UNIVERSITY OF SOUTHAMPTON

FACULTY OF ENGINEERING, SCIENCE AND MATHEMATICS

INSTITUTE OF SOUND AND VIBRATION RESEARCH

PASSIVE VIBRATION ISOLATORS WITH HIGH-STATIC-LOW-DYNAMIC-STIFFNESS

by

Alessandro Carrella

Thesis for the degree of Doctor of Philosophy

April 2008

UNIVERSITY OF SOUTHAMPTON
FACULTY OF ENGINEERING, SCIENCE AND MATHEMATICS
INSTITUTE OF SOUND AND VIBRATION RESEARCH

Thesis for the degree of Doctor of Philosophy

Passive Vibration Isolators with High-Static-Low-Dynamic-Stiffness

by Alessandro Carrella

ABSTRACT

In many engineering applications there is need to reduce the level of vibrations that are transmitted from a source to a receiver. Amongst several different techniques, the most commonly adopted solution is to interpose an *isolation mount* between the source and the receiver. Ideally, a vibration isolation mount would have a high static stiffness to prevent too large a static displacement to occur, but a low dynamic stiffness which reduces the natural frequency and extends the frequency range of isolation. For linear mounts these two features are mutually exclusive. However, an improved compromise can be reached by employing nonlinear mounts. In this thesis the advantages and the limitations of nonlinear isolation mechanisms with a *high-static-low-dynamic-stiffness*(HSLDS) characteristic are investigated.

A study of the static characteristics of two mechanisms with HSLDS is presented. This desired property is obtained by connecting in parallel elements with positive and negative stiffness. For both systems the positive stiffness is given by linear springs. In one model the geometry of the system is exploited to achieve the desired negative stiffness. This is obtained by a pair of linear springs placed at a certain angle to the horizontal (oblique springs). In the second model considered the required negative stiffness is provided by a set of magnets in attracting configuration. In both cases the force and stiffness are approximated to a symmetric cubic polynomial and a quadratic function of the displacement respectively. From a dynamical point of view this allows the system to be treated as a Duffing oscillator. It is argued that for small oscillations about the static equilibrium position the mechanism behaves linearly. A lab-scale rig which reproduces the HSLDS system with magnets and springs is designed and built. The excitation level is chosen to comply with the assumption of small displacement so that the experimental results show that the system responds in a rather linear fashion. The natural frequency of the HSLDS is half that of a linear model with the same static displacement and its transmissibility also compares favourably.

A nonlinear analysis is also carried out in order to predict the response of the system when the assumption of linearity no longer holds true. Both cases of harmonic excitation of the payload and of the base are studied. For the two instances an approximate solution to the nonlinear equation of motion is found by applying the method of Harmonic Balance to a first order expansion. The main feature of the dynamic response of a Duffing oscillator is the jump phenomenon. Herein this is described and analytical expressions for the jump frequencies are also provided. The isolation properties of an HSLDS isolation system are evaluated in terms of the transmissibility and its performance is compared with that of an equivalent linear system. It is shown that the HSLDS has a higher isolation capability.

Contents

1 Introduction **1**
1.1 Motivation of the research 1
1.1.1 Vibration isolation of a SDOF system 2
1.1.2 Influence of damping 3
1.1.3 Influence of stiffness 4
1.1.4 A solution with a nonlinear spring 4
1.2 Literature survey 6
1.2.1 Vibration isolation techniques 6
1.2.2 Passive vibration isolation with HSLDS mechanisms 10
1.3 Objectives and contributions 14
1.4 Thesis outline 16

2 Static characteristics of two HSLDS systems **27**
2.1 Introduction 27
2.2 Negative stiffness - restoring force of a system with two oblique springs 28
2.3 A hardening HSLDS system 30
2.3.1 Approximation to the stiffness of the HSLDS isolator . . . 33
2.3.2 Equation of motion 35
2.4 A softening system with HSLDS stiffness 36
2.5 The magnetic spring 37
2.5.1 Repelling magnets 38
2.5.2 Attracting magnets 39
2.6 HSLDS with springs and magnets 40
2.6.1 Approximate force and stiffness expressions 42
2.6.2 Equation of motion 43
2.7 Effect of the weight of the isolated object 44
2.8 Conclusions 46

3 Basic aspects of nonlinear dynamics **61**
3.1 Introduction . . . 61
3.2 Fundamental concepts . . . 62
3.3 Local stability and the phase plane . . . 63
3.3.1 Linear stability analysis of the hardening and softening Duffing's equation . . . 66
3.3.2 Conservative systems and motion in the large . . . 67
3.4 Non-autonomous systems: response to a harmonic excitation . . . 70
3.4.1 Perturbation methods . . . 71
3.4.2 The Harmonic Balance method . . . 72
3.5 Parametric system and bifurcation . . . 75
3.6 Conclusions . . . 78

4 Vibration isolation of a SDOF system with an HSLDS isolator: force transmissibility **88**
4.1 Introduction . . . 88
4.2 Response to a harmonic force . . . 90
4.2.1 Approximate periodic solution . . . 91
4.2.2 Bifurcation and stability analysis . . . 93
4.3 The jump frequencies . . . 95
4.4 Force transmissibility . . . 99
4.4.1 Peak transmissibility . . . 100
4.4.2 Comparison between the transmissibility of an HSLDS mechanism and an equivalent linear isolator . . . 101
4.5 Conclusions . . . 104

5 Vibration isolation of a SDOF system with an HSLDS isolator: motion transmissibility **117**
5.1 Introduction . . . 117
5.2 Response to a harmonic excitation of the base . . . 119
5.2.1 Approximate periodic solution: relative transmissibility . . . 120
5.2.2 The jump frequencies . . . 122
5.3 Absolute motion transmissibility . . . 125
5.3.1 Comparison between the motion transmissibility of an HSLDS mechanism excited at the base and that of an equivalent linear isolator . . . 127
5.4 Conclusions . . . 130

6 Experimental work: rig design and transmissibility measurement of a HSLDS isolator **143**
6.1 Introduction . . . 143
6.2 Isolator configuration . . . 144
6.3 Experiments . . . 146
6.3.1 Comparison with theoretical transmissibility curves . . . 149
6.4 Discussion . . . 151
6.5 Conclusions . . . 152

7 Concluding remarks and suggestions for future work **159**
7.1 Future work . . . 163

References **165**

Appendix **172**

A On the dynamic behaviour of a mass supported by a parallel combination of a spring and an elastically connected damper **172**

B Static analysis of a passive vibration isolator with quasi-zero-stiffness characteristic **173**

C Lab demonstrator of the HSLDS characteristic **174**
C.1 Linear mathematical model . . . 174
C.2 Experimental rig and results . . . 176
C.3 Conclusions . . . 177

List of Figures

1.1 The problem of vibration isolation: the vibration source generates vibration which is then transmitted to the receiver via the transmission path. With a passive vibration isolation approach a reduction of the level of vibrations passed on to the receiver can be achieved by modifying the transmission path 18

1.2 Single-degree-of-freedom (SDOF) vibration isolator model. The source can be a force, f_e, applied to the mass in which case the receiver is the base of the system which is subject to the force transmitted f_t, or a motion of the base z in which case the receiver is the mass m experiencing a motion x. In both cases the disturbance travels from the source to the receiver through the spring k_l and the dashpot c which therefore constitute the transmission path 19

1.3 Absolute transmissibility of a SDOF system with viscous damping. Effect of changing the damping ratio. An increase of ζ_l causes the peak to decrease. However, at higher frequencies $\Omega_l > \sqrt{2}$, the higher the damping the higher the transmissibility with consequent deterioration of the isolation performance 20

1.4 Absolute transmissibility of a SDOF system with viscous damping. Effect of changing the stiffness. The solid line is the transmissibility of a mount with a spring 4 times softer than the original system (dashed line) if the damping coefficient c is maintained constant. If c is varied to keep ζ_l constant the transmissibility is given by the dotted line 21

1.5 Natural frequency of a linear SDOF system as a function of the static displacement. With a soft spring the natural frequency decreases but the static displacement increases 21

1.6 Comparison of the nondimensional force-displacement characteristic of a linear and a nonlinear spring. The static and dynamic stiffness of the linear spring are equal. At the static equilibrium point, the static stiffness stiffness of the nonlinear mount is the same of the linear one, but for oscillations about this position the slope of the nonlinear force-displacement curve (dynamic stiffness) is much smaller and this results in a lower natural frequency . . . 22
1.7 Schematic representation of an air spring 22
1.8 Main system, m, k with the an undamped DVA m_a, k_a fitted . . . 23
1.9 Magnitude of the response of the isolated mass to a harmonic force: dashed line without DVA; solid line with undamped DVA. $\mu = 0.2$ 23
1.10 Schematic representation of a Belleville or disc spring 24
1.11 Load-Deflection plot for a Belleville Spring with different geometrical parameters 24
1.12 Schematic model of system with HSLDS characteristic. (a) HSLDS mechanism in its loaded condition. (b) Oblique springs which provide the necessary negative stiffness, in their initial position. (c) Vertical spring which provides the static support 25
1.13 Stiffness-displacement characteristic of a HSLDS model. The dotted line is the stiffness, which becomes negative, of the system depicted in Fig. 1.12(b). The dashed line is the positive, constant stiffness of a spring such as that shown in Fig. 1.12(c). The sum of these two curves is the solid line which is the curve of the HSLDS mechanism of Fig. 1.12(a). This particular example illustrates the special case in which the stiffness becomes zero 26

2.1 Schematic representation of a system with two oblique springs. The springs oppose the applied load f, and the geometry gives rise to a non-linear force-displacement characteristic 48
2.2 Force-deflection characteristic of the system represented in Fig. 2.1. When $\gamma = 0$ the springs are vertical and when $\gamma = 1$ they are horizontal. After the maximum the curves have a region with negative stiffness 49
2.3 Schematic representation of an isolator with HSLDS characteristic 49

2.4 Stiffness-displacement characteristic of a HSLDS mount: by connecting in parallel (summing the stiffness) a linear spring (with positive stiffness, dashed line) with one with 2 oblique springs (negative stiffness, dotted line) the total stiffness (solid line) at the static equilibrium position can be made as small as desired, e.g. even zero as in this case 50
2.5 Non-dimensional force-displacement characteristic of a HSLDS mechanism when $\mu = 1$: the solid line has a flat region in which that system has quasi-zero stiffness 51
2.6 Non-dimensional stiffness of a HSLDS mechanism when $\mu = 1$: the solid line is representative of a stable system (always positive stiffness) with zero stiffness at the static equilibrium position. The symbol 'o' denotes the static equilibrium position $\hat{x}_e = \sqrt{1-\gamma^2}$, i.e. when the oblique springs are horizontal 51
2.7 Non-dimensional force-displacement characteristic when $\mu = \mu_{opt}$ and $\gamma = 2/3$. The solid line shows the plot of the exact expression Eqn.(2.13) in the new coordinate system. The other lines are for the approximate expressions of third, fifth and seventh order Taylor's series expansions about $\hat{y} = 0$ 52
2.8 Approximation error between the quadratic and exact stiffness when $\mu = \mu_{opt}$ and $\gamma = 2/3$ 53
2.9 Isolation system with coil springs and magnets 54
2.10 **Magnets in repelling configuration**: Nondimensional force and stiffness characteristic as function of the nondimensional displacement 55
2.11 **Magnets in attracting configuration**: Nondimensional force and stiffness characteristic as function of the nondimensional displacement; $\hat{x} = x/d$ 56
2.12 Force and stiffness characteristics of a system with attracting magnets and coil springs. The system parameter ν is changed so as to achieve several values of maximum stiffness $\hat{k}_0$ 57
2.13 Maximum excursion from the static equilibrium position which guarantees positive stiffness as a function of ν. Both exact (solid line) and approximate (dashed line) are plotted. This figure clearly shows the compromise between the desired low stiffness and width of stability region 58

2.14 Relationship between the maximum stiffness of the HSLDS system, $\hat{k}_0$, and the system parameter ν required to achieve it 58
2.15 Percentage error introduced by assuming the stiffness to be a quadratic function of the displacement. Two values of ν have been chosen and the smaller ν (the higher the maximum stiffness) the smaller the error 59
2.16 Percentage error introduced by the approximate expression for the maximum displacement from the static equilibrium position which ensures positive stiffness 59
2.17 HSLDS system with 3 springs: (a) unladen condition; (b) loaded with a tuned mass m so that at the static equilibrium position the oblique springs lie horizontal; (c) system loaded with an untuned mass m_u and the static equilibrium position is $x = h_e$. The dashed line in (b), (c), is relative to the initial unladen position 60

3.1 Phase-plane (a) and motion space (b) representation of the undamped system $\ddot{x} + x + x^3 = 0$. The initial conditions are $x(0) = 1$ and $\dot{x}(0) = 0$ 80
3.2 Phase-plane (a) and motion space (b) representation of the damped system $\ddot{x} + 0.1\,\dot{x} + x + x^3 = 0$. The initial conditions are $x(0) = 1$ and $\dot{x}(0) = 0$ 80
3.3 Definition of stability in the sense of Liapunov. The equilibrium point $\mathbf{u_e}$ is stable for system I as if perturbed within the neighbourhood (circle) δ the solution $\mathbf{u}(t)$ remains within ε for all $t \geq 0$; $\mathbf{u_e}$ asymptotically stable for system II for, in the limit for $t \to \infty$ the solution tends to the equilibrium point; the equilibrium point is unstable for the system III 81
3.4 Stability regions according to the trace (T) and determinant (D) of the Jacobian matrix: Saddle Points (SP); Unstable Nodes (UN); Unstable Focus (UF); Stable Focus (SF); Stable Nodes (SN); Centres (C), [45] 82
3.5 Hardening Duffing oscillator. (a) phase-plot (b) potential energy, V as function of displacement. The only stable singular point is a centre in the phase plane, $x_1 = x_2 = 0$ 82

3.6 Softening Duffing oscillator. (a) phase-plot (b) potential energy, V as function of displacement. There are three singular points on the x-axis: one is stable, $x_1 = 0$ and two are unstable $x_1 = \pm 1$. These are respectively a centre, C and two saddle points, S, in the phase plane 83
3.7 Potential energy of a softening Duffing oscillator as function of displacement. The black circle represents the system: when it is at point C is in a stable condition; when is at points S is unstable 83
3.8 Fourier coefficients and harmonic decomposition of the numerical solution of the undamped Duffing equation $\hat{x''} + \hat{x} + \hat{x}^3 = 0$, with initial condition $\hat{x}(0) = 7.35$, $\hat{x'}(0) = 0$. The response contains only odd-ordered harmonics (1, 3, 5) 84
3.9 Qualitative representation of the frequency response function of a hardening Duffing oscillator. The dashed line is the *unstable branch* 84
3.10 Equilibrium points of a system depending on the parameter α. The points on segments $\overline{CA}$ and $\overline{CB}$ are unstable. At the value α_0 there are three equilibrium points of which one is unstable . . 85
3.11 Catastrophe manifold: this is the surface of singular points in the x_1, ξ, ρ space. The $x_1 - \xi$ plane correspond to the unforced system. The segment connecting the 'upper' and 'lower' part of the surface denote unstable equilibrium points 86
3.12 Bifurcation set for the parameters of the Duffing oscillator. In the region $D < 0$ there are three equilibrium points, whilst in the area where $D > 0$ only one. The lines mark the passage from one condition to the other and are the bifurcation points. 87

4.1 Single-degree-of-freedom system with an HSLDS mount with viscous damping: a mass m is suspended on a dashpot c in parallel with a nonlinear spring with HSLDS k_{HSLDS}. The excitation force acting on the mass is $f_e = F_e \cos \omega t$. f_t is the force transmitted to the base through the spring and the dashpot 106
4.2 Frequency response function of the Duffing oscillator described by Eqn.(4.3). The sign of the cubic coefficient defines a softening (-) or hardening (+) behaviour. When $\alpha = 0$ the system becomes linear 106

4.3 Plot of the frequency response of the Duffing oscillator, given by Eqns.(4.7) with $\zeta = 0.01$. Hardening system (a): as the frequency is increased the amplitude increases following the upper or *resonant* curve. At the frequency Ω_d, marked with the letter D, it suddenly drops to the lower or *non-resonant* branch. Similarly, decreasing the frequency, the response follows the non-resonant branch until the frequency Ω_u, marked with the letter U. A further decrease in frequency causes the response to jump up to the resonant branch. When the system has a softening spring, (b), the jump down occurs by decreasing the frequency and the jump up increasing the frequency. The dashed line denotes unstable equilibrium points. This part of the curve cannot be observed experimentally 107

4.4 Stability analysis of the forced response of the Duffing equation using a linear perturbation method. For both hardening (a) and softening systems (b) $\zeta = 0.02$. The part of the FRF included in the unstable region denotes unstable equilibrium points and is the branch between the resonant and non-resonant curves 108

4.5 Nature of the equilibrium points of the FRF of a Duffing equation with softening nonlinearity. The stable points are centres, whilst the unstable points are saddles 109

4.6 FRF of a softening system with $\alpha = 1.33 \times 10^{-4} = -5\,\alpha_{max}$ and $\zeta = 0.01$. The jump-down phenomenon does not take place, but as the frequency is decreased the response follows the resonant curve until $\Omega = 0$ 109

4.7 FRF of a hardening (a) and softening (b) system. In both cases the jump-down frequency is strongly dependent on the damping ratio ζ, whilst the jump-up frequency is mostly unaffected by the change in ζ 110

4.8 Comparison between the analytical and numerical jump-frequencies as a function of α for two different values of ζ 111

4.9 FRF of a softening (red) and hardening (blue) system with $\zeta = 0.02$ and critical value of the coefficient coefficient of the nonlinear term, $|\alpha| = |\alpha_{cr}| = 1.31 \times 10^{-4}$. The dashed line has been replaced by a solid line as no jump occurs 112

4.10 Absolute Transmissibility of an isolator with symmetric cubic nonlinearity. For both hardening (a) and softening (b) systems $\zeta = 0.01$. The maximum transmissibility calculated with Eqn.(4.30) is also shown 113
4.11 Comparison between the absolute transmissibility curves of a linear (-.) and HSLDS (–) mount. The peak transmissibility values have been calculated analytically. For the linear system $\zeta_l = 0.005$ and for the HSLDS mount $\zeta = 0.01$ ($\beta = 0.5$) 114
4.12 Absolute transmissibility. Same plots of Fig.4.11 but with the transmissibility expressed in dB. The increase of the frequency isolation region is highlighted 115
4.13 Transmissibility curves of a linear mount (-.) and of a two HSLDS (–) system with $\alpha = \alpha_{lim}$ and $\alpha = 2\,\alpha_{lim}$. For the linear system $\zeta_l = 0.005$ and for the HSLDS mount $\zeta = 0.01$ ($\beta = 0.5$) 116

5.1 Single-degree-of-freedom model of HSLDS mount with viscous damping: a mass m is suspended on a dashpot c in parallel with a nonlinear mount with HSLDS k_{HSLDS}. The base undergoes harmonic motion $z = Z\,\cos(\omega\,t)$ 132
5.2 Relative transmissibility of the HSLDS isolator for a harmonic motion of the base. Hardening (a) and softening systems (b). The damping ratio is $\zeta = 0.01$. The part of the FRF included in the unstable region delimited by the dash-dot lines, denotes unstable equilibrium points and is therefore plotted with a dashed line . . . 133
5.3 Relative transmissibility. (a) hardening, (b) softening for different values of ζ. Despite the damping has doubled the jump-up frequency has remained substantially unchanged 134
5.4 Comparison between the analytical and numerical jump-frequencies as function of α for two different values of ζ 135
5.5 Comparison between the jump frequencies of a system with symmetric cubic restoring force excited by a harmonic force applied to the mass (solid line) and by a harmonic motion of the base. In both cases is $\zeta = 0.01$ 136
5.6 Relative transmissibility of a softening (red) and hardening (blue) system with $\zeta = 0.02$ and critical value of the coefficient coefficient of the nonlinear term, $|\alpha| = |\alpha_{cr}| = 1.31 \times 10^{-4}$. The dashed line has been replaced by a solid line as no jump occurs 137

5.7 Absolute transmissibility of a (a) softening HSLDS isolator and (b) hardening isolator. For both systems is $\zeta = 0.01$. The maximum transmissibility calculated with Eqn.(5.24) is also shown 138
5.8 Comparison of the absolute force and motion transmissibility, Eqns.(4.29) and (5.22) respectively. The symbols 'o' and '×' mark the maximum force and motion transmissibility calculated with Eqns.(4.30) and (5.24) respectively 139
5.9 Comparison of the absolute transmissibility of a HSLDS and a linear isolation mount. The frequency on the x-axis is normalised by the natural frequency of the linear system, Ω_l. The linear system (dash-dot line) has a damping ratio $\zeta_l = 0.005$ and the scaling factor is $\beta = 0.5$. Thus the damping ratio of the HSLDS isolator is $\zeta = 0.01$. Both HSLDS mechanisms offer improved isolation performance 140
5.10 Comparison of the absolute transmissibility of a HSLDS and a linear isolation mount. The frequency on the x-axis is normalised by the natural frequency of the linear system, Ω_l. The linear system (dash-dot line) has a damping ratio $\zeta_l = 0.005$ and the scaling factor is $\beta = 0.5$. Thus the damping ratio of the HSLDS isolator is $\zeta = 0.01$. Both HSLDS mechanisms offer improved isolation performance 141
5.11 Transmissibility of a hardening HSLDS mechanism compared with that of the equivalent linear isolator (with $\zeta_l = 0.005$) when $\alpha = \alpha_{lim}$ and $\alpha = 1.25\,\alpha_{lim}$. When $\alpha = \alpha_{lim}$ the jump-down frequency becomes equal to the natural frequency of the equivalent linear system and also the peak transmissibility of the HSLDS equals that of an equivalent linear model (dashed-dotted line). If $\alpha \geq \alpha_{lim}$ there is no advantage in using a HSLDS isolator 142

6.1 Schematic representation of an isolation system with coil springs and magnets: the middle magnets has a mass m and is free to move along the vertical smooth bar. The upper and lower magnets are fixed to the bar and both attract the central piece. The mechanical springs separate the middle magnets from the others 153
6.2 Ratio between the magnitudes of the nonlinear and linear terms of the restoring force as a function of the non-dimensional displacement when $\nu = 0.72$ 154

6.3 Magnetic isolator. Experimental rig fixed at the base to a vertical shaker . . . 154
6.4 Measured modulus of the transmissibility to determine the mount properties. Transmissibility of the system without the coil springs and the magnets arranged in a repelling configuration (dashed line and data points marked with 'x'). Transmissibility of the mass-spring system without the magnets at the extremities of the bar (solid line and data points marked with '+') . . . 155
6.5 Steady-state measurements of the base (a) and mass (b) displacement at different frequency of excitation. The distance of the central magnet from the extremities is $d = 3.81$ cm . . . 155
6.6 Comparison of the transmissibility of a linear mass-spring system (dashed line and crosses) and that of the HSLDS mount for a 3 mm base amplitude excitation (solid line and diamonds) and 4 mm base amplitude excitation (dotted line and squares) . . . 156
6.7 Comparison of the transmissibility predicted theoretically and that measured. The diamonds and squares are the data points of the measured transmissibility for a 3 and 4 mm base amplitude excitation respectively. The dashed and the solid line are the theoretical curves, Eqn.(5.22) with the values of ζ and α given in Eqns.(6.12) and (6.14) respectively. The measured transmissibility of the linear system is shown as data points $\times$ whilst the dotted line is the analytical transmissibility Eqn.(1.1) with $\zeta_l = 0.177$. . . . 157
6.8 Ratio between the Fourier coefficients of the third and first harmonic of the measured response of the HSLDS system at each excitation frequency for base displacement with maximum amplitude of 3 mm . . . 158

C.1 Schematic representation of the HSLDS demonstrator . . . 179
C.2 *Experimental Rig* . . . 180
C.3 Transient response of the system for different values of a: the period of the simple pendulum is more than 4 times shorter than the period of the HSLDS mechanism when $a = 15.5$cm (c) . . . 181
C.4 DFT magnitude of the measured acceleration. The analysis of the frequency content clearly shows the reduction in natural frequency achieved with the insertion of the corrective springs . . . 182

Declaration of authorship

I, Alessandro Carrella, declare that the thesis entitled PASSIVE VIBRATION ISOLATORS WITH HIGH-STATIC-LOW-DYNAMIC-STIFFNESS and the work presented in it are my own. I confirm that: the work was done wholly whilst in candidature at this university; where I have consulted the published work of others this has been clearly attributed and I have acknowledged all main sources of help.

Acknowledgements

I am deeply indebted to my supervisors Tim Waters and Mike Brennan to whom goes my deepest gratitude for their superb job. They have made me passionate about research and I have made treasure of their teachings. The hours of discussion greatly improved me as a researcher as well as a person. I recall once Mike saying "You need a good reason to get out of the bed in the morning"; in another occasion Tim told me "The process is much more important than the research outcome. So think about your PhD as cultivating skills, and everything else is a bonus".

I would also like to thank all the Dynamic Group of the ISVR: here I have felt to belong to a family where academics, staff and researcher contributed to make it a great place to work in.

A PhD can be likened to a roller coster ride. However, going through three years of roller coster requires strength and balance. I received most of these from my friends here in Southampton. I like to mention here those who have been constantly there for me to support and advice: Alessandro Beda, Paolo, Sabrina, Ismath, Fay, Cassandra, Stefano, Davide, Cecio, Beppe, Gianluca. And Elisabetta who deserves a special mention for having stood by me and for having been the source and the recipient of my strongest emotions.

However, all these professional and personal developments would not have been possible without the constant presence, care and support of my family. I hope my mum and dad, my brother and sister can accept this my achievement as a reward for their enduring love and these lines as a sign of mine for them.

List of symbols and abbreviations

FRF Frequency response function

HB Harmonic Balance

HSLDS High-static-low-dynamic-stiffness

SDOF Single-degree-of-freedom

$\hat{}$ Denotes nondimensional quantities

$\cdot$ Differentiation with respect to time

$'$ Differentiation with respect to non-dimensional time

α Nondimensional coefficient of the cubic term of the polynomial nondimensional restoring force

β Nondimensional coefficient of the linear term of the polynomial nondimensional restoring force

γ Initial angle at which the oblique springs of the hardening HSLD model

ϵ Fractional change in the value of optimal design parameters

δ_{st} Static displacement

μ Ratio of the springs coefficients of the hardening HSLD model

ν Coefficient relating magnetic and mechanical stiffnesses

ω_l Natural frequency of standard linear system (or of the equivalent linear isolator)

ω_n Natural frequency of linearised HSLDS system and characteristic frequency of the HSLDS isolator

ζ	Damping ratio
L_0	Initial length of the oblique springs
k_o	Spring coefficient of the oblique springs
k_v	Spring coefficient of the vertical springs
k_1	Coefficient of the linear term of the restoring force
k_3	Coefficient of the cubic term of the restoring force
T_a	Force transmissibility - excitation force applied to the mass
T_m	Motion transmissibility - excitation of the base

Chapter 1

Introduction

'If a man will begin with certainties, he shall end with doubts;
but if he will be content to begin with doubts,
he shall end in certainties.'

Francis Bacon, (1561-1626)

1.1 Motivation of the research

The isolation of vibrations is a problem that affects most engineering structures and, despite the decades of previous studies, it remains a problem that is solved on a case-by-case basis. Furthermore, it is also an issue that relates to everyday life. For instance, a ride in a car, a hand-held power tool or an underground-train, generate a certain amount of vibration that is transmitted to the surrounding environment.

The problem is depicted schematically in Fig. 1.1. The vibrations generated by a source (e.g. car, power-tool, train) are inevitably transmitted to a receiver (e.g. passenger, hands, building) attached to it. The disturbance reaches the receiver via the transmission path as shown schematically in Fig. 1.1. To reduce the level of vibrations transmitted to the receiver different approaches can be followed. Ideally, the source could be designed to generate a lower vibration level. Alternatively, an external device such as a force actuator or a vibration absorber can be added in order to reduce transmitted vibrations. However, usually the preferred choice is to insert a device between the source and the receiver called a

vibration isolator, or **isolation mount**; in other words, the transmission path is modified, [1]. The next section illustrates the modelling of a vibration isolator and the strategies employed to improve the isolation performance of a mount.

1.1.1 Vibration isolation of a SDOF system

The model of a single-degree-of-freedom (SDOF) that is often used to represent a vibration isolation system is shown in Fig. 1.2. A mass m is suspended on a parallel combination of a spring of coefficient k_l and a dashpot c (which are both considered massless).

There are two different problems related to the transmission of vibration from a source to a receiver, and these are also shown in Fig. 1.2. In one case the mass is directly excited by a force f_e, and therefore acts as the source of the disturbance. The objective of a vibration isolator is then to reduce the force transmitted to the base f_t, which is the receiver. In the other situation, the disturbance comes from the motion of the base z (source), in which case the purpose of the isolator is to reduce the motion of the mass (receiver), x, attached to the vibrating base. Either way, the isolation mount that separates the source and the receiver can be schematised with a spring and a dashpot connected in parallel. In order to minimise the level of transmitted vibrations without the intervention of external forces (i.e. passive isolation) these two elements should be opportunely chosen.

The quantity that is often used to evaluate the performance of an isolation mount is a nondimensional function called **absolute transmissibility** and is a function of frequency. If the system is excited by a harmonic force applied to the mass the absolute transmissibility is the ratio between the magnitude of the transmitted force to a rigid foundation and the magnitude of the excitation force, in steady-state vibration and at a given excitation frequency. When the source is a harmonic motion of the base, the absolute transmissibility is the ratio between the amplitude of the displacement of the mass and that of the base, at a given frequency of oscillation of the base. Expressions for the absolute transmissibilities of systems with linear isolators are given in textbooks, e.g. [1–3]. For a linear system with viscous damping subject to harmonic excitation (force or base), such as that shown in Fig. 1.2, the absolute transmissibility is given in non-dimensional

quantities by

$$|T_a| = \frac{|x|}{|z|} = \frac{|f_t|}{|f_e|} = \sqrt{\frac{1 + 4\,\zeta_l^2\,\Omega_l^2}{(1 - \Omega_l^2)^2 + 4\,\zeta_l^2\,\Omega_l^2}} \tag{1.1}$$

where ζ_l is the damping ratio of the system and Ω_l is the frequency ratio given respectively by[a]

$$\zeta_l = c/2m\omega_l \qquad \Omega_l = \omega/\omega_l \qquad \omega_l^2 = \tfrac{k}{m}$$

in which ω_l is the undamped natural frequency and ω the excitation frequency.

When evaluating the isolation properties of an isolator, it can be argued that two very important values are: i) the frequency at which the isolation begins, that is the frequency above which $|T_a| < 1$ and ii) the peak-transmissibility, $|T_a|_{max}$ which (for a linear system) occurs approximatively at the natural frequency $\Omega_l = 1$ provided that $\zeta_l \ll 1$. These values can be found from Eqn.(1.1) and are respectively $\sqrt{2}$ times the natural frequency and, for small damping, $|T_a|_{max} \approx 1/2\zeta$. It remains now to investigate the influence of the damping and the stiffness on these transmissibility properties.

1.1.2 Influence of damping

Fig.1.3 shows the transmissibility of a linear system with different values of the damping ratio. Some interesting features can be observed. The isolation region begins at $\Omega_l = \sqrt{2}$ regardless of the damping ratio. An increase of the damping ratio causes the peak to decrease but also an increase of the transmissibility at high frequencies. This phenomenon is attributed to the dynamic stiffness of the damper which increases with frequency and can far exceed that of the spring thus becoming the primary transmission path. This drawback can be mitigated against, for example, by connecting a spring in series with the damper. The system thus obtained is referred to as the Zener model. In reference [6] (reported in this thesis in Appendix A) it is shown that this system performs poorly in the case of white-noise random excitation and does not provide any benefits in terms of the bandwidth of the isolation region.

[a] The subscript $_l$ is used in this thesis to denote the parameters of a linear system

1.1.3 Influence of stiffness

The other way of modifying the path through which the vibrations are transmitted from the source to the receiver, is to change the stiffness of the isolator. The effect of changing k_l cannot be inferred directly from Eqn.(1.1) as k_l is implicitly contained in Ω_l. The way in which stiffness changes the transmissibility is illustrated in Fig. 1.4. In the example shown the stiffness is reduced by a factor of four. The natural frequency of the system is thus halved (solid line). The reduction of the natural frequency implies that the isolation frequency bandwidth is larger. Furthermore, a change in the natural frequency affects also the damping ratio and this produces the effects seen in Section 1.1.2. These considerations may lead to the conclusion that improved isolation performance can be obtained simply by employing a softer spring. This, however, is not the case.

The spring (or resilient element) also has the function of providing the static support to the mass suspended on it. A characteristic parameter of the isolation system is in fact the *static deflection*, δ_{st}. This is directly related to the natural frequency as follows, [3]

$$\omega_l = \sqrt{\frac{g}{\delta_{st}}} \tag{1.2}$$

The dilemma between better isolation (characterised by the natural frequency in Hz, $f_l = \omega_l/2\pi$) and the travel on the isolator (i.e. the static displacement), is plotted in Fig. 1.5. It can be seen that in order to achieve a low natural frequency, there is need to accommodate a large static displacement.

1.1.4 A solution with a nonlinear spring

In conclusion, when adjusting the parameters of an isolator, increased damping performs a useful function at resonance but is detrimental at high frequencies and a softer springs helps to widen the isolation frequency bandwidth but comes at the price of a higher static displacement.

If it is chosen to improve vibration isolation through changes in stiffness rather than the damping, the trade-off is clearly defined. The reason why there seems not to be an optimal solution is because the spring considered is a linear element.

Consider a linear spring of coefficient k_l: it exerts the restoring force $f_k = k_l\, x$

which is shown as solid line in Fig. 1.6. If a mass of weight W is placed on this spring it displaces by δ_{st} reaching the static equilibrium position. The constant of proportionality between force and displacement is the *static stiffness*. If the mass is forced to oscillate about the static equilibrium position, in the range $\Delta\, x$ say, the slope of this part of the force-deflection curve defines the *dynamic stiffness* which, in the case of a linear spring, is constant and thus static and dynamic stiffnesses are equivalent.

Consider now a nonlinear spring with a cubic force-deflection curve

$$f_k = k_1\, x + k_3\, x^3 \tag{1.3}$$

In this case the stiffness is no longer constant but is a quadratic function of the displacement. Furthermore, the nonlinear spring can be designed in such a way that the load W produces the same static displacement as the linear spring. This is depicted by the dashed line in Fig.1.6. The main difference between the linear and nonlinear spring is that for oscillations about the static equilibrium position, in the range $\Delta\, x$ say, the nonlinear spring has a smaller dynamic stiffness (local slope of the curve).

In summary, the nonlinear spring described by Eqn.(1.3) has a relatively high static stiffness but a low dynamic stiffness. A spring with this characteristic is herein referred to as a ***High-Static-Low-Dynamic-Stiffness*** (**HSLDS**) spring (or mechanism, or isolation mount). Furthermore, for small oscillations about the static equilibrium position Eqn.(1.3) can be linearised and the natural frequency of the system is smaller than that of the system with a standard linear spring. This characteristic gives the HSLDS spring potential as a vibration isolator.

The problem of vibration isolation embraces a variety of techniques and applications; therefore only a brief survey of the different approaches to the problem of vibration isolation will be presented in the literature review that follows. More emphasis will be given to the area of literature which pertains to mechanisms with low natural frequency and their exploitation for vibration isolation purposes.

1.2 Literature survey

Amongst the different approaches to vibration isolation, this thesis is concerned with **passive isolation** systems, that is when the characteristics of the isolation mount (e.g. spring and/or damper coefficients) are not changed by means of devices which need an external power supply. There are different models to describe a passive isolation system which can be found in references [1, 3].

1.2.1 Vibration isolation techniques

Before focussing entirely on passive isolation with low natural frequency systems, it has to be said that passive devices are not the only, or necessarily the best, way to achieve a good isolation performance. In fact, also active and semi-active isolators play a major role in the field of vibration isolation:

1. **active isolation**: this type of isolator uses a force produced by an external device (actuator); for example, the control force can be chosen to minimise the response of the system.

2. **semi-active isolation**: in this case the isolation is produced by 'passive' elements, but their properties can be modified (e.g. electro-rheological (ER) or magneto-rheological (MR) dampers). However, unlike active control systems, external forces do not contribute to the isolation effect (and very little power supply is required);

Active Control In actively controlled vibration isolators the reduction of transmitted vibrations between the base and the payload mounted on it is due to the action of an actuator. This device is controlled and is activated and deactivated in order to exert the force required to counteract obnoxious vibrations. Although very versatile and able to adapt to different operating conditions this kind of isolator has the drawback of being power-consuming and, in some cases, instability is also a problem. This field of research, thanks to the advances of computational power, has been very active particularly during the 1970's and 1980's. Ever since papers have been produced to a rate of several hundreds per year and their application concerns all fields of engineering. A comprehensive reference on the subject is found, for example in [7]. As other examples of active control of vibrations, in [8] a study on how to prevent a tall building from excessive vibration is presented. An example of a vibration control applied to a car suspension system is

presented in [9]. Many other papers that study and describe several applications for these devices are available in the literature. However, as there is no intention to pursue an active-control approach, no further attention will be given to this class of isolator.

Semi-active Isolation A semi-active isolator, in some circumstances, offer both the robustness of a passive system and the versatility of an active control system. As discussed above, these systems need very small external power sources. This is needed only to modify the stiffness or the damping coefficients. One widespread way to change the damping coefficient is the use of fluids which can change their viscosity when immersed in an electrical or magnetic field. These fluids, discovered in the late 1940's are known respectively as *electrorheological* (ER) and *magnetorheological* (MR) fluids. These are most commonly colloidal suspensions: when an electric or magnetic field is applied to the fluid, the particles react changing the viscosity of the liquid. Therefore, ER or MR have the ability to alter the dynamic behaviour of the system [10, 11]. When dealing with ER or MR fluids there seems still to be issues on how to model the complex physics of the phenomenon, although several models have been proposed to describe controllable fluid dampers [12–15]. On the other hand, smart stiffness can be achieved by modifying, for example, the temperature or the shape of the supporting element. Rustighi *et al* [16] investigated a tunable vibration absorber whose elastic modulus changed by about 47.5% when the supporting beams were heated thus changing the frequency range of suppression. The drawback highlighted was the long response time because of its thermal inertia. Bonello *et al* [17] considered instead several mechanisms in which the change in stiffness was due to the a change in shape of the support but encountered a limitation in the variation of the tuned frequency due to the limits of the actuator. A reference textbook on the subject is [18], whilst a review of semi-active control of vibrations is presented by Jalili, [19]. In the article particular emphasis is put on the 'adjustable semi-active dampers' such as MR and ER elements, but variable-rate springs are also discussed.

Passive Isolation In the majority of engineering applications, passive vibration isolators are usually the first solution to the problem of vibration transmission. This is mainly due to the fact that they are rather simple, do not require any external power source or computer control and therefore are also not ex-

pensive. When attempting a literature search on passive vibration isolation the works available are of the order of the thousands. In this section a brief overview of conventional passive isolators is presented. The mathematical models are not introduced here but only a brief description is given. Only for one system more details will be provided. A comprehensive analysis for these passive isolation systems can be found in the two main references used for this section [1, 3].

In general, as seen, the essential features of an isolator are a load-supporting element and an energy dissipating means. A common isolator device in which these two functions are performed by a single element is a mount made of **natural or synthetic rubber**. Such isolators return to their approximate original state with virtually no damage or change of shape even if they undergo large deformations. Their main advantage is that, for a given amount of elasticity, deflection capacity, energy storage, and dissipation, they require less space and less weight; also, they can be made in a variety of shapes and are usually cheap. However, the behaviour of rubber mounts is complex because of the viscoelastic nature of the material: there are several models that describe the mechanical properties of the rubber (e.g. the Zener model) but research is still ongoing to characterise these properties. The damping and stiffness are dependant on a series of factors (e.g. temperature, material, manufacturing, etc) which makes necessary a case-by-case analysis. The most widely element for energy storage (resilient element) is the **helical (or coil) spring**. These can work in tension or compression and have a linear load-deflection characteristic. Coil springs offer the advantages of low cost, compactness, and efficient use of material but dissipate a very small amount of energy and are ineffective at high frequencies. Amongst the metal springs, it is worthy to mention the **leaf spring** which is not as efficient as a helical spring (in terms of energy stored per unit weight) but it can act as a structural member (a common application of these springs is suspensions in trucks). Other than rubber or metal, resilient elements can be made also with gas. In general the gas in question is air and therefore these springs are referred to as **air springs**. The load is supported by the pressurised gas contained in a sealed pressure vessel and a flexible member. Thus, the static deflection can be maintained small by opportunely pressurising the gas. This does not imply (as it would for a coil spring) that the stiffness is high. In fact, air springs enable a reduction of the natural frequency by one order of magnitude compared to a metal or rubber spring with the same static displacement. A simple schematic representation of an air spring

is shown in Fig.1.7. A piston with surface S acted upon by a force F moves by a distance x and compresses the gas initially at pressure P and volume V. Boyle's law states that

$$P\,V^n = P_i\,V_i^n \tag{1.4}$$

where P_i is the gas pressure after the displacement, V_i is the volume of the gas and n is the ratio of specific heat of gas (1.4 for air). Assuming that the change in volume is small, i.e. $S\,x \ll V_i$ the stiffness of the air spring is given by

$$k = \frac{n\,P_i\,S^2}{V_i} \tag{1.5}$$

In this type of springs the damping is nonlinear and is due to friction, gas dynamic, motion of the wall.

A different, but also widely used, passive system for vibration control is the **dynamic vibration absorber** (DVA), invented by Frahm in 1909, [4]. It is employed in a variety of applications (for example it can be seen on top of the rotor hub of Lynx helicopters). For this reason a more detailed analysis is given here. A scheme of an undamped DVA is depicted in Fig. 1.8. A harmonic force $F_0\,\cos(\omega\,t)$ acts on a mass m (mass to be isolated); attached to this mass by a spring k_a, there is the mass m_a. Theoretically, if the natural frequency of the DVA is equal to the excitation frequency, the isolated mass m does not vibrate. When the DVA is perfectly tuned its natural frequency is equal to that of the main system and equal to the excitation frequency; in this case the ratio between the displacement of the isolated mass, x and its static displacement x_{st} due to the amplitude of the applied harmonic force is

$$\left|\frac{x}{F_0/k}\right| = \left|\frac{x}{x_{st}}\right| = \left|\frac{1-\Omega_a^2}{(1-\Omega_a^2)\,(1-\Omega_a^2+\mu)-\mu}\right| \tag{1.6}$$

where Ω_a is the nondimensional frequency ratio between the excitation frequency and the natural frequency of the DVA, ω/ω_a and μ is the ratio of the absorber mass to the isolated mass. By setting the denominator to zero it is possible to determine the two natural frequencies of the 2-dof system which are

$$\Omega_a^2 = \left(1+\frac{\mu}{2}\right) \pm \sqrt{\mu+\frac{\mu^2}{4}} \tag{1.7}$$

The solid line in Fig.1.9 depicts the magnitude of the response of the main mass

m when $\mu = 0.2$, whilst the dashed line is relative to the main mass only without the DVA attached. It can be seen that at the resonant frequency $\Omega_a = 1$ there is a notch in the displacement of the main mass. The case of a damped DVA requires a deeper analysis and is therefore omitted here for it goes beyond the scope of this section. In general, the dynamic absorber is effective only for a system that is subjected to a constant frequency excitation. Besides, it introduces an additional degree-of-freedom and an additional natural frequency into the primary system and there are many factors that need to be controlled.

In the next section it is presented a survey of the literature that concern isolators with a nonlinear stiffness characteristic and exhibits a load-deflection curve which is of interest for the purposes discussed in this thesis.

1.2.2 Passive vibration isolation with HSLDS mechanisms

In section 1.1.4 it was highlighted the potential benefits for vibration isolation offered by nonlinear springs with a certain load-deflection characteristic. There are commercially available springs, such as the *Belleville spring* or *disc spring*, which can be designed to have a nonlinear force-deflection curve similar to the dashed line in Fig.1.6. The cross section of a Belleville spring is schematically shown in Fig.1.10. The central horizontal part is where the load is applied. The restoring force is a cubic function of the displacement and is given by [1],

$$f = \frac{\pi\, E\, s}{6(D - D_0)^2} x \left[\left(h - \frac{x}{2} \right) (h - x) + s^2 \right] \ln \frac{D}{D_0} \tag{1.8}$$

which can be written in nondimensional form as

$$\hat{f} = \frac{f}{C\, h^4} = (s/h)\, \hat{x}^3 - \frac{3}{2} (s/h)\, \hat{x}^2 + (s/h) \left[1 + (s/h)^2 \right] \hat{x} \tag{1.9}$$

where the constant C is $\frac{\pi\, E}{6(D-D_0)^2} \ln \frac{D}{D_0}$ and $\hat{x} = x/h$. Thus the spring's characteristic depends on the material (taken into account by means of the Young's modulus E) and the geometrical properties. These can be adjusted to obtain the desired load-deflection curve. In Fig.1.11 several load-deflection curves are plotted for different geometries (h/s). The force, f (normalised by the force necessary to flatten the spring, F_0) is plotted against the displacement, x (normalised by the height of the spring, h). It can be seen that by changing the ratio s/h

the load-deflection curve can be *linear* (if $s/h \gg 1$ the linear term prevails) or nonlinear (as s/h becomes smaller the quadratic and cubic terms become not negligible). It is noticeable that for small displacements $x/h \ll 1$ the nonlinear terms are small compared to the linear one. Practical applications of a disc spring are described in [20]. Hunt [21] has suggested the use of a softening Belleville spring to increase the suppression bandwidth of a vibration absorber, whilst La Rosa *et al* [22] have investigated the possibility of discs with variable stiffness in order to achieve zero stiffness at the flat position. There are several disadvantages that make the Belleville spring unsuitable for vibration isolation purposes: in most applications the flat position is the limit of travel [23]; it is difficult to quantify the friction damping due to the sliding between the spring and the support surface [1]; finally these springs do not work in tension and often have dimensions (the width D) too large for practical applications [20].

A reference book for studying isolation systems with high-static-low-dynamic-stiffness characteristic is reference [24]. Therein, different strategies for realising an HSLDS characteristic for *Vibration Protecting Systems* (VPS) are illustrated. The principle is to combine elastic elements (e.g. springs) in a definite manner so that these result in a parallel combination of elements with negative and positive stiffness. This way the total stiffness, can be made as small as desired, theoretically zero. This can be clarified with an example. Consider the system shown in its loaded condition in Fig.1.12(a). Fig.1.12(b) shows the initial, unladen position of the two lateral springs, of coefficient k_o. The vertical spring, of stiffness k_v is also shown separately in Fig.1.12(c). The purpose of the lateral (oblique) springs is to provide the required negative stiffness, whilst the vertical spring grants the static load bearing capability. In Fig. 1.13 the stiffness-displacement curves of each sub-system of Fig. 1.12 are shown. The dotted line is for the two oblique spring and has a region with negative stiffness; the dashed line traces the positive, constant stiffness of the vertical spring. When combined (connected in parallel) the total stiffness is given by the sum of the curves and is shown as solid line. In this particular example the special case is shown of zero stiffness at the equilibrium position. In reference [24] several other systems with the same principle are presented. For each system the static characteristics are derived. The nonlinear restoring force (or moment in the case of a rotational degree-of-freedom) is expressed as a polynomial and the dynamic response of the system determined numerically. However, the isolation performance, i.e. the transmissibility curves

are not defined and the effectiveness of the VPS compared with a standard linear mount is not discussed.

Winterflood's PhD thesis focusses on vibration isolation of apparatus for gravitational wave detectors, [25]. The accuracy of these measuring systems is compromised for seismic motion of just a fraction of a Hertz in both vertical and horizontal directions. In his work he explores different ultra-low-frequency (ULF) isolation systems for both horizontal and vertical vibration. In the thesis different ingenious isolators are presented. For vertical vibrations he introduces the 'torsion-crank' mechanism that for the particular system tested was capable of achieving a period of oscillation greater than 20 seconds.

Reference [25] also introduced the concept of Euler springs. These are vertical beams axially pre-compressed with the critical Euler load (hence the name). In general, buckling is not desired because of the potential total loss of stiffness and static support that can occur. However, there are systems that, even beyond the buckling load, maintain a considerable strength which can be exploited. In this case the post-buckling configuration of the beams is used to give springs with small dynamic stiffness. This results in a small natural frequency of the system which was calculated to be in the sub-Hertz region. The concepts of Euler buckling springs has also been considered by Virgin [26–28] who analysed their static and dynamic characteristics and also presented experimental results that show a reduction of the fundamental frequencies with consequent widening of the isolation region. A commercially available isolator that exploits the concept of negative stiffness of buckled structures has been presented by Platus [29]. However the paper shows only measurements and lacks theoretical background.

In the literature it is possible to find many examples of isolation systems with low dynamic stiffness for a variety of applications. Here are some examples. Peleg [30, 31] was interested in improving the isolation of packaging systems from vibration during transport. He studied a nonlinear spring with hardening cubic characteristic but failed to propose a way to achieve the desired load-deflection curve. The aim of the study presented in [32] was to design a system with very low natural frequency so as to simulate flight boundary conditions during ground testing. The requirement is for the natural frequency of the system tested on the ground to be substantially less than the natural frequencies of interest of the

structure. The proposed mechanism is a vertical spring in parallel with two horizontal compressed beams. Numerical simulations for both linear and nonlinear ranges of operation are presented that show the effectiveness of the device. As also pointed out by the authors, further work is required to include the effect of damping on the mechanism and to increase the robustness to manufacturing imperfections which have a considerable effect on the initial equilibrium position. Wan and Schimmel [33] argue that vibration isolation of a vehicle seat can be improved if this is suspended on a hardening spring with a cubic force deflection characteristic. In particular, after a numerical optimisation analysis, the authors conclude that the best solution would be to have zero stiffness at the equilibrium position (i.e. after the driver has sat on the seat). A numerical simulation of the time response of the seat is presented which shows a reduction in the level of vibration of the seat when subject to a random acceleration input of the base. Regrettably, only a numerical study is presented. Sokolov *et al* [34] have considered the case of a hand-held percussion machine. In the paper numerical and experimental results show that the operator is subject to a low level of vibration if the handle is opportunely suspended on a spring with zero rate. The zero-rate spring proposed in the paper is a curved wedge sliding between two horizontal springs. However, in the paper the benefit of this mechanism on the transmissibility is only mentioned in passing and the nonlinear dynamics are not investigated.

A number of researchers have exploited magnetic forces to improve the performance of a vibration isolator [35, 36]. A particularly interesting example has been reported by Mizuno et al. [37] in which a pair of magnets in an attracting configuration is placed in series with a mechanical spring. The series combination of a negative stiffness due to the magnets, with an equal but positive stiffness due to the mechanical spring, results in a system which has infinite stiffness. Although this arrangement relies on an active control mechanism and is not very useful for vibration isolation, it can be used to obtain very high natural frequencies and significantly reduce the motion of a mass suspended on such a system when subjected to direct rather than base excitation.

Finally, it is noteworthy that systems with low natural frequency are of interest not only for vibration isolation purposes. For example, in the early 1930's Lacoste designed a vertical pendulum capable of reaching a period of oscillation of 37 seconds (i.e. with a natural frequency of 0.02 Hz), [38]. Although at the

time it was only a course-work exercise, the system laid the basis for the development of a new type of instrument used to measure gravitational acceleration, the gravitometer [39]. In the paper it is shown that if the initial length of the spring is zero, the period can be made infinite. Because a spring of zero initial length is not physically feasible Lacoste ingeniously manufactured it by pre-compressing the coil during the manufacturing process.

1.3 Objectives and contributions

From the review of the literature it emerges that both academic and industrial establishments have a particular interest in isolators with an HSLDS characteristic. Because the equation of motion of a mass suspended on an HSLDS mount is a nonlinear differential equation, there are two issues associated with this class of isolators: the evaluation and improvement of the isolation performance of the mount, a task that usually engages engineers, and the solution of the nonlinear differential equation, which requires the knowledge of highly mathematical techniques. The survey of the literature has highlighted that further contributions to this field can be made if the use of HSLDS springs as vibration isolators is investigated further. This thesis addresses this issue and **aims** at investigating further the static and dynamic properties of different mechanisms with HSLDS characteristics and to determine the suitability of such systems for improving the reduction of transmitted vibrations.

In order to achieve this goals, several **objectives** have been set:

1. to investigate different models that exhibit an HSLDS characteristic, and to establish the dependence of this property on the parameters of the systems;

2. to establish the benefit of using such HSLDS mechanisms as vibration isolators in the quasi-linear regime of operation and the consequences of the operation in a nonlinear regime;

3. to illustrate and compare with a standard linear mount, the practical use of HSLDS isolators through experimentation;

This research has made several **contributions** by:

1. proposing an in-depth static analysis of an existing HSLDS mechanism and formulating the dynamic equation of motion of a mass suspended on such a spring in the form of the Duffing oscillator;

2. presenting an optimisation analysis of the mechanism introduced in 1) which aims to maximise the displacement from the static equilibrium position without exceeding a desired (low) stiffness, [40];

3. proposing a novel mechanism where the negative stiffness comes from commercially available magnets (mounted so that they exert an attracting force between each other) and the positive stiffness is provided by off-the-shelf compression springs. Based on this model a lab-scale rig has been designed and tested. The data collected have been compared with an equivalent standard linear isolator. The comparison shows that the HSLDS isolator outperforms the standard linear system, [41];

4. studying the forced response of a Duffing oscillator. An approximate solution to the nonlinear equation of motion is found by applying the Harmonic Balance method and considering the response to be harmonic. This way it is possible to re-write the expressions of the jump-up and jump-down frequencies for a softening and a hardening system with linear viscous damping and their corresponding response amplitudes as simple explicit functions of the system parameters (damping ratio and coefficient of the nonlinear term);

5. studying the dynamics of a system with a symmetric cubic restoring force when it is excited by a harmonic oscillation of the base. Also for this case the jump phenomenon is characterised by simple explicit expressions and the results compared with the case of harmonic force excitation;

6. introducing simple analytical expressions for the maximum absolute transmissibility of an HSLDS isolator in case of both harmonic force and base excitation;

7. presenting a consistent and concise analysis of the free and forced vibration of the Zener model. This is a linear vibration isolation system in which a spring is connected in parallel to a series connection of a damper and a spring, [6].

1.4 Thesis outline

In Chapter 2, the static analysis of two HSLDS isolators is presented. Firstly, a comprehensive analysis of one model taken from the literature is carried out; in the second part a new model with HSLDS characteristic that comprises attracting magnets and coil springs is studied. Eventually the restoring force of both mechanisms is approximated to a symmetric cubic polynomial which enables the equation of the motion to be written in the form of a Duffing oscillator. It is argued that the system can be linearised for small oscillations from the static equilibrium position. However should this assumption not hold true there is the onset of nonlinear behaviour.

The aim of Chapter 3 is to give a brief overview of the fundamental concepts of dynamic analysis of nonlinear systems.

In Chapter 4 the problem of the response of the HSLDS isolator to harmonic force excitation is studied. First, the frequency response function of the system is defined by applying the Harmonic Balance method. The characteristic jump phenomenon is described analytically and the known simple approximate expressions for the jump amplitudes and frequencies are derived with a consistent method and presented in a simple explicit form. Subsequently, the isolation properties are evaluated in terms of absolute transmissibility and an expression for the maximum transmissibility of the nonlinear isolator is given. Finally, numerical simulations show the effectiveness of the HSLDS isolator compared to a standard linear mount.

The case of harmonic excitation of the base is studied in Chapter 5. The layout of the chapter follows very closely that of Chapter 4. The relative transmissibility is first studied and expressions for the jump frequencies proposed. The absolute transmissibility is then defined and an expression for its maximum value given. Also in this case numerical simulations demonstrate that the HSLDS offers improved isolation performance when compared to a linear system.

In Chapter 6 an experimental case study is presented. The rig designed and built reproduces the HSLDS mechanism with springs and magnets discussed in Chapter 2. The system is excited by a harmonic motion of the base and its absolute transmissibility is compared with that of a linear system subject to the same

excitation. Measurements also indicate that the HSLDS isolator is more effective than a linear system. In accordance with the analysis carried out in Chapter 2 it is shown that the system behaves linearly for oscillations of small amplitude.

The design and measurements of another experimental rig are contained in Appendix C. This concerns an apparatus which has the sole purpose of providing a visual demonstration of the effect of combining elements with positive and negative stiffness. Appendices A and B are two articles published in a scientific journal and included for completeness. In Appendix A a comprehensive study of the Zener model is presented; in Appendix B the static characterisation of a system with quasi-zero-stiffness is presented and an optimisation analysis is carried out in order to maximise the displacement from the static equilibrium position without exceeding a desired low stiffness.

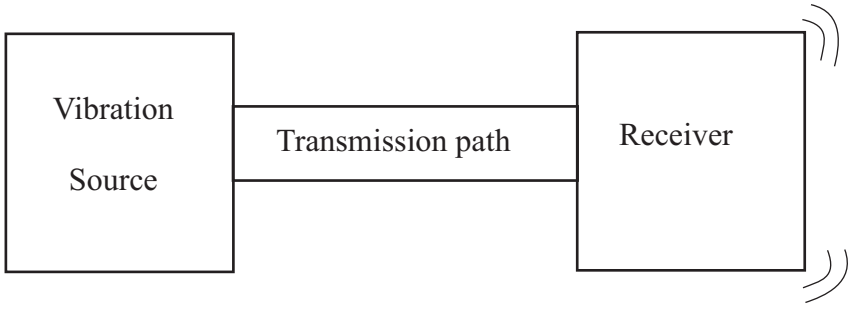

Figure 1.1: The problem of vibration isolation: the vibration source generates vibration which is then transmitted to the receiver via the transmission path. With a passive vibration isolation approach a reduction of the level of vibrations passed on to the receiver can be achieved by modifying the transmission path

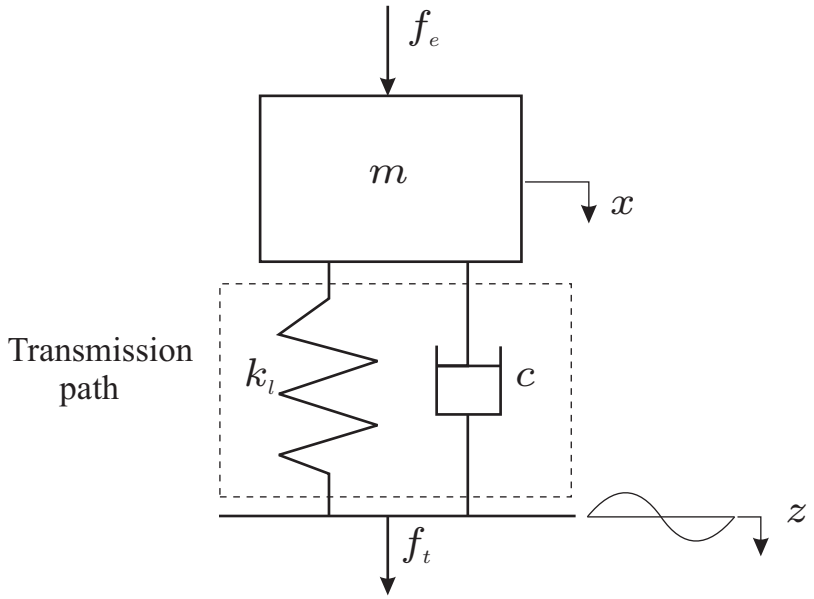

Figure 1.2: Single-degree-of-freedom (SDOF) vibration isolator model. The source can be a force, f_e, applied to the mass in which case the receiver is the base of the system which is subject to the force transmitted f_t, or a motion of the base z in which case the receiver is the mass m experiencing a motion x. In both cases the disturbance travels from the source to the receiver through the spring k_l and the dashpot c which therefore constitute the transmission path

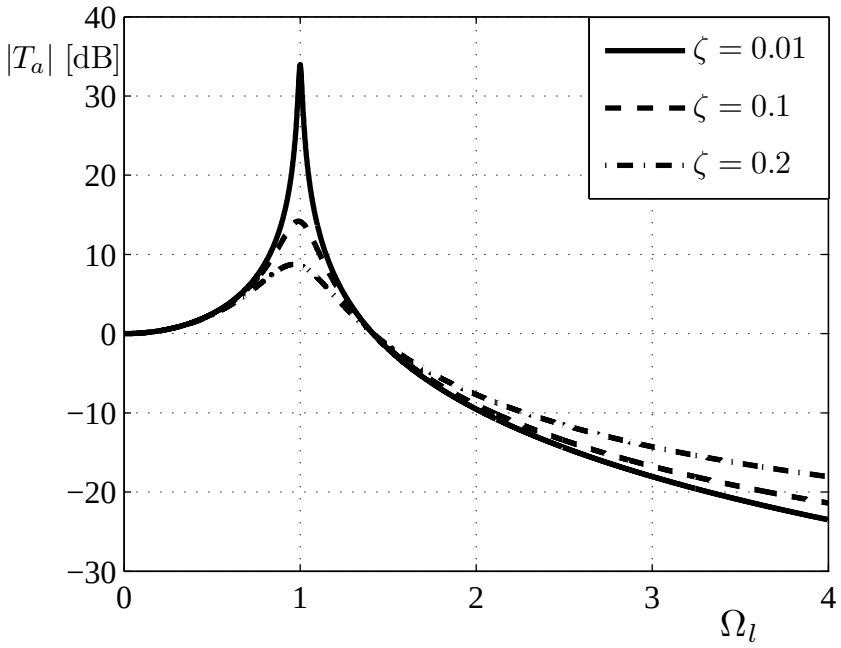

Figure 1.3: Absolute transmissibility of a SDOF system with viscous damping. Effect of changing the damping ratio. An increase of ζ_l causes the peak to decrease. However, at higher frequencies $\Omega_l > \sqrt{2}$, the higher the damping the higher the transmissibility with consequent deterioration of the isolation performance

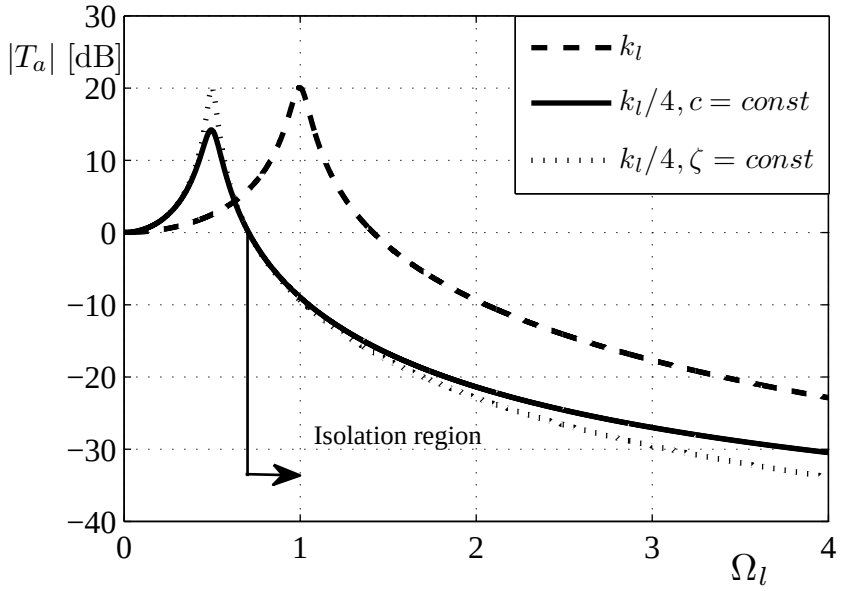

Figure 1.4: Absolute transmissibility of a SDOF system with viscous damping. Effect of changing the stiffness. The solid line is the transmissibility of a mount with a spring 4 times softer than the original system (dashed line) if the damping coefficient c is maintained constant. If c is varied to keep ζ_l constant the transmissibility is given by the dotted line

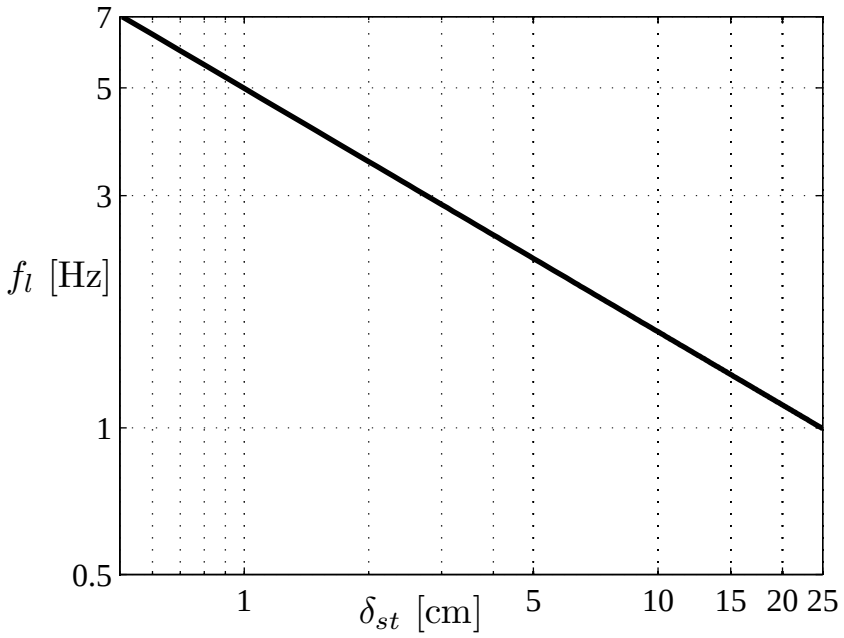

Figure 1.5: Natural frequency of a linear SDOF system as a function of the static displacement. With a soft spring the natural frequency decreases but the static displacement increases

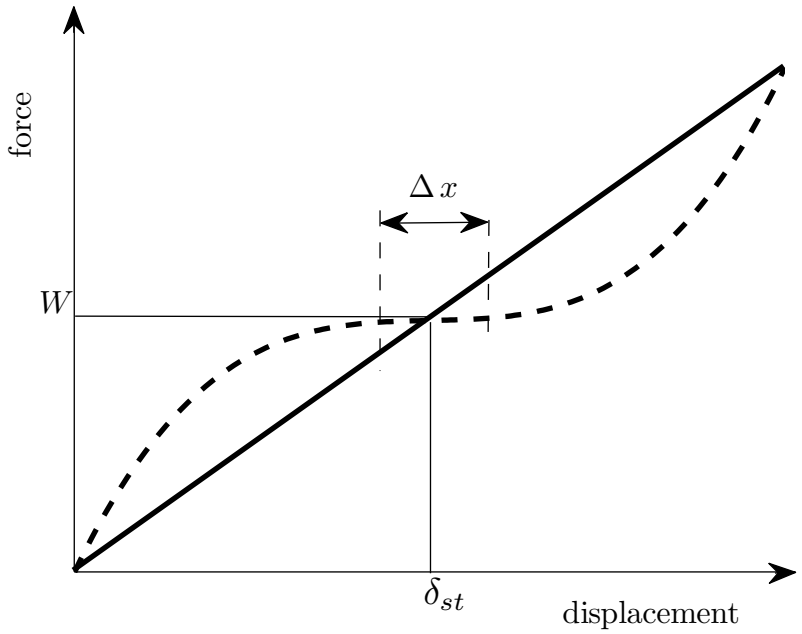

Figure 1.6: Comparison of the nondimensional force-displacement characteristic of a linear and a nonlinear spring. The static and dynamic stiffness of the linear spring are equal. At the static equilibrium point, the static stiffness stiffness of the nonlinear mount is the same of the linear one, but for oscillations about this position the slope of the nonlinear force-displacement curve (dynamic stiffness) is much smaller and this results in a lower natural frequency

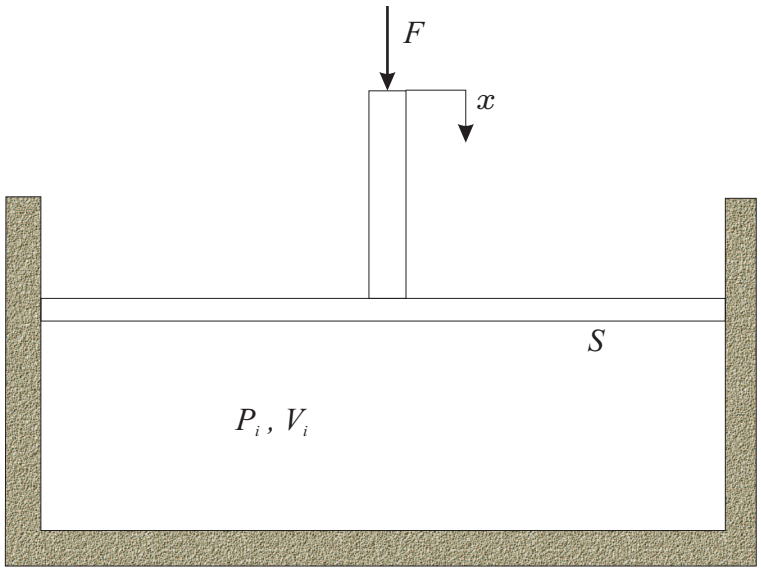

Figure 1.7: Schematic representation of an air spring

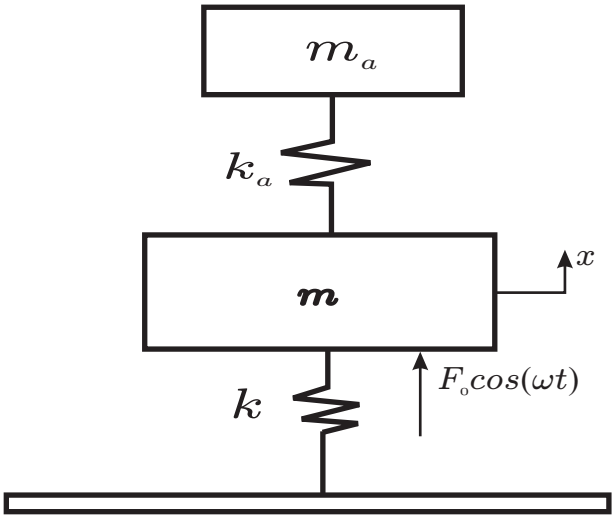

Figure 1.8: Main system, m, k with the an undamped DVA m_a, k_a fitted

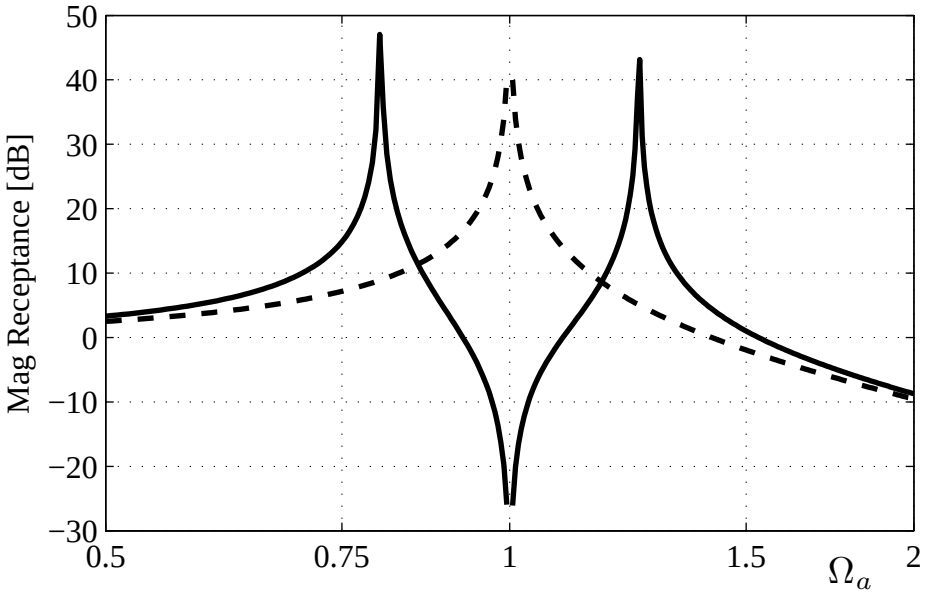

Figure 1.9: Magnitude of the response of the isolated mass to a harmonic force: dashed line without DVA; solid line with undamped DVA. $\mu = 0.2$

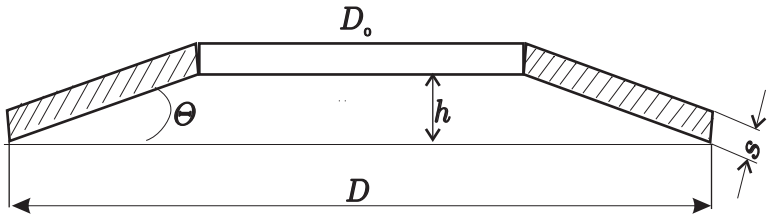

Figure 1.10: Schematic representation of a Belleville or disc spring

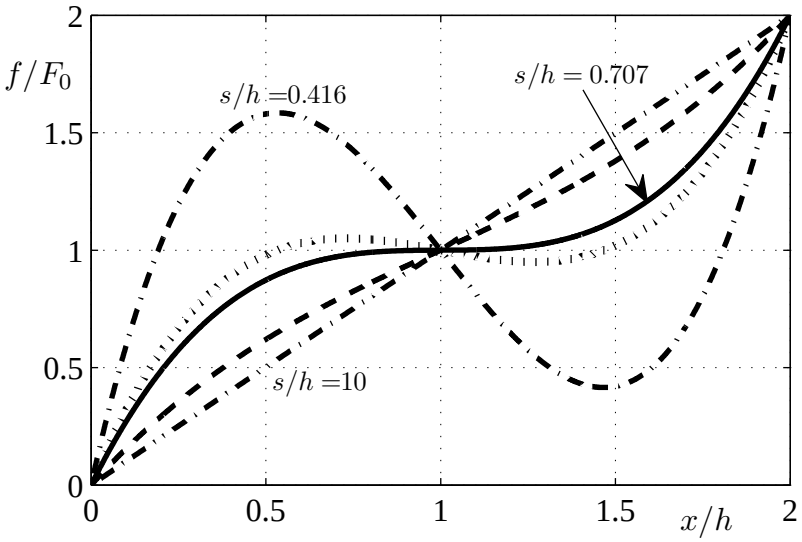

Figure 1.11: Load-Deflection plot for a Belleville Spring with different geometrical parameters

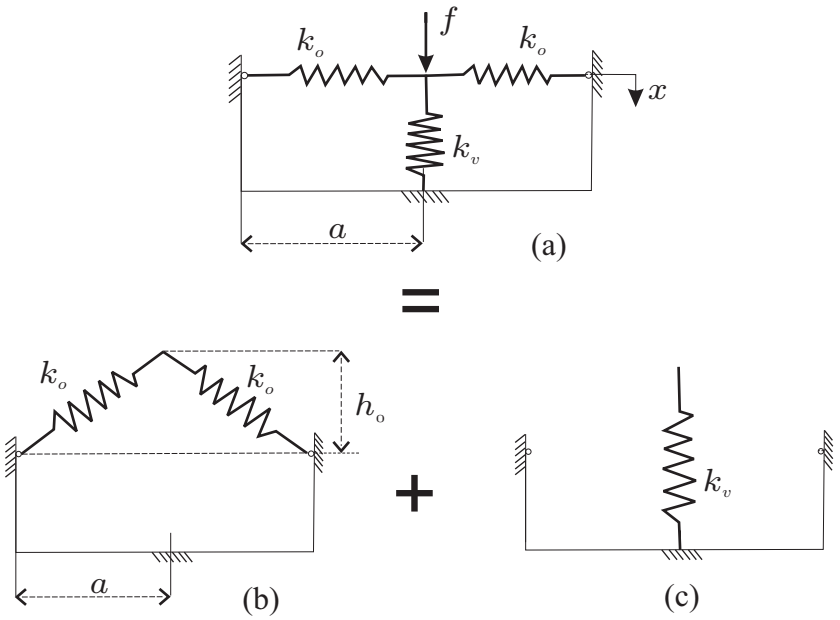

Figure 1.12: Schematic model of system with HSLDS characteristic. (a) HSLDS mechanism in its loaded condition. (b) Oblique springs which provide the necessary negative stiffness, in their initial position. (c) Vertical spring which provides the static support

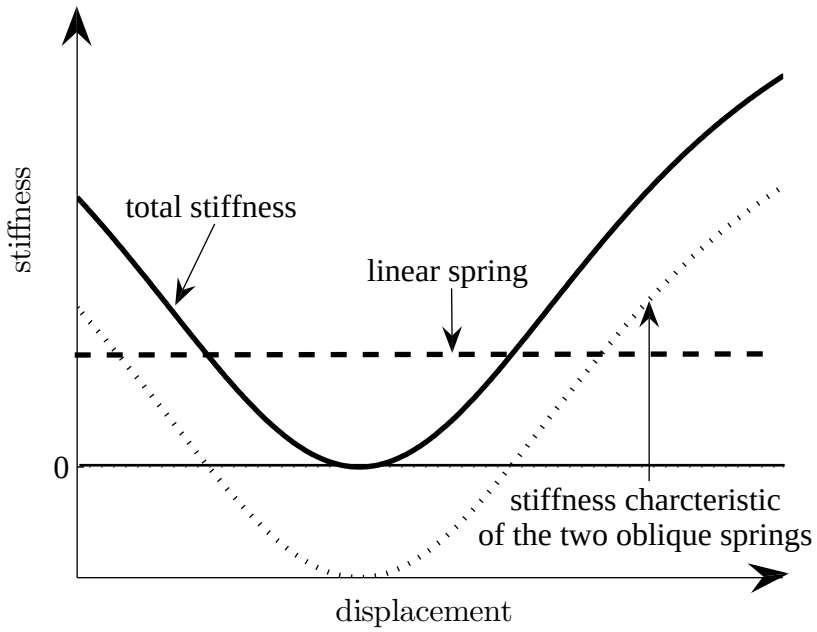

Figure 1.13: Stiffness-displacement characteristic of a HSLDS model. The dotted line is the stiffness, which becomes negative, of the system depicted in Fig. 1.12(b). The dashed line is the positive, constant stiffness of a spring such as that shown in Fig. 1.12(c). The sum of these two curves is the solid line which is the curve of the HSLDS mechanism of Fig. 1.12(a). This particular example illustrates the special case in which the stiffness becomes zero

Chapter 2

Static characteristics of two HSLDS systems

'The mathematics is not there till we put it there.'

Arthur Eddington (1882 - 1944)

2.1 Introduction

In the introductory chapter it has been argued that the frequency range over which a linear passive vibration isolator is effective, is often limited by the mount stiffness required to support a static load. It has been suggested that this can be improved upon by employing non-linear mounts which provide high-static and low-dynamic stiffness (HSLDS). One way to reduce the dynamic stiffness without paying the penalty of a low static stiffness is to connect in parallel elements with positive and negative stiffness. The direct benefit of a HSLDS mount is a wider frequency isolation region. Besides, if it is possible to linearise the stiffness by considering only small vibrations about the static equilibrium position, there may also be another advantage. The damping ratio is inversely proportional to the natural frequency but proportional to the damping coefficient. If the damping coefficient is not changed the damping ratio of the HSLDS isolator will be larger and thus the peak in transmissibility peak will be smaller. If this increase of damping ratio is too detrimental at high frequencies, then the damping coefficient can be adjusted accordingly.

In this chapter, the concept of negative stiffness is illustrated and two mechanisms with HSLDS are introduced and discussed. The first system comprises a vertical spring acting in parallel with two oblique springs. The two oblique springs provide the negative stiffness necessary to counteract the positive stiffness of the vertical spring and achieve the desired HSLDS characteristic. In the second mechanism with HSLDS stiffness the negative stiffness is provided by a set of magnets in attracting configuration separated by linear springs that provide the positive stiffness. The analysis carried out in this chapter aims to define the expressions for the force and stiffness as functions of the displacement and to describe the parameters that influence the systems' HSLDS property. Finally, for both models the equation of motion is defined.

2.2 Negative stiffness - restoring force of a system with two oblique springs

The system depicted in Fig. 2.1 has two linear springs with identical stiffness k_o and initial length L_0 mounted obliquely. A force f is applied as shown in the figure. The springs are hinged at M and N. P is the point of application of the force and is a horizontal distance a from M and N and initially at height h_0 from the horizontal line MN. It is assumed that $L_0 \geq a$. Initially, the springs are at an angle θ_0 from the horizontal. The application of the force f causes a vertical displacement x and the length of the springs becomes L. The force exerted by each of the springs is therefore

$$f_o = k_o(L - L_0) \tag{2.1}$$

However, only the vertical component resists the applied force f. Hence

$$f = 2k_o(L_0 - L)\sin\theta \tag{2.2}$$

where $\sin\theta = \frac{(h_0 - x)}{L}$. It should be noticed that when $\theta = 0$ the springs lie horizontally and do not exert any vertical force, i.e. $f = 0$.
Thus, the force-displacement relationship can be written as

$$f = 2k_o(h_0 - x)\left(\frac{L_0}{L} - 1\right) \tag{2.3}$$

From Fig. 2.1 it can also be seen that

$$L_0 = \sqrt{h_0^2 + a^2} \tag{2.4a}$$

and

$$L = \sqrt{(h_0 - x)^2 + a^2} \tag{2.4b}$$

Combining Eqn.(2.3) with Eqns.(2.4 a,b) gives

$$f = 2k_o(h_0 - x)\left(\frac{\sqrt{h_0^2 + a^2}}{\sqrt{(h_0 - x)^2 + a^2}} - 1\right) \tag{2.5}$$

This expression can be non-dimensionalised by normalising the displacement x by L_0 and the force f by $k_o L_0$. Thus, Eqn.(2.5) can be written as

$$\hat{f} = \frac{f}{k_o L_0} = 2(\sqrt{1-\gamma^2} - \hat{x})\left\{\left[\hat{x}^2 - 2\sqrt{1-\gamma^2}\hat{x} + 1\right]^{-1/2} - 1\right\} \tag{2.6}$$

where $\hat{x} = x/L_0$ is the *non-dimensional displacement* and

$$\gamma = \frac{a}{L_0} = \cos\theta_0 \tag{2.7}$$

is a fixed *geometrical parameter*. If $\gamma = 0$ the springs are initially vertical and if $\gamma = 1$ the springs, initially, lie horizontally.

Fig. 2.2 shows the non-dimensional force plotted against the non-dimensional displacement for different values of γ. It can be seen that the system has a non-linear characteristic and regions with negative stiffness. Following the application of the load f the springs deform. When the springs lie in the horizontal position ($x = h_0$, that is $\hat{x} = \sqrt{1-\gamma^2}$) the restoring force is zero and this is due to the fact that there is not a vertical component of the spring force able to resist the applied load f. At this point, any perturbation (e.g. a small displacement) would bring the system to a different position of equilibrium making the horizontal position a condition of unstable equilibrium. It can also be observed that each curve has a maximum and a minimum. The peak also represents a point of unstable equilibrium. Between the maximum and the minimum the gradient is negative, which means that the stiffness of the system becomes negative. If too large a force is applied the system snaps through the static equilibrium position until a new equilibrium position is reached. The maximum non-dimensional force that

the system can accept before it snaps through can be expressed as a function of the geometrical parameter γ and is given by

$$\hat{f}_{max} = 2\left[1 - \left(1 - \sqrt{1-\gamma^2}\right)^{1/3}\right]^{3/2} \tag{2.8}$$

which occurs at

$$\hat{x}_{max} = \sqrt{1-\gamma^2} - \gamma\sqrt{\gamma^{-2/3} - 1} \tag{2.9}$$

Finally, the stiffness of this system can be calculated by differentiating the force with respect to the displacement, and is given by

$$\hat{K} = \frac{d}{d\hat{x}}(\hat{f}(\hat{x})) = 2\left[1 - \frac{\gamma^2}{\left(\hat{x}^2 - 2\sqrt{1-\gamma^2}\hat{x} + 1\right)^{3/2}}\right] \tag{2.10}$$

The instability described above makes this system unsuitable for isolation purposes. However, the geometric non-linearity and negative stiffness of this system can be exploited in order to obtain a HSLDS system.

2.3 A hardening HSLDS system

Amongst the several model of systems with HSLDS characteristic presented in reference [24], one of particular interest is shown in Fig. 2.3. It represents a parallel combination of two oblique springs and a vertical spring. The dotted curve in Fig. 2.4 is a qualitative plot of the non-dimensional stiffness of two oblique springs as discussed in the previous section. The dashed line represents the non-dimensional stiffness of a linear spring element. If the two mechanisms are configured in parallel, the total stiffness is the sum of the stiffness of each mechanism. This is the solid line in the figure. At the static equilibrium position this could be made as small as desired (the curves plotted represent a special case in which the total stiffness becomes zero). Thus, unlike the system with only oblique springs, the one depicted in Fig. 2.3 always has a force that opposes the applied load f. When the correcting springs lie horizontal the supporting (vertical) spring resists the force f. By choosing the stiffness of the vertical mounting (positive) to be slightly larger than the maximum stiffness of the oblique springs (negative) the dynamic stiffness can be made very small at the equilibrium position maintaining

a relatively high static stiffness. This is the nature of a *high-static low-dynamic stiffness* (HSLDS) mechanism. Conceivably, the stiffness can be made zero by choosing the coefficient of the vertical spring to be equal to the maximum (negative) stiffness of the oblique springs. Systems with zero dynamic stiffness are referred to as *quasi-zero-stiffness* (QZS) mechanisms. A comprehensive study of the system shown in Fig. 2.3 with QZS characteristic is presented in [40].

In the HSLDS model depicted in Fig. 2.3 the three springs act as if connected in parallel, thus the restoring force of the system is the sum of the force exerted by the vertical spring and the vertical component of the restoring force exerted by the two oblique springs. If k_v denotes the stiffness of the vertical element, the restoring force is given by [a]:

$$f = L_0 \left\{ k_v \hat{x} + 2k_o(\sqrt{1-\gamma^2} - \hat{x}) \left[\left(\hat{x}^2 - 2\sqrt{1-\gamma^2}\hat{x} + 1 \right)^{-1/2} - 1 \right] \right\} \tag{2.11}$$

where again $\gamma = a/L_0$. By introducing the ratio of spring coefficients

$$\mu = \frac{k_o}{k_v} \tag{2.12}$$

Eqn.(2.11) can be re-written in non-dimensional form as

$$\hat{f} = \frac{f}{k_v L_0} = \hat{x} + 2\mu(\sqrt{1-\gamma^2} - \hat{x}) \left\{ \left[\hat{x}^2 - 2\sqrt{1-\gamma^2}\hat{x} + 1 \right]^{-1/2} - 1 \right\} \tag{2.13}$$

Note that now it has been chosen to use the coefficient of the linear spring k_v and the initial length of the oblique spring L_0 to normalise the restoring force. The non-dimensional force as a function of the non-dimensional displacement is plotted in Fig. 2.5 for several values of γ when $\mu = 1$.

The stiffness of the system, which is shown in Fig. 2.6, can be found by differentiating Eqn.(2.13) with respect to the displacement to give

$$\hat{k} = \frac{d}{d\hat{x}}(f(\hat{x})) = 1 + 2\mu \left[1 - \frac{\gamma^2}{\left(\hat{x}^2 - 2\sqrt{1-\gamma^2}\hat{x} + 1 \right)^{3/2}} \right] \tag{2.14}$$

At the static equilibrium position it can be positive, zero or negative depending

[a] A positive restoring force is defined here to be upwards

on the values of the system's parameters μ and γ. The combination of these two parameters that gives zero stiffness at the equilibrium position is found by setting the stiffness to zero when $\hat{x} = \hat{x}_e = \sqrt{1-\gamma^2}$. It results

$$\gamma_{opt} = \frac{2\mu}{2\mu + 1} \tag{2.15a}$$

or equivalently

$$\mu_{opt} = \frac{\gamma}{2\,(1-\gamma)} \tag{2.15b}$$

where the subscript $_{opt}$ is used to denote the values of the parameters that give zero stiffness at the static equilibrium position. Fig. 2.6 shows that if $\gamma < \gamma_{opt}$ the stiffness at the static equilibrium position becomes negative. Note that this condition is equivalent to $\mu > \mu_{opt}$. Obviously, a negative value of the stiffness has to be avoided because of the instability it implies. Although zero stiffness seems ideal for isolation purposes (zero natural frequency means that the isolation region begins at a frequency of zero Hz!), it is a hazardous condition that is not very convenient and is practically almost impossible to achieve [42]. For example, a small difference between nominal and real spring coefficients due to manufacturing tolerances could make the stiffness at the equilibrium position negative. A better choice of parameters for isolation purposes is to choose μ or γ so as to have a small positive stiffness at the equilibrium position. As mentioned previously, this is achieved by choosing $\mu < \mu_{opt}$ or $\gamma > \gamma_{opt}$. It remains to establish the relationship between the stiffness at the equilibrium position and the deviation of μ and γ from their optimum values.

Let ϵ be a fractional decrease in μ from its optimal value, that is $\mu = \mu_{opt}(1-\epsilon)$. Substituting this expression for μ into Eqn.(2.14) it gives

$$\hat{k} = 1 + 2\mu_{opt}(1-\epsilon)\left[1 - \frac{\gamma^2}{\left(\hat{x}^2 - 2\sqrt{1-\gamma^2}\hat{x} + 1\right)^{3/2}}\right] \tag{2.16}$$

which can be rearranged to give

$$\hat{k} = \hat{k}_{opt} - 2\epsilon\mu_{opt}\left[1 - \frac{\gamma^2}{\left(\hat{x}^2 - 2\sqrt{1-\gamma^2}\hat{x} + 1\right)^{3/2}}\right] \tag{2.17}$$

where $\hat{k}_{opt}$ is the stiffness of the QZS system. At the equilibrium position, $\hat{x} = \hat{x}_e = \sqrt{1-\gamma^2}$, so by definition $\hat{k}_{opt} = 0$ and thus from Eqn. (2.17) the stiffness is

$$\hat{k}\Big|_{\hat{x}=\hat{x}_e} = \epsilon \tag{2.18}$$

It can be concluded that the (nondimensional) stiffness at the equilibrium position is equal to fractional decrease of μ from its optimum value μ_{opt}. If instead, for a given value of μ, γ is made larger than its optimum value γ_{opt} as in $\gamma = \gamma_{opt}(1+\epsilon)$ then the stiffness at the equilibrium position is

$$\hat{k}\Big|_{\hat{x}=\hat{x}_e} = \frac{\epsilon\,(1+2\,\mu)}{1+\epsilon} \tag{2.19}$$

This way the stiffness and the static equilibrium position can be controlled by choosing an appropriate fractional change of one of the system's parameters.

2.3.1 Approximation to the stiffness of the HSLDS isolator

In the previous sections the force-displacement and stiffness characteristics of a HSLDS stiffness mechanism have been studied. The relationship between force and displacement is expressed by Eqn.(2.13) and is shown graphically in Fig. 2.5. It can be seen that the curves have a shape similar to that of a cubic function.

In this section a simplified cubic expression of the force is therefore sought and the error in the approximation is investigated. One way of approximating a function by a polynomial is to use the Taylor series expansion. In this specific case, the centre of expansion can be the static equilibrium position. In so doing, it is possible to linearise the motion about the static equilibrium position, that is if the oscillations from this position are small enough it is possible to consider the terms of order higher than one small compared to the linear term. Most generally, a smooth function can be expressed by a power series of order N. The expansion is given in [43] as

$$f(x) = f(x_0) + \sum_{n=1}^{N} \frac{f^n(x_0)}{n!}(x-x_0)^n \tag{2.20}$$

where x_0 is the point at which the function is expanded and f^n denotes the

n-th derivative of f. Since the system is designed to oscillate about the static equilibrium position it is of interest to expand the force characteristic around this point, i.e. $x_0 = \hat{x}_e$. By expanding Eqn.(2.13) using Eqn.(2.20), an approximate expression for the force can be found. The approximate nondimensional force is found to be

$$\hat{f}_{app}(\hat{x}) = \frac{\mu}{\gamma^3}\left(\hat{x} - \sqrt{1-\gamma^2}\right)^3 + \left[1 - 2\mu\frac{(1-\gamma)}{\gamma}\right]\left(\hat{x} - \sqrt{1-\gamma^2}\right) + \sqrt{1-\gamma^2} \tag{2.21}$$

where the subscript $_{app}$ denotes that this is an approximate expression.

Introducing the variable $\hat{y} = \hat{x} - \sqrt{1-\gamma^2}$ the deflection from the static equilibrium position is $\hat{y} = 0$. Beside, letting $\hat{F}_{app} = \hat{f}_{app} - \sqrt{1-\gamma^2}$ the restoring force can be rewritten as

$$\hat{F}_{app}(\hat{y}) = \beta^2\,\hat{y} + \alpha\,\hat{y}^3 \tag{2.22}$$

where the coefficients of the linear and the cubic term, β^2 and α respectively, are given by

$$\beta^2 = 1 - 2\mu\frac{(1-\gamma)}{\gamma} = \epsilon \qquad\qquad \alpha = \frac{1}{2\gamma^2(1-\gamma)} \tag{2.23}$$

It can be seen that $0 < \beta < 1$. Besides, if γ or μ are chosen according to one of Eqns.(2.15 a) or (2.15 b), $\beta = 0$ and the force-displacement relationship is given by the purely cubic function

$$\hat{F}_{app}(\hat{y}) = \alpha\,\hat{y}^3 \tag{2.24}$$

Eqn.(2.24) is plotted in Fig.2.7 for $\gamma = 2/3$. Also shown in the same figure are the curves of the fifth and seventh order polynomial expansions compared with the exact function. Expressing the restoring force as a cubic polynomial enables the equation of motion to be written in the form of a Duffing equation which has already been extensively studied, for example [44, 45].

An approximate expression for the stiffness can be obtained by differentiating Eqn.(2.22):

$$\hat{k}_{app} = 3\,\alpha\,\hat{y}^2 + \beta^2 \tag{2.25}$$

In the case when the parameters μ and γ are optimally related, $\beta = 0$ and the previous expression of the stiffness simplifies to

$$\hat{k}_{app} = \frac{3}{2}\frac{1}{\gamma^2(1-\gamma)}\hat{y}^2 \tag{2.26}$$

which, of course, becomes zero at $\hat{y} = 0$.

An estimate of the error is needed to determine the extent to which the approximate quadratic stiffness (equivalently a cubic force) can be used without introducing too large an error in the static analysis of this system. There are different ways to estimate the error when approximating a function with a finite power series, as opposed to an infinite power series. Some analytical expressions for the remainder have been provided by Lagrange and Cauchy [43]. However, here a numerical estimation of the error is calculated as

$$err(\%) = \left| 1 - \frac{\hat{k}_{app}}{\hat{k}_{ex}} \right| * 100 \tag{2.27}$$

where $\hat{k}_{app}$ is the approximate value of the function and $\hat{k}_{ex}$ is the exact one. The difference between the exact and approximate solution is expected to increase when large displacements from the equilibrium position occur. This is a direct consequence of having expanded the function about the static equilibrium point. Fig. 2.8 shows the error that is introduced when the approximate quadratic expression is used instead of the exact function when the constant term is zero. It can be seen that the error remains small (< 10 %) for relatively small displacements from the equilibrium position ($\pm$ 20% excursion range). Clearly, higher amplitudes of oscillation would invalidate the approximation of quadratic stiffness.

2.3.2 Equation of motion

Having approximated the restoring force and the stiffness to a cubic and quadratic function of the displacement respectively and having investigated the validity of this approximation in the vicinity of the static equilibrium position, it is possible to write the equation of motion of a mass m suspended on the HSLDS spring described in the previous section. If the weight is such that the mass reaches its static equilibrium position when the oblique springs are horizontal, i.e. $\hat{y} = 0$, using Eqn.(2.22) the equation of motion of the mass-HSLDS spring system is

$$m\,\ddot{y} + k_v\,(\beta^2 + \alpha\,\hat{y}^2)\,y = 0 \tag{2.28}$$

whence by assuming the displacement small enough so that

$$\hat{y} \ll \frac{\beta}{\sqrt{\alpha}} \tag{2.29}$$

the dynamics of the system can be assumed to be approximatively linear and is thus described by

$$m\,\ddot{y} + k_v\,\beta^2\,y = 0 \tag{2.30}$$

The natural frequency of the HSLDS system is thus

$$\omega_n = \beta\sqrt{\frac{k_v}{m}} \tag{2.31}$$

Note that since $\beta < 1$ this is smaller than that of a system with only the vertical spring (linear equivalent model) $\omega_l = \sqrt{k_v/m}$.

2.4 A softening system with HSLDS stiffness

As previously stated, there are different ways of engineering a system with high-static-low-dynamic-stiffness. Given its manufacturing simplicity, a particularly interesting method to achieve the required nonlinear stiffness is to employ magnets.

Magnets have been used in vibration isolation systems in the past, but have often been configured so that they act in repulsion and hence act as springs with positive stiffness. The advantage of such a system is that, for small oscillations, the natural frequency is independent of the isolated mass. Examples of such systems are given in references [35, 36, 46]. Examples of active vibration isolation devices with magnets can be found instead in [47, 48].

The novelty of the isolation mount presented in this section resides in the fact that the desired high-static-low-dynamic-stiffness is obtained by connecting in parallel linear mechanical springs (positive stiffness) with attracting magnets (negative stiffness). The system is shown in Fig.2.9 in its loaded condition, i.e. $x = 0$ is the equilibrium position. Two coil springs are inserted between three magnets, with the upper and lower elements fixed and the middle piece free to move only in the vertical (x) direction on a smooth bar. The linear springs take the static load whereas the magnets in an attracting configuration generate a

negative stiffness which is inversely proportional to the cube of the distance between the magnets, d. By adjusting d it is possible to achieve any desired value of stiffness at the equilibrium position (which, incidentally, is the position at which the stiffness is maximum). Finally, a polynomial cubic expression of the force is obtained via a Taylor expansion. In this way the equation of motion of the system is written in the form of a softening Duffing oscillator. The dynamic behaviour of a system described by this equation can be found in the literature (e.g. [44, 45]) details of which can be found in Chapter 3.

2.5 The magnetic spring

Before going into the details of the softening HSLDS system, it is necessary to define the interaction force between two magnets placed a short distance apart.

The laws that define the magnetic field between two permanent magnets which cannot be modelled as poles are generally of a rather complex nature. For example one theory often used is due to Bancel [49] who has proposed a method to calculate the magnetic force between cuboidal magnets superimposing the effect of equivalent magnetic monopoles placed at the corners of the cube. A simpler model for the magnetic force acting between two magnets, such as those shown in Fig. 2.9 when the coil springs are removed, is provided by Coulomb's law, [50], which states that the attractive or repelling force is inversely proportional to the square of the distance according to

$$F_m = \frac{C_m}{d^2} \tag{2.32}$$

where the constant $C_m = C\, p_1\, p_2$ with C being the magnetic permeability of the medium (which has units of Nm^2) and the scalars p_1 and p_2 are the pole strengths of the magnets; d is the distance between the magnets.

What is of interest here, is to determine the force needed to displace the middle magnets by a distance x or, in other words, the stiffness of the system. Initially, because the middle element is acted on either side by the same force it will remain in vertical equilibrium. However, the equilibrium condition is very different according to whether the magnets are in a repelling or attracting configuration.

The equilibrium position is stable in the former case, and is unstable in the second case.

2.5.1 Repelling magnets

Consider the system shown in Fig.2.9 but without the mechanical springs and where the middle piece is reversed so that equal polarities face each other. The central magnet is repelled by the upper element by a force

$$F_{up} = \frac{C_m}{(d-x)^2} \tag{2.33}$$

whilst the lower repels it with a force

$$F_{low} = \frac{C_m}{(d+x)^2} \tag{2.34}$$

where the subscripts $_{up}$ and $_{low}$ denotes the interaction of the middle magnet with the upper and lower magnet respectively.

Initially, at $x = 0$, the forces are equal and opposite and the middle element is in equilibrium. When displaced by a distance x, the net force acting on the central magnet is

$$F_{rep}(x) = F_{low} - F_{up} = C_m \frac{4\,d\,x}{(d^2-x^2)^2} \tag{2.35}$$

or in nondimensional form

$$\hat{F}_{rep} = \frac{F_{rep}}{C_m/d^2} = \frac{4\,\hat{x}}{(1-\hat{x}^2)^2} \tag{2.36}$$

where $_{rep}$ describes a system of magnets in repelling configuration and $\hat{x} = x/d$. The stiffness is given by

$$K_{rep}(x) = \frac{dF_{rep}}{dx} = 4\,C_m \frac{d\,(d^2+3\,x^2)}{(d^2-x^2)^3} \tag{2.37}$$

or in nondimensional terms

$$\hat{K}_{rep} = \frac{K_{rep}}{C_m/d^3} = \frac{4\,(1+3\,\hat{x}^2)}{(1-\hat{x}^2)^2} \tag{2.38}$$

In Fig. 2.10 both nondimensional force and stiffness curves are shown as func-

tions of the nondimensional displacement. Note that at the static equilibrium position, $\hat{x} = 0$, the force acting on the moving element is zero, whilst the stiffness is positive.

The potential energy of the system is defined as

$$V = -\int f(x)dx \tag{2.39}$$

where $f(x)$ is the spring force. Substituting Eqn.(2.36) into Eqn.(2.39) the nondimensional potential energy of this particular system is

$$\hat{V} = \frac{2}{1-\hat{x}^2} \tag{2.40}$$

and is always positive since $\hat{x} < 1$. According to the *principle of minimum potential energy* an equilibrium condition is stable if it corresponds to a minimum of the potential energy, [51]. Because $\hat{x} = 0$ is a point of minimum of the function $\hat{V}(\hat{x})$, Eqn.(2.39), it is a stable equilibrium position. In fact, should the magnet be displaced from $\hat{x} = 0$ it tends to return to its initial position.

2.5.2 Attracting magnets

If the three magnets are oriented as in Fig. 2.9, but without the coil springs, the net force acting on the middle element when it is displaced by x is

$$F_{att}(x) = -C_m \frac{4\,d\,x}{\left(d^2 - x^2\right)^2} \tag{2.41}$$

where the subscript $_{att}$ is used to denote that the magnets are in an attracting configuration.

Differentiating Eqn.(2.41) with respect to x yields the stiffness

$$K_{att}(x) = -4\,C_m \frac{d\left(d^2 + 3\,x^2\right)}{\left(d^2 - x^2\right)^3} \tag{2.42}$$

which can both written in non-dimensional form as

$$\hat{F}_{att} = -\frac{4\,\hat{x}}{(1-\hat{x}^2)^2} \tag{2.43}$$

and

$$\hat{K}_{att} = -\frac{4\,(1+3\,\hat{x}^2)}{(1-\hat{x}^2)^2} \tag{2.44}$$

The force and stiffness curves for this configuration are shown in Fig. 2.11 where it can be seen that the stiffness is always negative.

Unlike the configuration with repelling magnets, in this case the potential energy, Eqn.(2.39), has a maximum at the static equilibrium position $x = 0$. This means that the initial position is unstable. Any displacement from the initial position $x = 0$ would push the middle magnet further away from it.

2.6 HSLDS with springs and magnets

Consider the system in Fig. 2.9 with all the components. As mentioned, the device is shown in the loaded condition. The static load of the central element is taken up by the two coil springs which act as if in parallel. Without the upper and lower magnets this system would be a linear SODF system (linear equivalent model) with a mass m suspended on a spring of stiffness $2\,k_s$ with a natural frequency $\omega_l = \sqrt{2\,k_s/m}$. However, the effect of the upper and lower magnets, both attracting the central piece, is to produce a negative stiffness which can be made to neutralise the positive stiffness of the springs. If this is achieved, the static stiffness depends only on the vertical springs, whilst the dynamic stiffness comes from the combined effect of springs and magnets and can be made as small as desired.

This section is concerned with the study of the static characteristics of such a system. The force-displacement relationship as well as the stiffness-displacement curve are studied. The system parameters are defined and expressions that relate these parameters in such a way to achieve the desired low stiffness are provided. Optimisation criteria are also suggested and finally an approximate cubic expression of the force is proposed.

The force needed to displace by a distance x the central piece of the system in Fig. 2.9 is found to be

$$f = 2\,k_s\,x - 4\,C_m \frac{d\,x}{\left(d^2 - x^2\right)^2} \tag{2.45}$$

which can be written in nondimensional form as

$$\hat{f}(\hat{x}) = \frac{f}{2\,k_s\,d} = \hat{x} - \nu\frac{\hat{x}}{(1-\hat{x}^2)^2} \tag{2.46}$$

where

$$\nu = 2\,C_m/(k_s\,d^3) \tag{2.47}$$

and $-1 < \hat{x} = x/d < 1$. The condition $\hat{x} = \pm 1$ is not included as it would imply that the spring has a zero solid length.

The parameter ν can be seen as the relationship between the stiffness term due to the magnets, $4\,C_m/d^3$, and that due to the mechanical springs, $2\,k_s$. It can be varied by changing the springs, the magnets or the distance between the magnets. In practice, for a given set of magnets and springs, i.e. for given values of C_m and k_s, ν can be changed by varying the initial distance between the magnets, d.

The force-displacement characteristic is shown in Fig. 2.12(a) for several values of ν.
From Eqn.(2.45) the dimensional stiffness of the system is

$$k = 2\,k_s - 4\,C_m\frac{d\,(d^2+3\,x^2)}{(d^2-x^2)^2} \tag{2.48}$$

Similarly, from Eqn.(2.46) the non-dimensional stiffness is given by

$$\hat{k}(\hat{x}) = \frac{k}{2\,k_s} = 1 - \nu\frac{(1+3\,\hat{x}^2)}{(1-\hat{x}^2)^3} \tag{2.49}$$

Fig. 2.12(b) shows several stiffness curves with different values of ν. Two noticeable features are observable. Firstly, the stiffness has a maximum at $\hat{x} = 0$. This can be found analytically by differentiating $\hat{k}$ with respect to $\hat{x}$, setting it equal to zero and solving for $\hat{x}$. Secondly, the stiffness is positive only within a limited range of displacement. The value of the maximum displacement from the equilibrium position before the stiffness becomes zero can be found by setting Eqn.(2.49) to zero and solving for $\hat{x}$, which yields

$$\hat{x}_{max} = \sqrt{1 + \left[\nu\left(\sqrt{4+\nu} - 2\right)\right]^{1/3} - \frac{\nu}{\left[\nu\left(\sqrt{4+\nu} - 2\right)\right]^{1/3}}} \tag{2.50}$$

The solid line in Fig. 2.13 is a plot of the maximum displacement from the static equilibrium for which the stiffness is positive. As ν increases the the width of the stability region decreases.

As explained in Chapter 1, the advantage of a HSLDS isolation mount is to have a very low (dynamic) stiffness (i.e. a very low natural frequency without the drawback of a large static displacement. Suppose that $\hat{k}_0$ is the maximum desired stiffness. Because of the non-dimensionalisation, better isolation performance corresponds to $\hat{k}_0 \ll 1$, that is $k \ll 2\,k_s$. A direct relationship between a desired stiffness and the system characteristic, ν, can be found by considering that the maximum stiffness is measured at the static equilibrium position, $\hat{x} = 0$. Thus, from Eqn.(2.49)

$$\hat{k}_0 = 1 - \nu \tag{2.51}$$

which is equivalent to

$$\nu = 1 - \hat{k}_0 \tag{2.52}$$

Eqn.(2.52) is plotted in Fig. 2.14 and expresses a unique relationship that allows the control of the stiffness of the system, by appropriate choice of ν, fixing its maximum to $\hat{k}_0$. Note that $\nu \leq 1$ for the maximum stiffness not to be negative. In particular, $\nu = 1$ is a condition to be avoided because in this case the maximum stiffness would be zero. Considering that the stiffness curve is concave, any displacement from the static equilibrium would make the stiffness negative and the system unstable. Figures 2.13 and 2.14 clearly shows the compromise between maximum excursion allowed before the stiffness becomes negative with consequent onset of instability and low dynamic stiffness.

2.6.1 Approximate force and stiffness expressions

The analytical force-displacement characteristic of the HSLDS system is expressed by Eqn.(2.46) and is shown graphically in Fig. 2.12(a). It can be seen that the curves have a shape similar to that of a cubic function. In this section a simplified cubic expression for the force is therefore sought and the error in the approximation is investigated. Using the Taylor series expansion given by Eqn.(2.20) about the static equilibrium position $\hat{x} = 0$, the approximate non-

dimensional restoring force is found to be

$$\hat{f}(\hat{x}) \approx (1-\nu)\,\hat{x} \; - 2\nu\,\hat{x}^3 = \beta^2\,\hat{x} - \alpha\,\hat{x}^3 \tag{2.53}$$

whence the non-dimensional stiffness can be found by differentiating with respect to the displacement to give

$$\hat{k}(\hat{x}) \approx (1-\nu) - 6\nu\,\hat{x}^2 \tag{2.54}$$

The error can again be calculated numerically according to Eqn.(2.27). Fig. 2.15 shows the error introduced by the quadratic expression of the stiffness for two values of ν. It can be seen that a larger error results for the larger value of ν which corresponds to a lower value of maximum stiffness.

As already pointed out, the displacement range within which the stiffness is positive is limited, and its width depends only on the parameter ν. The smaller the maximum stiffness (large value of ν) the narrower is this range. The exact expression has been found in Eqn.(2.50). From Eqn.(2.54) a simpler formula can be derived. In fact, setting the stiffness to zero and solving for $\hat{x}$ the maximum excursion from the static equilibrium position with positive stiffness is found to be

$$\hat{x}_{max} = \sqrt{\frac{1-\nu}{6\,\nu}} \tag{2.55}$$

The approximate maximum displacement, Eqn.(2.55), is plotted in Fig. 2.13 together with the exact curve. It can be seen that the approximate value overestimates the exact one. The error (%) between the exact and approximate expressions is shown in Fig. 2.16. This shows that the error is less than 10% if $\nu > 0.65$. For smaller values of ν, the error introduced by the quadratic approximation of the stiffness would no longer be negligible.

2.6.2 Equation of motion

If the weight of the mass/magnet suspended on the elasto-magnetic HSLDS system, as depicted in Fig. 2.9, is such that its static equilibrium position is at $x = 0$, the equation of motion can be determined using Eqn.(2.53) to give

$$m\,\ddot{x} + 2\,k_s\,\left[(1-\nu)\; - 2\nu\,\hat{x}^2\right]\; x = 0 \tag{2.56}$$

or

$$m\,\ddot{x} + 2\,k_s\,\left(\beta^2 - \alpha\,\hat{x}^2\right)\,x = 0 \tag{2.57}$$

where m is the mass of the central magnet and $\beta = \sqrt{1-\nu}$ and $\alpha = 2\nu$ are the coefficients of the linear and cubic term of the restoring force respectively. Eqn.(2.57) is in the form of Duffing's equation whose solution can be found from many sources in the literature, e.g. [44, 45]. It should be noticed that the negative sign in front of the cubic term denotes the softening characteristic of the stiffness. Nevertheless, for small oscillations, that is if

$$\hat{x} \ll \frac{\beta}{\sqrt{\alpha}} \tag{2.58}$$

the equation of motion can be linearised as

$$m\,\ddot{x} + 2\,\beta^2\,k_s\,x = 0 \tag{2.59}$$

It should be noted that, just as for the hardening mechanism discussed in Section 2.3.2, the natural frequency of the linearised HSLDS system becomes β times smaller than that of the equivalent linear model (obtained by removing the upper and lower magnets), Eqn.(2.31).

2.7 Effect of the weight of the isolated object

In the previous sections it was implicitly assumed that the weight of the suspended object was tuned in such a way that at the static equilibrium position the mechanism with negative stiffness exerts no force. Namely, for the three-springs system the oblique springs were horizontal and for the elasto-magnetic model the central mass/magnet was at an equal distance from the magnets at the extremities of the shaft. In this section some further considerations are made on the effect of the weight on the equation of motion of the hardening HSLDS system.

The equation of motion of a mass suspended on the mechanism with three springs, as depicted in Fig.2.17(b,c), can be derived by imposing the equilibrium of all the forces acting on the system, which for the unforced and undamped case is

$$m\,\ddot{x} + f(x) = m\,g \tag{2.60}$$

where $m\,\ddot{x}$ is the inertial force and $f(x)$ is the spring restoring force, Eqn.(2.11). At the static equilibrium position $\ddot{x} = 0$

$$f(x) = m\,g \tag{2.61}$$

If it is desired that the static equilibrium position coincides with the oblique springs being horizontal, i.e. $\hat{x_e} = \sqrt{1-\gamma^2}$ or equivalently $x_e = h_0$, Fig.2.17(b), it can be seen from Eqn.(2.11) that it has to be that

$$k_v\,h_0 = m\,g \tag{2.62}$$

from which it can be deduced that

$$k_v = \frac{m\,g}{h_0} \Leftrightarrow m = \frac{k_v\,h_0}{g} \tag{2.63}$$

The implication of this condition is that the static displacement depends only on the vertical spring. If the expression of the force is Taylor expanded about this static equilibrium position, a symmetric cubic polynomial can be used to approximate the restoring force, Eqn.(2.22).

In this section it is considered the case of a system in which at the static equilibrium position the negative stiffness elements exert some force, i.e the oblique springs are not horizontal. The mistune can be caused by the mass or the stiffness of the vertical spring to be such that Eqn.(2.62) does not hold. In the example shown in Fig.2.17(c), the static equilibrium position of the untuned mass m_u is $x = x_e = h_e$, where $h_e < h_0$. By expanding the spring force, Eqn.(2.11), in a third-order Taylor's series about the static equilibrium position h_e, the approximate force-displacement relationship assumes the form

$$f_0(y_e) \approx k_0 + k_1\,y_e + k_2\,y_e^2 + k_3\,y_e^3 \tag{2.64}$$

where $y_e = x - h_e$ and the coefficients k_i, $i = 0..3$, depend on μ, γ and the static equilibrium position (these are not included as they have a very complex form and are not relevant to the rest of the thesis). Thus the undamped, free equation of motion for oscillations about the static equilibrium position $y_e = 0$ is

$$m_u\,\ddot{y_e} + k_1\,y_e + k_2\,y_e^2 + k_3\,y_e^3 = 0 \tag{2.65}$$

By differentiating the spring force (2.64) with respect to y_e the approximate stiffness of the system is

$$k_0(y_e) \approx k_1 + k_2\, y_e + k_3\, y_e^2 \tag{2.66}$$

Hence, for the static equilibrium position ($y_e = 0$) to be stable it has to be $k_1 > 0$.

In this thesis only the case of a tuned mass-spring system is considered, that is it assumed throughout that the weight of the mass suspended on the HSLDS spring is such that at the static equilibrium the negative stiffness elements exert no restoring force. This enables to write the equation of motion in the form of the Duffing equation, Eqns.(2.28) and (2.57).

2.8 Conclusions

In this chapter it has been shown that by connecting elements with positive and negative stiffness in parallel it is possible to design a vibration isolation mount which has a high static stiffness, i.e. small static deflection, and a low natural frequency, i.e. a wider isolation region. Systems with this properties have been termed HSLDS mechanisms and offer potential improvements in the isolation performance of a mount.

The first mechanism studied comprises three linear springs which are appropriately configured. The negative stiffness is provided by two oblique springs which are at a certain angle to the horizontal. The vertical mounting with a positive linear stiffness ensures an adequate load bearing capability. For this model two parameters are of major importance: the ratio of the coefficients of the springs (μ) and the initial angle at which the oblique springs are inclined (γ). The stiffness of this system increases with the displacement (hardening) and therefore the static stability is always guaranteed, provided that the two parameters are chosen in such a way to make the minimum stiffness (which occurs at the static equilibrium position) positive. The relationship that links the parameters with the minimum stiffness has been found. It has been shown that for a particular choice of parameter the stiffness of the mount can be set to zero at the static equilibrium position. However, this mechanism has a drawback. For large oscillations the linear analysis becomes invalid and the onset of nonlinear dynamic

effects might reduce the benefits of the HSLDS mechanism.

The main components in the second mechanism investigated are off-the-shelf magnets and coil springs. A magnet/mass is free to move vertically on smooth shaft. Two magnets fixed at the top and bottom of the device at a distance d exert an attracting force on a middle magnetic element to which they are connected by means of two coil springs. The negative stiffness due to the magnetic interaction is exploited to cancel partially some of the positive stiffness of the coil springs. An appropriate design of the system allows any value of desired low stiffness to be achieved. The static behaviour of the system has been described in terms of only one parameter, ν. Like the previous mechanism, also this presents a drawback: the stiffness is positive (stable system) only within a limited displacement range. Besides, this range becomes smaller as the maximum stiffness is decreased. In practice, in order to prevent too large a displacement from occurring, some form of restriction for the motion of the central piece has to be engineered.

For both systems the exact functions that describe the force and stiffness-displacement relationship have been simplified. In particular, the restoring force of the HSLDS spring has been expressed with a symmetric cubic polynomial. As a consequence, the equation of motion of a mass suspended on such a springs takes the form the Duffing equation. The conditions for the linearisation have been stated. In this case the natural frequency of the HSLDS mount is lower that than an equivalent linear system.

In the remaining chapters both nonlinear and linear behaviour will be further analysed: in chapters 3,4,5 a nonlinear analysis will be carried out in order to predict the system dynamics when the linear approximation is no longer applicable, whereas in chapter 6 the assumption of linearity will be validated experimentally.

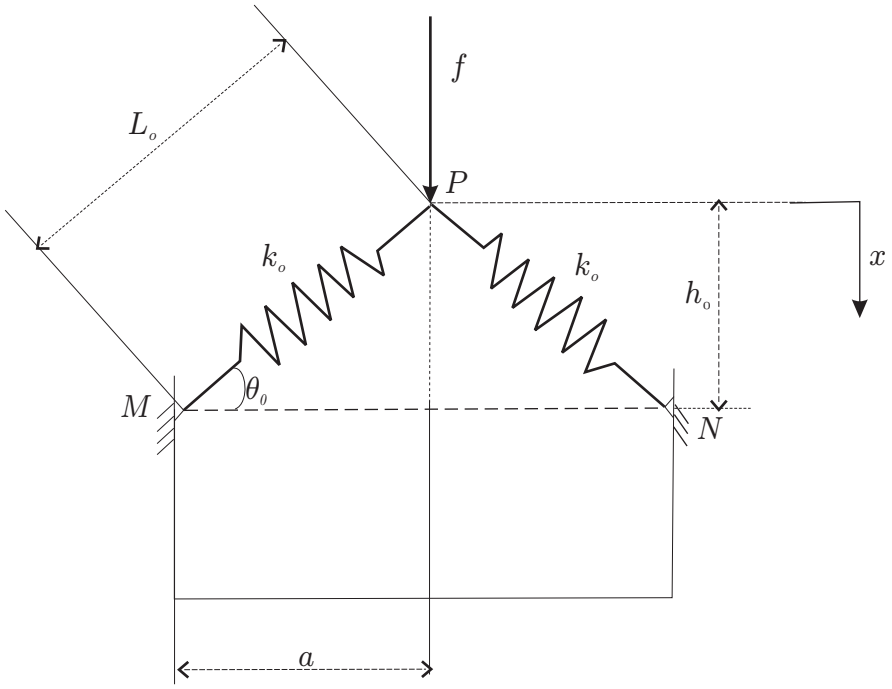

Figure 2.1: Schematic representation of a system with two oblique springs. The springs oppose the applied load f, and the geometry gives rise to a non-linear force-displacement characteristic

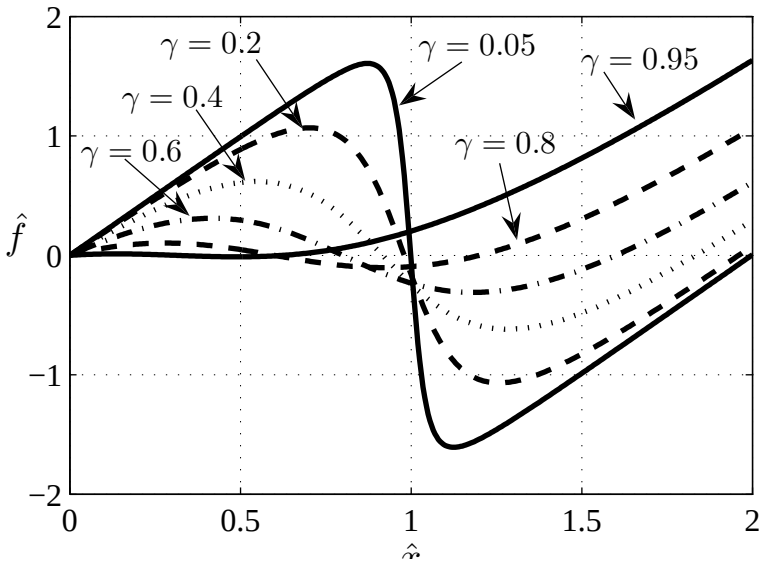

Figure 2.2: Force-deflection characteristic of the system represented in Fig. 2.1. When $\gamma = 0$ the springs are vertical and when $\gamma = 1$ they are horizontal. After the maximum the curves have a region with negative stiffness

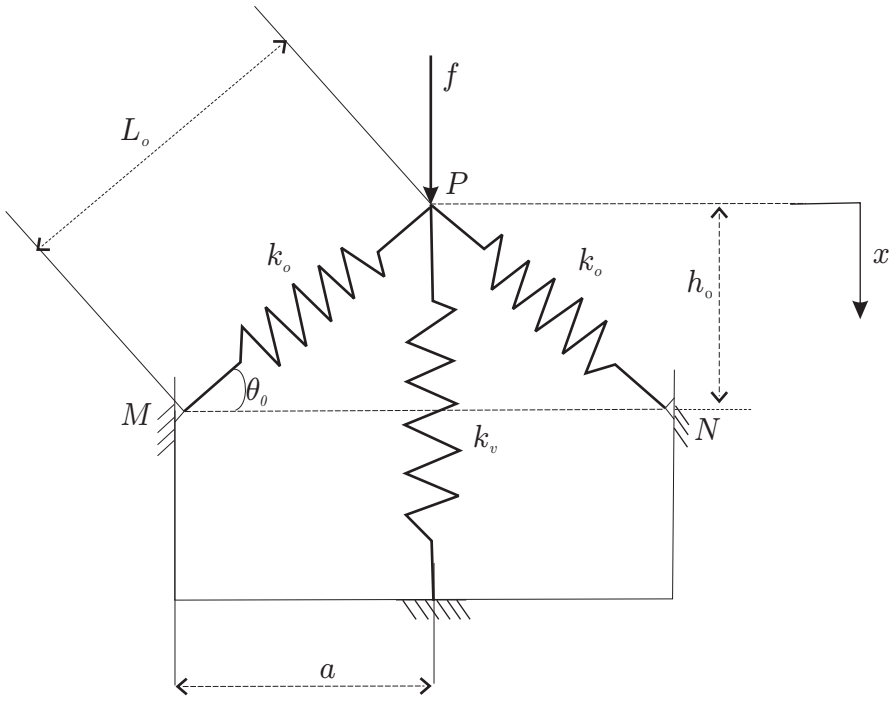

Figure 2.3: Schematic representation of an isolator with HSLDS characteristic

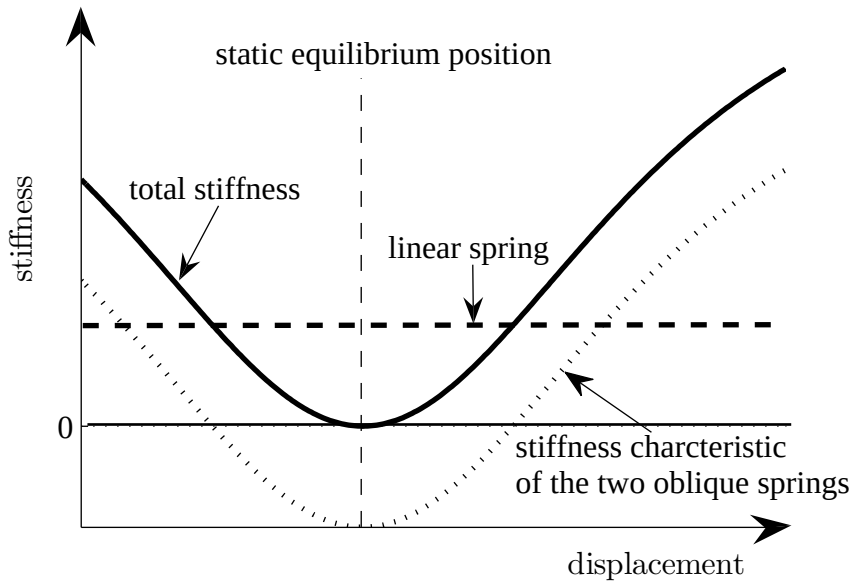

Figure 2.4: Stiffness-displacement characteristic of a HSLDS mount: by connecting in parallel (summing the stiffness) a linear spring (with positive stiffness, dashed line) with one with 2 oblique springs (negative stiffness, dotted line) the total stiffness (solid line) at the static equilibrium position can be made as small as desired, e.g. even zero as in this case

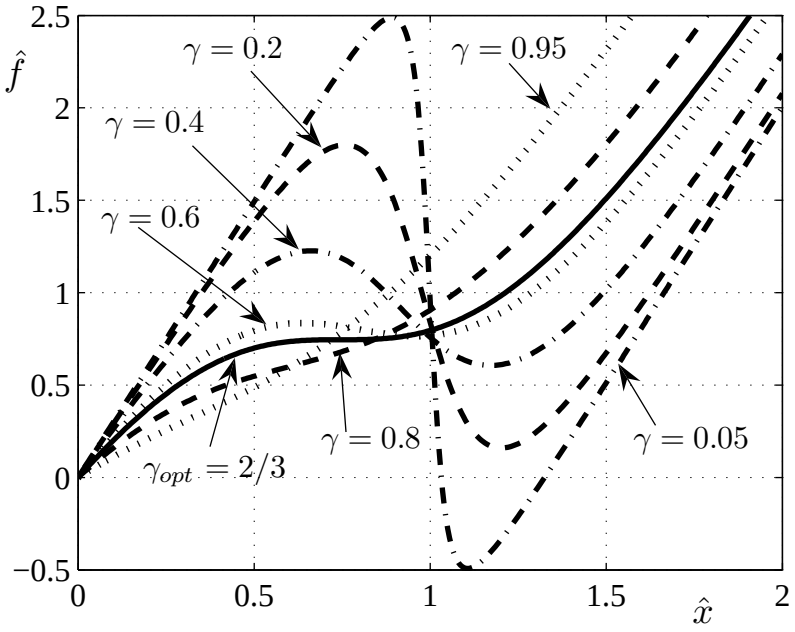

Figure 2.5: Non-dimensional force-displacement characteristic of a HSLDS mechanism when $\mu = 1$: the solid line has a flat region in which that system has quasi-zero stiffness

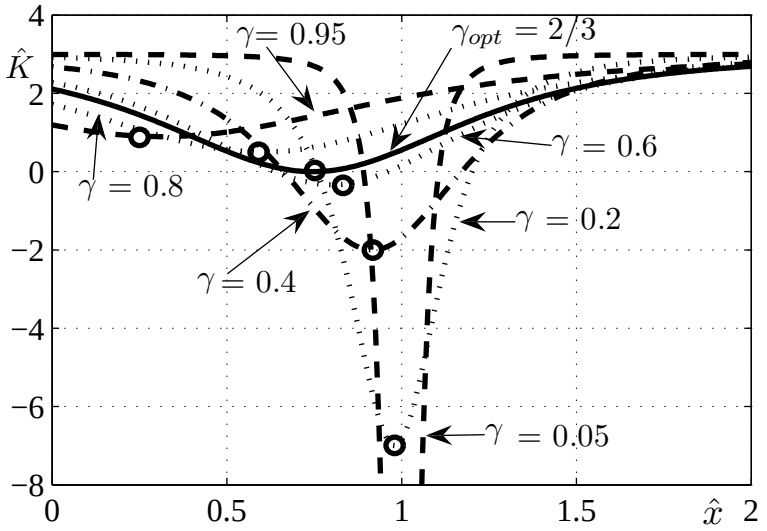

Figure 2.6: Non-dimensional stiffness of a HSLDS mechanism when $\mu = 1$: the solid line is representative of a stable system (always positive stiffness) with zero stiffness at the static equilibrium position. The symbol 'o' denotes the static equilibrium position $\hat{x}_e = \sqrt{1-\gamma^2}$, i.e. when the oblique springs are horizontal

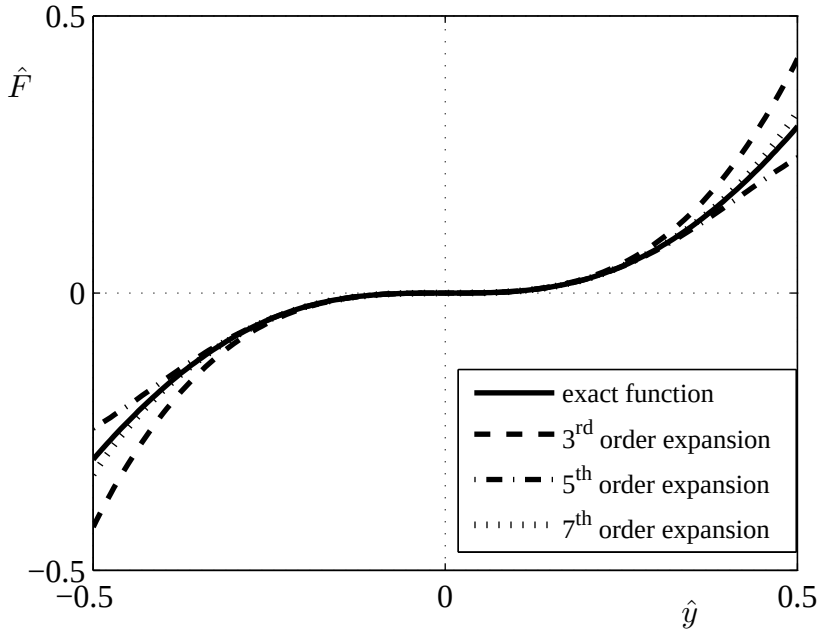

Figure 2.7: Non-dimensional force-displacement characteristic when $\mu = \mu_{opt}$ and $\gamma = 2/3$. The solid line shows the plot of the exact expression Eqn.(2.13) in the new coordinate system. The other lines are for the approximate expressions of third, fifth and seventh order Taylor's series expansions about $\hat{y} = 0$

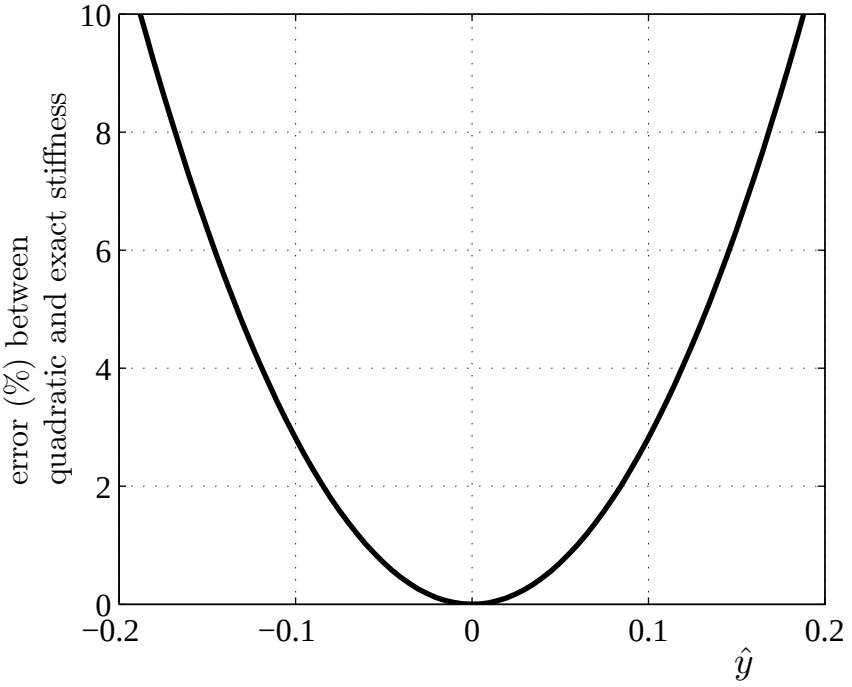

Figure 2.8: Approximation error between the quadratic and exact stiffness when $\mu = \mu_{opt}$ and $\gamma = 2/3$

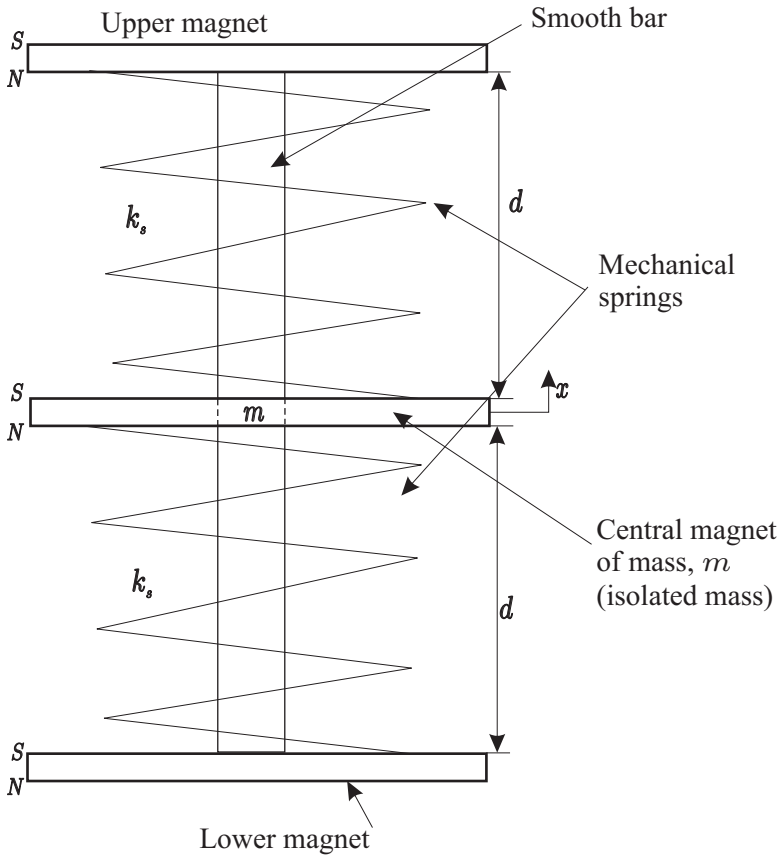

Figure 2.9: Isolation system with coil springs and magnets

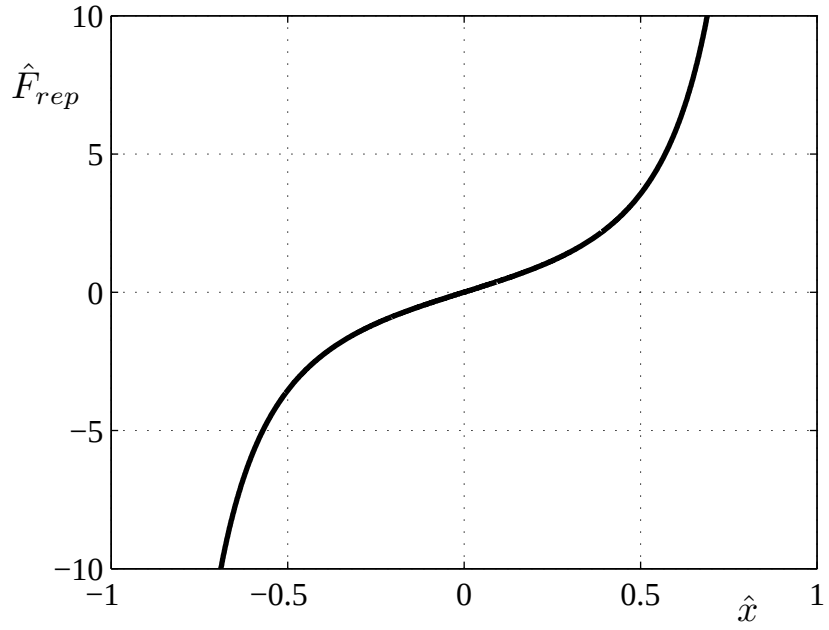

(a) Force

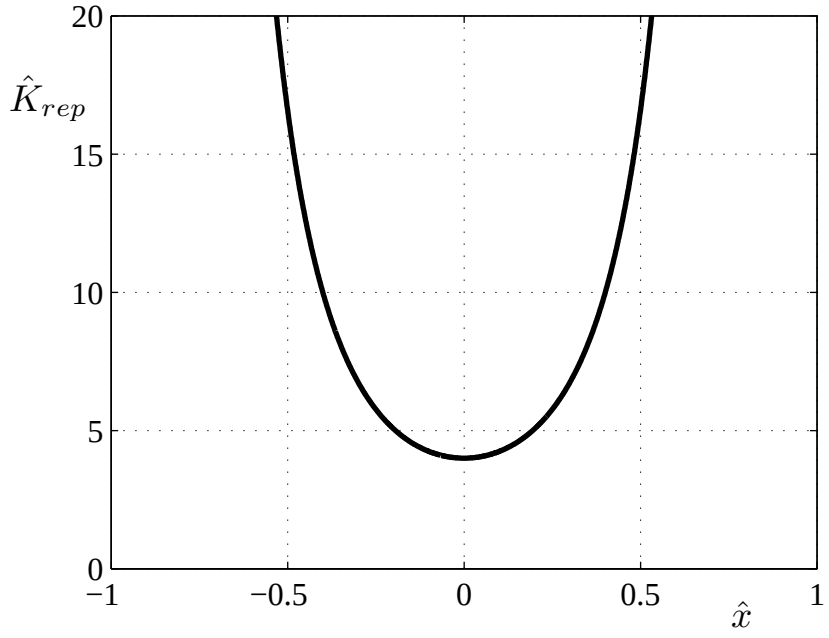

(b) Stiffness

Figure 2.10: **Magnets in repelling configuration**: Nondimensional force and stiffness characteristic as function of the nondimensional displacement

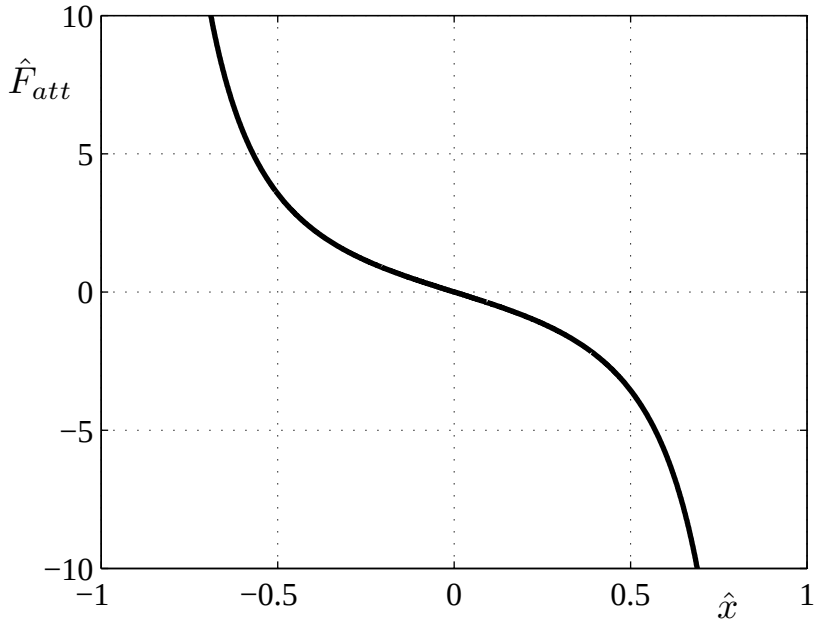

(a) Force

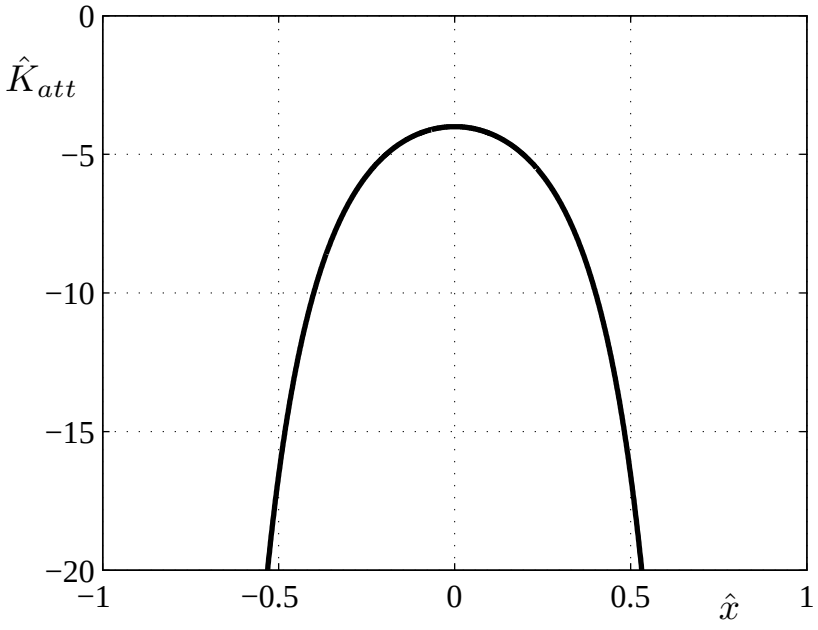

(b) Stiffness

Figure 2.11: **Magnets in attracting configuration**: Nondimensional force and stiffness characteristic as function of the nondimensional displacement; $\hat{x} = x/d$

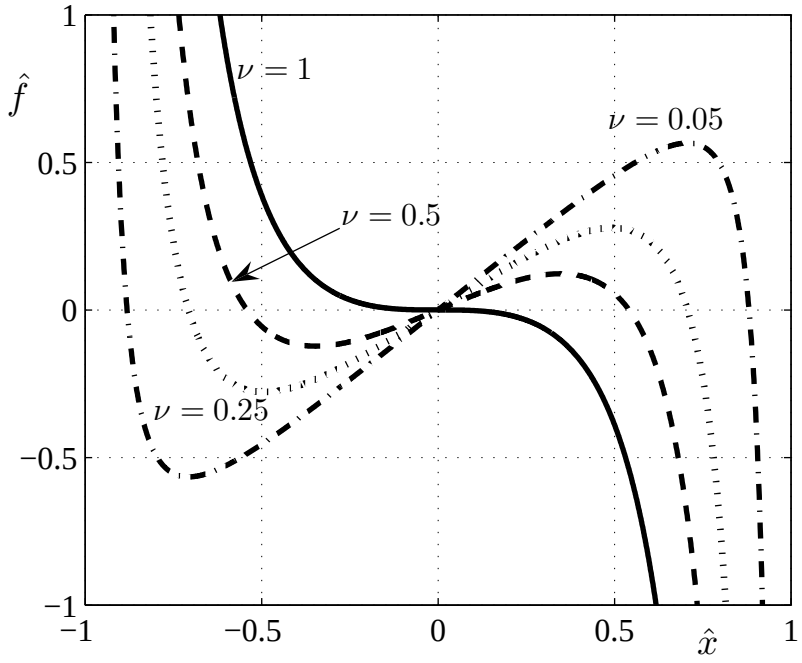

(a) force

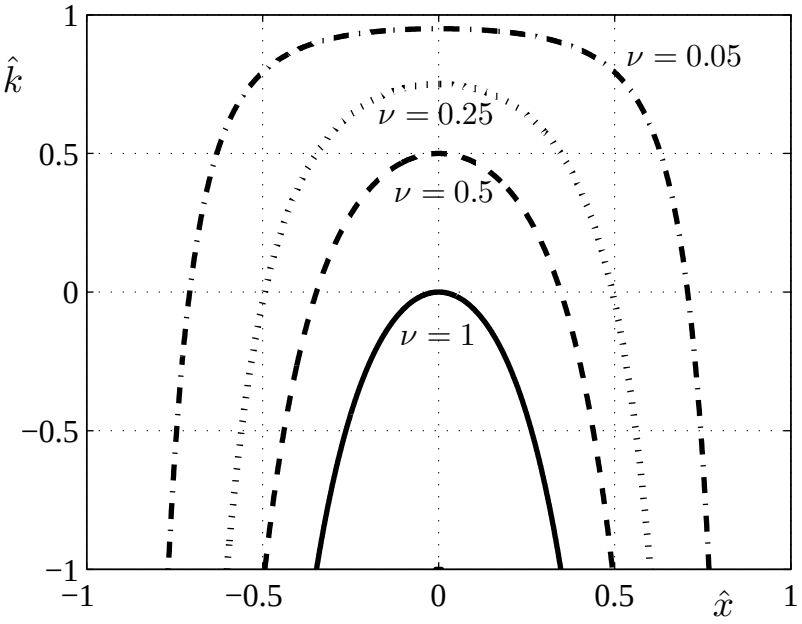

(b) stiffness

Figure 2.12: Force and stiffness characteristics of a system with attracting magnets and coil springs. The system parameter ν is changed so as to achieve several values of maximum stiffness $\hat{k}_0$

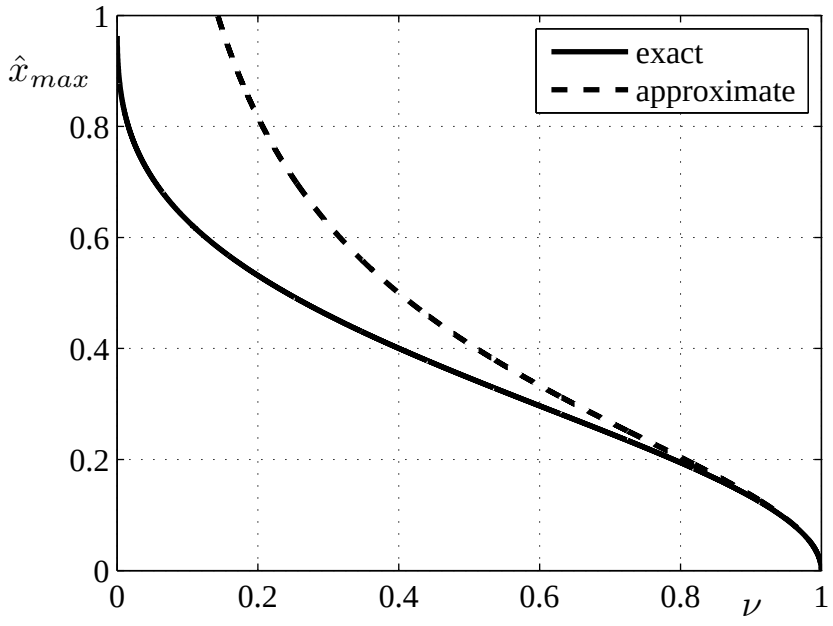

Figure 2.13: Maximum excursion from the static equilibrium position which guarantees positive stiffness as a function of ν. Both exact (solid line) and approximate (dashed line) are plotted. This figure clearly shows the compromise between the desired low stiffness and width of stability region

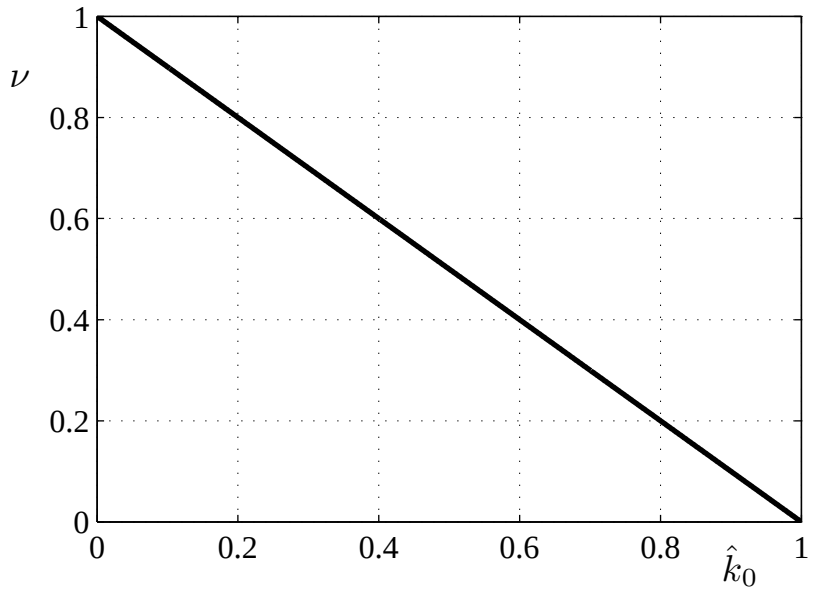

Figure 2.14: Relationship between the maximum stiffness of the HSLDS system, $\hat{k}_0$, and the system parameter ν required to achieve it

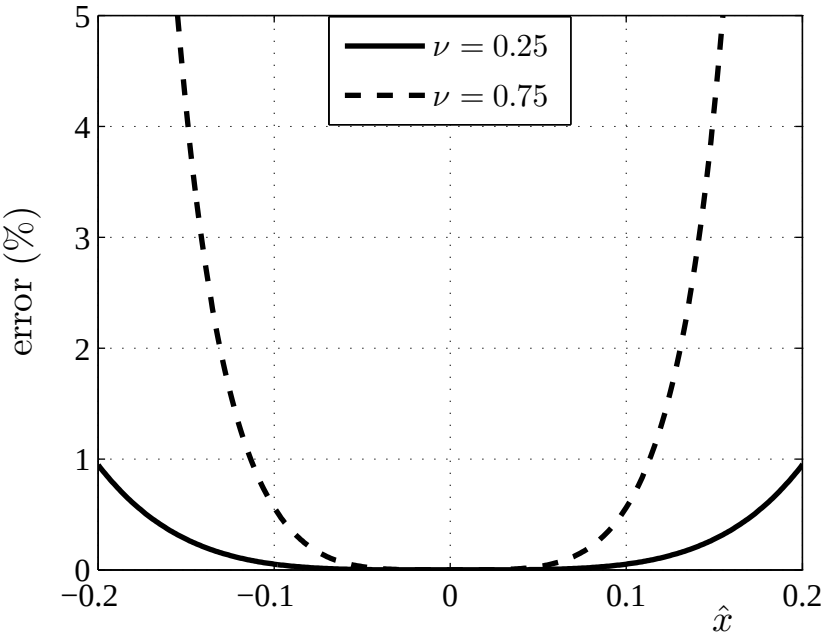

Figure 2.15: Percentage error introduced by assuming the stiffness to be a quadratic function of the displacement. Two values of ν have been chosen and the smaller ν (the higher the maximum stiffness) the smaller the error

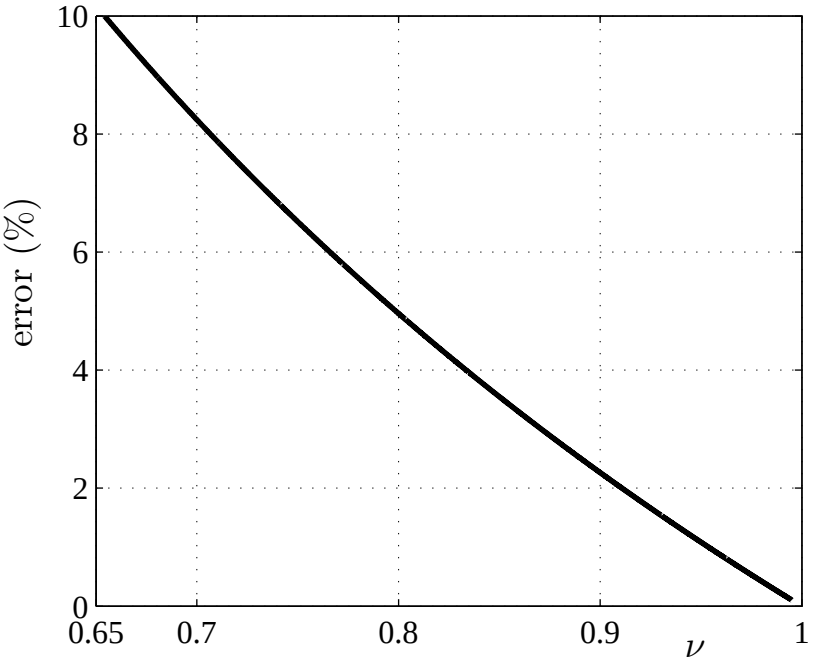

Figure 2.16: Percentage error introduced by the approximate expression for the maximum displacement from the static equilibrium position which ensures positive stiffness

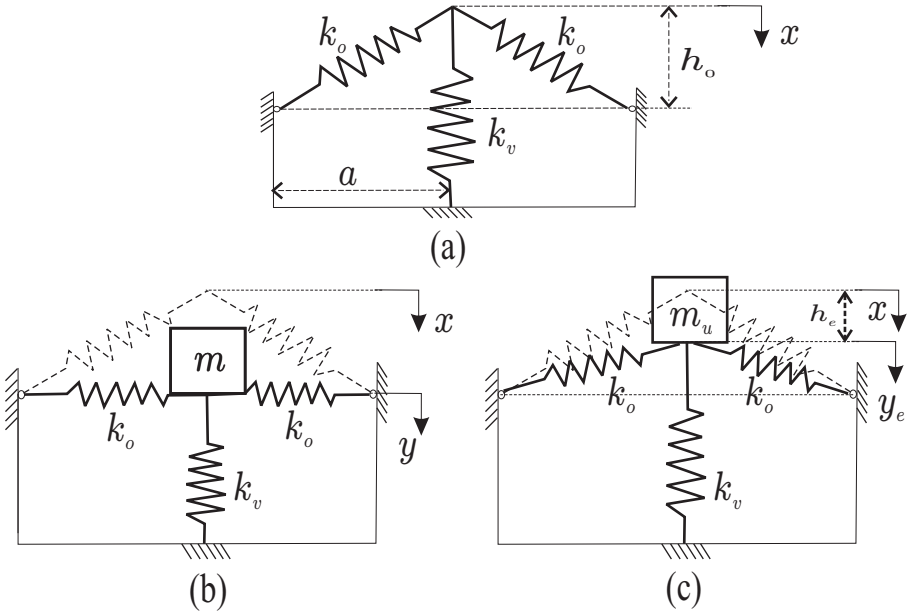

Figure 2.17: HSLDS system with 3 springs: (a) unladen condition; (b) loaded with a tuned mass m so that at the static equilibrium position the oblique springs lie horizontal; (c) system loaded with an untuned mass m_u and the static equilibrium position is $x = h_e$. The dashed line in (b), (c), is relative to the initial unladen position

Chapter 3

Basic aspects of nonlinear dynamics

'He who loves practice without theory is like the sailor who boards ship without a rudder and compass and never knows where he may cast.'

Leonardo da Vinci (1452 - 1519)

3.1 Introduction

The motion of a mass suspended on one of the HSLDS vibration isolation systems described in the previous chapter, which have a nonlinear (hardening or softening) restoring force, can be described by the Duffing equation. It has also been shown that for small oscillations about the static equilibrium position the system can be considered to be linear. Yet, for larger oscillations the nonlinearity in the system may not be negligible. In this case it is important to be able to identify the system's behaviour in the nonlinear regime.

The aim of this chapter is thus to give an overview of the fundamental concepts of dynamical analysis of nonlinear systems which will be used subsequently in the next chapter that concerns the forced response of the Duffing oscillator. Because the study of the nonlinear isolation system is more directed towards engineering applications rather than a mathematical study of the system, emphasis is placed on the stability of equilibrium points, the phase-space and bifurcation

concepts only. Methods for the solution of nonlinear differential equations are also discussed with particular focus on the harmonic balance method. Where appropriate, the examples given are with regard to the Duffing equation.

3.2 Fundamental concepts

The systems considered in this thesis are single-degree-of-freedom (SDOF) systems described by the ordinary differential equation (ODE) of the type

$$\ddot{x}_1 = f(x_1, \dot{x}_1, t) \tag{3.1}$$

with a given vector of initial conditions $\mathbf{u_0} = [x_1(0), \dot{x}_1(0)]$.
When the time variable, t, explicitly appears in the function f the system is called **non-autonomous**[a]. If t is only implicit then is called **autonomous**.

It is possible to write Eqn.(3.1) as two first order ODEs

$$\begin{aligned} \dot{x}_1 &= x_2 \\ \dot{x}_2 &= f(x_1, x_2, t) \end{aligned} \tag{3.2}$$

In this way the solution of the dynamical system can be displayed graphically in the two-dimensional space, x_1, x_2 (*displacement-velocity*), called the **phase plane**. The vector $\mathbf{u}(t) = [x_1(t), x_2(t)]$, is also called the *state vector* because it defines at any time the **state** of a dynamical system. The path traced in the phase plane by the state vector changes as the initial set of initial conditions, $\mathbf{u_0}$, is changed. The total of all the solutions (paths) is called the *phase portrait*. For a given set of initial conditions, the system's path can be projected onto the phase plane (autonomous systems) or plotted in a 3-dimensional space (x_1, x_2, t) (useful for non-autonomous systems). The former representation is referred to as the *trajectory*, whereas the latter is called the *motion space*. Fig.3.1 shows the trajectory and motion space of an undamped hardening Duffing's equation, whilst Fig.3.2 depicts those of a damped case.

A system is said to be in **static equilibrium** if the velocity and acceleration

[a] **forced equations** are an example of non-autonomous systems

are simultaneously zero, that is

$$\dot{x}_1 = 0 \qquad\qquad \dot{x}_2 = 0 \tag{3.3}$$

The points that satisfy Eqn.(3.3) are called *equilibrium points* or *singular points*[52]. From Eqns.(3.2) and (3.3) it follows that the state of the system at an equilibrium point is stationary.

3.3 Local stability and the phase plane

In this section the static stability of autonomous systems is discussed. Conceptually, stability may be defined as the capacity of a physical system to return to its initial equilibrium state when slightly disturbed.

A more rigourous definition widely used is due to Liapunov, [45, 53], and states that, an equilibrium point $\mathbf{u_e}$ is **stable** *in the sense of Liapunov* if for every neighbourhood ε there exist one neighbourhood δ such that any solution $\mathbf{u}(t)$ starting in δ, $\mathbf{u_0}$, remains in ε for all $t \geq 0$, that is

$$||\mathbf{u_0}|| < \delta \Longrightarrow ||\mathbf{u}(t)|| < \varepsilon \qquad 0 \leq t < \infty \tag{3.4}$$

If $\mathbf{u_e}$ is not stable is **unstable**. If the equilibrium point is Liapunov stable and $\mathbf{u}(t) \rightarrow \mathbf{u_e}$ for $t \rightarrow \infty$ then $\mathbf{u_e}$ is **asymptotically stable**. These 3 cases are depicted in Fig.3.3. Because this stability criteria focusses on the response of the system close to singular points and with respect to small perturbations it is also referred to as *local stability*. Further considerations on the equilibrium points of an autonomous system and their stability may be made from the analysis of their trajectories.

Consider the autonomous SDOF system described by two first order ODEs

$$\begin{aligned} \dot{x}_1 &= f(x_1, x_2) \\ \dot{x}_2 &= g(x_1, x_2) \end{aligned} \tag{3.5}$$

where f, g are nonlinear functions.

Let $\mathbf{u_e} = (x_{1_e}, x_{2_e})$ be a singular point, which means that $f(x_{1_e}, x_{2_e}) = g(x_{1_e}, x_{2_e}) = 0$. In order to study the behaviour of the system in the proximity of this point, the two functions can be expanded using Taylor's series. This expansion can be simplified and made more meaningful if the centre of expansion is the origin $(0, 0)$ of the phase-plane (McLaurin's expansion). Shifting the equilibrium point to the origin is a licit mathematical operation which does not undermine the generality of the problem and is always possible by scaling the phase plane appropriately, [53].

Expanding the functions f, g using the McLaurin's series yields

$$\begin{aligned} \dot{x}_1 &= A_{11}\, x_1 + A_{12}\, x_2 + \varepsilon_1(x_1, x_2) \\ \dot{x}_2 &= A_{21}\, x_1 + A_{22}\, x_2 + \varepsilon_2(x_1, x_2) \end{aligned} \tag{3.6}$$

where the functions ε_1 and ε_2 are the reminders of the McLaurin's expansion and therefore of order of at least two. Eqn.(3.6) can be written in matrix form as

$$\left\{ \begin{array}{c} \dot{x_1} \\ \dot{x_2} \end{array} \right\} = \left[\begin{array}{cc} A_{11} & A_{12} \\ A_{21} & A_{22} \end{array} \right] \left\{ \begin{array}{c} x_1 \\ x_2 \end{array} \right\} + \left\{ \begin{array}{c} \varepsilon_1 \\ \varepsilon_2 \end{array} \right\} \tag{3.7}$$

on in compact form

$$\dot{\mathbf{u}} = \mathbf{A}\,\mathbf{u} + \varepsilon \tag{3.8}$$

where the matrix $\mathbf{A}$ is the matrix of the partial derivatives (Jacobian matrix) evaluated at the equilibrium points, with constant elements $\mathbf{A}_{ij}$ given by

$$A_{11} = \frac{\partial f}{\partial x_1} \qquad A_{12} = \frac{\partial f}{\partial x_2} \qquad A_{21} = \frac{\partial g}{\partial x_1} \qquad A_{22} = \frac{\partial g}{\partial x_2} \tag{3.9}$$

For small displacements from the equilibrium point Eqn.(3.8), known as the *complete variational nonlinear equations*, can be approximated by the *linearised equations*

$$\dot{\mathbf{u}} = \mathbf{A}\,\mathbf{u} \tag{3.10}$$

A system described by Eqn.(3.10) has solution

$$\mathbf{u}(t) = \mathbf{\Phi}\, e^{\lambda t} \tag{3.11}$$

where λ are the *eigenvalues* of the linearised system and $\mathbf{\Phi}$ the corresponding

eigenvectors. The eigenvalues can be found by solving the *eigenproblem*

$$det\ (\mathbf{A} - \lambda\,\mathbf{I}) = 0 \tag{3.12}$$

Eqn.(3.12) is equivalent to

$$\lambda^2 - T\,\lambda + D = 0 \tag{3.13}$$

where T is the *trace* and D the *determinant* of Jacobian matrix evaluated at the equilibrium point

$$\begin{array}{rclcl} T & = & A_{11} + A_{22} & = & tr[\mathbf{A}] \\ D & = & A_{11}\,A_{22} - A_{12}\,A_{21} & = & det[\mathbf{A}] \end{array} \tag{3.14}$$

Thus the eigenvalues are given by

$$\lambda_{1,2} = \frac{T}{2} \pm \frac{1}{2}\sqrt{T^2 - 4\,D} \tag{3.15}$$

The stability of the equilibrium will depend on the eigenvalues. Depending on the eigenvalues the singular points can be classified as follows:

1. $\lambda_{1,2}$ *are real and distinct* $(T^2 > 4\,D)$. If the eigenvalues have the same sign $(D > 0)$ the equilibrium point is a **node**. If they are both negative $(T < 0)$ the singular point is an *(asymptotically) stable node*, if $\lambda_{1,2}$ are positive $(T > 0)$ the point is an *unstable node*.
   An equilibrium point is said to be a **saddle point** which is *unstable* if the two eigenvalues have different sign $(D < 0)$.

2. $\lambda_{1,2}$ *are real and coincident* $(T^2 = 4\,D)$. An equilibrium point with real and coincident eigenvalues is a **stable degenerate node** if $T < 0$ and an **unstable degenerate node** if $T > 0$ (this case requires that $\mathbf{A}_{12}$ and $\mathbf{A}_{21}$ have different sign).

3. $\lambda_{1,2}$ *are complex and conjugate* $(T^2 < 4\,D)$. In this case the equilibrium point is a **focus** or **spiral**. If the real part is positive $(T > 0)$ the focus is *unstable*; if it is negative $(T < 0)$ is a *stable* focus. If the two eigenvalues have zero real part $(T = 0)$ then the equilibrium point is called a **centre** and is stable.

All the above cases are shown in Fig. 3.4

The parabola $T^2 = 4\,D$ separates oscillatory from nonoscillatory motion, that is foci from nodes. Saddle points ($D < 0$), as previously stated, are always unstable. More specifically, *if one root is real and positive or complex with positive real part, there is instability; if, on the other hand, the eigenvalues are either real and negative or complex with negative real part the equilibrium point is asymptotically stable*. If the eigenvalues of the linearised variational equation have non-zero real parts, i.e. when $T \neq 0$, the equilibrium points (nodes, foci and saddle points) are also referred to as *hyperbolic*. If the eigenvalues have zero real part, i.e. $T = 0$ the equilibrium points are said to be *non-hyperbolic*.

The stability analysis presented has concerned the linearised system. If an equilibrium point is a node, or focus or a saddle point of the linearised system it will be the same also for the complete nonlinear model, [53]. However, this cannot be said of centres. If a singular point of the linearised system is a centre (stable), it does not imply that it is a stable point for the nonlinear model too (it could be a stable or unstable focus). In order to asses the nature of centres, there is need either to consider the nonlinear terms neglected in the linearised analysis or extend the analysis to what is called *motion in the large* which considers the motion of the system at some distance away from the equilibrium point. As it will be shown shortly, for the Duffing equation the characteristics of the equilibrium points are conserved when considering the complete nonlinear equation.

3.3.1 Linear stability analysis of the hardening and softening Duffing's equation

Consider the Duffing equation

$$\ddot{x}_1 + x_1 + x_1^3 = 0 \tag{3.16}$$

which can be rewritten in the form of Eqn.(3.5) as

$$\begin{aligned} \dot{x}_1 &= x_2 \\ \dot{x}_2 &= -x_1\,(1 + x_1^2) \end{aligned} \tag{3.17}$$

The only equilibrium point of the system Eqn.(3.17) is

$$\mathbf{u_e} = (0, 0) \tag{3.18}$$

The Jacobian matrix for the hardening Duffing oscillator, from Eqn.(3.9) is

$$[\boldsymbol{A}] = \begin{bmatrix} 0 & 1 \\ -1 & 0 \end{bmatrix} \tag{3.19}$$

whose trace and determinant are

$$T = 0 \qquad\qquad D = 1 \tag{3.20}$$

The eigenvalues are thus

$$\lambda_{1,2} = \pm j \tag{3.21}$$

From Fig.3.4 it can be seen that the equilibrium point is a centre, as also shown in the phase-plot of Fig. 3.5(a).

The softening Duffing oscillator is described by

$$\ddot{x}_1 + x_1 - x_1^3 = 0 \tag{3.22}$$

or

$$\begin{aligned} \dot{x}_1 &= x_2 \\ \dot{x}_2 &= x_1\,(x_1^2 - 1) \end{aligned} \tag{3.23}$$

This system possess three equilibrium points at

$$\mathbf{u_{e1}} = (0, 0) \qquad\qquad \mathbf{u_{e2,3}} = (\pm 1, 0) \tag{3.24}$$

It can be verified that the trace is zero for all the singular points, i.e. $T = 0$. The Jacobian determinant of the first equilibrium point is $D_1 = 1$, whereas for the other two is $D_{2,3} = -2$. From Fig.3.4 it can be seen that the equilibrium point $\mathbf{u_{e1}} = (0,0)$ is a centre, whilst the other two, $\mathbf{u_{e2,3}}$, are saddle points, as depicted in the phase-plot of Fig. 3.6(a).

3.3.2 Conservative systems and motion in the large

The results of the linear stability analysis have a certain degree of uncertainty when the equilibrium point is a centre. In fact, the equilibrium point of the non-linear model can indeed be a centre but it could also be a focus.

Consider the conservative system described by

$$\ddot{x}_1 = f(x_1) \tag{3.25}$$

or

$$\begin{aligned} \dot{x}_1 &= x_2 \\ \dot{x}_2 &= f(x_1) \end{aligned} \tag{3.26}$$

where $f(x_1)$ is a generic restoring force function.

The motion of a point in the x_1, x_2 (phase) plane, the trajectory, is given by the solution of the *integral curve* [54]

$$\frac{dx_2}{dx_1} = \frac{\frac{dx_2}{dt}}{\frac{dx_1}{dt}} = \frac{f(x_1)}{x_2} \tag{3.27}$$

Integrating Eqn.(3.27) yields

$$\frac{x_2^2}{2} - \int f(x_1)\, dx_1 = const \tag{3.28}$$

Eqn.(3.28) coincides with the application of the principle of conservation of energy

$$E = K + V = \text{constant} \tag{3.29}$$

where E is the total energy, and the kinetic energy, K, and the potential energy, V, are defined respectively as

$$K = \frac{1}{2}\, x_2^2 \tag{3.30a}$$

$$V = -\int f(x_1)\, dx_1 \tag{3.30b}$$

By the definition given in Eqn.(3.3), the singular points can be found by solving

$$x_2 = 0 \qquad \dot{x}_2 = f(x_1) = 0 \tag{3.31}$$

which is equivalent to

$$\frac{dV}{dx_1} = -f(x_1) = 0 \tag{3.32}$$

Hence, it can be deduced that the equilibrium points are stationary points of the potential energy. The two following examples help to establish the relationship

between the equilibrium points of the system and the stationary points of the potential energy.

First, consider the hardening Duffing equation with restoring force

$$f(x_1) = x_1 + x_1^3 \tag{3.33}$$

According to Eqn.(3.31) the only singular point is $\mathbf{u_e} = (0, 0)$ and is a point of minimum of the potential energy. Fig. 3.5(b) shows the potential energy of the hardening Duffing equation. It can be seen that there is a minimum of V when $x_1 = x_2 = 0$ which result in a centre for the orbits in the phase-plane, shown Fig. 3.5(a).

As a second example, consider the softening Duffing oscillator with restoring force

$$f(x_1) = x_1 - x_1^3 \tag{3.34}$$

From Eqn.(3.31) it is found that the system has three equilibrium points at

$$\mathbf{u_{e1}} = (0, 0) \qquad \mathbf{u_{e2,3}} = (\pm 1, 0) \tag{3.35}$$

which coincide with the results obtained in Eqn.(3.24). Moreover, u_{e1} is a minimum, whilst $u_{e2,3}$ are maxima of the potential energy function. This is also depicted in Fig. 3.6 which shows that the minimum of the potential energy is a centre of the phase plane, whilst the two maxima are two saddle points. The trajectory passing through the saddle points is called *separatrix*.

From the two examples illustrated it is possible to establish a link to a theorem attributed to Lagrange (who formulated it) and Dirichlet (who proved it) which states that *if the potential energy has an isolated minimum at an equilibrium point, the equilibrium state is stable*, [53, 55]. They also relate to a converse Liapunov theorem according to which *if the potential energy at an equilibrium point is not a minimum, the equilibrium state is unstable* [53]. With reference to Fig. 3.7, these theorems can be physically interpreted as follows. If the system is at a point of maximum of the potential energy, S in the figure, any displacement from it would require a reduction in potential energy. Therefore, in order for the principle of energy conservation to hold, the kinetic energy has to increase, i.e

the velocity increases. This indicates that the system starts to move away from S at increasing speed. If instead the system is at a point of minimum, as in C, a displacement would cause an increase of potential energy which would make the velocity decrease, with the consequence that the system would eventually return to its initial position.

3.4 Non-autonomous systems: response to a harmonic excitation

This section deals with the nonlinear, non-autonomous equation of motion of a damped single-degree-of-freedom (SDOF) system harmonically excited by a force applied to the mass. Suitable examples of such systems are the two models considered in Chapter 2, whose non-dimensional equation of motion is in the form of the forced Duffing equation

$$\hat{x}'' + 2\,\zeta\,\hat{x}' + \hat{x} + \alpha\,\hat{x}^3 = \hat{F}_0\,\cos(\Omega\,\tau) \tag{3.36}$$

where $\hat{x}$ is the non-dimensionalised displacement, $\zeta \ll 1$ is the damping ratio and $\hat{F}_0$ and Ω are respectively the non-dimensional magnitude and frequency ratio of the excitation force. The $'$ operator denotes differentiation with respect to non-dimensional time τ.

In general, exact analytical solutions of nonlinear differential equations rarely exist. Results are obtained either by numerical integration or with mathematical techniques that yield approximate closed-form expressions. However the mathematical techniques needed for obtaining the approximate solution of nonlinear differential equations are not always straightforward and can be complex in nature. Reference textbooks for these analytical methods are [44, 56], but also [45, 52–54, 57] contain sections dedicated to the topic.

In accordance with the scope of this thesis, only a brief survey of the most used techniques is provided here, placing emphasis on the method of Harmonic Balance (HB). The reason why the HB method has been chosen to find the approximate solution of the nonlinear differential equation is described rather clearly by Worden [67]:

"*The purpose of applied mathematics is to describe and elucidate experiment. Theoretical analysis should yield information in a form which is readily comparable with observation. The method of the harmonic balance conforms to this principle beautifully as a means of approximating the FRFs*[b] *of nonlinear systems.*"
Furthermore, as stated by Hamdan *et al* [60] is not restricted to *weakly* nonlinear problems and, for smooth systems, the assumed harmonic solutions always converge to the exact solution.

3.4.1 Perturbation methods

There are different implementations of the perturbation technique that enable one to obtain an approximate solution to Eqn.(3.36). However they all have some common features and limitations, [58]. The solution is found by applying small nonlinear perturbations (hence the name) to the linearised equation, but the implementation of these methods is restricted to *weakly nonlinear* systems. A system is said to be *weakly nonlinear* when its motion is described by a differential equation that can be separated in one part containing linear terms and a part with nonlinear terms which are small relatively to the linear ones [53].

The basic idea behind any perturbation method is contained in the **straightforward expansion method** in which the solution of a nonlinear differential equation such as Eqn.(3.36) is assumed to be

$$\hat{x}(\tau,\alpha) = \hat{x}_0(\tau) + \alpha\,\hat{x}_I(\tau) + \alpha^2\,\hat{x}_{II}(\tau) + \alpha^3\,\hat{x}_{III}(\tau) + \dots \tag{3.37}$$

where $\hat{x}_0(\tau)$ is the solution to the linear system and $\alpha \ll 1$ is the 'perturbation'. Although this method is the basic perturbation method it is flawed because: 1) the expansion (3.37) is not periodic; 2) the frequency-amplitude relationship is not taken into consideration, [44, 53].

With the **method of multiple scales** it is assumed that the solution is dependent on multiple independent variables (two in its simplest form). This is because the solution depends on both the time t and the small parameter α, but

[b] Frequency Response Functions

also from a combination of the two $\alpha\, t \ll t$. Thus the solution is expanded as

$$\hat{x}(\tau) = \hat{x}_0(\tau) + \alpha\, \hat{x}_I(\tau,\, \eta) + \alpha^2\, \hat{x}_{II}(\tau,\, \eta) + \ldots \tag{3.38}$$

where $\eta = \alpha\, t$ and is called *slow time*. Nayfeh and Mook, [44] studied the system described by (3.36) assuming that the damping, the amplitude of the excitation force and the nonlinear coefficient are small and of the same order. First, they treated the case of primary resonance, deriving the first order differential equation for the amplitude and phase motion. For steady-state motion, the frequency-response equation was also obtained. The corresponding *backbone* curve, *jump phenomenon* and stability were then discussed. In addition, the superharmonic and subharmonic resonances of the system subject to hard excitation were analysed with a view to obtaining the frequency response equation for steady-state motions and defining the condition for their existence.

A different variant of the perturbation analysis is the **averaging method**. The most used version goes under the name of Krylov-Bogoliubov method [44, 56] which assumes that the two unknowns (amplitude and phase) are slowly varying functions of time, that is

$$\hat{x}(\tau) = \hat{X}(\alpha\, \tau)\, \cos(\Omega\, \tau + \varphi(\alpha\, \tau)) \tag{3.39}$$

where $\hat{X}(\alpha\, t)$ and $\varphi(\alpha\, t)$ are the slow-time-varying amplitude and phase respectively. Because they change slowly with the time they can be assumed constant over the period $T = 2\,\pi$. The result is obtained by averaging over this period. However, when applied to its first order approximation and compared with the result produced with different techniques, not all the nonlinear corrections to the frequency are accounted for. In order to obtain results which are consistent with those yielded by other methods it is suggested to apply the *generalised method of averaging*, which is fully explained in [56].

3.4.2 The Harmonic Balance method

As previously mentioned, the approximate analytical method chosen to carry out the analysis of the forced response of a Duffing's oscillator (presented in the next chapter) is the Harmonic Balance (HB) method. The main benefit of HB is that, in principle and unlike the other perturbation methods, it is not restricted to

weakly nonlinear problems [60]. However, neglecting the terms which contains higher order harmonics and assuming the response to be harmonic is an unacceptable solution for the Duffing equation (3.36) [67]. Yet, when the linear term of the restoring force is dominant over the nonlinear term, the application of the HB to a first order expansion provides a good approximate solution, especially when the major interest is in the response of the system at the excitation frequency. In this case the mathematical analysis is greatly simplified. Also the simplicity of its application makes it rather popular [59–61]. The main drawback of the HB is that the study of the system's stability requires a separate analysis.

The general approach when solving a nonlinear differential equation using HB is to assume that the solution has the form

$$\hat{x}(t) = \sum_{n=0}^{N} A_n \cos(n\,\Omega\,\tau + n\,\varphi_0) \tag{3.40}$$

which has $N+3$ unknowns Ω, φ_0, A_n.
Substituting Eqn.(3.40) into Eqn.(3.1) and equating the coefficients of equivalent harmonics it is possible to obtain a system of $N+1$ algebraic equations. Usually the $N+1$ unknown coefficients Ω, A_0, A_2 ..., A_N are expressed as functions of A_1 and φ_0, which can be determined by the initial conditions, [52]. Clearly the solution will be 'exact' only if an infinite number of harmonics are considered. However, the HB can be very simple and effective if something is known about the system's response.

Consider the unforced Duffing's equation which is obtained by setting $F = 0$ in Eqn.(3.36). A numerical simulation shows that the undamped, unforced system oscillates at its fundamental frequency (that depends on the amplitude of the initial displacement) but it also contains odd-ordered harmonics. Fig. 3.8 shows the frequency content of the undamped, unforced Duffing oscillator system, Eqn.(3.36) with $\alpha = 1$ and $\hat{F}_0 = 0$, with initial conditions $\hat{x}(0) = 7.35$ and $\hat{x}'(0) = 0$. This is expected because the restoring force is a nonlinear symmetric function. This *a priori* information allows the exclusion of the even harmonics A_{2n} from the solution.

In this thesis the interest is in the system response at the excitation frequency (as in many other engineering applications). It is thus a reasonable approxima-

tion to truncate the series to first order, but in doing so it is implicitly assumed that the linear term of the restoring force is dominant over the nonlinear term.

Thus, given the 'pre-analysis' of the response of a Duffing's oscillator to an harmonic excitation force, the solution in the region of the principal resonance can be assumed to be a first order series ($N = 1$)

$$\hat{x}(\tau) = \hat{X}\,\cos(\Omega\,\tau + \varphi) = \hat{X}\,\cos\,\theta \tag{3.41}$$

which implies

$$\hat{x}' = -\Omega\,\hat{X}\,\sin\,\theta \qquad\qquad \hat{x}'' = -\Omega^2\,\hat{X}\,\cos\,\theta \tag{3.42}$$

Substituting Eqn.(3.41) and (3.42) into Eqn.(3.36) yields

$$-\,\Omega^2\,\hat{X}\,\cos\,\theta - 2\,\zeta\,\Omega\,\hat{X}\,\sin\,\theta + \hat{X}\,\cos\,\theta + \alpha\,\hat{X}^3\,\cos^3\,\theta = \hat{F}_0\,\cos(\Omega\,\tau) \tag{3.43}$$

By neglecting harmonics of order higher than 1, one can simplify the trigonometric identity

$$\cos^3\,\theta \equiv \frac{1}{4}\,(3\cos\,\theta + \cos\,3\theta) \approx \frac{3}{4}\,\cos\,\theta \tag{3.44}$$

The forcing term can be rearranged as

$$\hat{F}_0\,\cos(\Omega\,\tau) = \hat{F}_0\,\cos(\theta - \varphi) = \hat{F}_0\,\cos\,\theta\,\cos\,\varphi + \hat{F}_0\,\sin\,\theta\,\sin\,\varphi \tag{3.45}$$

Finally, inserting Eqns.(3.44) and (3.45) into Eqn.(3.43) gives

$$-\Omega^2\,\hat{X}\,\cos\,\theta - 2\,\zeta\,\Omega\,\hat{X}\,\sin\,\theta + \hat{X}\,\cos\,\theta + \frac{3}{4}\,\alpha\,\hat{X}^3\,\cos\,\theta = \hat{F}_0\,\cos\,\theta\,\cos\,\varphi + \hat{F}_0\,\sin\,\theta\,\sin\,\varphi \tag{3.46}$$

Equating the coefficients of similar functions yields the system of two coupled algebraic equations

$$\frac{3}{4}\,\alpha\,\hat{X}^3 + (1 - \Omega^2)\,\hat{X} = \hat{F}_0\,\cos\,\varphi \tag{3.47a}$$

$$-\,2\,\zeta\,\Omega\,\hat{X} = \hat{F}_0\,\sin\,\varphi \tag{3.47b}$$

from which the two unknowns $\hat{X}$ and φ can be determined. The relationship between the response amplitude and frequency of excitation (the *frequency response function*) can be calculated by squaring and adding both equations (3.47

a,b) which results in

$$\frac{9}{16}\,\alpha^2\,\hat{X}^6 + \frac{3}{2}\,(1-\Omega^2)\,\alpha\,\hat{X}^4 + \left[(1-\Omega^2)^2 + 4\,\zeta^2\,\Omega^2\right]\,\hat{X}^2 = \hat{F}_0^2 \tag{3.48}$$

Eqn.(3.48) can be seen either as a cubic in $\hat{X}^2$ or a quadratic in Ω^2. A typical plot for $\alpha > 0$ is shown in Fig. 3.9: it presents the typical *jump phenomenon* of the Duffing oscillator. A detailed analysis of the forced response is presented in the next chapter.

3.5 Parametric system and bifurcation

In the examples so far considered, the state of the system, i.e. displacement and velocity, did not depend on any coefficient or parameter. As a consequence the equilibrium points were uniquely defined. However, in many case the equation of motion contains one or more parameters which influence the system dynamics. A generic conservative physical system is described by the differential equation

$$\ddot{x} = f(x, \alpha) \tag{3.49}$$

The equilibrium points are given by Eqn.(3.31), which corresponds to

$$f(x, \alpha) = 0 \tag{3.50}$$

The curve in Fig. 3.10 depicts the generic system described (3.50). In the shaded area $f(x, \alpha) > 0$. All the points of the curve which have a shaded region below them are stable points. Those parts of the curve below a shaded area are unstable, i.e $\overline{CA}$ and $\overline{CB}$. For example, at the value α_0 shown, there exist three equilibrium points, one of which is unstable, [45]. The points at which the equilibrium of the system changes qualitatively (i.e. from stable to unstable) or quantitatively, (e.g. from one to three) are called *bifurcation points*, and are denoted with the letters A, B, C in the figure. This simple rule can be explained by considering Lagrange's theorem on minimum potential energy law: a point of minimum of the potential energy is stable. Mathematically this means that for a stable point, as x increases, $\partial V/\partial x$ goes from negative to positive. However, from Eqn.(3.30b), $f(x, \alpha) = -\partial V/\partial x$, thus, for stability it is required that $f(x, \alpha)$ goes from positive to negative as x increases. Consider Fig. 3.10. For a fixed value of α the

points on the curve above a shaded area, go from positive to negative as x is increased, and hence are stable. The opposite happens for those with shaded area above ($\overline{CA}$ or $\overline{CB}$) which are therefore unstable.

A system whose response changes radically (e.g. appearance of new equilibrium points) as a result of a small change in one of its parameters, is said to be *structurally unstable*, [45]. The concept of **structural stability** is very different from that of Liapunov stability discussed earlier. Whilst Liapunov stability is concerned with the response of particular points (singular points) of the phase plane to perturbation, structural stability regards the response of the system to a small variation of its parameter(s). For a structurally unstable system, the **bifurcation point** is the critical value of a parameter that triggers a sudden or 'catastrophic' change in the response. Note that since every parameter might have one or more bifurcation points, a system dependent on many parameters can display extremely complex behaviour [45]. Note also that bifurcation points cannot exist if the system is structurally stable. One way to check the structural stability is to examine the eigenvalues of the system: if none of the equilibrium points has eigenvalues with zero real part ($T = 0$), i.e. if all the stationary points are *hyperbolic* the system is structurally stable.

The bifurcation concept can be envisioned by considering the simple linear system described by

$$\ddot{x} + \sigma\, x = 0 \tag{3.51}$$

or

$$\dot{x} = y \qquad\qquad \dot{y} = -\sigma\, x \tag{3.52}$$

where σ is a real number.

The system dynamics depend on the parameter σ. The equilibrium point is $\mathbf{u_e} = (0, 0)$ and the Jacobian matrix has trace and determinant

$$T = 0 \qquad\qquad D = \sigma \tag{3.53}$$

Because $T = 0$ the roots have zero real part and therefore the system is structurally unstable. Moreover, examining Fig. 3.4 it can be seen that if $\sigma > 0$ the equilibrium point will be a centre (stable) but if σ becomes negative then the singular point will be a saddle point (unstable). It follows that $\sigma = 0$ is the critical

value of the system's parameter at which the equilibrium point suddenly passes from stable to unstable as σ is decreased. In conclusion, zero is the bifurcation point for the parameter σ.

Amongst the different types of bifurcations observed in dynamical systems, of interest in the system is the *cusp bifurcation* because this kind of bifurcation is observed in the type of undamped Duffing equation considered in this thesis. The system changes drastically as the number of its equilibrium points goes from one to three for a small change in the system parameters. Take for example the equation of motion in non-dimensional form of the harmonically-forced softening undamped Duffing oscillator

$$x_1'' + x_1 - \alpha\, x_1^3 = f \tag{3.54}$$

where $f = F\,\cos(\Omega\,\tau)$ is the (non-dimensional) harmonic excitation force.

Eqn.(3.54) is dependent upon two parameters and can be written as

$$\begin{aligned} \dot{x_1} &= x_2 \\ \dot{x_2} &= f - x_1 + \alpha\, x_1^3 \end{aligned} \tag{3.55}$$

The equilibrium points all lie all on the x_1-axis of the phase plane ($x_2 = 0$) and are found by solving the cubic equation

$$\alpha\, x_1^3 - x_1 + f = 0 \tag{3.56}$$

which can be written in canonical form

$$x_1^3 - \xi\, x_1 + \rho = 0 \tag{3.57}$$

where $\xi = 1/\alpha$ and $\rho = f/\alpha$.

Eqn.(3.57) can have different type and number of solutions depending on the value of the discriminant of the cubic equation

$$D(\xi, \rho) = -4\,\xi^3 + 27\,\rho^2 \tag{3.58}$$

If $D > 0$, there is one real solution and two complex one; if $D = 0$ there is one

double real root; finally, when $D < 0$ there are three different real roots. As one of the parameters ρ or ξ changes, the number of equilibrium points of the system will pass from one to three. The surface x_1, ξ, ρ plotted in Fig.3.11 is called *catastrophe manifold*. The term catastrophe is used because of the catastrophic consequences that the passage from one stable solution to another may have. The curves in the x_1, ξ and x_1, ρ plane can be related to the simple case with only one parameter described by Eqn.(3.49) and illustrated at the beginning of this section; for the reasons therein explained the segment that connects the 'upper' and the 'lower' part of the surface represent unstable equilibrium points.

The bifurcation set, instead, is obtained by setting Eqn.(3.58) equal to zero. The result is plotted in Fig.3.12. Note that the curve is equivalent to the projection of the manifold onto the ρ, ξ plane (marked in Fig. 3.11). The name for this type of bifurcation is due to the cusp shown by the bifurcation set. In the region between the two branches of the curve there are three equilibrium points, and outside there is one.

The examples given in this chapter were taken from the literature and had the scope of illustrating the main theoretical aspect of nonlinear dynamic. For example the bifurcation set was determined in terms of the parameters ξ and ρ that represent the linear coefficient and the forcing term respectively. In the next chapter the equation of motion is non-dimensionalised in such a way that the dynamics of the system is described in terms of the cubic coefficient, the damping ratio and the forcing frequency.

3.6 Conclusions

This chapter has given a brief overview of the analysis and solution of nonlinear physical systems whose dynamics are described by nonlinear differential equations with cubic non-linearity. The aim was to introduce concepts such as stability, bifurcation and methods of solution for the forced equation (namely the Harmonic Balance Method) which will be used in the analysis of the forced response of the HSLDS mechanism in later chapters.

The topics discussed bridge the static analysis of the models of the HSLDS systems introduced in Chapter 2 (eventually approximated to the Duffing equa-

tion) with the dynamic analysis which is presented in the next chapters.

The analysis presented in this chapter has focussed on a nonlinear differential equation with cubic restoring force with both hardening and softening characteristic. It has been shown that, although both systems have a stable equilibrium point, the softening Duffing oscillator (negative cubic term) can become unstable in the sense of Liapunov; this behaviour does not occur in the hardening system, which is always stable. Amongst others, the method of Harmonic Balance has been chosen to solve the equation of motion when the system is subject to a harmonic excitation. Finally, it has also been shown that Duffing's equation is structurally unstable and therefore bifurcation points exist for the system's parameters.

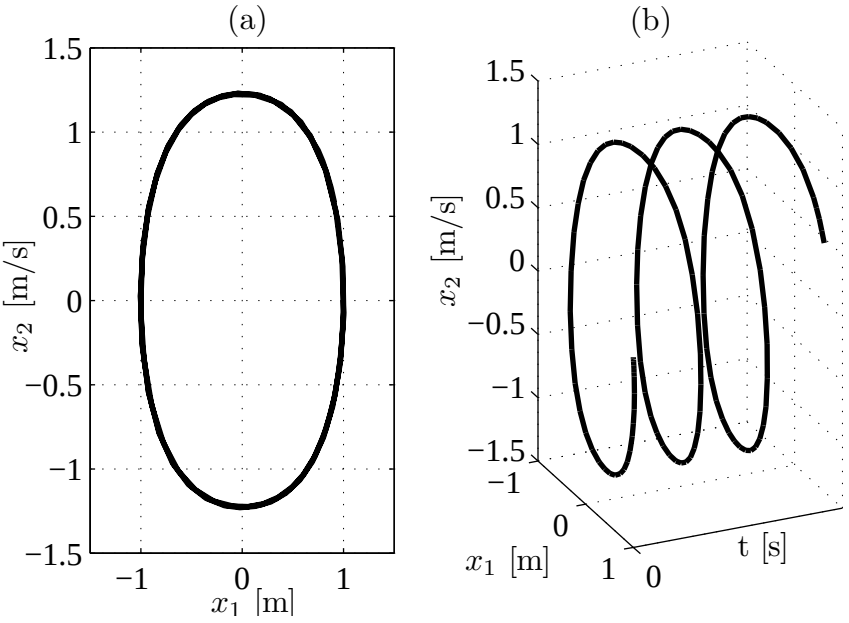

Figure 3.1: Phase-plane (a) and motion space (b) representation of the undamped system $\ddot{x} + x + x^3 = 0$. The initial conditions are $x(0) = 1$ and $\dot{x}(0) = 0$

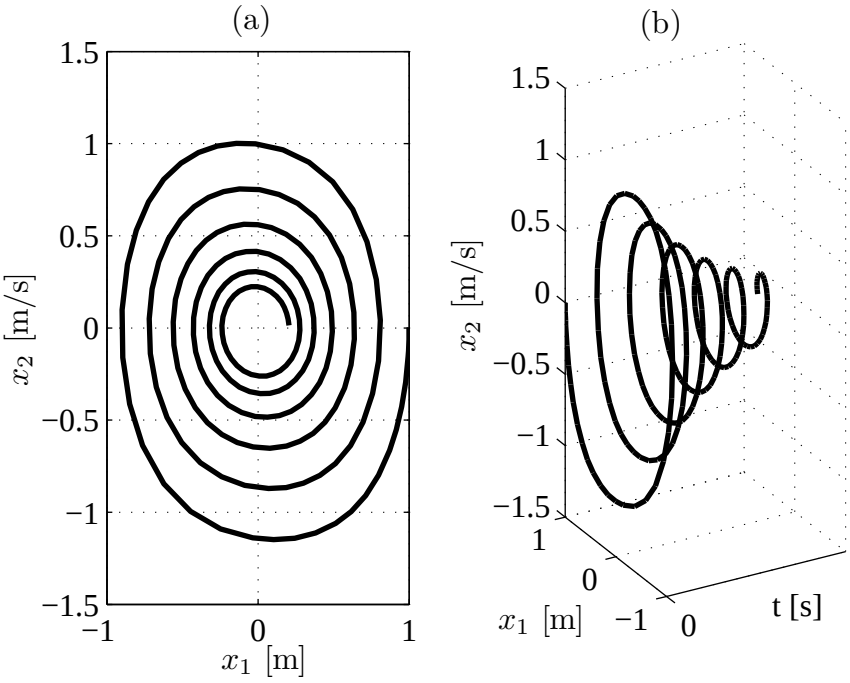

Figure 3.2: Phase-plane (a) and motion space (b) representation of the damped system $\ddot{x} + 0.1\,\dot{x} + x + x^3 = 0$. The initial conditions are $x(0) = 1$ and $\dot{x}(0) = 0$

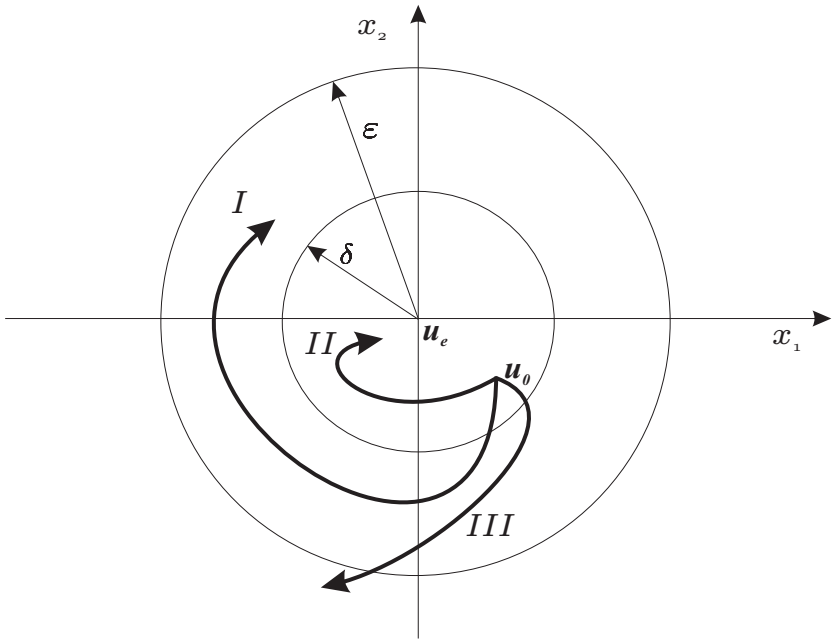

Figure 3.3: Definition of stability in the sense of Liapunov. The equilibrium point $\mathbf{u_e}$ is stable for system I as if perturbed within the neighbourhood (circle) δ the solution $\mathbf{u}(t)$ remains within ε for all $t \geq 0$; $\mathbf{u_e}$ asymptotically stable for system II for, in the limit for $t \to \infty$ the solution tends to the equilibrium point; the equilibrium point is unstable for the system III

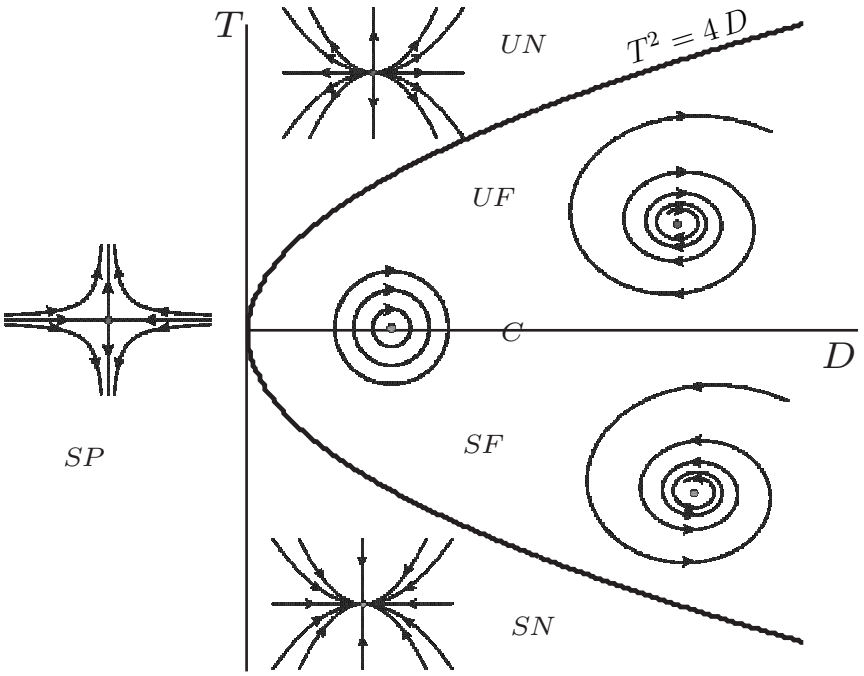

Figure 3.4: Stability regions according to the trace (T) and determinant (D) of the Jacobian matrix: Saddle Points (SP); Unstable Nodes (UN); Unstable Focus (UF); Stable Focus (SF); Stable Nodes (SN); Centres (C), [45]

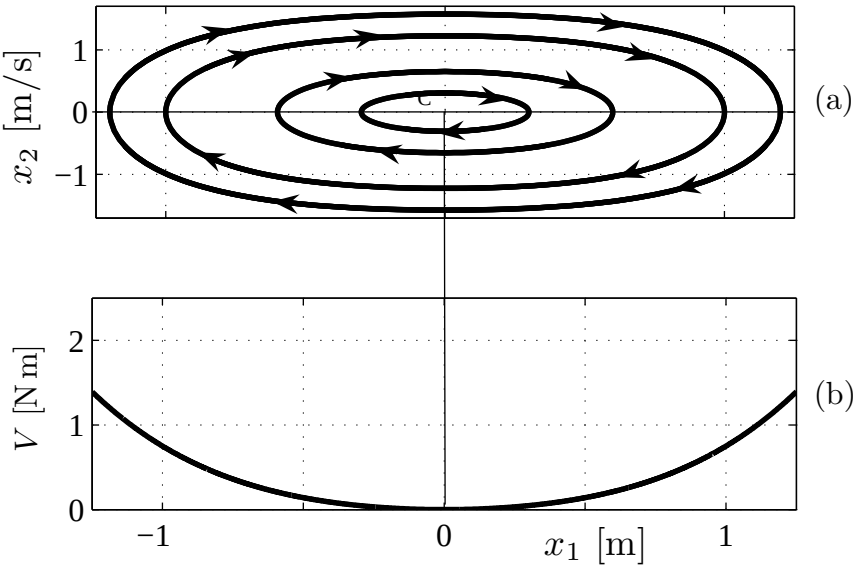

Figure 3.5: Hardening Duffing oscillator. (a) phase-plot (b) potential energy, V as function of displacement. The only stable singular point is a centre in the phase plane, $x_1 = x_2 = 0$

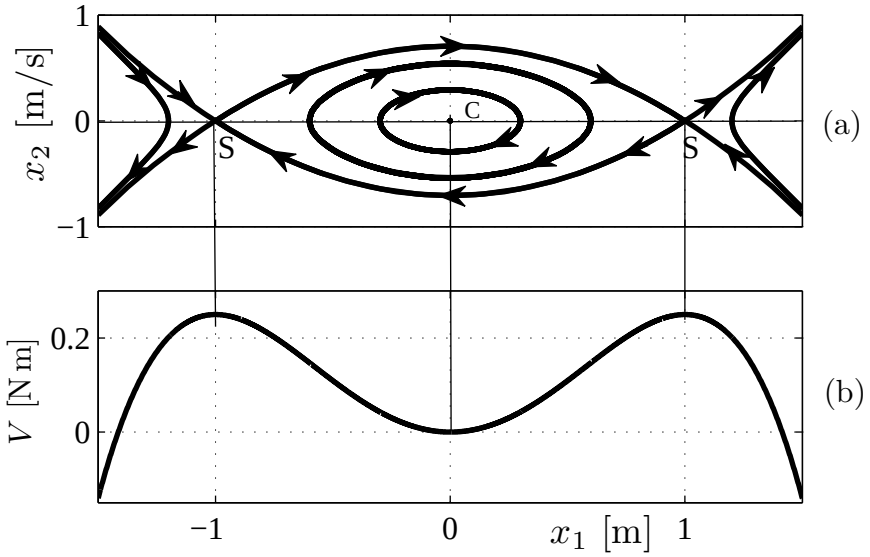

Figure 3.6: Softening Duffing oscillator. (a) phase-plot (b) potential energy, V as function of displacement. There are three singular points on the x-axis: one is stable, $x_1 = 0$ and two are unstable $x_1 = \pm 1$. These are respectively a centre, C and two saddle points, S, in the phase plane

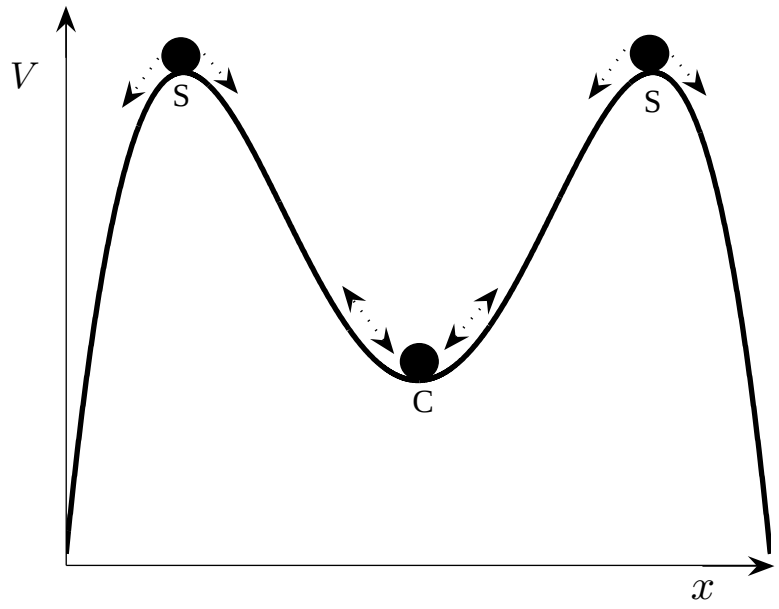

Figure 3.7: Potential energy of a softening Duffing oscillator as function of displacement. The black circle represents the system: when it is at point C is in a stable condition; when is at points S is unstable

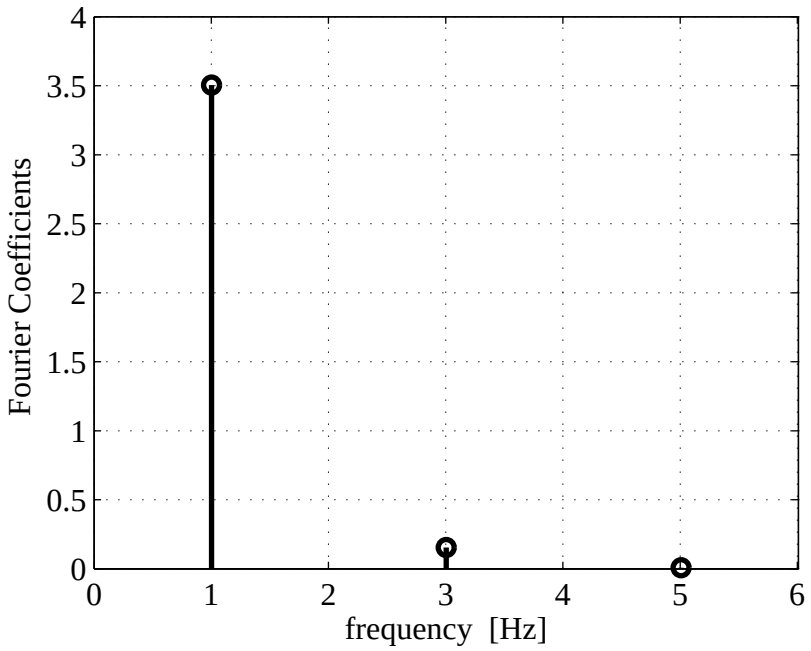

Figure 3.8: Fourier coefficients and harmonic decomposition of the numerical solution of the undamped Duffing equation $\hat{x''} + \hat{x} + \hat{x}^3 = 0$, with initial condition $\hat{x}(0) = 7.35$, $\hat{x'}(0) = 0$. The response contains only odd-ordered harmonics (1, 3, 5)

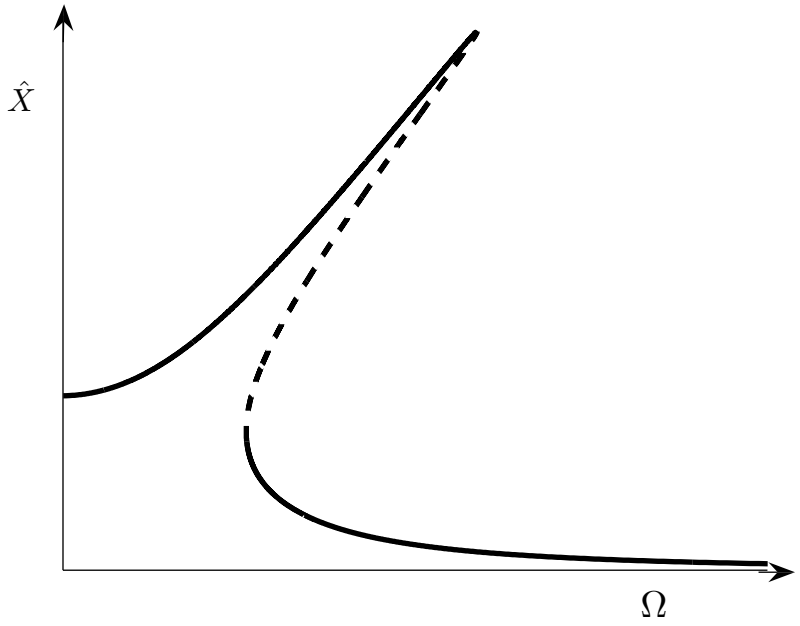

Figure 3.9: Qualitative representation of the frequency response function of a hardening Duffing oscillator. The dashed line is the *unstable branch*

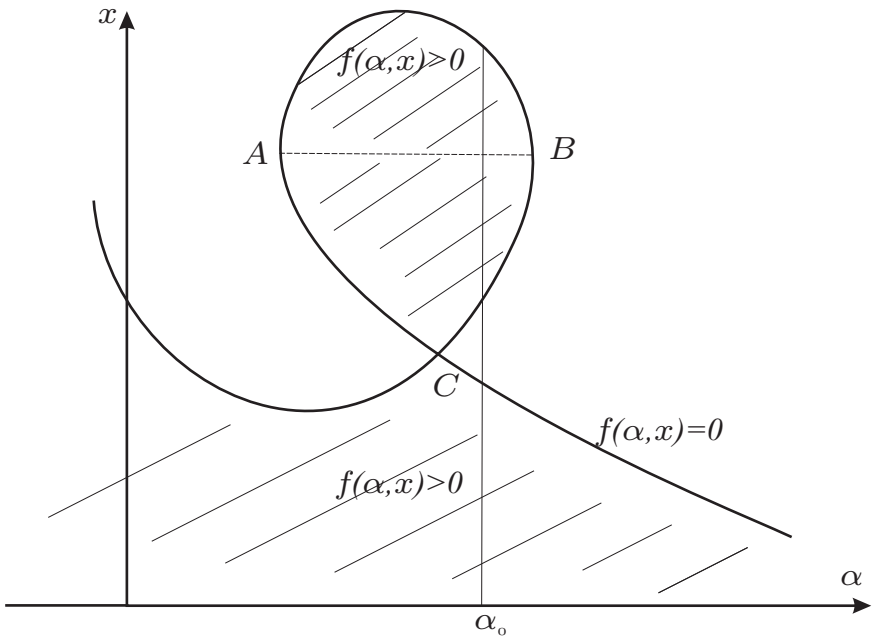

Figure 3.10: Equilibrium points of a system depending on the parameter α. The points on segments $\overline{CA}$ and $\overline{CB}$ are unstable. At the value α_0 there are three equilibrium points of which one is unstable

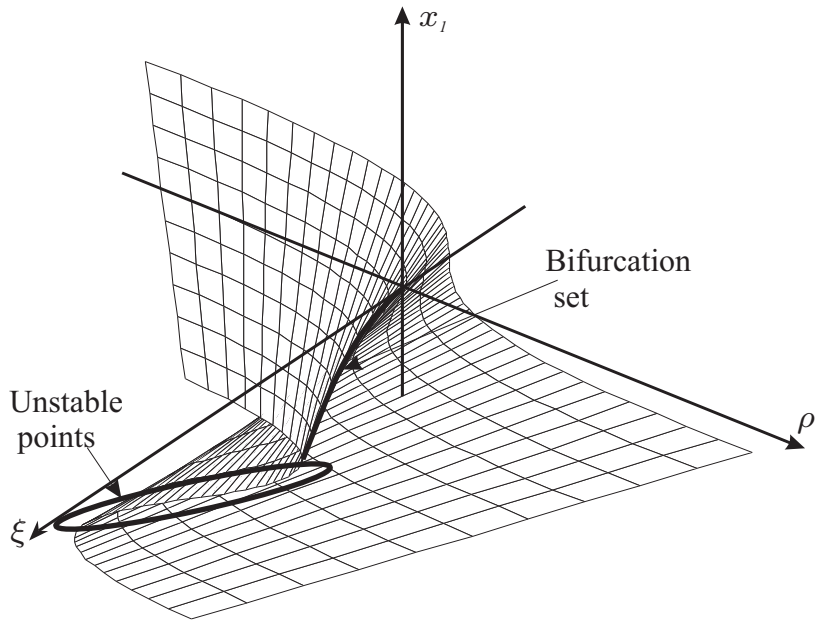

Figure 3.11: Catastrophe manifold: this is the surface of singular points in the x_1, ξ, ρ space. The $x_1 - \xi$ plane correspond to the unforced system. The segment connecting the 'upper' and 'lower' part of the surface denote unstable equilibrium points

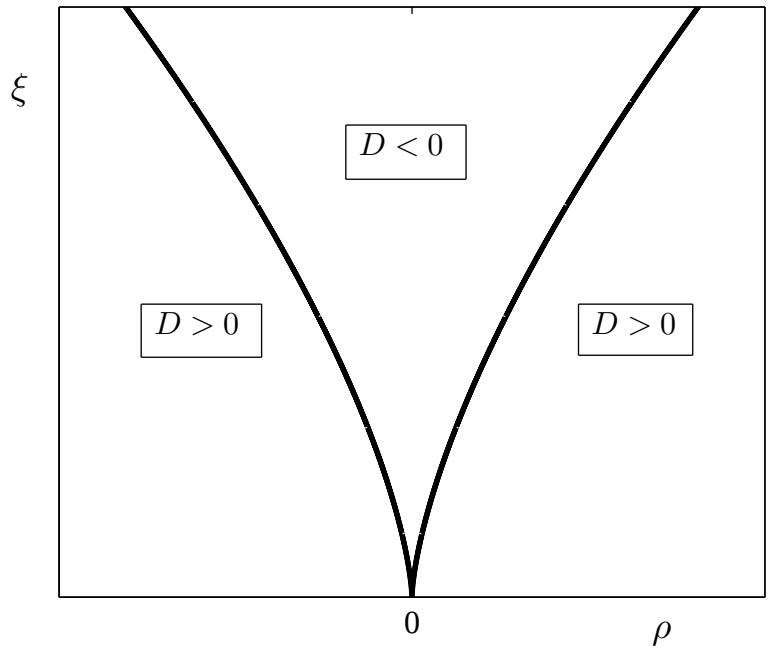

Figure 3.12: Bifurcation set for the parameters of the Duffing oscillator. In the region $D < 0$ there are three equilibrium points, whilst in the area where $D > 0$ only one. The lines mark the passage from one condition to the other and are the bifurcation points.

Chapter 4

Vibration isolation of a SDOF system with an HSLDS isolator: force transmissibility

'The important thing in science is not so much to obtain new facts as to discover new ways of thinking about them.'

Sir William Bragg (1862 - 1942)

4.1 Introduction

In Chapter 2 it was shown that by connecting elements with positive and negative stiffness in parallel it is possible to design a vibration isolation mount with a small dynamic stiffness without having to compromise its static load-bearing capability. This type of vibration isolator has been called a *high-static-low-dynamic stiffness* (HSLDS) isolator. Mechanisms with this characteristic have a nonlinear force-deflection curve, i.e. the stiffness varies with displacement. It was also shown that for small displacements about the static equilibrium position the restoring force can be linearised, and the stiffness of the HSLDS mount is smaller than that of its equivalent linear model. Nonetheless, should the assumption of small displacements not be applicable the system can no longer be considered to be linear and there is thus a need to study also the nonlinear dynamic response of the HSLDS system.

The aim of this chapter is to investigate the isolation performance of a single-degree-of-freedom (SDOF) system with an HSLDS isolation mount acted upon by a harmonic excitation force. A measure of the isolation properties of a system, in the frequency domain, is the absolute transmissibility. When the mass is excited by a harmonic force it is defined as the ratio of the force transmitted to a rigid base to the excitation force at a given frequency of excitation (*force transmissibility*). The dynamic analysis of a base excited HSLDS mechanism is carried out in the next chapter.

Studies that focus on passive nonlinear vibration isolators are generally based on the numerical solution of the system equations [62–64]. Here the quest is for analytical expressions that describe the performance of the isolator, i.e. peak-transmissibility and extension of the isolation region compared with that of a standard linear isolator model. Achieving this may help to improve the design of this type of isolator. To obtain these closed-form expressions, there is need to establish an analytical relationship between the response amplitude and the frequency of excitation. Herein, as in many practical problems, only the amplitude of the response at the excitation frequency is of interest. The forced response of a nonlinear system described by the Duffing equation (such as the HSLDS model), has been extensively studied, for example [44, 53, 57]. It features the *jump phenomenon*, which occurs because of the existence of bifurcation points at which the system response 'jumps' from one stable branch to another. Herein, for the sake of completeness, some known results on the dynamic stability of systems described by the Duffing equation are also included.

In this chapter, by solving the nonlinear differential equation of motion with the method of Harmonic Balance, simple, approximate formulae for the description of the jump phenomenon are proposed. These are subsequently used to describe the isolation properties of the HSLDS isolator. Finally, numerical simulations are performed and it is shown that the transmissibility of a HSLDS isolator compares favourably with that of an equivalent linear system.

4.2 Response to a harmonic force

In this section the equation of motion of a HSLDS isolator mount is shown to be of the form of Duffing's equation. The Duffing oscillator was a milestone of nonlinear dynamics [65] and has been extensively studied over the past 9 decades. A collection of the conclusions of the studies of interest to this thesis is presented and discussed.

Fig. 4.1 is a schematic representation of a SDOF system with an HSLDS mount and viscous damping. A mass m is suspended on a dashpot c and a nonlinear mount with HSLDS characteristic, k_{HSLDS}. As shown in Chapter 2, the restoring force can be expressed approximately as

$$f_{k_{\text{HSLDS}}} = k_1\, x + k_3\, x^3 \tag{4.1}$$

It is very important to recall that if the elements with negative stiffness (which confer the desired HSLDS characteristic) are removed, i.e. $k_3 = 0$, the isolator becomes a standard linear model with stiffness $k_l \neq k_1$. If the mass of the system shown in Fig. 4.1 is excited by a harmonic force $f_e = F_e\, \cos(\omega\, t)$ the equation of motion of the HSLDS model is

$$m\ddot{x} + c\dot{x} + k_1\, x + k_3\, x^3 = F_e\, \cos(\omega\, t) \tag{4.2}$$

where k_1 and k_3 are the coefficients of the linear and nonlinear terms of the cubic restoring force respectively, and the sign of k_3 denotes the stiffness behaviour, hardening (+) or softening (-). It is helpful to nondimensionalise Eqn.(4.2), so that

$$\hat{x}'' + 2\,\zeta\,\hat{x}' + \hat{x} + \alpha\,\hat{x}^3 = \cos(\Omega\,\tau) \tag{4.3}$$

where:

$$\zeta = \frac{c}{2m\omega_n} \qquad \omega_n^2 = \frac{k_1}{m} \qquad \alpha = \frac{k_3\, x_0^2}{k_1} \qquad \Omega = \frac{\omega}{\omega_n} \qquad \tau = \omega_n\, t$$

$$\hat{x}'' = \frac{\ddot{x}}{\omega_n^2\, x_0} \qquad \hat{x}' = \frac{\dot{x}}{\omega_n\, x_0} \qquad \hat{x} = x/x_0$$

with the symbol '$\prime$' denoting differentiation with respect to the nondimensional time τ and

$$x_0 = \left.\frac{F_e}{k_1}\right|_{k_3=0,\,\omega=0}$$

It is noteworthy that ω_n *is not* the natural frequency of the HSLDS system but is a characteristic frequency which is the natural frequency of the linearised HSLDS isolator, i.e. when the amplitude of oscillations are small enough to make $\alpha\,\hat{x}^2 \ll 1$. Note also that α is a factor related to the type and degree of non-linearity. Besides, α also takes into account the magnitude of the applied force because of its dependency on the displacement x_0. The role played by the sign of α is qualitatively shown in Fig. 4.2. When α is negative the FRF curve bends to the left, marking a softening behaviour. When $\alpha = 0$ the system becomes linear and the FRF assumes its standard shape with a peak at $\Omega = 1$ (when damping is small). Finally, as α is made positive, the plot leans over to the right because of its hardening characteristic. In the next section a detailed procedure to obtain the curves of Fig. 4.2 is illustrated.

4.2.1 Approximate periodic solution

As discussed in Chapter 3, there are several analytical methods that enable one to obtain an approximate solution of Eqn.(4.3). In this thesis the method used to seek an approximate solution is that of the Harmonic Balance. The basic assumption is that the system responds predominantly at the excitation frequency, i.e. the response is assumed to be harmonic at the excitation frequency. Thus,

$$\hat{x} = \hat{X}\,\cos(\Omega\,\tau + \varphi) \tag{4.4}$$

where $\hat{X}$ is the amplitude and φ the phase of the response.

As shown in Section 3.4.2, the application of the HB method leads to the equation of the magnitude of the frequency response function (FRF), which can be written either as

$$\frac{9}{16}\,\alpha^2\,\hat{X}^6 + \frac{3}{2}\,(1-\Omega^2)\,\alpha\,\hat{X}^4 + \left[(1-\Omega^2)^2 + 4\,\zeta^2\,\Omega^2\right]\,\hat{X}^2 = 1 \tag{4.5}$$

or as

$$\Omega^4 - 2\left[1 + \frac{3}{4}\,\alpha\,\hat{X}^2 - 2\,\zeta^2\right]\,\Omega^2 + \left[\left(1 + \frac{3}{4}\,\alpha\,\hat{X}^2\right)^2 - \frac{1}{\hat{X}^2}\right] = 0 \tag{4.6}$$

which, for given ζ and α, relate the frequency and the amplitude of the response.

Thus the FRF can be seen either as a cubic function of the amplitude squared $\hat{X}^2$ or a quadratic in Ω^2. The values of $\hat{X}$ that satisfy Eqn.(4.5) are equilibrium points of the system. However, it will be shown shortly that not all of them are stable.

The equation of the FRF magnitude expressed as a quadratic in Ω^2, as in Eqn.(4.6), can be solved analytically and the two positive roots are, [66]

$$\Omega_1 = \sqrt{\left(1 + \frac{3}{4}\alpha\,\hat{X}^2 - 2\,\zeta^2\right) - \frac{1}{\hat{X}}\sqrt{1 - 4\,\zeta^2\,\hat{X}^2\left(1 - \zeta^2 + \frac{3}{4}\alpha\,\hat{X}^2\right)}} \tag{4.7a}$$

$$\Omega_2 = \sqrt{\left(1 + \frac{3}{4}\alpha\,\hat{X}^2 - 2\,\zeta^2\right) + \frac{1}{\hat{X}}\sqrt{1 - 4\,\zeta^2\,\hat{X}^2\left(1 - \zeta^2 + \frac{3}{4}\alpha\,\hat{X}^2\right)}} \tag{4.7b}$$

In order to extract simple expressions, throughout this chapter, it is assumed that the damping is small, i.e. $\zeta^2 \ll 1$. This assumption is legitimate in many practical cases. If the radicand of the nested square root is negative then Ω_1 and Ω_2 become complex. Thus, for Ω_1 and Ω_2 to be positive, the following condition has to hold

$$3\alpha\,\hat{X}^4\,\zeta^2 + 4\,\zeta^2\left(1 - \zeta^2\right)\,\hat{X}^2 - 1 \leq 0 \tag{4.8}$$

which implies that, for a given damping ratio and coefficient of the nonlinear term, Eqn.(4.8) can be solved for the response amplitude to give four values of $\hat{X}$. The solutions of interest are when

$$\hat{X} \leq \hat{X}_{max} \tag{4.9}$$

where

$$\hat{X}_{max} \approx \sqrt{\frac{2}{3\,\alpha}\left[\sqrt{1 + \frac{3\,\alpha}{4\,\zeta^2}} - 1\right]} \tag{4.10}$$

In case of softening system, i.e. $\alpha < 0$, Eqn.(4.10) is real only if

$$|\alpha| \leq |\alpha|_{max} \tag{4.11}$$

with

$$|\alpha|_{max} = \frac{4}{3}\,\zeta^2 \tag{4.12}$$

Note that throughout this chapter the condition expressed by Eqn.(4.12) will be

used as limiting value for the coefficient of the nonlinear term of the Duffing equation. Eqn.(4.12) expresses the fact that, when a softening system with a given damping ratio has too large a nonlinear coefficient, i.e. $|\alpha| > |\alpha|_{max}$, the two curves Ω_1 and Ω_2 never meet and the jump-down does not occur, [60].

When $\hat{X} = \hat{X}_{max}$ the nested square root in Eqns.(4.7) becomes zero and the two solutions are real and coincident, $\Omega_1 = \Omega_2 = \Omega_d$[a].

Fig. 4.3(a) is a plot of the curves given by Eqns.(4.7 a,b) with $\zeta = 0.01$ and $\alpha = 5.32 \times 10^{-4}$ as $\hat{X}$ is varied between 0 and $\hat{X}_{max}$. It shows the *jump phenomenon* that characterises the forced response of the Duffing oscillator [57, 66, 67]. When the frequency is increased from 0, the response amplitude increases following the upper branch, also called *resonant branch* [63], until the maximum value $\hat{X}_{max}$. This point corresponds to the *jump-down* frequency Ω_d. Any further increase of the frequency causes the response to 'jump' to the lower curve, also referred to as the *non-resonant branch* [63]. Similarly, if the frequency is decreased (in the limit from ∞), $\hat{X}$ follows the non-resonant branch until the *jump-up* frequency Ω_u. A further decrease of Ω triggers a sudden 'jump' up of the response to the resonant branch. Fig. 4.3(b) depicts the FRF of a system with softening nonlinearity. The jump phenomenon can also be observed, although in this case the order of the jumps is reversed: the response amplitude jumps up as the frequency is increased and jumps down when Ω is decreased.

4.2.2 Bifurcation and stability analysis

For the sake of completeness, this section illustrates an established technique for the determination of the unstable region of the FRF of a Duffing oscillator.

From both plots in Fig.4.3 it can be observed that the system has either one equilibrium point (up to Ω_u and after Ω_d) or three possible equilibrium states (between Ω_u and Ω_d). From the definition given in Section 3.5, it follows that Ω_u and Ω_d are bifurcation points of the frequency. When three equilibrium points co-exist, which one occurs depends on the initial conditions [44]. However, by applying a first order perturbation analysis it has been shown previously that

[a]The more complicated case of $\hat{X} < \hat{X}_{max}$ will be illustrated shortly

the points corresponding to the dashed line in the figure are unstable points, [57, 60, 68]. The principle behind this first order perturbation analysis is a direct application of the very concept of stability: a perturbation is applied to the response of the system and its evolution in time is studied. If the equilibrium point is stable, it will return to its initial position; if it is unstable it will move away from it.

Introducing a small perturbation ε so that, near the periodic solution, the response of the system is given by

$$\hat{x} = \hat{X}\,\cos(\Omega\,\tau + \varphi) + \varepsilon = \hat{X}\,\cos(\theta) + \varepsilon \tag{4.13}$$

Applying first order perturbation analysis, which means neglecting terms of order higher than those $O(\varepsilon^2)$, and assuming a harmonic response, i.e. neglecting higher order harmonics in the response, the motion of the system is expressed in terms of the perturbation as [68]

$$\varepsilon'' + 2\,\mu\,\varepsilon' + (p - 2\,q\,\cos\,2\theta)\,\varepsilon = 0 \tag{4.14}$$

with

$$\mu = \frac{\zeta}{\Omega} \tag{4.15a}$$

$$p = \frac{1}{\Omega^2}\left(1 + \frac{3}{2}\alpha\,\hat{X}^2\right) \tag{4.15b}$$

$$q = -\frac{3}{4}\frac{\alpha}{\Omega^2}\,\hat{X}^2 \tag{4.15c}$$

Eqn.(4.14) is known as Mathieu's equation [56, 68] and has been extensively studied, [45, 56, 68]. Thus, the stability of the equilibrium points of the Duffing equation coincides with the stability of the Mathieu equation. Using a linear perturbation analysis it is shown in reference [68] that the solution of Eqn.(4.14) is unstable if it lies outside the parabola

$$p = 1 \pm \sqrt{q^2 - 4\,\mu^2} \tag{4.16}$$

By substituting Eqns.(4.15 a,b,c) into Eqn.(4.16) the region of instability is found

to be enclosed by the curves

$$\Omega_{unst_1} = \sqrt{1 - 2\,\zeta^2 + \frac{3}{2}\,\alpha\,X^2 - 2\sqrt{\left(\frac{3}{8}\,\alpha\,X^2 + \zeta^2\right)^2 + \zeta^2\left(\frac{3}{4}\,\alpha\,X^2 - 1\right)}} \quad (4.17a)$$

$$\Omega_{unst_2} = \sqrt{1 - 2\,\zeta^2 + \frac{3}{2}\,\alpha\,X^2 + 2\sqrt{\left(\frac{3}{8}\,\alpha\,X^2 + \zeta^2\right)^2 + \zeta^2\left(\frac{3}{4}\,\alpha\,X^2 - 1\right)}} \quad (4.17b)$$

Eqns.(4.17 a,b) are plotted in Fig. 4.4 for both softening (a) and hardening (b) systems together with the FRF. As expected the unstable equilibrium points fall between the jump frequencies Ω_u and Ω_d. It is also shown that the unstable branch is the one between the upper (resonant) and lower (non-resonant) curves. In reference [54] it is shown that, because the trace of the Jacobian matrix is zero, the equilibrium points of the Duffing equation are either stable centres or unstable saddle points (see Section 3.3 and Fig. 3.4). Fig. 4.5 shows the nature of the equilibrium points for a softening system as an example, but the case of a hardening stiffness is identical.

4.3 The jump frequencies

Because of the crucial role played by the jump frequencies on the dynamic response of a Duffing oscillator, it is desirable to seek some simple analytical expressions which allow the prediction, at least within engineering approximation, of these frequencies. These expressions will facilitate a better understanding of the physics of the HSLDS isolator, and the role played by the damping ratio and the coefficient of the nonlinear term. Besides, they are of paramount importance for the evaluation of the performance of a vibration isolator with HSLDS characteristic.

In the literature it is possible to find several references in which analytical expressions for the jump frequencies are proposed. Magnus [66] gives an expression for the jump-down frequency but does not provide one for the jump-up. In reference [69], Hagedorn solves the nonlinear equation of motion with the HB method and finds the frequency of vertical tangency of the FRF (jump frequencies) expressed as function of the response amplitude. Hayashi [57] also used the HB

method to derive the frequency response of the harmonic oscillation. Then, while studying the stability of the periodic solutions he considered the Mathieu equations and derived implicit expressions for the point of vertical tangency. Friswell and Penny [59] computed the jump-frequencies using a numerical approach based on Newton's method. Worden [61] considered the FRF expressed as a cubic function in the square of the amplitude, Eqn.(4.5), and computed the frequencies that set the discriminant to zero. Also, in this case a numerical technique was needed to solve a 10-th order equation. Some recent work on the calculation of the jump frequencies has been carried out by Malaktar and Nayfeh [70]. Although their primary concern was to establish what is the minimum forcing amplitude required for the nonlinear 'jump' phenomenon to appear, they also proposed a method for the calculation of the jump frequencies by using a numerical technique based on the Gröbner basis method.

It appears that since Duffing's original paper [65], a consistent method for the calculation of the jump frequencies and congruous reference trail from the earlier analytical works to the modern numerical studies would benefit the engineering community. One of the contributions of this thesis is to present simple explicit analytical expressions for the jump-up and jump-down frequencies for a softening and a hardening system with linear viscous damping and the corresponding response amplitudes, in consistent manner, and presenting the results in a compact form with particular emphasis on the physical behaviour of the system.

The jump-down frequency can be assumed to be the frequency at which $\hat{X} = \hat{X}_{max}$. In fact, the difference between this frequency at that of vertical tangency to the resonant branch is small and decreases as damping is decreased, [63]. This is shown in Fig. 4.3(a,b). When $\hat{X} \approx \hat{X}_{max}$ the two curves expressed by Eqns.(4.7) are equal and are given by

$$\Omega_d = \sqrt{\frac{3}{4}\alpha\,\hat{X}_{max}^2 + (1 - 2\,\zeta^2)} \tag{4.18}$$

By substituting Eqn.(4.10) into (4.18), and because of the assumption $\zeta^2 \ll 1$ a simple expression for Ω_d can be found, which is

$$\Omega_d \approx \frac{1}{\sqrt{2}}\sqrt{1 + \sqrt{1 + \frac{3\,\alpha}{4\,\zeta^2}}} \tag{4.19}$$

Fig.4.6 shows the FRF of a softening Duffing system with $\alpha = -1.33 \times 10^{-4} = -5\,\alpha_{max}$ ($\zeta = 0.01$). Increasing the frequency (from zero) the jump-up occurs at frequency Ω_u. However, if the frequency is reduced (in the limit from ∞) the amplitude of the response increases, without the advent of the typical jump down, until the frequency becomes zero. Because of the definition of the parameter α, this phenomenon is exacerbated when the system is strongly nonlinear and/or for high amplitudes of excitation.

Expressions for the jump-up frequency, Ω_u, can be found in references [69] and [71]. In the former, Ω_u is expressed as function of the nonlinear coefficient and amplitude of response; the expressions given in the latter reference are instead obtained by applying a perturbation analysis and based on the assumption that damping, nonlinear coefficient and forcing amplitude are small parameters. Figures 4.7(a) and 4.7(b) show the FRF curves of a hardening and a softening system respectively for a fixed value of α in each case and two different damping ratios. It can be observed that the jump up frequency is mostly unaffected by changing ζ. This observation can be exploited for the search of an approximate analytical expression for the jump-up frequency, Ω_u. Note that this can be found by imposing the condition of vertical tangency to the non-resonant branch. When $\alpha < 0$ (softening mount) the non-resonant branch is Eqn.(4.7a). The point with vertical tangent if found by setting $\zeta = 0$ (because it is assumed that it is independent of damping), and imposing

$$\left.\frac{d\,\Omega_1}{d\hat{X}}\right|_{\zeta=0} = \frac{3\,\alpha\,\hat{X}^3 + 2}{2\,\hat{X}\sqrt{\hat{X}\left(3\,\alpha\,\hat{X}^3 + 4\,\hat{X} - 4\right)}} = 0\,, \qquad \alpha < 0 \tag{4.20}$$

If $\alpha > 0$ (hardening system) the vertical tangent to the non-resonant branch, Eqn.(4.7b), is found by setting

$$\left.\frac{d\,\Omega_2}{d\hat{X}}\right|_{\zeta=0} = \frac{3\,\alpha\,\hat{X}^3 - 2}{2\,\hat{X}\sqrt{\hat{X}\left(3\,\alpha\,\hat{X}^3 + 4\,Y + 4\right)}} = 0\,, \qquad \alpha > 0 \tag{4.21}$$

Solving both Eqns.(4.20) and (4.21) for $\hat{X}$ gives

$$\hat{X}_u = \left(\frac{2}{3\,|\alpha|}\right)^{1/3} \tag{4.22}$$

The expressions for the jump-up frequencies can be determined by substituting Eqn.(4.22) into Eqns.(4.7a) and (4.7b) to give respectively

$$\Omega_{u_h} \approx \sqrt{1 + \left(\frac{3}{2}\right)^{4/3} |\alpha|^{1/3}} \tag{4.23a}$$

$$\Omega_{u_s} \approx \sqrt{1 - \left(\frac{3}{2}\right)^{4/3} |\alpha|^{1/3}} \tag{4.23b}$$

where the subscripts h and s stand for hardening and softening respectively. Eqn(4.23a,b) are the same as the expressions provided in [71].

In order to assess the correctness of the analytical expressions proposed, a comparison with numerical results is carried out. The jump frequencies calculated with the analytical expressions proposed, Eqns. (4.19), (4.23b) and (4.23a) are compared with the results obtained by numerical integration of Eqn.(4.3) with the 4-th order Runge-Kutta method (Matlab® built-in solver ODE45). For this analysis, two different values of damping are used, $\zeta = 0.02$ and $\zeta = 0.05$. For the numerical solution α is varied discretely, that is $\alpha = n\,\alpha_{max}$ with $n = -1, -0.5, 0, 1, 2, 3, 4, 5$ for each value of ζ. The analytical curves have been plotted by changing α (with a step $\Delta\alpha = 10^{-5}$) between $-\alpha_{max}$ and $5, \alpha_{max}$.

The comparison between the numerical and analytical values of the jump frequencies is shown in Fig. 4.8. From Fig. 4.8(a) it is possible to see that the numerical results for the jump-up frequency, Ω_u have a weak dependence of on damping. The analytical expressions for of the jump-up frequency, $\Omega_u(\alpha)$, are Eqns.(4.23b) and (4.23a). These are superimposed with the numerical results for comparison and are, of course, independent of damping.

The jump-down frequencies as a function of α are calculated using the analytical expression Eqns.(4.19). The corresponding numerical results are plotted in Fig.4.8(b). It can be seen that, in this case, the jump frequencies are heavily dependent upon damping.

Avoidance of the jump The jump phenomenon, especially the jump-up, has potentially catastrophic effects. For this reason there is interest in determining

the combination of parameters that ensures this event does not take place [64, 72]. In general, it can be expected that the jump does not occur for a small enough excitation. Malatakar and Nayfeh [70] have found a critical value of the forcing amplitude that prevents the appearance of the jump by calculating the point of inflection of the frequency response curve where there are three real and coincident solutions. Unlike the study described in reference [70], in this chapter the forcing amplitude is embedded in the coefficient of the nonlinear term α. Nonetheless, a correspondence between the different notation used can be found and the results therein obtained can be transposed in terms of the variables defined in this thesis. In particular, the expression provided in [70] for a jump *not* to occur corresponds to the condition

$$|\alpha| = |\alpha_{cr}| < \frac{2^8}{3^{5/2}}\,\zeta^3 \tag{4.24}$$

Fig.4.9 depicts a softening and a hardening system with a nonlinear coefficient set to its critical value, defined by Eqn.(4.24). In order to mark the absence of the jump both curves have been plotted with solid lines.

4.4 Force transmissibility

The *transmissibility* is a measure of the reduction of the vibrations transmitted from a source to a receiver, i.e. it is an index of the performance of an isolator. Mathematically, the transmissibility is defined in the frequency domain and is the ratio between the magnitude of the transmitted and excitation force at a given frequency. As illustrated in Chapter 1, in a linear system this ratio is the same whether the source of the disturbance is a force acting on the suspended mass (force transmissibility) or whether the base is excited (motion transmissibility). However, this is not the case for a nonlinear system. This section concerns the force transmissibility only. The aim is to compare the isolation performance of a HSLDS mount with that of the equivalent linear isolator.

Fig. 4.1 depicts a SDOF model of an HSLDS isolator. The harmonic excitation force (source) acting on the mass is $f_e = F_e\,\cos(\omega\,t)$. The force transmitted to the base (receiver) is $f_t = F_t\,\cos(\omega\,t + \varphi_t)$. By definition the absolute transmissibility is

$$|T_a| = \frac{F_t}{F_e} \tag{4.25}$$

Expressing the equation of motion in nondimensional form as in Eqn.(4.3), the nondimensional transmitted force – through the spring and the dashpot – is

$$\hat{f}_t = 2\,\zeta\,\hat{x}' + \hat{x} + \alpha\,\hat{x}^3 \tag{4.26}$$

where $\hat{f}_t = (c\,x + k_1\,x + k_3\,x^3)/(k_1\,x_0)$. Being interested in the response at the excitation frequency only, as expressed by Eqn.(4.4), the transmitted force can be written as

$$\hat{f}_t = -2\,\zeta\,\Omega\,\hat{X}\,\sin\,\theta_t + \left(\hat{X} + \frac{3}{4}\,\alpha\,\hat{X}^3\right)\,\cos\,\theta_t = A\,\sin\,\theta_t + B\,\cos\,\theta_t \tag{4.27}$$

where $\theta_t = \cos(\Omega\,\tau + \varphi_t)$.

Thus, the magnitude of the transmitted force is, [63]

$$\hat{F}_t = \sqrt{A^2 + B^2} \tag{4.28}$$

On the other hand, from Eqn.(4.2), the nondimensional magnitude of the applied force is $\hat{F}_e = 1$. It follows that the magnitude of the force transmissibility is

$$|T_a| = \hat{F}_t = \hat{X}\,\sqrt{\left(1 + \frac{3}{4}\,\alpha\,\hat{X}^2\right)^2 + 4\,\zeta^2\,\Omega^2} \tag{4.29}$$

Fig.4.10 shows a typical plot of the force transmissibility. The transmissibility of a hardening system with $\zeta = 0.01$ and $\alpha = 10^{-4}$ is plotted in Fig. 4.10(a). The transmissibility of a system with softening nonlinearity with $\zeta = 0.01$ and $\alpha = -10^{-4}$ is instead shown in Fig. 4.10(b). Note that the curves have been obtained by substituting Eqns.(4.7) into Eqn.(4.29) and letting $\hat{X}$ vary between 0 and $\hat{X}_{max}$.

4.4.1 Peak transmissibility

It can be argued that there are two indices to measure the effectiveness of a vibration isolator: one is the bandwidth of the isolation region, which is the frequency region within which the transmitted force becomes smaller than the excitation force, that is when $|T_a| < 1$[b]; the other is the peak-transmissibility, which is the maximum amplitude of the transmitted force for a given amplitude of the input

[b]For a linear system this begins at $\sqrt{2}$ time the natural frequency [1, 3]

force.

In order to find an expression for the maximum transmissibility, the maximum amplitude response, $\hat{X}_{max}$, and the jump-down frequency Ω_d, equal to a very good approximation to Eqns.(4.10) and (4.19) respectively, are substituted into Eqn.(4.29). The resulting expression, valid for small damping, $\zeta^2 \ll 1$, is

$$|T_a|_{max} \approx \frac{1}{2\sqrt{2}\,\zeta}\sqrt{1+\sqrt{1+\frac{3\,|\alpha|}{4\,\zeta^2}}} \tag{4.30}$$

Recall that for a linear system the peak-transmissibility is given by, [1, 3]

$$|T_a|_{max(linear)} \approx \frac{1}{2\,\zeta} \tag{4.31}$$

It should also be noted that the expression for the peak transmissibility of a non-linear isolator with symmetric cubic restoring force given by Eqn.(4.30), reduces to that of a linear system Eqn.(4.31) when $\alpha = 0$.

4.4.2 Comparison between the transmissibility of an HSLDS mechanism and an equivalent linear isolator

In order to assess the vibration isolation performance of an HSLDS mount, its transmissibility is now compared with that of an equivalent linear model.

As discussed in Chapter 2, the principle behind an HSLDS mechanism, is to combine elements with constant positive stiffness (e.g. a mechanical spring) with others that have negative stiffness (e.g. oblique linear springs or attracting magnets). As previously said, the equivalent linear model is the HSLDS system with the negative stiffness elements removed.

For the HSLDS mechanisms studied in Sections 2.3.1 and 2.6.1 the restoring force can be approximated by a cubic polynomial with positive (hardening) or negative (softening) cubic coefficient. It is important to observe that examining Eqns.(2.22) and (2.53) the linear term of the restoring force has the form

$$k_1 = \beta^2\,k_l \tag{4.32}$$

where k_l is the stiffness of the element with positive stiffness, i.e. the stiffness of the equivalent linear isolator, and $0 < \beta^2 < 1$ depends on the type of negative stiffness mechanism. If there were no mechanism with negative stiffness then $\beta = 1$ and, of course, $k_1 = k_l$ and $k_3 = 0$. This observation is important when comparing the transmissibility curves of a linear and a HSLDS isolator. In fact, the dynamic properties of the HSLDS isolation mount (jump frequencies, maximum transmissibility, etc) have been derived in terms of the nondimensional parameters of Eqn.(4.3). A key parameter in the nondimensionalisation is the characteristic frequency $\omega_n^2 = k_1/m$ which is clearly different for a linear and a HSLDS system. In particular, for a linear system

$$\omega_l = \sqrt{\frac{k_l}{m}} \tag{4.33}$$

whilst for an HSLDS mount is

$$\omega_n = \sqrt{\frac{\beta^2\, k_l}{m}} = \beta\, \omega_l \tag{4.34}$$

As a consequence, the value of the damping ratio also changes between a linear and a HSLDS isolator. The damping ratio of a linear system is given by

$$\zeta_l = \frac{c}{2\, m\, \omega_l} \tag{4.35}$$

whereas for an HSLDS model is

$$\zeta = \frac{c}{2\, m\, \omega_n} = \frac{\zeta_l}{\beta} \tag{4.36}$$

Eqns.(4.34) and (4.36) can be seen as 'scaling laws', by means of which the transmissibility curves of the HSLDS and linear isolator models can be plotted on the same graph.

Recall that for a linear system, the transmissibility is, [3]

$$|T_a|_{(linear)} = \sqrt{\frac{1 + 4\,\zeta_l^2\,\Omega_l^2}{\left(1 - \Omega_l^2\right)^2 + 4\,\zeta_l^2\,\Omega_l^2}} \tag{4.37}$$

where the nondimensional frequency ratio is $\Omega_l = \omega/\omega_l$.
On the other hand, the transmissibility of the HSLDS mount is given by Eqn.(4.29)

where $\Omega = \omega/\omega_n$ or

$$\Omega_l = \Omega\,\beta \tag{4.38}$$

For sake of consistency, when plotting the transmissibility of a HSLDS and a linear isolator on the same graph, the values on the frequency axis have to comply with Eqn.(4.38). Fig. 4.11(a) shows the comparison between the transmissibility curves of a linear system with $\zeta_l = 0.005$ and that of a hardening HSLDS isolator. For this example $\beta = 0.5$ and $\alpha = 10^{-4}$. These values have not only a purely numerical meaning. As it will be shown in Chapter 6, $\beta = 0.5$, i.e. halving the natural frequency of the linear model, is feasible in practice. Also such a small value of α can be justified. In fact, the experimental measurements show that, for low excitation level, the cubic term can be neglected altogether; furthermore, for a softening system the nonlinear coefficient cannot be larger than a certain value dictated by Eqn.(**??**), which, for small damping, is a rather small number.

Because the frequency ratio on the x-axis is $\Omega_l = \omega/\omega_l$, the value of Ω used to compute the transmissibility of the HSLDS system, given by Eqn.(4.29), had to be scaled according to Eqn.(4.38). As expected, the transmissibility of the linear system reaches its peak value of $1/2\zeta = 100$ at $\Omega_l = 1$. To appreciate the benefit offered by the HSLDS isolator, the transmissibility curves of Fig. 4.11 have been plotted on a decibel scale in Fig. 4.12. The wider range of the frequency isolation region and the reduction of the peak transmissibility are clearly visible. From both Figures 4.11(a,b) and 4.12(a,b) it can be seen that the HSLDS mount does indeed offer better isolation performance than its equivalent linear model. The peak value is smaller and the isolation region is extended.

However, it is worthy to remember that the 'bend' of the transmissibility curve depends on the coefficient of the nonlinear term α which, in turn, depends on the amplitude of the applied force and the coefficient of nonlinearity, k_3. If a system with a hardening HSLDS mount is subject to large amplitudes of excitation or has a strong nonlinearity, its transmissibility curve might intersect and even go beyond that of the linear mount[c]. In order to set a criterion for comparing the isolation performance, it can be argued that the benefits of a HSLDS mount cease when the jump-down frequency coincides with the natural frequency of its equivalent linear model. The limiting value of α can be thus found by imposing

[c]For a softening system this issue does not exist.

that

$$\beta\,\Omega_d = 1 \tag{4.39}$$

If it is assumed that $\zeta^2 \ll 1$, substituting Eqn.(4.19) in Eqn.(4.39) and solving for α yields

$$\alpha_{lim} = \frac{16}{3}\frac{\zeta^2\,(1-\beta^2)}{\beta^4} \tag{4.40}$$

Fig. 4.13 shows the transmissibility curves of an HSLDS with $\beta = 0.5$ and $\zeta = 0.01$ when $\alpha = \alpha_{lim} = 0.0065$ and $\alpha = 2\,\alpha_{lim} = 0.013$. It can be seen that when $\alpha = \alpha_{lim}$ the jump-down frequency is equal to the natural frequency. The figure also shows that when $\alpha = \alpha_{lim}$ the linear and HSLDS isolator mounts have the same peak-transmissibility.

4.5 Conclusions

An isolation mount with HSLDS characteristics is a nonlinear system. However, if it is possible to assume that only small oscillations about its static equilibrium position take place, then it is possible to linearise its equation of motion. In this case, a lower natural frequency and the consequent extended frequency isolation region confer to the HSLDS isolator outstanding isolation performance.

Nonetheless, it is necessary to carry out a nonlinear analysis in order to include the case in which the amplitude of displacement become too large and the hypothesis of linear response no longer holds true. The dynamic response to a harmonic excitation force of a system with symmetric cubic restoring force harmonically force has been long studied and many references can be found in the literature. Fewer works instead focus on the isolation properties of this kind of system. Nonetheless, the study presented in this chapter has added some new results to the available knowledge.

The periodic response of the system at the excitation frequency using the Harmonic Balance, characterised by the known jump phenomenon, has been investigated. In addition to the information already present in the literature, the assumptions used have made it possible to derive simple expressions for the jump frequencies in a consistent manner. The accuracy of these expressions has been 'validated' by comparison with the numerical solution of the equation of motion.

The jump-down frequency is heavily dependent upon the damping ratio, whilst the jump-up frequency is unaffected by a change in the dissipative properties of the system.

A new expression for the maximum transmissibility has also been proposed. The expression found shows that the maximum transmitted force reduces with damping: besides this new analytical expression collapses to the known expression of maximum transmissibility of a linear isolator when the coefficient of the nonlinear term is set to zero. Finally, the numerically-generated transmissibility curves of a HSLDS isolation mount and that of equivalent standard linear model have been compared. In order to carry out the comparison, the equivalent linear model has been defined as the HSLDS system without the elements with negative stiffness. By plotting the transmissibility curves of the two systems on the same graph it been possible to appreciate the advantages of an HSLDS isolation mount, in terms of extension of the isolation region and the reduction of the maximum transmissibility.

It is noticeable that the magnitude of the nonlinear coefficient determines how much the transmissibility curve bends to the left (softening) or to the right (hardening). Of particular interest is the case of a hardening system because a strong nonlinearity may become detrimental for isolation purposes. As an arbitrary criterion to relate and compare directly the isolation performance of an HSLDS against a linear isolator, it has been argued that if the jump-down frequency coincides with the natural frequency of the equivalent linear model the small gain in the extension of the isolation region is outweighed by the manufacturing and computational complications introduced by a HSLDS mount. The value of nonlinear coefficient that prevents this from occurring has been shown to be proportional to the square of the damping ratio. In conclusion it is advantageous to employ a HSLDS isolator as long as the excitation level or the degree of nonlinearity is not strong enough to render the nonlinear coefficient greater than a specific value.

Following a similar pattern, the next chapter will focus on the isolation characteristics of an HSLDS isolation system excited at the base.

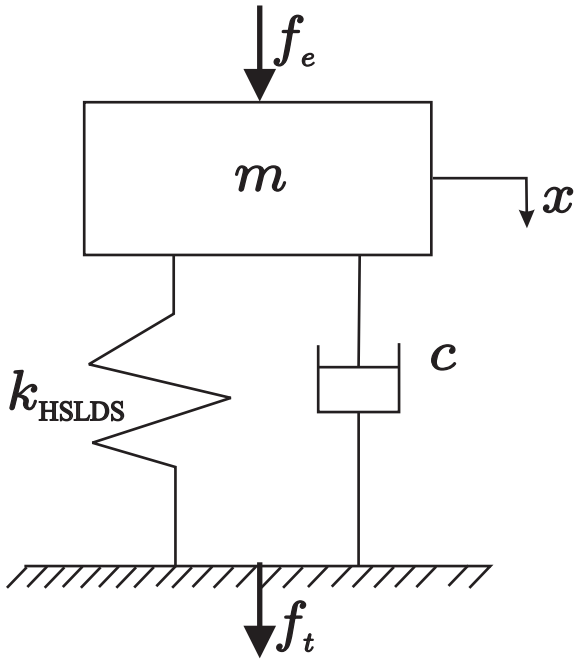

Figure 4.1: Single-degree-of-freedom system with an HSLDS mount with viscous damping: a mass m is suspended on a dashpot c in parallel with a nonlinear spring with HSLDS k_{HSLDS}. The excitation force acting on the mass is $f_e = F_e \cos \omega t$. f_t is the force transmitted to the base through the spring and the dashpot

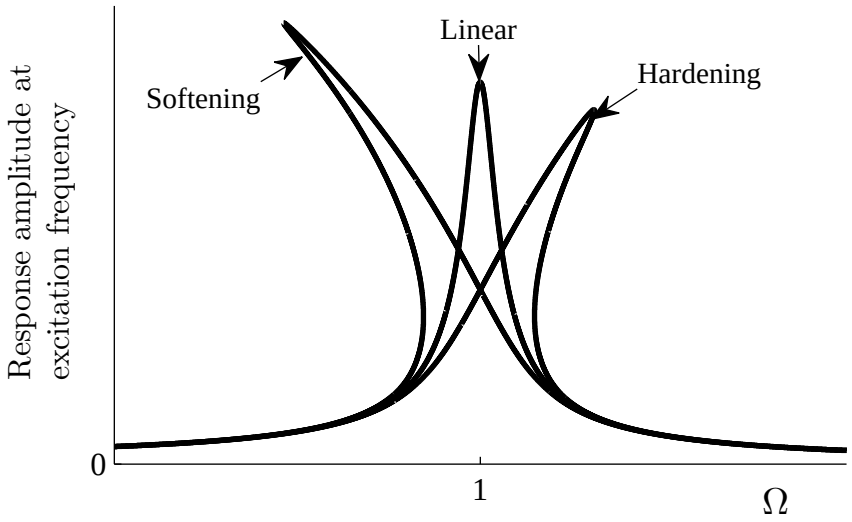

Figure 4.2: Frequency response function of the Duffing oscillator described by Eqn.(4.3). The sign of the cubic coefficient defines a softening (-) or hardening (+) behaviour. When $\alpha = 0$ the system becomes linear

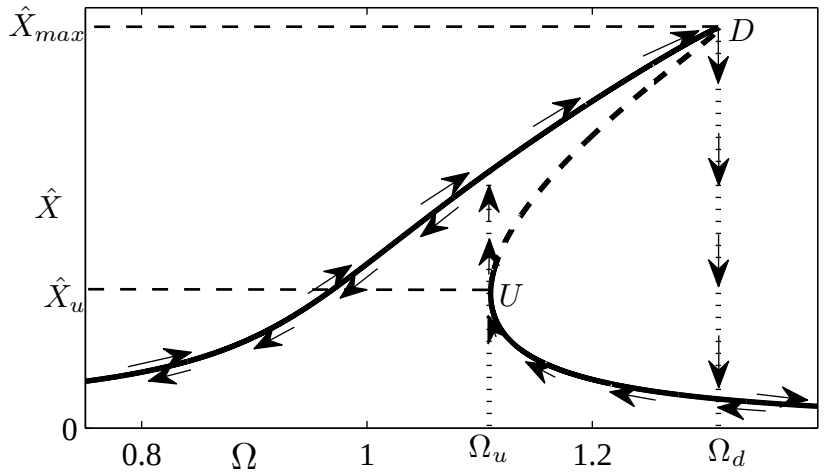

(a) $\alpha = 5.32 \times 10^{-4}$

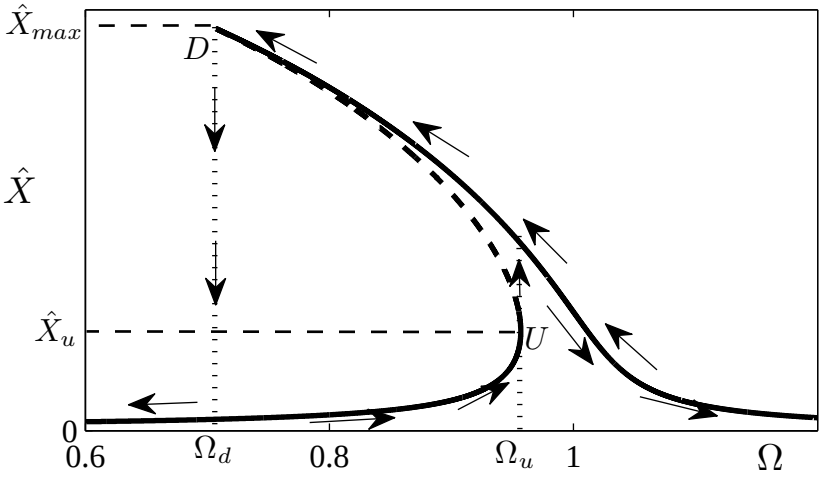

(b) $\alpha = -1.33 \times 10^{-4}$

Figure 4.3: Plot of the frequency response of the Duffing oscillator, given by Eqns.(4.7) with $\zeta = 0.01$. Hardening system (a): as the frequency is increased the amplitude increases following the upper or *resonant* curve. At the frequency Ω_d, marked with the letter D, it suddenly drops to the lower or *non-resonant* branch. Similarly, decreasing the frequency, the response follows the non-resonant branch until the frequency Ω_u, marked with the letter U. A further decrease in frequency causes the response to jump up to the resonant branch. When the system has a softening spring, (b), the jump down occurs by decreasing the frequency and the jump up increasing the frequency. The dashed line denotes unstable equilibrium points. This part of the curve cannot be observed experimentally

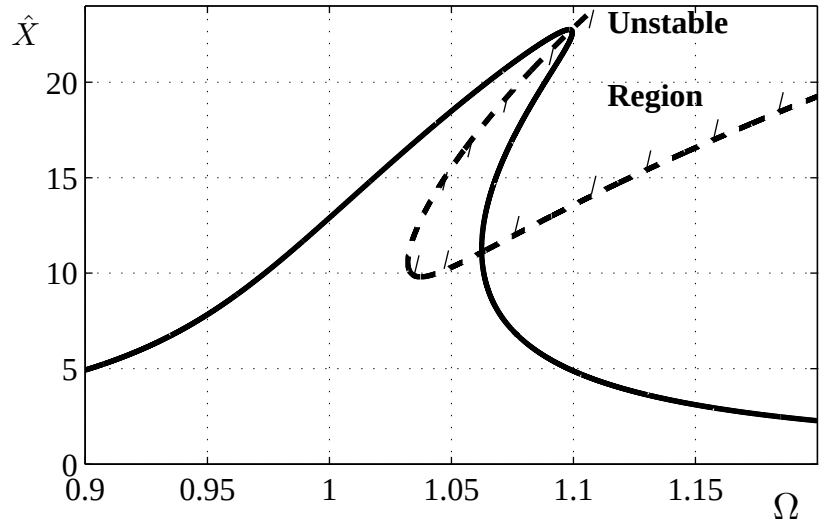

(a) $\alpha = 5.33 \times 10^{-4}$

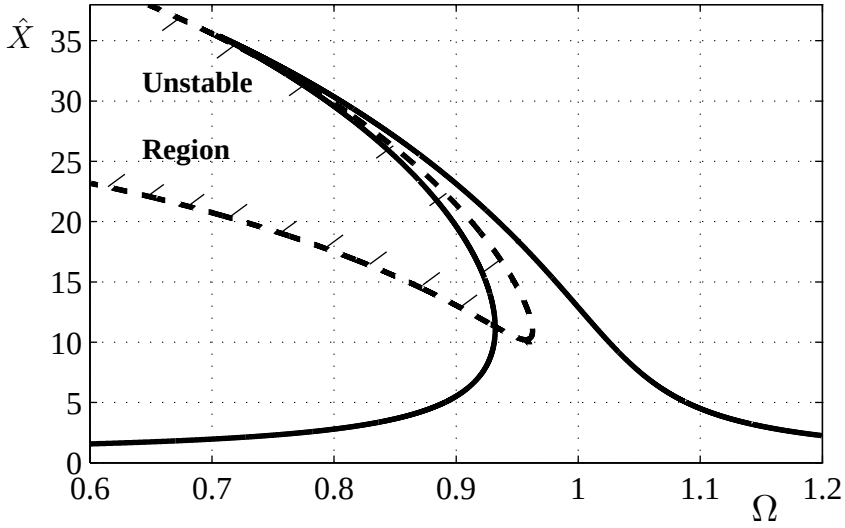

(b) $\alpha = -1.33 \times 10^{-4}$

Figure 4.4: Stability analysis of the forced response of the Duffing equation using a linear perturbation method. For both hardening (a) and softening systems (b) $\zeta = 0.02$. The part of the FRF included in the unstable region denotes unstable equilibrium points and is the branch between the resonant and non-resonant curves

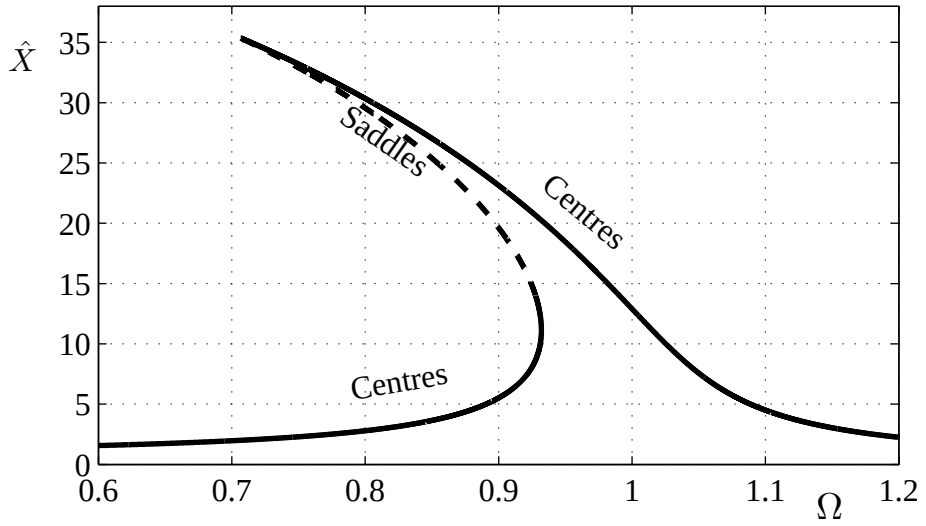

Figure 4.5: Nature of the equilibrium points of the FRF of a Duffing equation with softening nonlinearity. The stable points are centres, whilst the unstable points are saddles

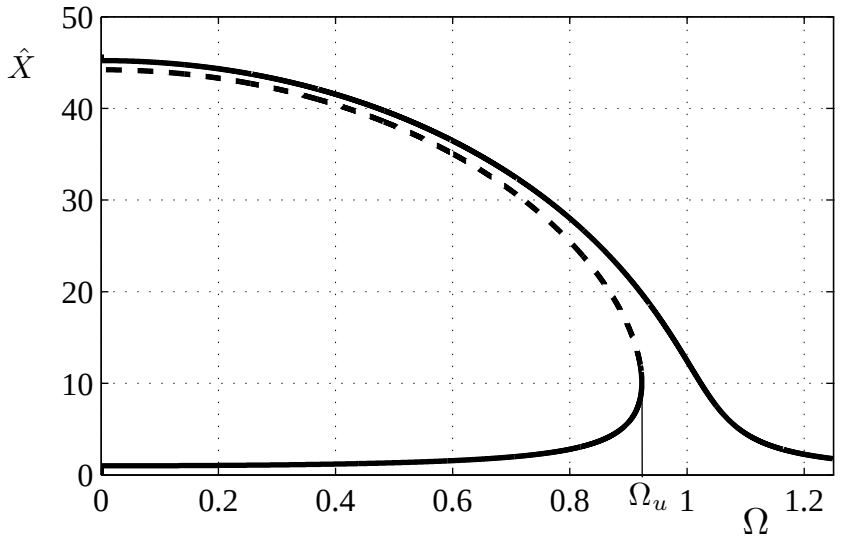

Figure 4.6: FRF of a softening system with $\alpha = 1.33 \times 10^{-4} = -5\,\alpha_{max}$ and $\zeta = 0.01$. The jump-down phenomenon does not take place, but as the frequency is decreased the response follows the resonant curve until $\Omega = 0$

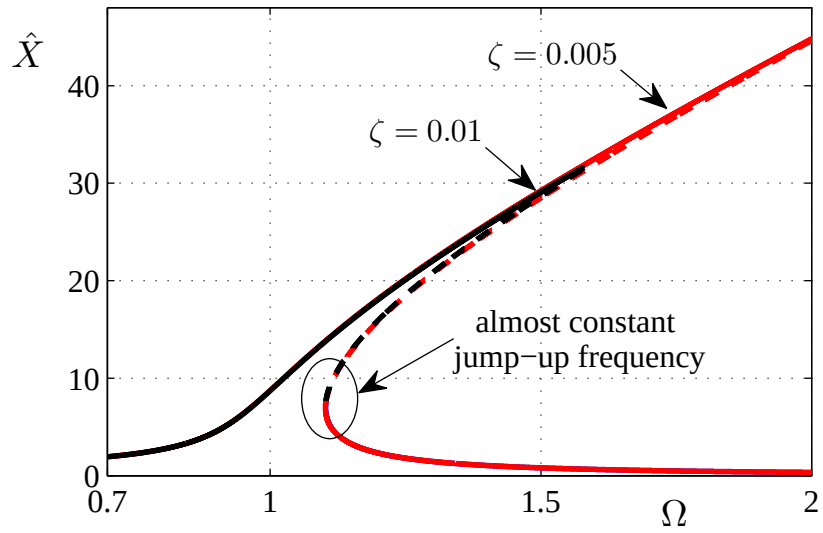

(a) $\alpha = 0.002$

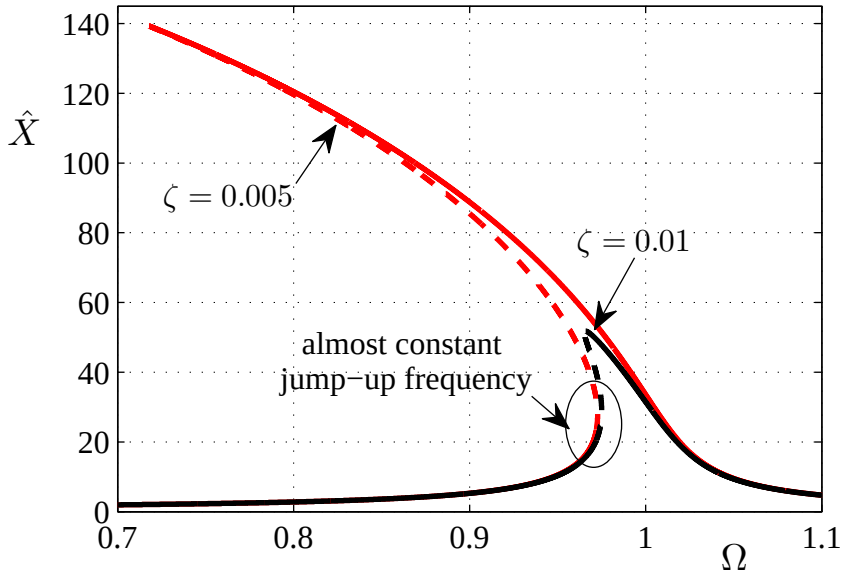

(b) $\alpha = -3.33 \times 10^{-5}$

Figure 4.7: FRF of a hardening (a) and softening (b) system. In both cases the jump-down frequency is strongly dependent on the damping ratio ζ, whilst the jump-up frequency is mostly unaffected by the change in ζ

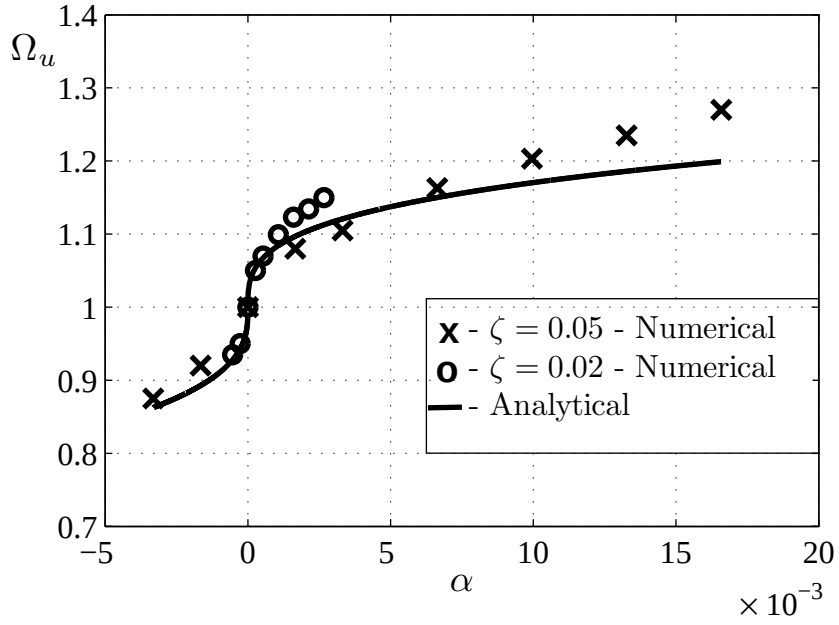

(a) Jump-up frequency

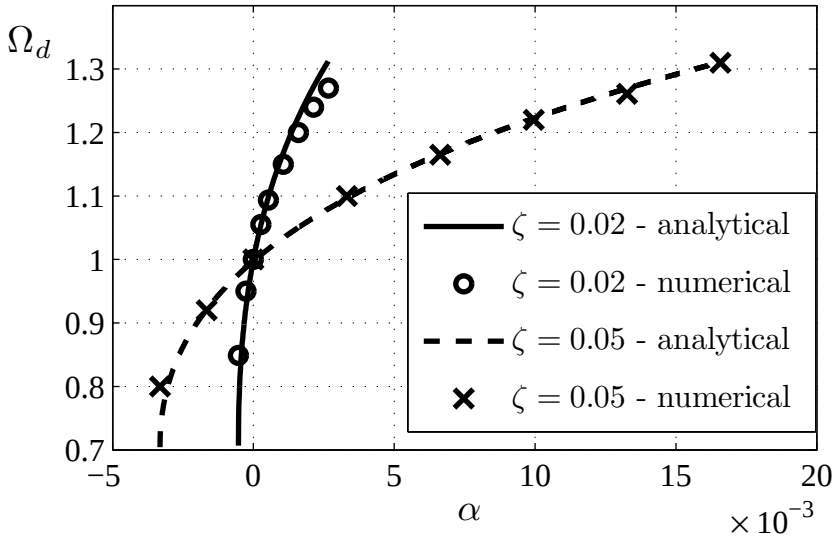

(b) Jump-down frequency

Figure 4.8: Comparison between the analytical and numerical jump-frequencies as a function of α for two different values of ζ

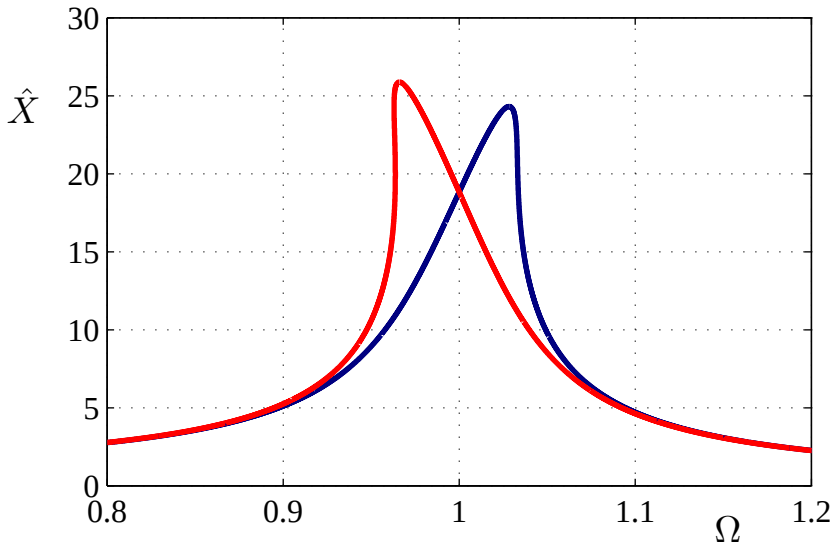

Figure 4.9: FRF of a softening (red) and hardening (blue) system with $\zeta = 0.02$ and critical value of the coefficient coefficient of the nonlinear term, $|\alpha| = |\alpha_{cr}| = 1.31 \times 10^{-4}$. The dashed line has been replaced by a solid line as no jump occurs

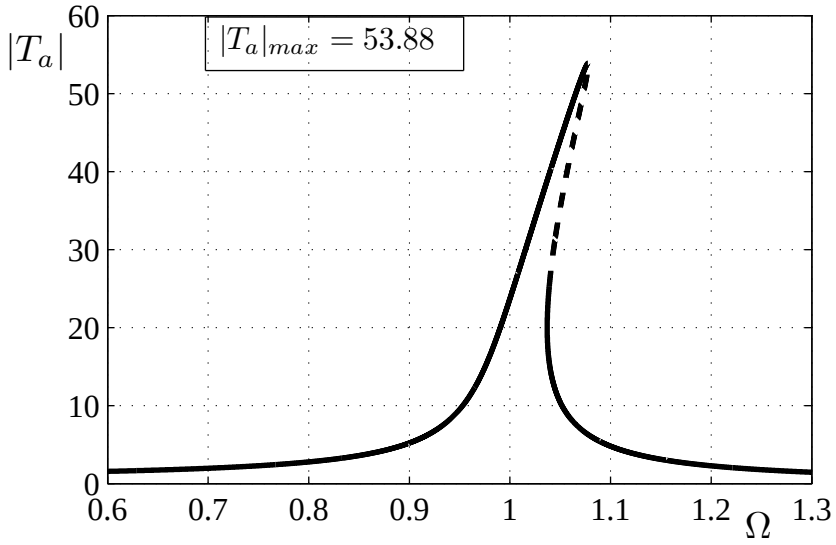

(a) $\alpha = 10^{-4}$

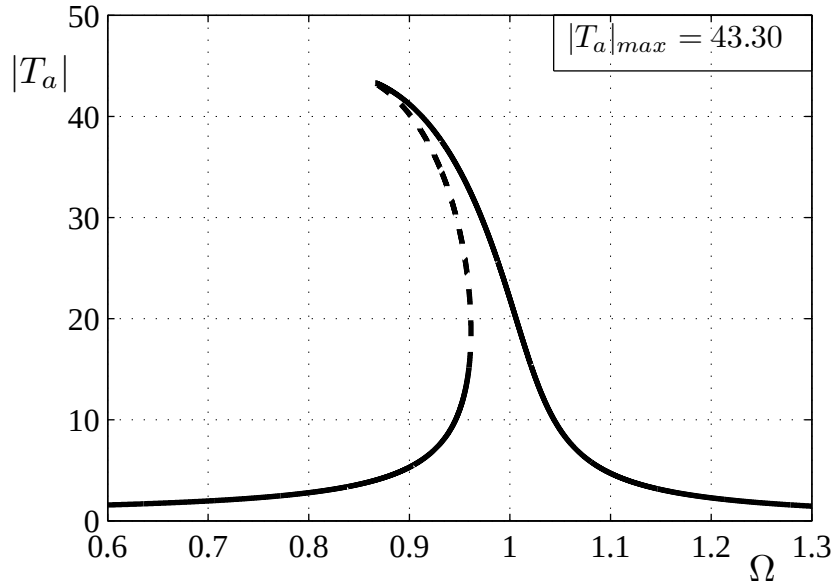

(b) $\alpha = -10^{-4}$

Figure 4.10: Absolute Transmissibility of an isolator with symmetric cubic nonlinearity. For both hardening (a) and softening (b) systems $\zeta = 0.01$. The maximum transmissibility calculated with Eqn.(4.30) is also shown

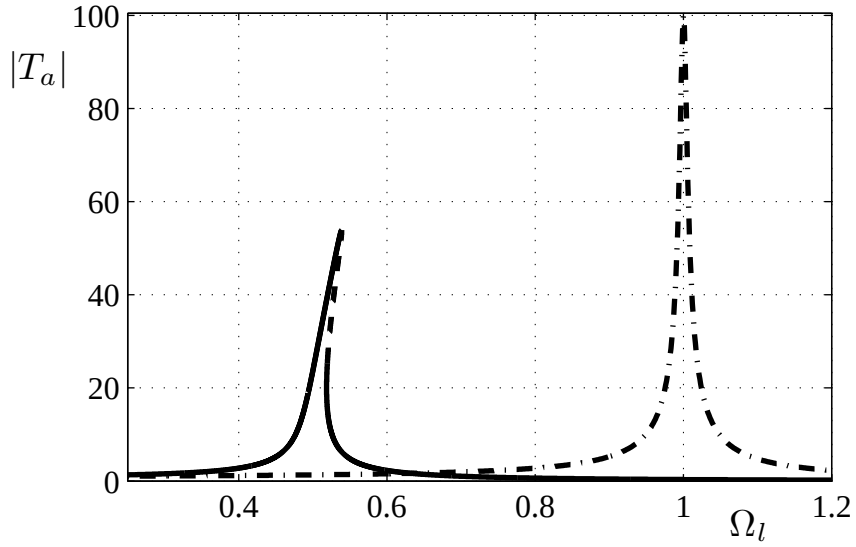

(a) $\alpha = 10^{-4}$

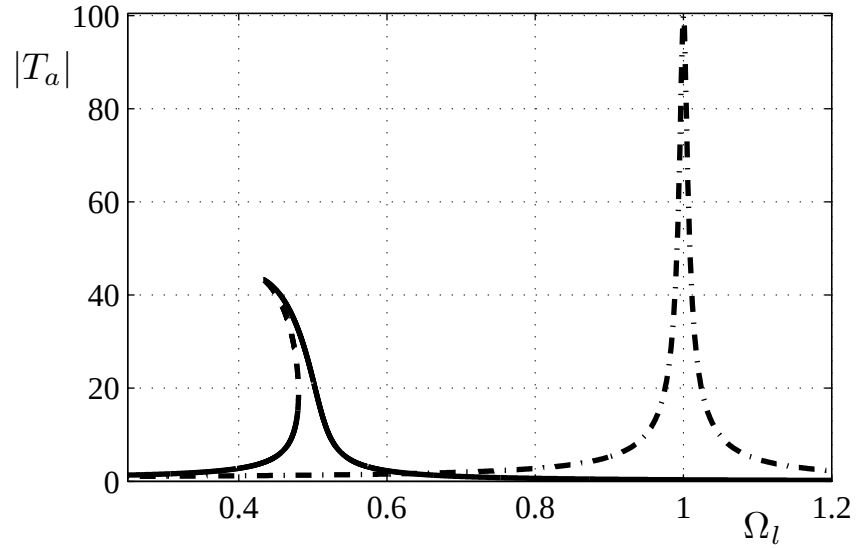

(b) $\alpha = -10^{-4}$

Figure 4.11: Comparison between the absolute transmissibility curves of a linear (-.) and HSLDS (–) mount. The peak transmissibility values have been calculated analytically. For the linear system $\zeta_l = 0.005$ and for the HSLDS mount $\zeta = 0.01$ ($\beta = 0.5$)

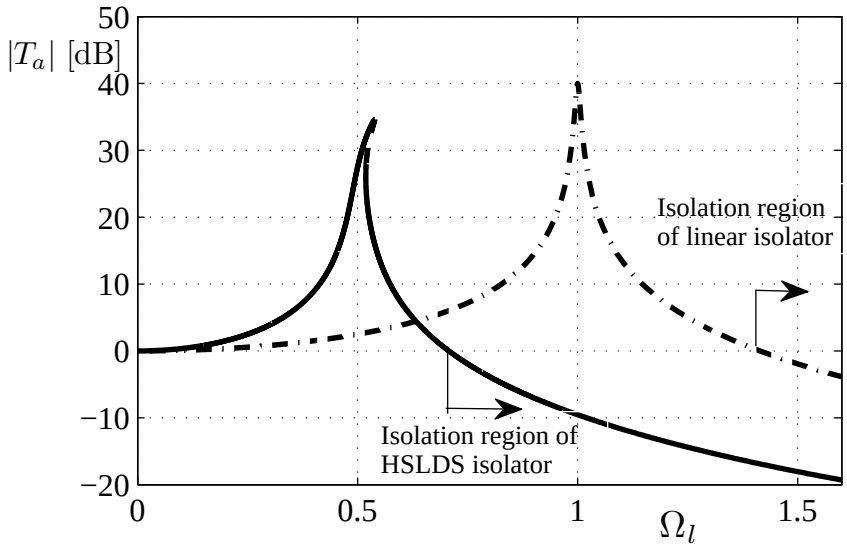

(a) $\alpha = 10^{-4}$

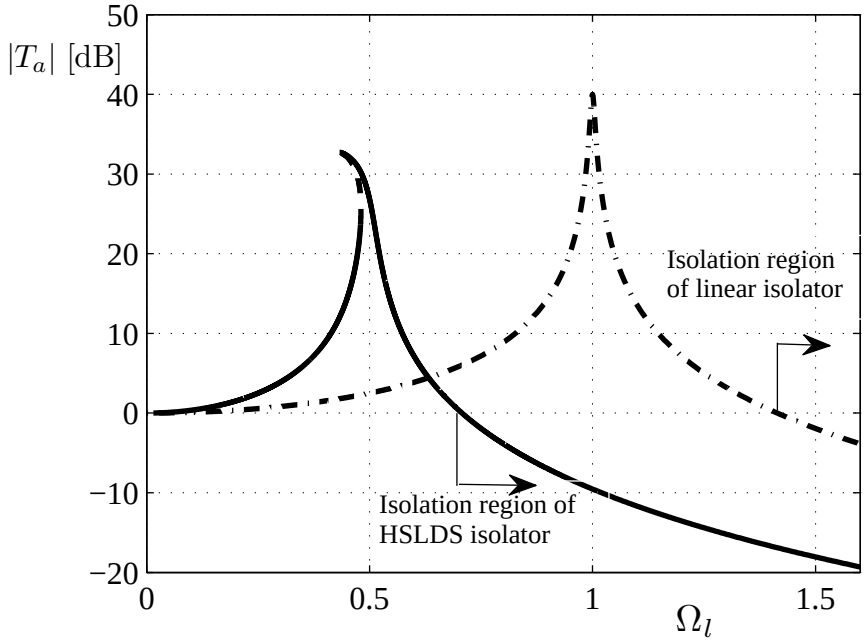

(b) $\alpha = -10^{-4}$

Figure 4.12: Absolute transmissibility. Same plots of Fig.4.11 but with the transmissibility expressed in dB. The increase of the frequency isolation region is highlighted

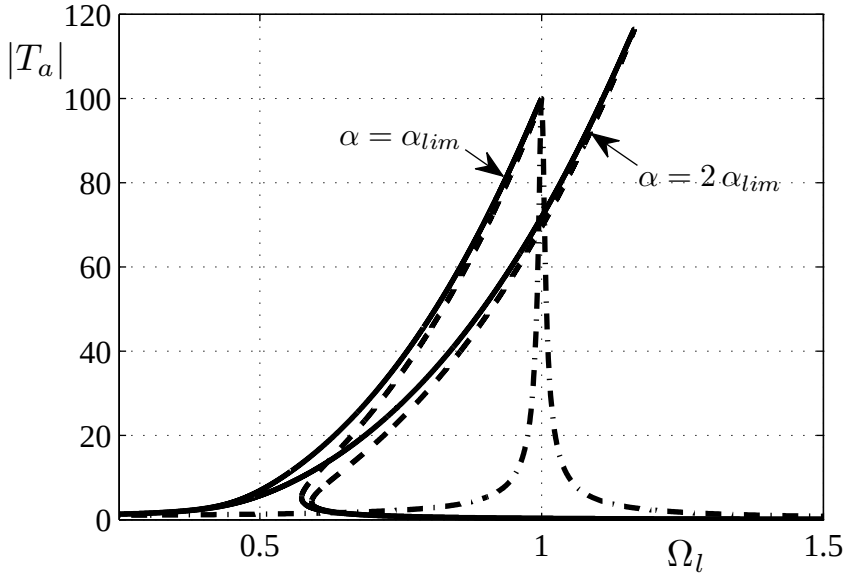

Figure 4.13: Transmissibility curves of a linear mount (-.) and of a two HSLDS (–) system with $\alpha = \alpha_{lim}$ and $\alpha = 2\,\alpha_{lim}$. For the linear system $\zeta_l = 0.005$ and for the HSLDS mount $\zeta = 0.01$ ($\beta = 0.5$)

Chapter 5

Vibration isolation of a SDOF system with an HSLDS isolator: motion transmissibility

'Science may be described as the art of systematic over-simplification.'

Karl Popper (1902 - 1994)

5.1 Introduction

This chapter aims to investigate the isolation properties of a mount with HSLDS characteristic and compare its isolation performance with that of an equivalent linear mount when the source of the disturbance is harmonic excitation of the base. In this case the absolute transmissibility is a measure of the ratio between the mass and base displacements at a given frequency of excitation and is referred to as *motion transmissibility*.

Although not as many studies as for the forced case can be found in the literature, studies of the dynamic response of a base-excited isolation system with cubic restoring force are given in [30, 63, 64]. Mallik *et al* [63] have studied the isolation properties of a system with a purely cubic restoring force and the effect of damping nonlinearity; in Jazar *et al* [64] the transmissibility curves of an engine isolation mount with quadratic stiffness and linear and/or quadratic

damping was studied; finally Peleg [30] has investigated the transmissibility of a base excited system with a hardening spring with viscous and friction damping. All the studies have a hybrid analytical-numerical approach. Thus simple, explicit expressions for the calculation of the characteristic parameters, i.e. jump frequencies and transmissibility-peak, are not available yet. Nor can these be assumed *a priori* to be the same as for the force excitation case because, given the nonlinear spring, the dynamic response may be different according to the excitation modality (force or base motion).

Determining these expressions would aid understanding of the system behaviour and of the influence of the parameters. There could also be another advantage. Most generally, given the highly mathematical analysis required to study nonlinear problems, engineers prefer to carry-out linear analysis wherever possible. With some simple, but approximate, expressions for the characterisation of the nonlinear effects (such as the jump phenomenon) it is possible that, to a first approximation, major nonlinear effects may be accounted for in many engineering applications.

The structure of this chapter follows very closely that of the previous one. In the first instance, the equation of motion is written by choosing as degree of freedom the relative displacement between mass and base. The system dynamic behaviour is thus described in terms of its frequency response function, which, incidentally, in the case of relative displacement response is called relative transmissibility, [3]. As for the case studied in Chapter 4, analytical expressions for the jump frequencies are sought and exploited for determining an expression for the maximum transmissibility. The equations can be drastically simplified if it is assumed that the damping ratio is small ($\ll 1$), which is a legitimate assumption for many engineering applications. Finally, the isolation properties of the HSLDS isolator are evaluated in terms of absolute transmissibility which is compared with that of an equivalent linear model.

5.2 Response to a harmonic excitation of the base

If the excitation is a motion of the base, the resulting response usually is expressed in terms of the amplitude of the motion of the mass relative to the amplitude of the motion of the base. This relative deflection is an important characteristic of a vibration isolator because it is a measure of the clearance required in the isolator [3].

Fig.5.1 depicts a SDOF system with HSLDS mount and viscous damping excited at the base. A mass m is suspended on a dashpot c and a nonlinear mount with HSLDS characteristic, k_{HSLDS}. The support of the system undergoes harmonic motion $z = Z\cos(\omega t)$. The equation of motion of this system can be written in the form of the Duffing equation

$$m\ddot{u} + c\dot{u} + k_1 u + k_3 u^3 = -m\ddot{z} \tag{5.1}$$

where $u = x - z$ is the relative displacement between the mass and the base. The equation of motion can be nondimensionalised to give

$$\hat{u}'' + 2\zeta\hat{u}' + \hat{u} + \alpha\hat{u}^3 = \Omega^2\cos(\Omega\tau) \tag{5.2}$$

where:

$\zeta = \frac{c}{2m\omega_n}$ $\omega_n^2 = \frac{k_1}{m}$ $\alpha = \frac{k_3 Z^2}{k_1}$ $\Omega = \frac{\omega}{\omega_n}$ $\tau = \omega_n t$

$\hat{u}'' = \frac{\ddot{u}}{\omega_n^2 Z}$ $\hat{u}' = \frac{\dot{u}}{\omega_n Z}$ $\hat{u} = \frac{u}{Z}$

with the symbol '$\prime$' denoting differentiation with respect to nondimensional time τ.

As for the case of the force excited system, ω_n is the natural frequency of the linearised HSLDS isolator, i.e. when the amplitude of oscillations are small enough to make $\alpha\hat{u}^2 \ll 1$, and the coefficient of the nonlinear term, α, takes into account the type (hardening or softening) and the degree of nonlinearity (including the amplitude of the excitation).

5.2.1 Approximate periodic solution: relative transmissibility

An approximate solution to the equation of motion can be found, as in the case of the force excitation, by applying the HB method, which is based on the assumption that the response (in this case the relative displacement) is harmonic at the excitation frequency and can be expressed as

$$\hat{u} = \hat{U}\,\cos(\Omega\,\tau + \phi) \tag{5.3}$$

where $\hat{U}$ is the amplitude and ϕ the phase. Note that because the relative displacement has been non-dimensionalised with respect to the amplitude of the base motion, the magnitude $\hat{U}$ is equivalent to the modulus of the *relative transmissibility*, $|T_r|$ defined as the ratio of the magnitude of the relative displacement to that of the base [3].

The application of the harmonic balance method, as detailed in Section 3.4.2, leads to the frequency response function which relates the amplitude of the response, $\hat{U}$, to the frequency ratio, Ω, as

$$\frac{9}{16}\,\alpha^2\,\hat{U}^6 + \frac{3}{2}\,(1-\Omega^2)\,\alpha\,\hat{U}^4 + \left[(1-\Omega^2)^2 + 4\,\zeta^2\,\Omega^2\right]\,\hat{U}^2 = \Omega^4 \tag{5.4}$$

which can also be written as

$$(\hat{U}^2-1)\,\Omega^4 + \left[\left(4\,\zeta^2-2\right)\,\hat{U}^2 - \frac{3\alpha}{2}\,\hat{U}^4\right]\,\Omega^2 + \frac{9}{16}\,\alpha^2\,\hat{U}^6 + \frac{3}{2}\,\alpha\,\hat{U}^4 + U^2 = 0 \tag{5.5}$$

Eqn.(5.4) is the same as the one obtained for the forced case, given in Eqn.(4.6), except for the term on the right-hand-side (RHS) where there is a Ω^4 instead of 1.

Solving Eqn.(5.5) for Ω yields

$$\Omega_1 = \sqrt{\frac{3\alpha\,\hat{U}^4 + 4\,\hat{U}^2(1-2\zeta^2) - \hat{U}\sqrt{(3\alpha\,\hat{U}^2+4)^2 - 64\hat{U}^2\zeta^2(1-\zeta^2) - 48\alpha\,\zeta^2\,\hat{U}^4}}{4\,\left(\hat{U}^2-1\right)}} \tag{5.6a}$$

$$\Omega_2 = \sqrt{\frac{3\alpha\,\hat{U}^4 + 4\,\hat{U}^2(1-2\zeta^2) + \hat{U}\sqrt{(3\alpha\,\hat{U}^2+4)^2 - 64\hat{U}^2\zeta^2(1-\zeta^2) - 48\alpha\,\zeta^2\,\hat{U}^4}}{4\left(\hat{U}^2-1\right)}} \tag{5.6b}$$

Before studying Eqns.(5.6 a,b) it should be noted that rearranging Eqn.(5.5) for $\hat{U}$ and setting α to zero, the known expression for the relative transmissibility of a linear system is obtained [3]

$$\hat{U} = |T_r| = \sqrt{\frac{\Omega^4}{(1-\Omega^2)^2 + 4\,\zeta^2\,\Omega^2}} \tag{5.7}$$

For $\Omega_{1,2}$ to be real the nested radicand in Eqns.(5.6 a,b) have to be positive, that is

$$(3\alpha\hat{U}^2+4)^2 - 64\hat{U}^2\zeta^2(1-\zeta^2) - 48\alpha\,\zeta^2\,\hat{U}^4 > 0 \tag{5.8}$$

which if solved for $\hat{U}$ and assuming, as previously stated in Chapter 4, that $\zeta^2 \ll 1$ yields four roots of which the only real positive one is

$$\hat{U} < \hat{U}_{max} \tag{5.9}$$

where

$$\hat{U}_{max} = 2\sqrt{\frac{8\,\zeta^2\,\left(1-\sqrt{1+\frac{3\,\alpha}{4}}\right) - 3\,\alpha}{3\,\alpha\,\left(3\,\alpha - 16\,\zeta^2\right)}} \tag{5.10}$$

which can be further simplified if it imposed that α is 'small', in which case Eqn.(5.10) becomes

$$\hat{U}_{max} \approx \frac{2}{\sqrt{16\zeta^2 - 3\,\alpha}} \tag{5.11}$$

The order of magnitude of α is set for the analysis that follows in this chapter to be

$$|\alpha| = |\alpha|_{max} < 16/3\,\zeta^2 \tag{5.12}$$

This restriction on the maximum value of the nonlinear coefficient α justifies the validity of the HB analysis as well as the simplification made in the equations (e.g. from Eqn.(5.10) to Eqn.(5.11)).

It should be noted that when $\alpha = 0$ (i.e., linear system) Eqn.(5.11) collapses to the known expression for the maximum relative transmissibility of a lightly

damped linear system [2, 3]

$$|T_r|_{max(linear)} \approx \frac{1}{2\,\zeta} \tag{5.13}$$

When $\hat{U} = \hat{U}_{max}$ the nested square root in Eqns.(5.6) becomes zero and the two solutions Ω_1 and Ω_2 become real and coincident, but if $\hat{U} > \hat{U}_{max}$ the frequency is complex. In other words, $\hat{U}$ cannot become greater than $\hat{U}_{max}$. However, the frequency of excitation can, of course, be increased (hardening) or decreased (softening), but the response amplitude can only decrease. This is the jump down phenomenon.

Fig. 5.2(a) is a plot of the curves given by Eqns.(5.6 a,b) with $\zeta = 0.01$ and $\alpha = 1.33 \times 10^{-4}$ as $\hat{U}$ is varied between 0 and $\hat{U}_{max}$. It shows that also in the case of base excitation the response of an HSLDS isolator is characterised by the *jump phenomenon*. In the same plot also the results of the linear perturbation stability analysis are shown. The linear perturbation stability analysis can be carried out as shown in the previous chapter and thus is not repeated here. Similarly to the case of the force excited mass, the problem reduces to the study of the stability of the Mathieu equation and the stability region is again defined in the region of the $\hat{U} - \Omega$ plane that lies outside of the parabola Eqn.(4.17).

Fig.5.2(b) depicts instead the relative transmissibility of a softening HSLDS isolation mount excited at the base with $\zeta = 0.01$ and $\alpha = -5.33 \times 10^{-4}$. Also in this case the figure is obtained by plotting Eqns.(5.6) as $\hat{U}$ goes from 0 to $\hat{U}_{max}$. The dash-dot lines are the boundary of the dynamically unstable response obtained as illustrated in the next section.

5.2.2 The jump frequencies

Finding analytical expressions for the jump frequencies would provide an important tool for the understanding and the prediction of a phenomenon which might have serious consequences on the integrity of the system but also for the evaluation of the isolation properties of an HSLDS mount supporting a mass.

Unlike the case of the forced response, where an analytical expression of the jump frequencies have been previously found, from a survey of the literature it

appears that simple, closed-form expressions to describe the dynamics of a base-excited Duffing oscillator have not been proposed yet. Peleg [31] has analysed a base excited system with a hardening spring and has proposed implicit analytical expressions for the jump frequencies and amplitudes. Some 10 years later the same author describes a 'grapho-analytic' method for studying a SDOF system with cubic restoring force and linear and nonlinear damping, [30]. In reference [64] the isolation properties of a nonlinear engine mount with cubic restoring force and linear and nonlinear damping are studied. The closed-form expressions provided have a rather complicated form. The absolute transmissibility was also defined but its main properties (extension of the frequency isolation region and peak-transmissibility) were not described analytically.

In this section, simple and explicit formulae to calculate the jump frequencies for base excitation are proposed. Subsequently, their accuracy is quantified by comparison with numerical solution of the equation of motion. The expression of the jump-down frequency will be used in the next section to define a formula for calculating the absolute peak transmissibility of the HSLDS isolator. The mathematical analysis can become prohibitive even given the approximation of harmonic response. However, it is possible to produce some simple analytical expressions if it is assumed that the damping is small $\zeta^2 \ll 1$.

With very good approximation, the jump-down frequency, Ω_d, can be assumed to be the frequency at which the response attains its maximum value (this is even more true when the damping is small). Thus, in a sense, Ω_d could be seen as the 'resonance' frequency of the nonlinear system. Of course it depends on the amplitude of the excitation and therefore this definition has to be taken only as indicative for one particular excitation level. A simplified analytical expression for the jump-down frequency, Ω_d, can be found by substituting Eqn.(5.10) into one of Eqns.(5.6 a,b). This results in

$$\Omega_d \approx \sqrt{\frac{2\,\left[3\,\alpha\,\zeta^2\,(3\,\alpha+4)+6\,\alpha\,\zeta^2\sqrt{3\,\alpha+4}\right]}{(16\,\zeta^2-3\,\alpha)\left(3\,\alpha-8\,\zeta^2+4\,\zeta^2\sqrt{3\,\alpha+4}\right)}} \tag{5.14}$$

This expression can be further simplified if $\alpha \ll 4/3$, in which case Eqn.(5.14) becomes

$$\Omega_d \approx \frac{4\,\zeta}{\sqrt{16\,\zeta^2-3\,\alpha}} \tag{5.15}$$

For the approximate value of the jump-down frequency of a hardening system the condition $\alpha < \alpha_{max}$ has to hold.

The approach to find an analytical expression for Ω_u differs from that followed in the previous chapter because the mathematical expressions that result from applying the condition of vertical tangency, as in Eqns.(4.20) and (4.21), become extremely complicated. In order to avoid this, the cubic equation in $\hat{U}^2$, given by Eqn.(5.4), is used instead of the quadratic in Ω^2, Eqn.(5.5). The cubic Eqn.(5.4) has either one real and two complex conjugate roots or three real roots [43]. At the bifurcation points, namely at the frequency Ω_u, the imaginary part of the complex pair becomes zero and two real solutions exist. Using software for symbolic mathematical analysis (in this case Maple), it is possible to find a closed form solution for the values of Ω that give a zero imaginary part. A simple expression for the jump-up frequency Ω_u is obtained if it assumed that this is independent of the damping (i.e. setting $\zeta = 0$), as shown in Fig. 5.3 where the relative transmissibility is plotted for one value of α and two different damping ratios. For both softening, Fig. 5.3(b), and hardening, Fig. 5.3(a), doubling the damping ratio has not produced any significant change in the jump-up frequency. Considering the limitation on the magnitude of α Eqn.(5.12), approximate analytical expressions for Ω_u are found to be

$$\Omega_{u_h} \cong 1 + \frac{27}{32} |\alpha|^{1/3} \tag{5.16a}$$

$$\Omega_{u_s} \cong 1 - \frac{27}{32} |\alpha|^{1/3} \tag{5.16b}$$

where the subscripts h and s stand for hardening and softening respectively.

A comparison between the results obtained with the proposed analytical expressions, Eqns.(5.16a,b) and (5.14), with the jump frequencies obtained by numerical integration of the equation of motion (as shown in the previous chapter) is shown in Fig. 5.4. The equation of motion has been solved with the built-in solver (based on a 4-th order Runge-Kutta routine) of Matlab®. α was changed discretely as $\alpha = n\,\alpha_{max}$ where $n = -2, -1.75, -1.5, -1, -0.5, 0, 0.25, 0.5, 0.75$. The line in Fig. 5.4(a) is the plot of Eqn.(5.16) and, of course, is independent of the damping ratio. The points marked with '×' are the numerical results for $\zeta = 0.005$. The figure shows that the trend of the analytical expression follows that of the numerically computed values. It can be seen that the match is bet-

ter when α is small (i.e. weak nonlinearity). Fig. 5.4(b) shows the comparison between the numerical and analytical values of the jump-down frequency. Also in this case the difference between the analytical and numerical result increases with α.

In order to investigate the difference between the jump frequencies of the system considered when it is force or base excited, the jump-up expressions for both cases Eqns.(4.23a,b) and (5.16a,b), and the jump-down, Eqns.(4.19) and (5.15) have been plotted in Fig.5.5(a,b) for a given value of damping ratio, $\zeta = 0.01$. It can be observed that the difference in the value of the jump-up frequency is small and increases with the magnitude of the nonlinear coefficient, Fig.5.5(a). Conversely, the analytical expressions for the jump-down frequency yield rather different results apart from when α is very small, Fig.5.5(b).

Avoidance of the jump Applying the method shown by Malatakar and Nayfeh [70] it is possible to calculate a 'critical' value of the nonlinear coefficient α_{cr} which does not produce the jump phenomenon. This value is equal to that of the forced system and is given by

$$|\alpha| = |\alpha_{cr}| < \frac{2^8}{3^{5/2}}\zeta^3 \tag{5.17}$$

The curves plotted in Fig. 5.6 are the relative transmissibility of a softening (red) and a hardening system (blue) with $\zeta = 0.02$ and $|\alpha| = |\alpha_{cr}| = 1.31 \times 10^{-4}$.

5.3 Absolute motion transmissibility

The dynamic analysis carried out so far has investigated the relative transmissibility. A more valuable parameter for the assessment of the isolation properties of an isolation mount is the *absolute transmissibility* which is defined as the ratio between the displacement of the mass and that of the base,

$$|T_m| = \frac{|x|}{|z|} \tag{5.18}$$

where the subscript m is used to indicate that this is the absolute motion transmissibility.

This is related to the relative transmissibility as follows

$$|T_m| = \frac{|x - z + z|}{Z} = \frac{|u + z|}{Z} \tag{5.19}$$

The vectors u and z rotate at the same angular speed but with a phase lag ϕ. When divided by Z their modulus become $\hat{U}$ and 1 respectively. Hence, the absolute motion transmissibility is the sum of two vectors with magnitude $\hat{U}$ and 1 at an angle ϕ. The modulus of the resulting vector is

$$|T_m| = \sqrt{1 + 2\,\hat{U}\,\cos\phi + \hat{U}^2} \tag{5.20}$$

where $\cos\phi$ is determined directly from the application of the HB method, as in Eqn.(3.47a)[a], and is given by

$$\cos\,\phi = \frac{[1 - \Omega^2 + 3/4\,\alpha\,U^2]\,U}{\Omega^2} \tag{5.21}$$

Substituting Eqn.(5.21) into Eqn.(5.20) the absolute transmissibility is thus given by, [62, 63]

$$|T_m| = \sqrt{1 + \hat{U}^2 + \frac{2\,\hat{U}^2}{\Omega^2}(1 - \Omega^2 + \frac{3}{4}\,\alpha\,\hat{U}^2)} \tag{5.22}$$

where Ω is a function of $\hat{U}$ according to Eqns.(5.6). From Eqn.(5.22) it can be seen that the absolute transmissibility reaches its maximum when $\hat{U} = \hat{U}_{max}$ and this, as seen earlier, occurs when $\Omega = \Omega_d$. Hence

$$|T_m|_{max} = \sqrt{1 + \hat{U}_{max}^2 + \frac{2\,\hat{U}_{max}^2}{\Omega_d^2}(1 - \Omega_d^2 + \frac{3}{4}\,\alpha\,\hat{U}_{max}^2)} \tag{5.23}$$

The analytical expression for the peak absolute motion transmissibility $|T_m|_{max}$ is obtained by substituting Eqns.(5.11) and (5.15) into (5.23). Having assumed that $\zeta^2 \ll 1$ the approximate expression for the peak absolute transmissibility is found to be

$$|T_m|_{max} \approx \sqrt{1 + \frac{4}{16\,\zeta^2 - 3\,\alpha}} \tag{5.24}$$

For Eqn.(5.24) to be real it is required that for a hardening system the condition $\alpha < \alpha_{max}$ has to hold.

[a] In the case of base excitation treated here in Eqn.(3.47a) $X = \hat{U}$ and $F = \Omega^2$

It should be noted that when $\alpha = 0$, i.e. for a linear system, Eqn.(5.24) reduces to the expression of the maximum absolute transmissibility of a linear system with small damping [3]

$$|T_m|_{max(linear)} \approx \frac{1}{2\,\zeta} \tag{5.25}$$

The absolute transmissibility of a HSLDS mechanism with a hardening characteristic is plotted in Fig. 5.7(a), whilst Fig. 5.7(b) shows that of a softening HSLDS system. For both plots the same damping ratio $\zeta = 0.01$ and nonlinear coefficient $\alpha = \pm 10^{-4}$ have been chosen to be consistent with the examples illustrated for the relative transmissibility. In the figures also included is the value of the maximum absolute transmissibility calculated from Eqn.(5.24) to show the validity of the newly proposed analytical expression for the cases considered.

Before assessing the isolation performance of an HSLDS mechanism by comparison with its equivalent linear model, it is of interest to compare the force and motion transmissibility curves, given by Eqns.(4.29) and (5.22) respectively. As mentioned, for a linear system the transmissibility is the same regardless of whether the excitation is due to a harmonic force directly applied to the mass or to a harmonic base motion. The force and motion absolute transmissibility are shown in Fig.5.8(a) for a hardening system and Fig.5.8(b) for a system with softening characteristic. In both figures the peak transmissibility has also been marked. For the case of force excitation it has been calculated with Eqn.(4.30) and marked with 'o'. When the excitation is a base motion the maximum value has been determined with Eqn.(5.24) and marked with '×'.

5.3.1 Comparison between the motion transmissibility of an HSLDS mechanism excited at the base and that of an equivalent linear isolator

This section aims to show the benefits of employing an HSLDS isolation mount. This is done by comparing the absolute motion transmissibility of an HSLDS mount with that of an equivalent linear support.

In Section 4.4.2 the nondimensional parameters which define the dynamic behaviour of the HSLDS mechanism were scaled to match the equivalent linear

quantities. Namely, the characteristic frequency, ω_n, of the HSLDS isolator is different from the natural frequency of the linear model, ω_l. These define the frequency ratio, Ω and Ω_l respectively, which therefore delineates a different frequency range. By virtue of the analysis presented in Chapter 2 and recalled in Section 4.4.2, the characteristic frequency of the HSLDS mount is

$$\omega_n = \beta\,\omega_l \tag{5.26}$$

and thus

$$\Omega = \frac{\Omega_l}{\beta} \tag{5.27}$$

where $\beta < 1$ is the nondimensional coefficient of the linear term of the approximated cubic polynomial restoring force (as in Eqns.(2.22) and (2.53)). Thus, when the transmissibility (as a function of the nondimensional frequency ratio) of a linear model is plotted together with that of the HSLDS system, the x-axis has to be scaled according to Eqn.(5.26). Clearly, the scaling factor β affects also the damping ratio because

$$\zeta = \frac{c}{2\,m\,\omega_n} = \frac{\zeta_l}{\beta} \tag{5.28}$$

where ζ_l is the damping ratio of the linear system. As a consequence of the fact that $\beta < 1$ the HSLDS system has a higher damping ratio and a lower peak transmissibility.

As an example, consider a linear system with $\zeta_l = 0.005$. Its absolute transmissibility is the dash-dotted curve in Fig. 5.9(a) and 5.9(b). Suppose now some elements with negative stiffness are added in order to obtain an HSLDS isolator, e.g. using a set of oblique springs or magnets as discussed in Chapter 2. As an example, the nondimensional coefficients of the linear and cubic term of the HSLDS system are $\beta = 0.5$ and $\alpha = \pm 10^{-4}$ respectively. The transmissibility curves of the hardening and softening HSLDS isolation mount are also plotted in Fig. 5.9(a) and 5.9(b) respectively. The following observations are made:

1. The frequency on the x-axis is normalised by the natural frequency of the linear model, hence the peak of the linear transmissibility is at $\Omega_l = 1$;

2. If the damping coefficient c remains constant it follows, from Eqn.(5.28), that the damping ratio of the HSLDS isolator increases to $\zeta = 0.01$;

3. The peak values can be found readily found from Eqns.(5.24) and (5.25).

The maximum transmissibility of the linear system is $|T_m|_{max(linear)} = 100$. For the hardening HSLDS is $|T_m|_{max} = 55.48$ and for the softening is $T_{m_{max}} = 45.90$;

4. The advantages of employing a vibration isolator with an HSLDS characteristic are better shown in Fig.5.10 where the same curves depicted in Fig.5.9 are displayed on a decibel scale. The isolation region (frequency range for which $|T_m| < 0$ dB) of the HSLDS isolator is wider and also the maximum value is smaller. It can also be appreciated that a softening mount is even better that a hardening one. This conclusion agrees with that of Ravindra and Mallik [62].

When the HSLDS system has a hardening stiffness, as for the case of force excitation, it can outperform a linear mount as long as the nonlinear coefficient is small enough to guarantee that the peak transmissibility and the jump-down frequency do not become equal or larger than the values of the linear model. The limiting value of α will depend on β and can be found by solving for α one of these two identities

$$|T_m|_{max} = |T_m|_{max_{(linear)}} \Leftrightarrow |T_m|_{max} = \frac{1}{2\,\beta\,\zeta} \tag{5.29a}$$

or

$$\beta\,\Omega_d = 1 \tag{5.29b}$$

Substituting Eqn.(5.24) into (5.29a) and solving for α yields

$$\alpha_{lim} = \frac{16}{3}\,\zeta^2\,\left[1 - \beta^2\,(1 + 4\,\zeta^2)\right] \tag{5.30}$$

which, when $\zeta^2 \ll 1/\sqrt{2}$ simplifies to

$$\alpha_{lim} \approx \frac{16}{3}\,\zeta^2\,\left(1 - \beta^2\right) = \alpha_{max}\left(1 - \beta^2\right) \tag{5.31}$$

Fig. 5.11 shows the comparison between the linear transmissibility with $\zeta_l = 0.025$ (dash-dotted line) and the transmissibilities of two hardening HSLDS systems with $\beta = 0.5$ and $\alpha = \alpha_{lim},\ 5/4\,\alpha_{lim}$.

5.4 Conclusions

In this chapter the dynamic response of an isolation mount with high-static-low-dynamic-stiffness to a harmonic excitation of the base has been investigated and its isolation performance compared with that of an equivalent linear.

The HSLDS system is described in terms of three nondimensional parameters: the damping ratio, the frequency of excitation and the coefficient of the cubic term of the restoring force which not only describes the type and degree of nonlinearity but also accounts for the amplitude of the excitation.

Initially, the dynamic response has been studied in terms of the relative transmissibility, that is the ratio of the relative displacement between the oscillating mass and the base to the amplitude of the base excitation as function of frequency. This problem has been investigated previously but the approach involved hybrid analytical-numerical solutions. Herein, within the validity of the assumptions made, an analytical theory has been developed to study the nonlinear dynamics of the model.

Simple expressions that describe the main dynamic behaviour of the nonlinear system considered have been derived: the maximum relative transmissibility, the jump-frequencies and the maximum absolute transmissibility.

A comparison between the absolute force and motion transmissibility has revealed that, unlike the linear case, these two functions are different.

To assess the vibration isolation performance of the proposed HSLDS isolator model, its absolute transmissibility has been compared with that of an equivalent linear system. In general, the nonlinear mount outperforms the standard mass spring model. A wider isolation region and a lower transmissibility-peak make the HSLDS mount a better isolator, with a softening giving better results than a hardening isolator.

However, both softening and hardening isolation systems have some drawbacks. For a softening system the limit is the excursion from the static equilibrium position within which the system is stable (i.e. the stiffness is positive). This effect is exacerbated for large amplitudes of excitation or a large nonlinear coefficient

and will be discussed again in the next chapter. When the HSLDS system has a hardening stiffness a strong nonlinearity or amplitude of excitation might increase its 'resonance' frequency and its peak-transmissibility until they become equal or larger than those of an equivalent linear model. Clearly when this happens a standard linear system is preferred.

In the next chapter a HSLDS that was designed and built is described. Its measured transmissibility is compared with that of its equivalent linear isolator.

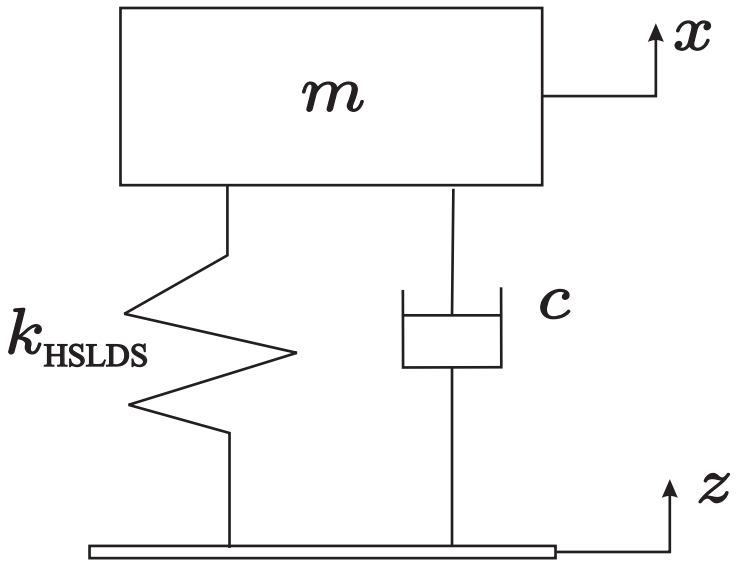

Figure 5.1: Single-degree-of-freedom model of HSLDS mount with viscous damping: a mass m is suspended on a dashpot c in parallel with a nonlinear mount with HSLDS k_{HSLDS}. The base undergoes harmonic motion $z = Z\,\cos(\omega\,t)$

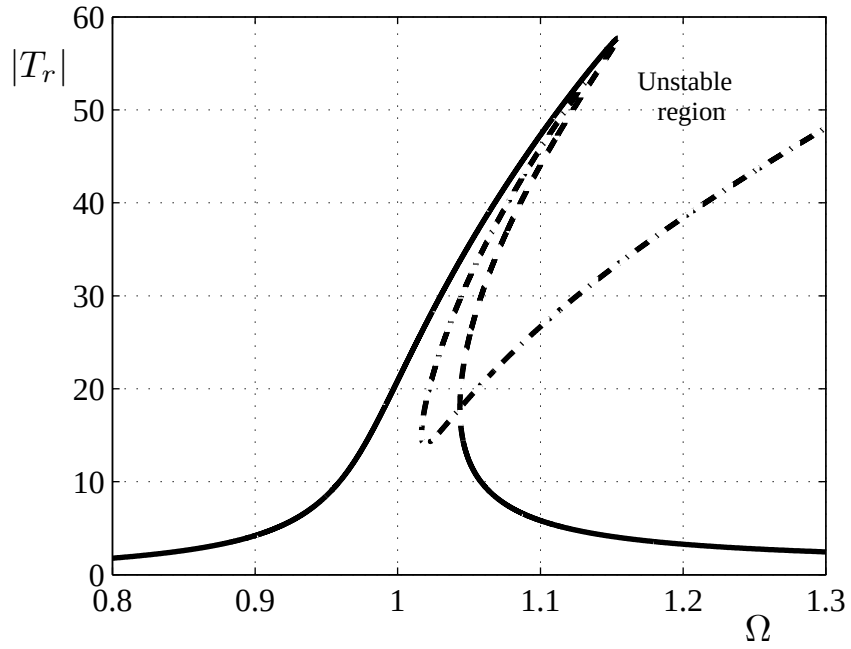

(a) $\alpha = 1.33 \times 10^{-4}$

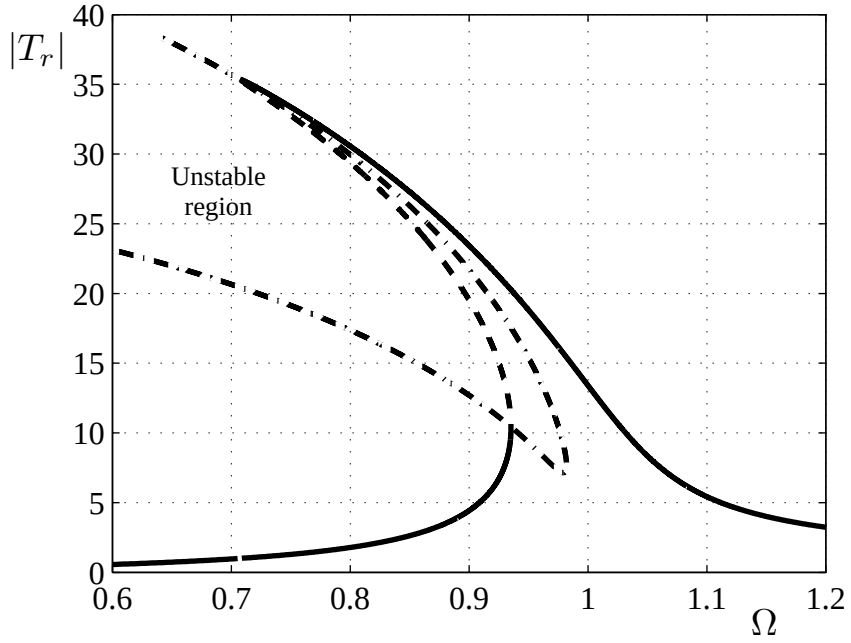

(b) $\alpha = -5.33 \times 10^{-4}$

Figure 5.2: Relative transmissibility of the HSLDS isolator for a harmonic motion of the base. Hardening (a) and softening systems (b). The damping ratio is $\zeta = 0.01$. The part of the FRF included in the unstable region delimited by the dash-dot lines, denotes unstable equilibrium points and is therefore plotted with a dashed line

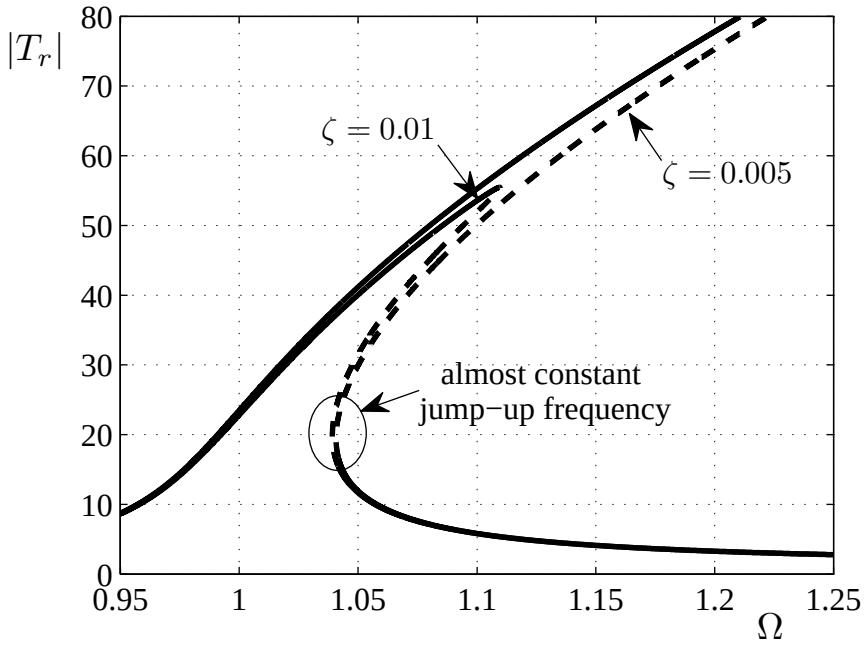

(a) $\alpha = 10^{-4}$

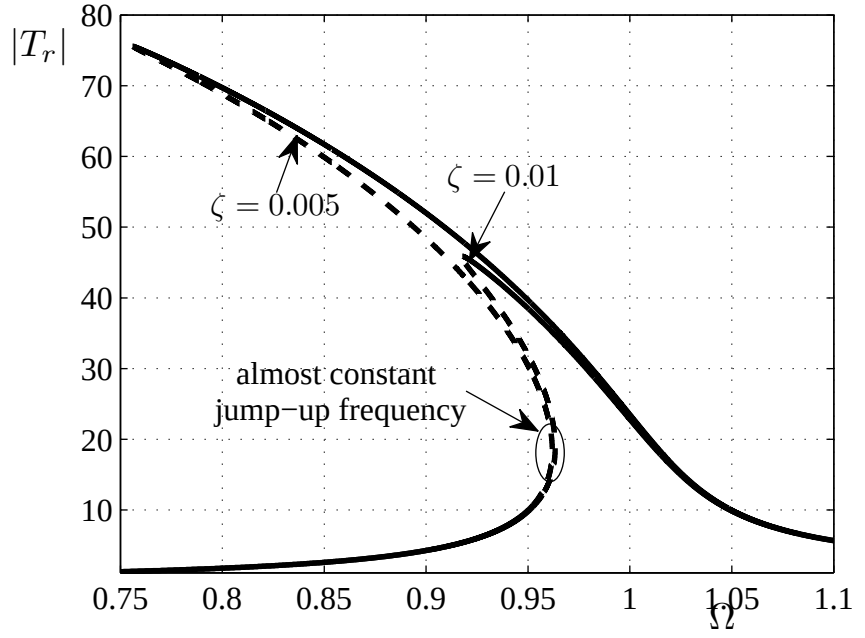

(b) $\alpha = -10^{-4}$

Figure 5.3: Relative transmissibility. (a) hardening, (b) softening for different values of ζ. Despite the damping has doubled the jump-up frequency has remained substantially unchanged

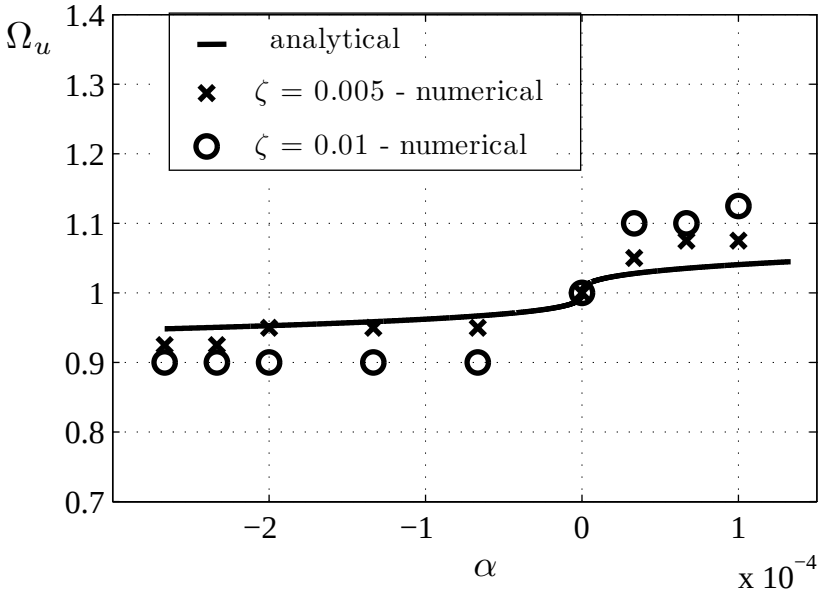

(a) Jump-up frequency

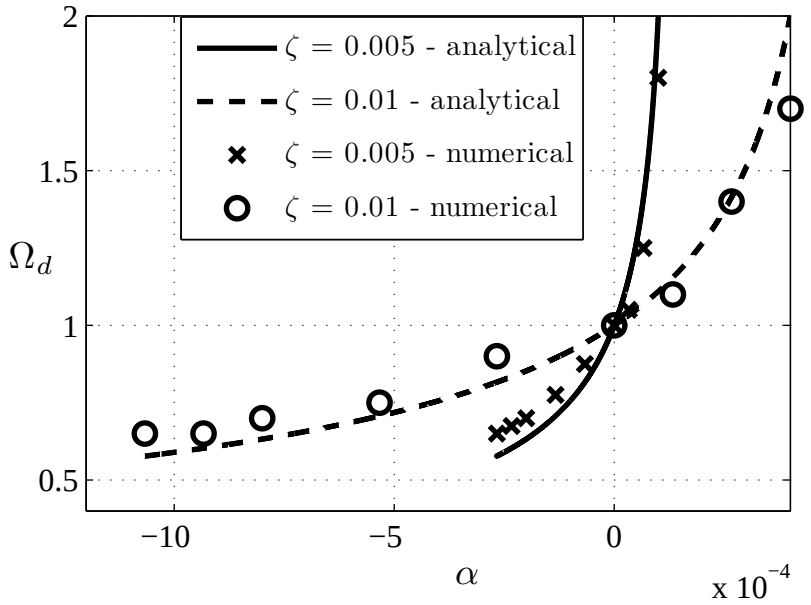

(b) Jump-down frquency

Figure 5.4: Comparison between the analytical and numerical jump-frequencies as function of α for two different values of ζ

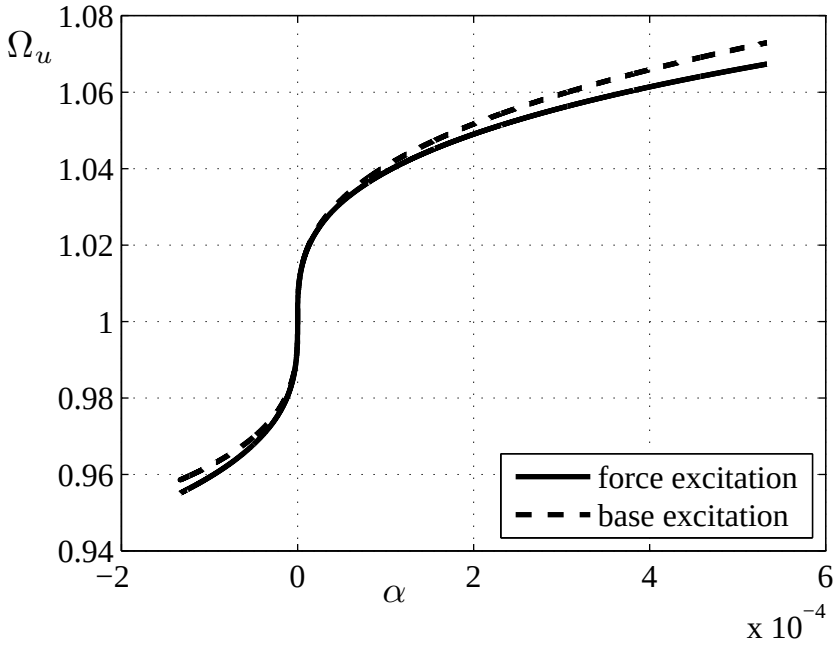

(a) Jump-up frequency

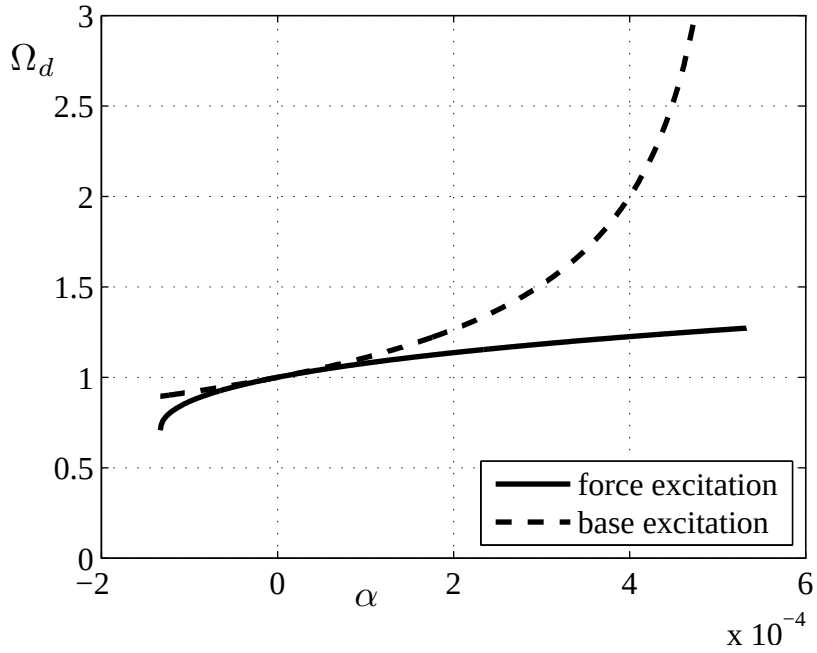

(b) Jump-down frquency

Figure 5.5: Comparison between the jump frequencies of a system with symmetric cubic restoring force excited by a harmonic force applied to the mass (solid line) and by a harmonic motion of the base. In both cases is $\zeta = 0.01$

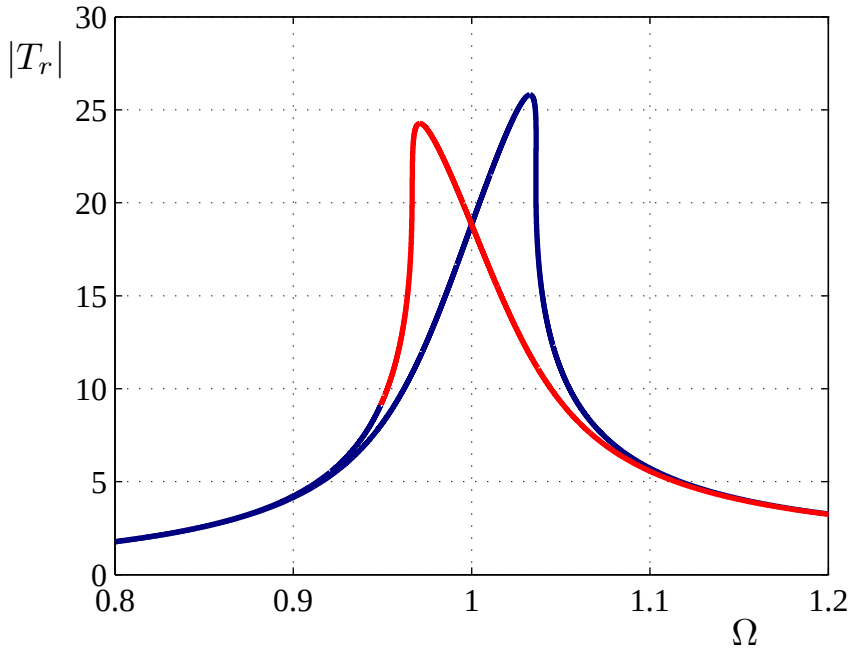

Figure 5.6: Relative transmissibility of a softening (red) and hardening (blue) system with $\zeta = 0.02$ and critical value of the coefficient coefficient of the non-linear term, $|\alpha| = |\alpha_{cr}| = 1.31 \times 10^{-4}$. The dashed line has been replaced by a solid line as no jump occurs

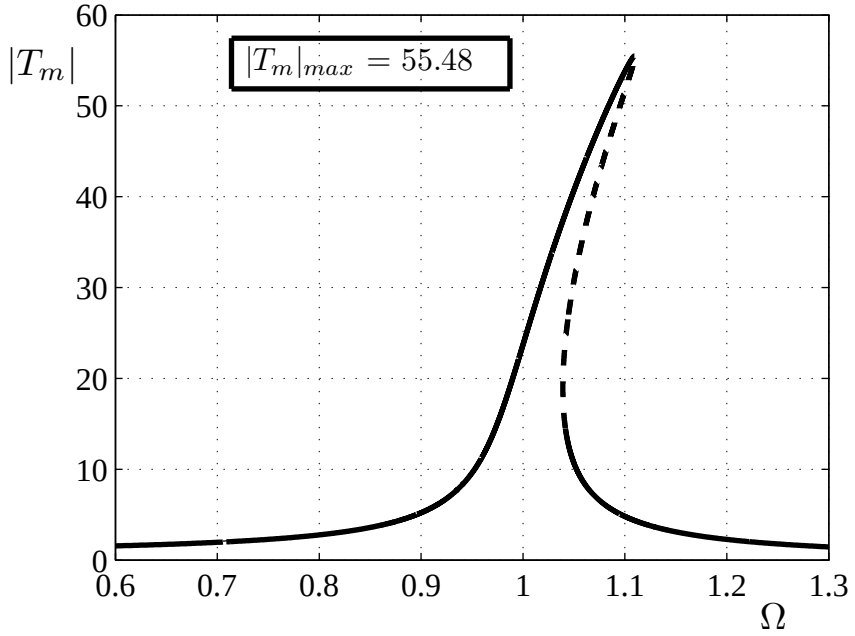

(a) $\alpha = 10^{-4}$

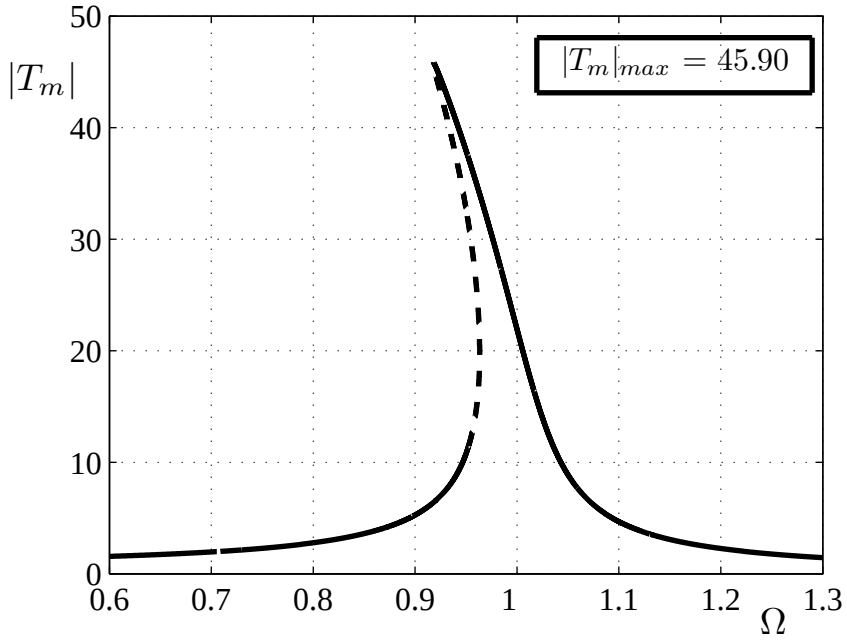

(b) $\alpha = -10^{-4}$

Figure 5.7: Absolute transmissibility of a (a) softening HSLDS isolator and (b) hardening isolator. For both systems is $\zeta = 0.01$. The maximum transmissibility calculated with Eqn.(5.24) is also shown

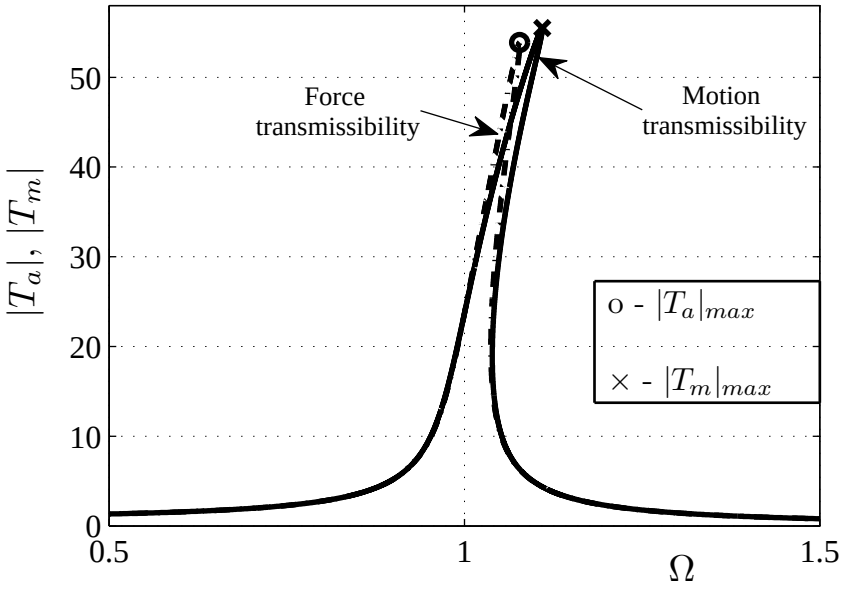

(a) $\alpha = 10^{-4}$

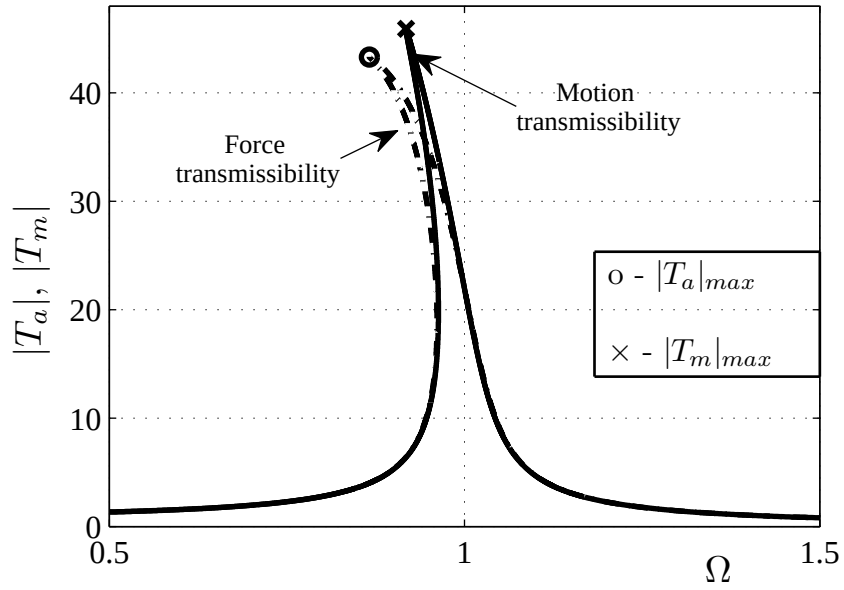

(b) $\alpha = -10^{-4}$

Figure 5.8: Comparison of the absolute force and motion transmissibility, Eqns.(4.29) and (5.22) respectively. The symbols 'o' and '×' mark the maximum force and motion transmissibility calculated with Eqns.(4.30) and (5.24) respectively

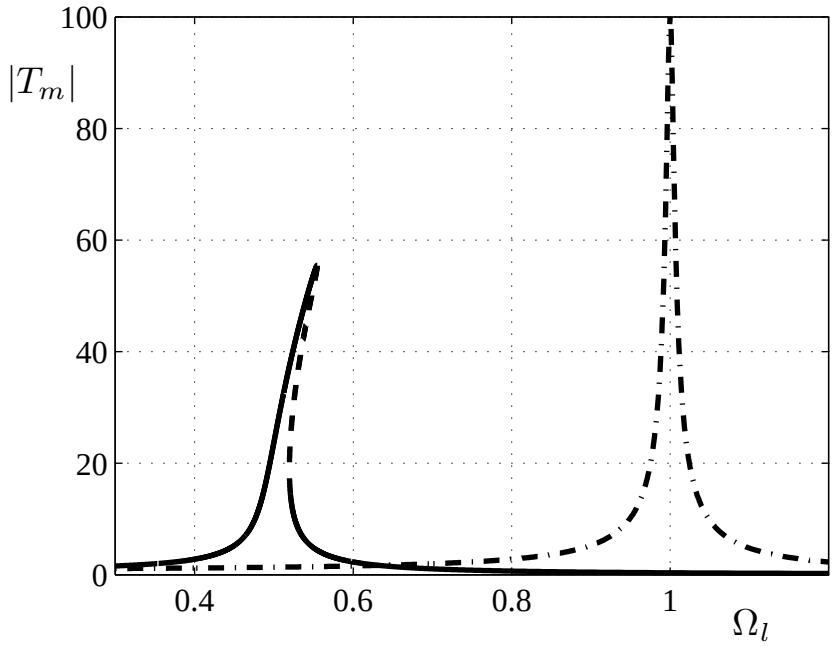

(a) $\alpha = 10^{-4}$

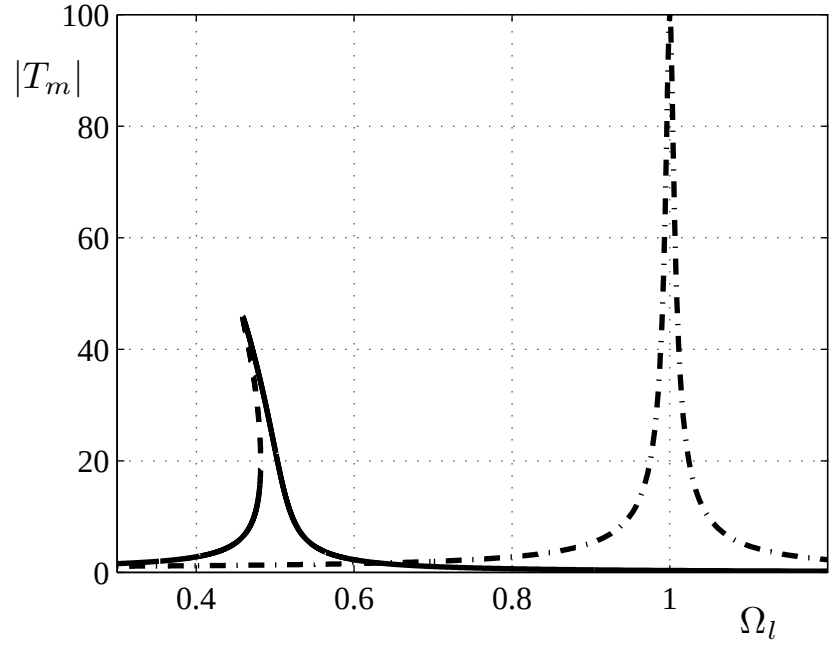

(b) $\alpha = -10^{-4}$

Figure 5.9: Comparison of the absolute transmissibility of a HSLDS and a linear isolation mount. The frequency on the x-axis is normalised by the natural frequency of the linear system, Ω_l. The linear system (dash-dot line) has a damping ratio $\zeta_l = 0.005$ and the scaling factor is $\beta = 0.5$. Thus the damping ratio of the HSLDS isolator is $\zeta = 0.01$. Both HSLDS mechanisms offer improved isolation performance

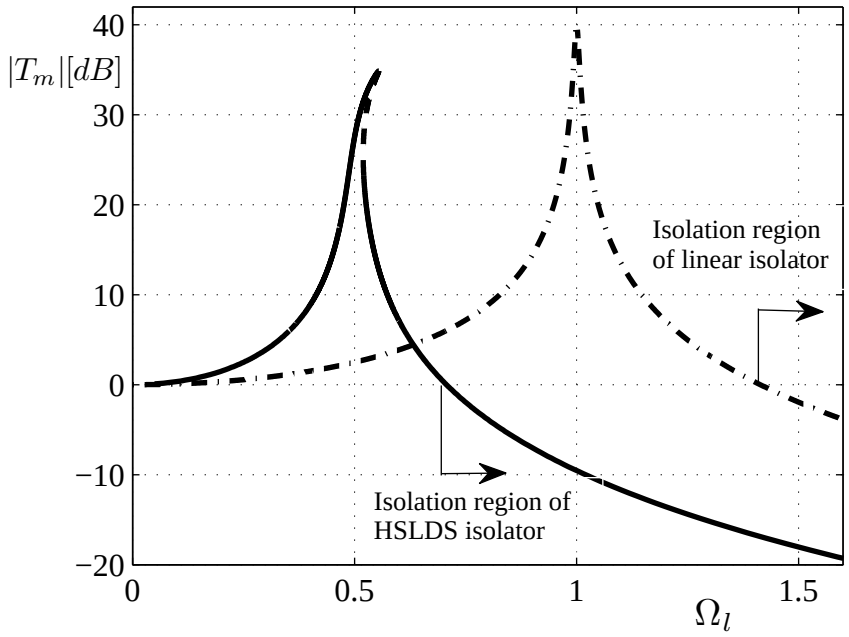

(a) $\alpha = 10^{-4}$

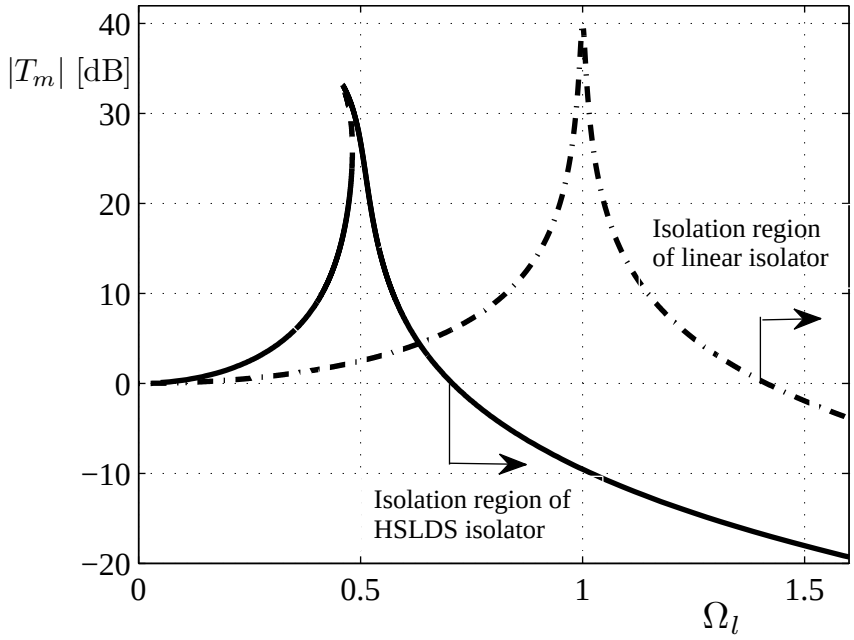

(b) $\alpha = -10^{-4}$

Figure 5.10: Comparison of the absolute transmissibility of a HSLDS and a linear isolation mount. The frequency on the x-axis is normalised by the natural frequency of the linear system, Ω_l. The linear system (dash-dot line) has a damping ratio $\zeta_l = 0.005$ and the scaling factor is $\beta = 0.5$. Thus the damping ratio of the HSLDS isolator is $\zeta = 0.01$. Both HSLDS mechanisms offer improved isolation performance

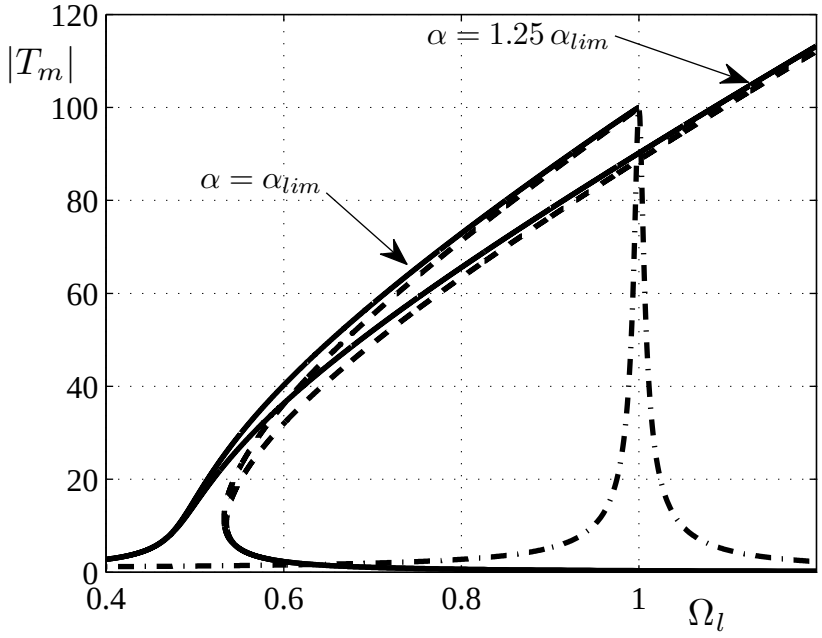

Figure 5.11: Transmissibility of a hardening HSLDS mechanism compared with that of the equivalent linear isolator (with $\zeta_l = 0.005$) when $\alpha = \alpha_{lim}$ and $\alpha = 1.25\,\alpha_{lim}$. When $\alpha = \alpha_{lim}$ the jump-down frequency becomes equal to the natural frequency of the equivalent linear system and also the peak transmissibility of the HSLDS equals that of an equivalent linear model (dashed-dotted line). If $\alpha \geq \alpha_{lim}$ there is no advantage in using a HSLDS isolator

Chapter 6

Experimental work: rig design and transmissibility measurement of a HSLDS isolator

'By three methods we may learn wisdom:
First, by reflection, which is noblest;
Second, by imitation, which is easiest;
and third by experience, which is the bitterest.'

Confucius (551 BC - 479 BC)

6.1 Introduction

Chapter 2 described the static analysis of two systems with HSLDS characteristics. The first system comprised three linear springs and had a hardening stiffness. The desired nonlinear characteristic was obtained because two of the springs were placed at an angle to the horizontal and provided the necessary negative stiffness. The second system studied had a softening characteristic. The HSLDS property was due to the action of linear springs (positive stiffness) and a set of magnets in an attracting configuration.

It was shown that despite their nonlinear restoring forces, for small oscillations the dynamic behaviour of both systems could be described by linear theory. Moreover, the HSLDS characteristic gave them a natural frequency that was lower

than an equivalent linear isolation model[a] without having to compromise on the static load bearing capability. Thus they have potential use as vibration isolators.

The aim of this chapter[b] is to demonstrate practically the principle of an HSLDS vibration isolator by using springs and magnets. As discussed in Chapter 2, magnets have been used in vibration isolation systems in the past [35–37, 46–48] but not in an HSLDS system.

A detailed analysis of the static characteristics of the system has been given in Section 2.6.1, but the relevant theoretical aspects will be repeated here for the sake of convenience. The drawbacks and other issues of this physical system are discussed.

In Appendix C the details of other experimental work carried out on a different HSLDS mechanism are given. The rig is rather bulky and not suitable for isolation purposes and its sole purpose was to provide a visual demonstration of the principle behind an HSLDS mechanism.

6.2 Isolator configuration

Consider three equally spaced magnets arranged in an attracting configuration, as shown in Fig.6.1. The middle magnet is free to move in the vertical (x) direction on a smooth shaft whilst the other two magnets are fixed with respect to each other.

The magnets thus arranged generate a negative stiffness which is inversely proportional to the third power of the distance between the middle and the other magnets, d, and counteracts the positive stiffness provided by linear springs inserted between each pair of magnets. By judicious choice of the system parameters, the effects of the springs and magnets can be made to cancel at the equilibrium position resulting in a very low (in the limit zero) stiffness.

[a] The equivalent linear model has been defined as the HSLDS system deprived of its elements with negative stiffness

[b] The content of which is published in reference [41]

Modelling the magnetic force with Coulomb's law the force and the stiffness can be approximated by

$$\hat{f} \approx (1-\nu)\,\hat{x} \; - 2\nu\,\hat{x}^3 \tag{6.1a}$$

$$\hat{k} \approx (1-\nu) - 6\,\nu\,\hat{x}^2 \tag{6.1b}$$

where $\hat{x}$ is the displacement of the mass normalised by the distance between the magnets, d, and ν is a nondimensional parameter that relates the stiffness from the magnets to the stiffness of the springs given by

$$\nu = 2\,C_m/(k_s\,d^3) \tag{6.2}$$

in which C_m is the magnetic constant (that depends on the magnets' strength and medium) and k_s is the coefficient of the mechanical springs.

As mentioned in the introduction, the function of the nonlinear magnetic stiffness is to reduce the overall dynamic stiffness of the isolator. Ideally, this should not cause undesirable nonlinear dynamic behaviour. One way of estimating whether this will occur is to examine the relative contributions of the nonlinear and linear stiffness forces given in Eqn.(6.1a). The ratio of these forces is given by $R_{nl} = -2\,\nu\,\hat{x}^2/(1-\nu)$, the magnitude of which is plotted in Fig.6.2 for $\nu = 0.72$, which is the value of ν for the isolator used in the experimental work discussed in the next section. It can be seen that the nonlinear component of stiffness is less than about 5% of the linear component of the stiffness provided that the maximum excursion of the mass from the static equilibrium position is less than about 0.1 d. If this condition holds then the system can be assumed to be linear with constant stiffness given by

$$\hat{k} \approx (1-\nu) \tag{6.3}$$

so that the ratio of the natural frequency of the HSLDS isolator ω_n, to the natural frequency of the isolator with the mechanical springs alone ω_l, is given by

$$\frac{\omega_n}{\omega_l} = \sqrt{1-\nu} \tag{6.4}$$

Thus, because of the magnets, the frequency at which isolation occurs is reduced by a factor of $\sqrt{1-\nu}$. There is an additional benefit of lowering of the isolator natural frequency if the damping is viscous. The transmissibility of a

linear mass-spring-damper system (the system without the magnets) at the resonance frequency ω_l is given approximately by $m\,\omega_l/c$ where m is the isolated mass and c is the viscous damping coefficient. Hence, the transmissibility of the HSLDS mount is given by $m\,\omega_n/c$. It follows that if the viscous damping in the isolator is constant, the peak in the transmissibility is reduced by a factor of $\omega_n/\omega_l = \sqrt{1-\nu}$. As discussed in the Chapter 1 an increase of the damping ratio also causes a poorer isolation at high frequencies. This penalty could be mitigated by changing the damping constant. However, the aim of the experiment carried out was to demonstrate the effectiveness of the HSLDS mechanism in reducing the natural frequency and extending the frequency region of isolation and therefore the damping coefficient was not made controllable.

6.3 Experiments

A laboratory scale experimental rig was designed and built to illustrate the principle described in the previous section. It is shown attached to the base of a vertical shaker in Fig.6.3. Similar to the model described above, it comprises three magnets, two coil springs and a smooth bar. Two magnets are fixed at the top and the bottom of the shaft at a distance $d = 3.81$ cm from the central magnet of mass $m = 0.04$ kg which is free to move vertically, sliding on the central bar. To take into account the static displacement of the isolated mass due to gravity and ensure symmetry of the magnetic force, a washer of about 2 mm thickness was inserted between the lower spring and the magnet to which it was attached.

The main aim of the experiment was to compare the transmissibility curves of the isolator with that of a conventional mass-spring system, which was realised by simply replacing the magnets at each end of the central bar with non-magnetic elements.

First, the magnetic constant, C_m, was measured using two different techniques. The first approach for measuring the strength of the magnets was dynamical. The springs were removed and the central magnet was reversed so that it was repelled by the magnets fixed at the end of the smooth bar. In this case the stiffness has a hardening characteristic. However, the isolator was excited using a stepped-sine generated by an HP analyser 35656A such that the relative amplitude between

the base and the suspended mass was small. Thus it was possible to assume that the stiffness was constant. The dashed line in Fig.6.4 shows the absolute value of the ratio between the acceleration of the suspended mass and the acceleration of the base (transmissibility). The peak occurs at the resonance frequency at about 13.25 Hz which, given the oscillating mass, gives the stiffness to be 277.23 N/m. Setting $x = 0$, $k_s = 0$ and $k = 277.23$ N/m in Eqn.(2.48) results in

$$C_m = 2.72 \times 10^{-3} \text{ Nm}^2 \tag{6.5}$$

A different way of calculating the magnetic constant is by means of static measurements. For this measurement only two magnets are needed. One magnet is fixed at the bottom of the shaft. The other is slid on the shaft so that it is repelled from the fixed one. The only forces acting are the weight and the repulsive magnetic force which is inversely proportional to the square of the distance, according to Coulomb's law Eqn.(2.32). At the static equilibrium position these forces balance

$$F_m = \frac{C_m}{d^2} = m\,g = W \tag{6.6}$$

where m is the mass of the free magnet, $g = 9.81$ ms^{-2} is the acceleration of gravity and W is the weight. The distance between the two magnets when in equilibrium was measured to be $d = 5.9$ cm. Knowing the mass of the free magnet $m = 0.04$ kg, it was possible to work out the value of magnetic constant as

$$C_m = m\,g\,d^2 = 1.36 \times 10^{-3}\text{Nm}^2 \tag{6.7}$$

This value doubles when two magnets are acting simultaneously on the middle piece and coincides with that derived by dynamic means and given in Eqn.(6.5).

Next, the stiffness of the coil springs was measured by suspending the mass only on the two springs and removing the lower and upper magnets (equivalent linear system). The corresponding transmissibility measurement is shown as a solid line in Fig. 6.4. It can be seen that the resonance peak is at a frequency of 13.1 Hz, which means that the combined stiffness of the springs is

$$2\,k_s = 277.24\text{N/m} \tag{6.8}$$

The non-dimensional parameter ν can be thus calculated and is found to be

$$\nu = \frac{2\,C_m}{k_s\,d^3} = 0.72 \tag{6.9}$$

From Eqn.(6.4), the natural frequency of the HSLDS system is thus predicted to be about 7 Hz.

Note that, as illustrated in Section 2.6, the system parameter ν defines not only the maximum stiffness of the system (hence its natural frequency), but also the maximum excursion from the static equilibrium position within which the stiffness is positive. Therein, exact and approximate expressions for the maximum displacement were provided, Eqns.(2.50) and (2.55). For the value of ν measured, the maximum approximate displacement (which overestimates the exact expression by about 7.5%) is $x_{max} = 0.97$ cm. Increasing ν would certainly reduce the natural frequency, and thus benefit the isolation performance, but it would also reduce the range of oscillations that guarantee the stability of the system. This trade-off between maximum stiffness and available excursion, as discussed in 2.6, is an important aspect of this type of HSLDS mechanism.

Having estimated the natural frequency of the HSLDS isolator, an experiment was conducted to see if the isolator performed as expected. It was assembled as shown in Fig.6.3 and placed on the vertical shaker. It was excited at discrete frequencies from 6 Hz to 10 Hz, and the base displacement amplitude of 3 mm was kept constant throughout the tests. At each frequency, once the system was at steady-state, fifteen seconds of data were captured using a NI DAQPad-6020E acquisition card. The acceleration of the base was measured using an ENDEVCO 2256-100 accelerometer and the acceleration of the isolated mass was measured using a PCB type 352C22 accelerometer.

Fig.6.5 shows a concatenation of the acquired time histories for each excitation frequency of the mass and base displacements. The amplitude of the base excitation (constant at 3 mm) is shown in Fig.6.5(a). In Fig. 6.5(b) is shown the corresponding measured steady-state displacement of the mass. The ratio of the root-mean-square (rms) displacement of the isolated mass to the rms displacement of the base was calculated for each excitation frequency and this is plotted in Fig.6.6 where it is labelled as transmissibility. This was repeated for an exci-

tation level of 4 mm and this is also plotted in Fig.6.6. As well as these graphs the transmissibility of the isolator without the magnets fitted is also plotted for comparison. It can be seen that the HSLDS stiffness system has a peak at 7 Hz as predicted, which is roughly half that of the isolator without the magnets. It should be noted that the amplitude of vibration at the resonance frequency has also been reduced by a factor of two, which is consistent with a halving of the damping ratio.

To assess whether the HSLDS isolator was behaving as a linear system, the spectral content of the acceleration time history of the isolated mass was calculated for each excitation frequency. As expected from a system with cubic nonlinearity, odd higher order harmonics were observed. In Fig.6.8 the ratio between the largest higher order harmonic (the 3rd), $|A_3|$, and that at the excitation frequency, $|A_1|$, are plotted when the peak amplitude of the base displacement was maintained constant at 3 mm at any frequency of excitation. It can be seen that the amplitude of the 3rd harmonic is smaller than that of the fundamental frequency $|A_1|$ for each frequency of excitation by a factor of about 30. This demonstrates that the nonlinearity in the isolator is very weak for the excitation levels used.

6.3.1 Comparison with theoretical transmissibility curves

From the measurements it is now possible to determine both the linear and nonlinear the system's parameters. However, it has to be pointed out that, as mentioned, the aim of the experiment was to measure the decrease in natural frequency and therefore the damping mechanism has been assumed to be linear and of viscous type. This of course might not be the case given the multiple sources of damping (e.g. friction, springs, magnetic interaction) which, in reality, can give rise to nonlinear damping. The damping coefficient, c, can be extracted from the measured transmissibility of the linear system. In this case, the analytical expression of the peak transmissibility is

$$(|T_a|_l)_{max} = \sqrt{1 + \frac{1}{4\,\zeta_l^2}} \tag{6.10}$$

which has been measured to be $(|T_a|_l)_{max} \approx 3$ at a frequency $\omega_l = 81.68$ rad/sec. From Eqn.(6.10) the damping ratio is

$$\zeta_l = \frac{c}{2\,m\,\omega_l} = 0.177 \tag{6.11}$$

from which the damping coefficient is $c = 1.16$ Ns/m.

Using this value of damping coefficient, the damping ratios for the other two measured curves can be calculated. For an amplitude of the base excitation of 3 mm the measured resonance frequency is $\omega_1 = 44$ rad/sec whilst for a 4 mm excitation amplitude is $\omega_2 = 43$ rad/sec. This information combined with the value of damping coefficient calculated enable one to determine the damping ratios for the two excitation levels which are

$$\zeta_1 = \frac{c}{2\,m\,\omega_1} = 0.33 \tag{6.12a}$$

$$\zeta_2 = \frac{c}{2\,m\,\omega_2} = 0.34 \tag{6.12b}$$

From the theory presented in Chpater 2, with the assumption of cubic restoring force Eqn.(6.1a), together with the measured nondimensional coefficient $\nu = 0.72$ and the measured distance between central and extremities magnets, d =3.81 cm, the linear and nonlinear coefficients of the restoring force can be calculated to give

$$f(x) = k_1\,x + k_3\,x^3 \tag{6.13}$$

where k_1 =77.62 N/m and $k_3 = -275\times10^3$ N/m^3. The nondimensional coefficient α as defined in Chapter 5 can be thus calculated for each level of excitation. It results in

$$\alpha_1 = \frac{k_3\,Z_{01}^2}{k_1} = -0.032 \tag{6.14a}$$

$$\alpha_2 = \frac{k_3\,Z_{02}^2}{k_1} = -0.056 \tag{6.14b}$$

For the higher excitation level, the nondimensional equation of motion, Eqn.(5.2) can be thus written as

$$\hat{u}'' + 2\,\zeta\,\hat{u}' + \hat{u}\,(1 - 0.056\,\hat{u}^2) = \Omega^2\,\cos(\Omega\,\tau) \tag{6.15}$$

where the same notation as in Chapter 5 has been maintained. It can be noted

that the nonlinear term becomes equal to the linear coefficient (=1), when $\hat{u} = 4.2$. As discussed in the next section the maximum measured relative displacement is u_{max} =2 mm which, for a base excitation amplitude of 4 mm gives $\hat{u}_{max} = 0.5$ which indicates that the nonlinear term is small compared to the linear. The theoretical curves, Eqn.(5.22), for both excitation levels are plotted together with the measured one in Fig.6.7. For completeness also the measured and theoretical linear transmissibility curves are plotted on the same figure.

6.4 Discussion

In the static analysis of the HSLDS isolator (detailed in Chapter 2) the magnetic force was modelled using Coulomb's law. Despite this being a very simple model, the analytical predictions and the experimental results agree reasonably well. It can be seen from Fig.6.6 that the peak transmissibility was about 1.5, which means that the absolute motion of the isolated mass was about 6 mm[c] for a 4 mm base displacement, and hence the relative displacement between the isolated mass and the base was about 2 mm. This is about 5.25% of the distance between the central magnet and the end magnets, which means that the non-linear component of the force is about 1.5% of the linear component. From the experimental and theoretical analysis it the non-linearity (i.e. the influence of the cubic term relatively to the linear one) is negligible for this isolator when subjected to reasonably high base excitation levels (4mm). It can be argued that disagreements between measured and predicted response and at different of excitation level might be due to inevitable measurement errors but most importantly to the damping mechanism which herein has been assumed to be linear and of viscous type. The main advantage of the HSLDS system is its load bearing capability. Reducing the natural frequency by a factor of two would be possible by using coil springs four times softer. A suspended mass of 40 grams will have a natural frequency of 7 Hz if it is suspended on a spring with a coefficient of 77.5 N/m. However, this would mean a static displacement of 5 mm. With the HSLDS mount the static displacement is dependent only on the coil springs which have a combined stiffness of 271 N/m resulting in a static displacement of only 1.5 mm.

Finally, the measured transmissibility has been compared with the analytical

[c]Note that the measured displacement of the mass is smaller than the maximum $x_{max} = 9.7$ mm allowed before the stiffness becomes negative

formulation. For the linear system (mass suspended only on the springs) there is an excellent agreement between theoretical and experimental results. For the HSLDS system, at both level of excitation, the measured natural frequency agrees well with the predicted result meaning that the stiffness calculation is correct. The mismatch between analytical and experimental curves seems thus due to the damping in the system.

The measurements taken have also highlighted some issues that need to be tackled in future works. The first is the need to engineer a mechanism that bounds the displacement of the mass within the region with positive stiffness. An adjustable mechanism that takes into account the static displacement of the mass and ensure that it is equidistant from both ends would also help to make the system more robust in practice. Furthermore, a measure of the damping and the understanding of the mechanism of energy dissipation is required in order to be accounted for with a suitable mathematical model.

6.5 Conclusions

The static and linearised dynamic behaviour of a mechanism with high-static-low-dynamic stiffness has been investigated. Magnets fixed at the top and bottom of the device exert an attracting force on a middle element to which they are connected by means of two coil springs. The negative stiffness due to the magnetic interaction is exploited to cancel partially the positive stiffness of the coil springs resulting in an ultra-low natural frequency.

A rig has been built using off-the-shelf magnets and coil springs to demonstrate the practicality of the proposed device and to validate the mathematical model. A reduction of the natural frequency by a factor of two has been achieved and the measured transmissibility from a displacement input compares favourably with an equivalent mass-spring system.

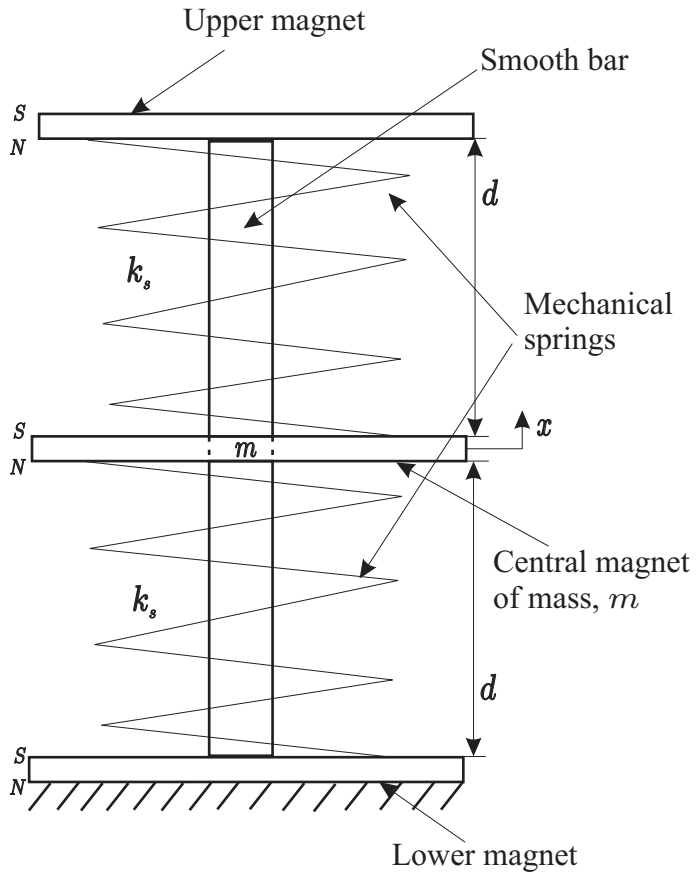

Figure 6.1: Schematic representation of an isolation system with coil springs and magnets: the middle magnets has a mass m and is free to move along the vertical smooth bar. The upper and lower magnets are fixed to the bar and both attract the central piece. The mechanical springs separate the middle magnets from the others

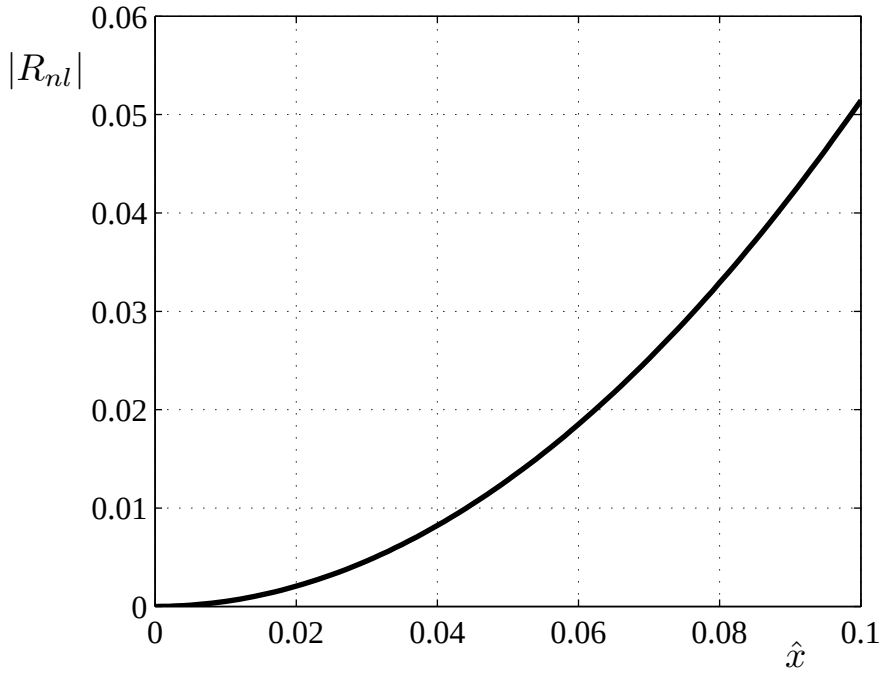

Figure 6.2: Ratio between the magnitudes of the nonlinear and linear terms of the restoring force as a function of the non-dimensional displacement when $\nu = 0.72$

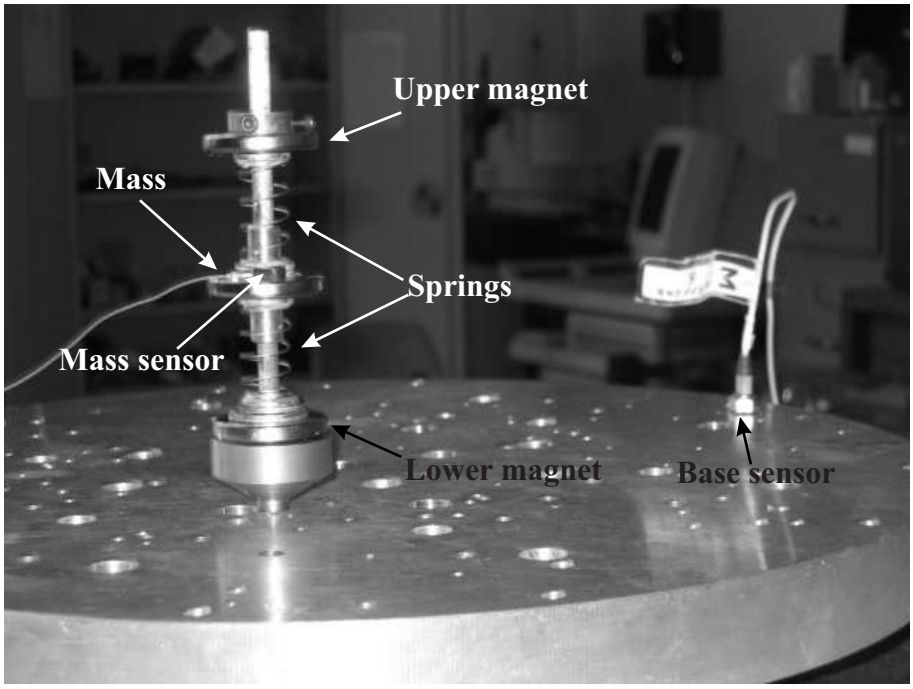

Figure 6.3: Magnetic isolator. Experimental rig fixed at the base to a vertical shaker

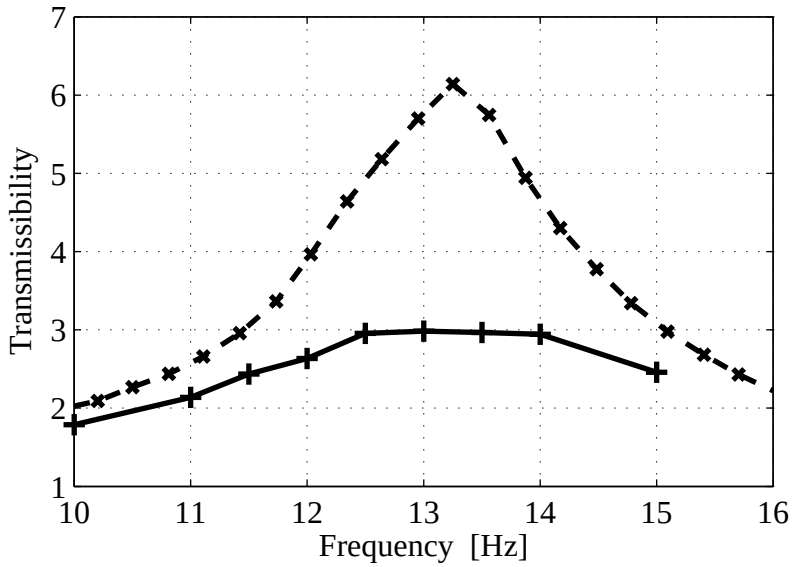

Figure 6.4: Measured modulus of the transmissibility to determine the mount properties. Transmissibility of the system without the coil springs and the magnets arranged in a repelling configuration (dashed line and data points marked with 'x'). Transmissibility of the mass-spring system without the magnets at the extremities of the bar (solid line and data points marked with '+')

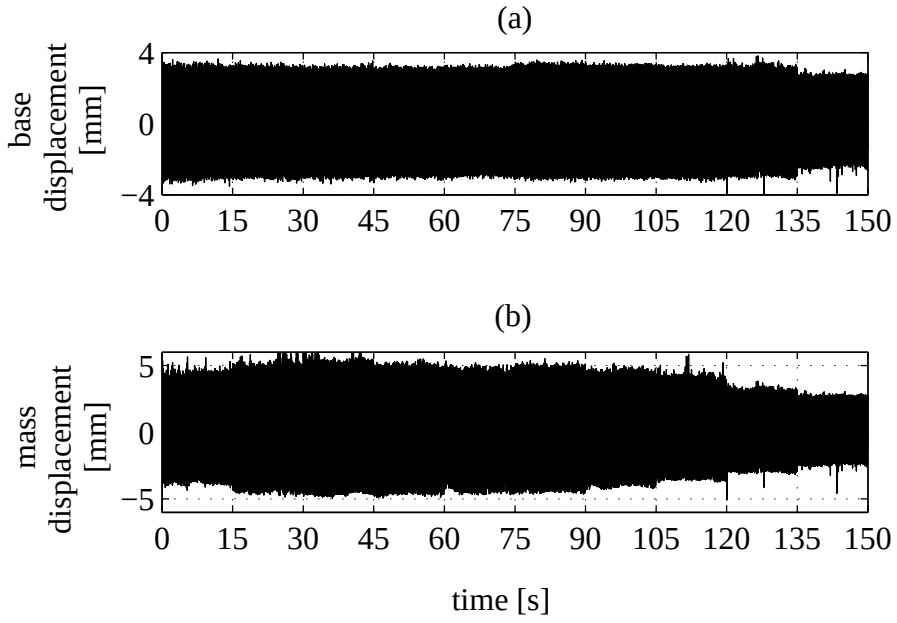

Figure 6.5: Steady-state measurements of the base (a) and mass (b) displacement at different frequency of excitation. The distance of the central magnet from the extremities is $d = 3.81$ cm

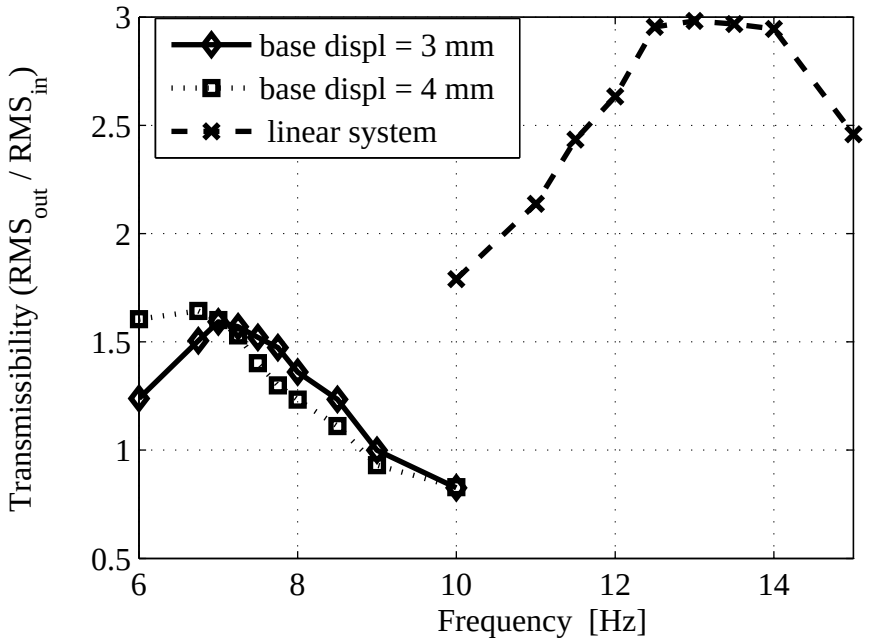

Figure 6.6: Comparison of the transmissibility of a linear mass-spring system (dashed line and crosses) and that of the HSLDS mount for a 3 mm base amplitude excitation (solid line and diamonds) and 4 mm base amplitude excitation (dotted line and squares)

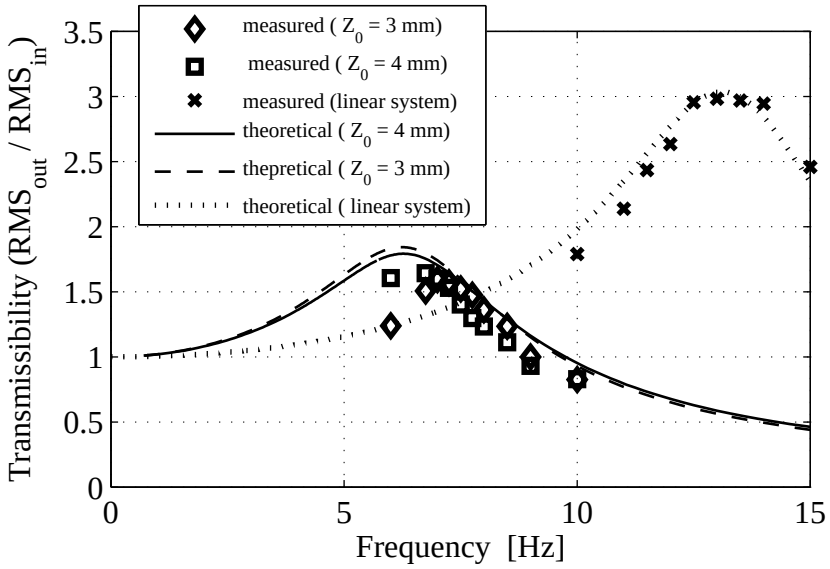

Figure 6.7: Comparison of the transmissibility predicted theoretically and that measured. The diamonds and squares are the data points of the measured transmissibility for a 3 and 4 mm base amplitude excitation respectively. The dashed and the solid line are the theoretical curves, Eqn.(5.22) with the values of ζ and α given in Eqns.(6.12) and (6.14) respectively. The measured transmissibility of the linear system is shown as data points $\times$ whilst the dotted line is the analytical transmissibility Eqn.(1.1) with $\zeta_l = 0.177$.

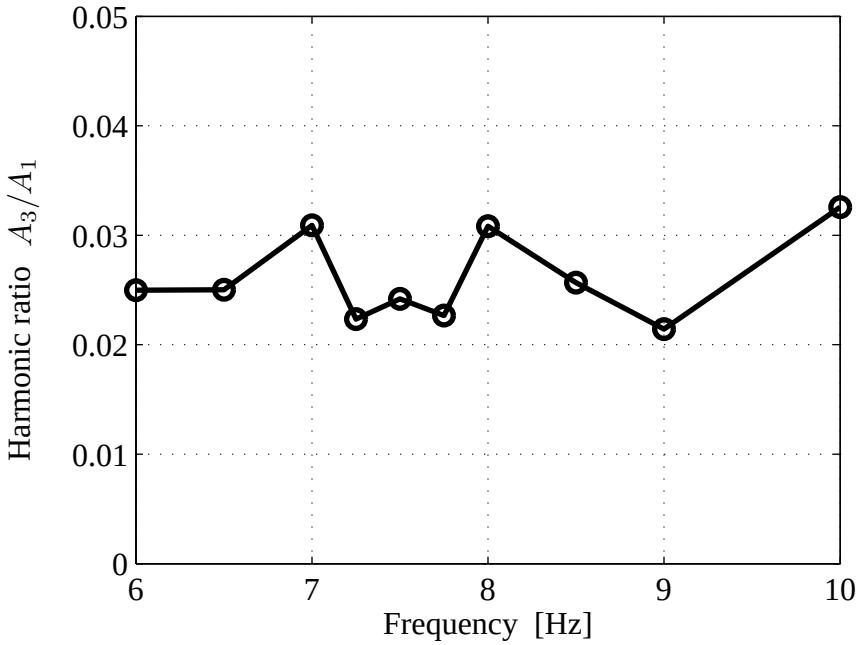

Figure 6.8: Ratio between the Fourier coefficients of the third and first harmonic of the measured response of the HSLDS system at each excitation frequency for base displacement with maximum amplitude of 3 mm

Chapter 7

Concluding remarks and suggestions for future work

The problem of vibration isolation interests many engineering applications. Therefore, a variety of solutions have been proposed over the years on a case-by-case basis. Most generally, the preferred choice to prevent too high a level of vibration from being transmitted from a source to a receiver is to alter the transmission path of the disturbance. The reasons for the preference of this passive approach are to be found in the cost, simplicity and reliability of this type of isolators.

A single-degree-of-freedom isolation system is modelled with a mass suspended on a parallel combination of a spring and a dashpot. These two elements constitute the transmission path. In principle, the stiffness of the spring or the coefficient of the dashpot need to be changed according to the case considered. However, when these elements are linear they both have drawbacks that need to be addressed.

An index of the isolation performance of an isolation mount is the transmissibility which measures the ratio between the transmitted and the excitation force or the ratio of the displacement of the receiver (mass) to that of the base, according to the type of excitation. The expression of the transmissibility of a linear system for harmonic excitation is the same in both cases. Examining the expression of the transmissibility, it can be seen that for the isolator to be effective the frequency of excitation has to be above $\sqrt{2}$ times the natural frequency of the system. Furthermore, the analysis of the transmissibility suggests that an increase of damping is beneficial in reducing the maximum level of transmitted vibration (at

the natural frequency), but is detrimental at higher frequencies. If, instead, the parameter to be changed is the stiffness, then a softer spring is beneficial because it decreases the natural frequency. This bears two important consequences: it increases the frequency region of isolation and potentially increases the damping ratio (which can be always changed by modifying the dashpot coefficient). However, a softer spring induces a greater static displacement which is not very practical in many cases where either there are space limitations or where isolators have limited travel.

A compromise can be found if the force-displacement characteristic of the spring is made nonlinear. In particular it has been shown that an optimal restoring force has a high static and a low dynamic stiffness. A review of the literature has revealed that there are different ways to obtain supports with low stiffness. It has been found that the literature lacks a consistent analysis of the isolation performance of such mechanisms and their comparison with standard linear mounts.

In this thesis the isolation properties of isolators with a high-static-low-dynamic-stiffness (HSLDS) characteristic have been investigated. The desired HSLDS feature derives from the parallel connection of elements with positive and negative stiffness. By appropriately choosing the system parameters it is possible to design a system with a good static load bearing capability and small dynamic stiffness for small oscillations about the static equilibrium position.

The static analysis of two of these mechanisms has been presented in chapter 2. The first model has been taken from the literature and its force and stiffness-deflection functions derived and studied. The stiffness is hardening and the combination of the parameter values that achieve zero stiffness at the static equilibrium position has been provided. It has been argued, though, that this condition is not recommended because if, for unforeseen circumstances (e.g. manufacturing tolerances) the parameters differ from the design values, the stiffness can become negative with undesired consequences (instability). The other HSLDS isolator is a new model which exploits the attracting magnetic force of a set of magnets to produce the necessary negative stiffness. In this case the stiffness is softening and the analysis has highlighted the compromise between a low dynamic stiffness and the excursion from the static equilibrium position before the unstable region (negative stiffness) is reached. For both models, a Taylor's series expansion has

allowed to write the restoring force as a symmetric cubic polynomial (i.e. only linear and cubic terms). It has been reasoned that if the displacement is very small, the cubic term can be neglected compared to the linear one and the system can be described with a linear theory.

However, when the assumption of small displacements does not hold true, the onset of undesired nonlinear effects occurs. Thus, the purpose of Chapters 3, 4 and 5 is to investigate the nonlinear behaviour of these systems. Nonlinear dynamics is a rather complicated matter. In this thesis, only a first-order nonlinear analysis has been carried out. The motion of the receiver (mass) has been supposed to be harmonic at the excitation frequency. This assumption, together with the postulation of small damping, has permitted the derivation of simple expressions for the description of the principal nonlinear phenomenon, namely the jump phenomenon. In Chapter 4 the case of a force-excited system has been discussed, whereas the case of base excitation has been studied in Chapter 5.

For both types of excitation, simple formulas for the prediction of the jump-frequencies have been provided: the jump-down frequency is strongly dependent on damping, whilst the jump-up is almost independent of it. In order to assess the validity of these analytical expressions the frequencies thus predicted have been compared with the values obtained by numerical integration of the equation of motion. The good agreement between the two approaches allows to conclude that the analytical formulae yield good results. A value of the coefficient of the cubic term which prevents the jump from occurring has also been proposed.

When a softening system is harmonically excited by a force acting on the mass, it has been found that, when the amplitude of excitation or the nonlinear coefficient are too large, as the frequency is decreased the jump-down does not occur and the response amplitude increases until the frequency becomes zero. This case has been observed also in previous research and can be ascribed to the fact that for large displacement the stiffness becomes negative and the system unstable.

The main purpose of this research, however, was to investigate the use of HSLDS mechanisms as vibration isolators. The general conclusion is that they do perform better than conventional standard linear isolators with equal static stiffness. The parameter used to evaluate the effectiveness of the isolator is the

transmissibility. Firstly, a numerical comparison between the transmissibilities of the HSLDS and its equivalent linear model has shown that the frequency region of isolation of the HSLDS isolation mount is wider as the result of the lower dynamic stiffness (i.e. lower linearised natural frequency). Also the peak transmissibility of the HSLDS system is smaller. When the system is hardening, regardless of the type of excitation, for large amplitude of oscillations or strongly nonlinear system, the HSLDS feature might become detrimental, in the sense that the isolation properties can become equal or worse than that of a simpler standard linear isolator. A criterion for the evaluation of this instance has been set and the relative value of the nonlinear parameter (which contains both information on the degree on nonlinearity and amplitude of excitation) has been determined.

A lab-scale isolation system has been designed and built reproducing a novel isolation system. Three off-the-shelf magnets were mounted so that their polarities were in attracting configuration and thus had negative stiffness. These were separated by two commercially available springs which provided the positive stiffness and the static load-bearing property. The source of the disturbance was a harmonic excitation of the base, the receiver was the central magnet/mass. The measured transmissibility (ratio between the magnet/mass and base rms displacement) was compared with that of the equivalent linear isolator composed by the springs only (without the two magnets that exerted the attraction force). Two different amplitude of oscillation of the base were used to excite the system. In both cases, the value of the cubic coefficient of the restoring force resulted small relatively to the linear term for the displacement measured. As a proof, the harmonic analysis has revealed that the magnitude of the third harmonic (the biggest after the response at the excitation frequency) is much smaller than the magnitude of the Fourier coefficient at the excitation frequency (by a factor of about 30). A comparison between the theoretical prediction and the measured transmissibility has shown that, for the cases considered, the natural frequency has decreased as predicted, hence increasing the isolation region of the HSLDS mount, and the peak transmissibility is also decreased. However, a certain degree of discrepancy between experimental data and the mathematical model of the HSLDS system has been observed. The mismatch is thought to be due to the simplified damping mechanism used in the analytical model: this has been assumed to be linear and of viscous type whereas a more complex and nonlinear mechanism can be the cause of energy dissipation of the system.

The original contributions can be summarised in brief as follow:

- in-depth static analysis of an existing HSLDS;
- study of a novel vibration isolation mount;
- proposition of simple and explicit expressions of the jump-up and jump-down frequencies for a softening and a hardening Duffing oscillator with linear viscous damping and their corresponding response amplitudes in case of mass and base harmonic excitation;
- introduction of simple analytical expressions for the maximum absolute transmissibility of an HSLDS isolator in case of both harmonic force and base excitation;
- presentation of a study for the free and forced vibration of the Zener model.

7.1 Future work

The analysis presented in this thesis has laid the basis for the development of a very effective isolation system. However, some issues remain open.

From a theoretical point of view, further investigations need to be carried out in order to shed more light on the nonlinear behaviour of the system. Extending the order of the nonlinear analysis might help to clarify issues such as the growth without bound of the response amplitude of a hardening system with a large nonlinear coefficient excited at the base. Chaotic behaviour might also be addressed in order to determine the conditions for its existence.

The experimental rig also has large margins for improvement. Because of its softening characteristic, the main problem is to prevent too large a displacement of the mass which might cause the stiffness to become negative and the system unstable. Also, implementing a variable magnetic force would increase the effectiveness of the isolator. Finally, a more robust isolator can be designed by engineering a control mechanism that, taking into account the effect of gravity, positions the moving mass at a equal distance from the magnets at the extremities of the bar.

The fundamental principle exploited in this thesis for obtaining an isolation system with HSLDS characteristic is to connect in parallel elements with positive and negative stiffness. However, different ways of obtaining the desired load-deflection curve can be explored. For example, in the aerospace industry there is a growing interest in morphing structures. Often these are obtained by thermally curing composite panels with an asymmetric stacking sequence. The result is a multistable structures that exhibits a snap-through mechanism in order to go from one stable state to another. As seen in this thesis, the snap-through mechanism is the evidence of a region with negative stiffness and therefore there is the possibility of exploiting morphing structures for vibration isolation purposes. Another field where the work presented in this thesis can open new possibilities is in the field of material engineering. In the last few years, auxetic materials have become of great interest. These materials (which come in the form of foams or structures with a particular geometry) have the rather unique property of having a negative Poisson's ratio. It has been shown that auxetic materials have a cubic load-deflection curve which makes them suitable for further investigation for vibration isolation purposes. More broadly, the simplified expressions presented herein that characterise the nonlinear dynamic behaviour of a system described by the Duffing equation will be of use for engineering applications which, for sake of simplicity, are too often based on the assumption of linear behaviour. Systems with a cubic restoring force are, for example, being studied in order to improve the amount of energy that can be harvested from a vibrating system.

References

[1] E. Rivin. *Passive Vibration Isolation*. AP, 2001.

[2] J.E. Ruzicka and T.E. Derby. *Influence of Damping in Vibration Isolation*. U.S. Dept. of Defense, 1972.

[3] Harris. *Shock and Vibrations Handbook*. McGraw Hill, IV Edn.

[4] J.P. Den Hartog. *Mechanical Vibrations*. Dover, IV Edn.

[5] S.S. Rao. *Mechanical Vibrations*. Prentice Hall, 2003

[6] M.J. Brennan, A. Carrella, T.P. Waters and V. Lopes Junior. On the dynamic behaviour of a mass supported by a parallel combination of a spring and an elastically connected damper. *Journal of Sound and Vibration*, 309:823-837, 2008.

[7] P. A. Nelson, C. C. Fuller, S. J. Elliott. *Active Control of Vibration*. Acedemic Press, 1997.

[8] K. Shiba, S. Mase, Y. Yabe and K. Tamura. Active/passive vibration control systems for tall buildings. *Smart Materials and Structures*, 7:588–598, 1998.

[9] T. Yoshimura, A. Kume, M. Kurimoto and J. Hino. Construction of an active suspension system of a quarter car model using the concept of sliding mode control. *Journal of Sound and Vibration*, 239(2):187–199, 2001.

[10] W.K. Tseng, J.D. Wu and R.J. Chen. A study of an electrorheological fluid-based mount for broadband vibration isolation in a squeeze mode. *Proceedings of the Institution of Mechanical Engineers, Part D: Journal of Automobile Engineering*, 220(3):313–320, 2006.

[11] X. Wang, D. York and F. Gordaninejad. A new mr fluid-elastomer vibration isolator. *Journal of Intelligent Material Systems and Structures*, 18:1221–1225, 2007.

[12] W.H. Liao and C.Y. Lai. Harmonic analysis of a magnetorheological damper for vibration control. *Smart Material and Structures*, 11:288–296, 2002.

[13] H.P. Gavin, R.D. Hanson and F.E. Filisko. Electrorheological dampers, part ii: Testing and modeling. *Journal of Applied Mechanics, Transactions ASME* , 63(3): 676–682,1996.

[14] F.E. Filisko and D.R. Gamota. Electrorheological materials: Mechanisms and mechanical properties. *American Society of Mechanical Engineers, Applied Mechanics Division, AMD*, 153:75 – 86, 1992.

[15] G. Yang, B.F. Spencer Jr., J.D. Carlson and M.K. Sain. Large-scale mr fluid dampers: Modeling and dynamic performance considerations. *Engineering Structures*, 24(3):309 – 323, 2002.

[16] M.J. Brennan, E. Rustighi and B.R. Mace. Shape memory alloy adaptive tuned vibration absorber: design and implementation. *Smart materials and structures*, 14(1):19–28, 2005.

[17] S.J. Elliott, J.F.V. Vincent, P. Bonello, M.J. Brennan and G. Jeronimidis. Designs for an adaptive tuned vibration absorber with variable shape stiffness element. *Proceedings of the Royal Society A- Mathematical Physical and Engineering Sciences*, 461(2064):3955–3976, 2005.

[18] D.M. McFarland and A.V. Srinivasan. *Smart Structures*. Cambridge University Press, 2001.

[19] N. Jalili. A comparative study and analysis of semi-active vibration control systems. *Journal of Vibration and Acoustic*, 124:593–605, October 2002.

[20] The application of disc springs. *Machinery and production engineering*, (7 February):189–190, 1973.

[21] J.C. Nissen and J.B. Hunt. The braodband dynamic vibration absorber. *Journal of Sound and Vibration*, 83(4):573 – 578, 1982.

[22] A. Risitano, G. La Rosa and M. Messina. Stiffness of variable thickness belleville springs. *Journal of Mechanical Design*, 123(2):294 – 299, 2001.

[23] F. Yeaple. Master the mysteries of spring washers. *Product Engineering*, (June):37 – 40, 1978.

[24] P. Alabuzhev, A. Gritchin, L. Kim, G. Migirenko, V. Chon and P. Stepanov. *Vibration Protecting and Measuring Systems with Quasi-Zero Stiffness*. Hemisphere Publishing, NY, 1989.

[25] J. Winterflood. *High Performance Vibration Isolation for Gravitational Wave Detection*. PhD thesis, University of Western Australia - Dept. of Physics, 2001.

[26] L.N. Virgin and R.B. Davis. Vibration isolation using buckled struts. *Journal of Sound and Vibration*, 260:965 – 973, 2003.

[27] R.H. Plaut, J.E. Sidbury and L.N. Virgin. Analysis of buckled and prebent fixed-end columns used as vibration isolators. *Journal of Sound and Vibration*, 283:1216 – 1228, 2005.

[28] R.H. Plaut, Sidbury J.E. and L.N. Virgin. Analysis of buckled and prebent fixed-end columns used as vibration isolators. *Journal of Sound and Vibration*, 283:1216 – 1228, 2005.

[29] D.L.Platus. Negative-stiffness-mechanism vibration isolation systems. In *Proceedings of SPIE Conference on Current Developments in Vibration Control for Optomechanical Systems*, volume 3786, pages 98 – 105, 1999.

[30] K. Peleg and S. Hinga. Parameter sensitivity of non-linear vibration systems. *Journal of Sound and Vibration*, 128(1):1–11, 1989.

[31] K. Peleg. Frequency response of non-linear single degree of freedom systems. *Int. J. Mech. Sci.*, 21:75–84, 1979.

[32] J.M. Housner and S.E. Woodard. Nonlinear behaviour of a passive zero-spring-rate suspension system. *Journal of Guidance*, 14(1):84 – 88, 1991.

[33] J.M. Schimmels and Y. Wan. Improved vibration isolating seat suspension designs based on position-dependant nonlinear stiffness and damping characteristic. *Journal of Dynamic Systems, Measurements and Control*, 125:330 – 338, 2003.

[34] N.A. Halliwell, I.J. Sokolov and V.I. Babitsky. Hand-held percussion machines with low emission of hazardous vibration. *Journal of Sound and Vibration*, 306:59 – 73, 2007.

[35] E. Puppin and V. Fratello. Vibration isolation with magnet springs. *Review of Scientific Instruments*, 73(11):4034 – 4036, 2002.

[36] E. Bonisoli and A. Vigliani. Identification techniques applied to a passive elasto-magentic suspension. *Mechanical Systems and Signal Processing*, 21:1479 – 1488, 2007.

[37] T. Mizuno, M. Takasaki, D. Kishita and K. Hirakawa. Vibration isolation system combining zero-power magnetic suspension with springs. *Control Engineering Practice*, 15:187–196, 2007.

[38] L. Lacoste. A new type long period vertical seismograph. *Physics*, 5:178, 1934.

[39] L. Lacoste. Lacoste and Romberg straight-line gravity meter. *Geophysics*, 48:606–610, 1983.

[40] A. Carrella, M.J. Brennan and T.P. Waters. Static analysis of a passive vibration isolator with quasi-zero-stiffness characteristic. *Journal of Sound and Vibration*, 301(3-5):678–689, 2007.

[41] A. Carrella, T.P. Waters, M.J. Brennan and K. Shin. On the design of a high-static-low-dynamic-stiffness isolator using linear mechanical springs and magnets. *Journal of Sound and Vibration*, article in press.

[42] T. Tarnai. Zero stiffness elastic structures. *International Journal of Mechanical Sciences*, 45:425–431, 2003.

[43] E. T. Whittaker and G. N. Watson. *A Course of Modern Analysis*. Cambridge Mathematical Library, IV Edn., 1990.

[44] A.H Nayfeh and D.T. Mook. *Nonlinear Oscillations*. John Wiley and Sons, II Edn., 1995.

[45] D.W. Jordan and P. Smith. *Nonlinear Ordinary Differential Equations*. Oxford, III Edn., 1999.

[46] A. D'Angola, G. Carbone, L. Mangialardi and C. Serio. Nonlinear oscillations in a passive magnetic suspension. *International Journal of Nonlinear Mechanics*, 41:1039 – 1049, 2006.

[47] T. Mizuno, T. Toumiya and M. Takasaki. Vibration isolation using negative stiffness. *JSME International Journal, Series C*, 46(3):807–812, 2003.

[48] W. Robertson, R. Wood, B. Cazzolato and A. Zander. Zero-stiffness magnetic springs for active vibration isolation. *Journal of Mathematical Physics*, 11(12):3413 – 3415, 1970.

[49] F. Bancel. Magnetic nodes. *Journal of Physics D: Appl. Phys.*, 32:2155 – 2161, 1999.

[50] A. Joseph, K. Pomerak, J. Prince and D. Sacher. *Physics for Engineering Technology*. Wiley, II Edn., 1977.

[51] G. Elert. *The Physics Hypertextbook*. http://hypertextbook.com/physics/mechanics/energy-potential/, 2007.

[52] Jon Juel Thomsen. *Vibration and Stability - Order and Chaos*. McGraw Hill, 1997.

[53] L. Meirovitch. *Elements of Vibration Analysis*. McGraw Hill, International Edn., 1986.

[54] A. Rand. *Lecture Notes on Nonlinear Vibration*. Wiley, 2005.

[55] N. V. Virgin. *Introduction to Experimental Nonlinear Dynamics*. Cambridge University Press, 2000.

[56] A.H. Nayfeh. *Perturbation Methods*. John Wiley and Sons, 1973.

[57] C. Hayashi. *Nonlinear Oscillations in Physical Systems*. McGraw Hill, 1964.

[58] J.H. He. Some asymptotic methods for strongly nonlinear equations. *International Journal of Modern Physics B*, 20(10):1141–1199, 2006.

[59] M.I. Friswell and J.E.T. Penny. The accuracy of jump frequencies in series solutions of the response of a duffing oscillator. *Journal of Sound and Vibration*, 169(2):261 – 269, 1994.

[60] M.N. Hamdan and T.D. Burton. On the steady state response and stability of non-linear oscillators using harmonic balance. *Journal of Sound and Vibration*, 166(2):255 – 266, 1993.

[61] K. Worden. On jump frequencies in the response of a duffing oscillator. *Journal of Sound and Vibration*, 198(4):522 – 525, 1996.

[62] B. Ravindra and A.K. Mallik. Hard duffing-type vibration isolators with combined coulomb and viscous damping. *Journal of Nonlinear Mechanics*, 28(4):427–440, 1993.

[63] B. Ravindra and A.K. Mallik. Performance of non-linear vibration isolators under harmonic excitation. *Journal of Sound and Vibration*, 170(3):325–337, 1994.

[64] G. Nakhaie Jazar, R. Houim, A. Narimarani and M.F. Golnaraghi. Frequency response and jump avoidance in a nonlinear passive engine mount. *Journal of Vibration and Control*, 12(11):1205 – 1237, 2006.

[65] G. Duffing. Erzwungene schwingungen bei vernderlicher eigenfrequenz und ihre technische bedeutung. *Vieweg Braunschweig*, 1918.

[66] K. Magnus. *Vibrations*. Blackie and Sons London, I Edn., 1965.

[67] K. Worden and G.R. Tomlinson. *Nonlinearity in Structural Dynamics: Detection, Identification and Modelling*. Institute of Physics Publishing, 2001.

[68] Taylor J.H. and K.S. Narendra. Stability region for damped Mathieu equation. *Siam - Journal of App. Math*, 17(2):343–352, 1969.

[69] P. Hagedorn. *Nonlinear Oscillations*. Clarendon Press, Oxford, I Edn., 1981.

[70] P. Malatakar and A.H. Nayfeh. Calculation of jump frequencies in the response of a s.d.o.f. non-linear system. *Journal of Sound and Vibration*, 254(5):1005 – 1011, 2002.

[71] J. Kevorkian and J.D. Cole. *Perturbation Methods in Applied Mathemathics*. Springer-Verlag, 1981.

[72] A. Murata, Y. Kume and F. Hashimoto. Application of catastrophe theory to forced vibration of a diaphgram air spring. *Journal of Sound and Vibration*, 112(1):31 – 44, 1987.

[73] M. Feldman. Nonlinear free vibration identification via the hilbert transform. *Journal of Sound and Vibration*, 208(3):475–489, 1997.

[74] A. Carrella, M.J. Brennan and T.P. Waters. A Demonstrator to Show the Effects of Negative Stiffness on the Natural Frequency of a Simple Oscillator. *Proceedings of the Institution of Mechanical Engineers, Part C, Journal of Mechanical Engineering Science*, in press.

Available online at www.sciencedirect.com
ScienceDirect
Journal of Sound and Vibration 309 (2008) 823–837
JOURNAL OF SOUND AND VIBRATION
www.elsevier.com/locate/jsvi

On the dynamic behaviour of a mass supported by a parallel combination of a spring and an elastically connected damper

M.J. Brennan[a,*], A. Carrella[a], T.P. Waters[a], Vicente Lopes Jr.[b]

[a]*Institute of Sound and Vibration Research, University of Southampton, Southampton, Hampshire SO17 1BJ, UK*
[b]*Department of Mechanical Engineering, Universidade Estadual Paulista—UNESP/Ilha Solteira, Av. Brasil, 5385-000 Ilha Solteira, SP, Brazil*

Received 14 October 2006; received in revised form 29 July 2007; accepted 30 July 2007
Available online 30 October 2007

Abstract

This paper presents a consistent and concise analysis of the free and forced vibration of a mass supported by a parallel combination of a spring and an elastically supported damper (a Zener model). The results are presented in a compact form and the physical behaviour of the system is emphasised. This system is very similar to the conventional single-degree-of freedom system (sdof)—(Voigt model), but the dynamics can be quite different depending on the system parameters. The usefulness of the additional spring in series with the damper is investigated, and optimum damping values for the system subject to different types of excitation are determined and compared.

There are three roots to the characteristic equation for the Zener model; two are complex conjugates and the third is purely real. It is shown that it is not possible to achieve critical damping of the complex roots unless the additional stiffness is at least eight times that of the main spring. For a harmonically excited system, there are some possible advantages in using the additional spring when the transmitted force to the base is of interest, but when the displacement response of the system is of interest then the benefits are marginal. It is shown that the additional spring affords no advantages when the system is excited by white noise.

1. Introduction

The classic mass–spring–damper single degree-of-freedom (sdof) system is the bedrock of vibration analysis and has been studied at length over many decades. Any elementary textbook on vibration analysis describes the free and forced vibration of a sdof system in detail. In the context of vibration isolation, where the parallel combination of the spring and damper are representative of the isolation system, the damper performs a useful function at the resonance frequency of the system, but is detrimental at high frequencies. It has therefore been suggested that elastically connecting the spring may offer some potential benefits [1]. A thorough investigation of the modified sdof has been conducted and is described comprehensively in Ref. [2].

*Corresponding author.
E-mail address: mjb@isvr.soton.ac.uk (M.J. Brennan).

0022-460X/$ - see front matter © 2007 Elsevier Ltd. All rights reserved.
doi:10.1016/j.jsv.2007.07.074

Combinations of springs and dampers are of interest to the materials community as they are used to represent the behaviour of viscoelastic materials [3]. The parallel combination of a spring and a mass is generally called the *Voigt* model, the series combination of a spring and a damper is called the *Maxwell* model and the parallel combination of a spring and an elastically supported damper is called the *Zener* model. These terms are used in this paper for such systems supporting a mass.

Free vibration of the Zener model was studied by Yamakawa [4]. Muller [5] also studied this model, some 44 years later, in terms of parameters more concerned with material properties such as "*relaxation time*". He also showed that the characteristic equation of the system comprises three roots, one of which is purely real and the other two being complex conjugates. His analysis demonstrated that the complex roots become real under certain situations. However, his approach was such that his explanation of this phenomenon was mathematical rather than physical. Muravyov and Hutton [6] have studied a system similar to the Zener model, where a mass is suspended by a parallel combination of a viscoelastic spring and a viscous dashpot. They showed that over- or under-damped oscillations occur depending on the parameters of the viscoelastic spring.

Because the Zener model is of interest in vibration isolation and in material characterisation it is perhaps surprising that the literature offers little other work on this subject other than the aforementioned references. It is worth noting that there is not a consistent reference trail from the later to the earlier papers. The present paper hopes to contribute by analysing the free and forced vibration of the Zener model in a consistent manner and presenting the results in a compact form with particular emphasis on the physical behaviour of the system.

Optimum damping values for various stated criteria for each of the situations (free vibration, harmonic excitation and white noise excitation) are derived for each case, and are compared. For forced vibration, the amplitude response of the mass is considered, as is the force transmitted to the rigid base.

2. Free vibration

The sdof system shown in Fig. 1 consists of a mass, m, supported by a parallel combination of a spring, k, and an elastically attached viscous damper, c, where the connecting spring has stiffness Nk ($N \geqslant 0$). The spring in series with the dashpot is referred to as the *secondary spring* as opposed to the *primary spring* which is the one in parallel with the damper. This system is commonly referred to as the Zener model, and its equation of

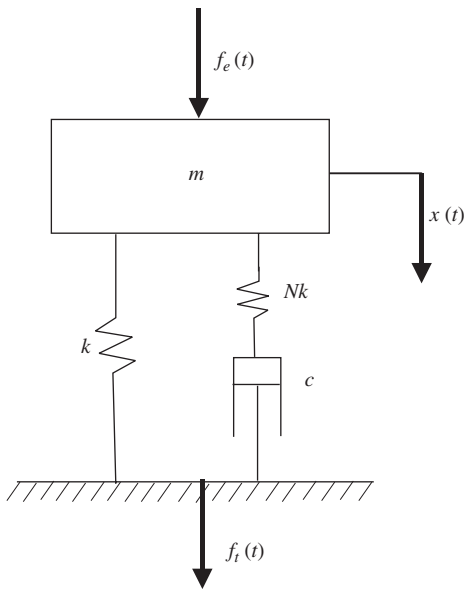

Fig. 1. A point mass supported on a parallel combination of a spring and an elastically attached viscous damper (Zener model).

motion of free vibration is given by [1,2]

$$\left(\frac{mc}{Nk}\right)\dddot{x} + m\ddot{x} + c\left(\frac{N+1}{N}\right)\dot{x} + kx = 0. \tag{1}$$

Eq. (1) can be written in terms of the non-dimensional damping coefficient $\varsigma = c/2\sqrt{mk}$ and the undamped natural frequency of the system when $N = 0$, $\omega_0 = \sqrt{k/m}$, as

$$\left(\frac{2\varsigma}{\omega_0 N}\right)\dddot{x} + \ddot{x} + 2\varsigma\omega_0\left(\frac{N+1}{N}\right)\dot{x} + \omega_0^2 x = 0. \tag{2}$$

Note that $\varsigma = c/2\sqrt{mk}$ is a convenient non-dimensional damping parameter and *not* the damping ratio of the system. As such, the usual symbol for damping ratio, ζ, has been deliberately avoided. Eq. (2) is a third-order differential equation with solutions of the form

$$x(t) = Ae^{s_1 t} + Be^{s_2 t} + Ce^{s_3 t}, \tag{3}$$

where A, B, C are constants that depend on the initial conditions and s_1, s_2, s_3 are the solutions of the system's characteristic equation

$$\left(\frac{2\varsigma}{\omega_0 N}\right)s^3 + s^2 + 2\varsigma\omega_0\left(\frac{N+1}{N}\right)s + \omega_0^2 = 0. \tag{4}$$

Alternatively, a non-dimensional form of the solution can be assumed

$$x(t) = Ae^{\hat{s}_1\tau} + Be^{\hat{s}_2\tau} + Ce^{\hat{s}_3\tau}, \tag{5}$$

where $\hat{s}_i = s_i/\omega_0$ and $\tau = \omega_0 t$ is non-dimensional time. The characteristic equation can then be written as

$$\hat{s}^3 + \left(\frac{N}{2\varsigma}\right)\hat{s}^2 + (N+1)\hat{s} + \left(\frac{N}{2\varsigma}\right) = 0. \tag{6}$$

The three roots of this equation are either all real, or include a complex conjugate pair that characterises under-damped motion [5]. The roots of this equation are given in Appendix A. To determine when critical damping occurs, the imaginary parts of the roots of Eq. (6) are set to zero and solved for ς. The algebraic steps for this procedure can also be found in Appendix A. For a given stiffness ratio N, the values of ς for which this can occur are found to be

$$\varsigma = N\frac{\sqrt{2}}{8}\sqrt{\frac{N^2+20N-8}{(N+1)^3} \pm \frac{\sqrt{N(N-8)^3}}{(N+1)^3}}. \tag{7}$$

There are no real solutions to Eq. (7) when $N<8$ which means that critical damping cannot be achieved if the secondary spring is too soft. This is illustrated by the root locus in Fig. 2(a) in which the roots have been calculated for $0.001 \leqslant \varsigma \leqslant 20$ in increments of 0.05. When $\varsigma = 0$ (no damping) the complex roots are purely imaginary with $\hat{s}_{2,3} = \pm j$, and the system becomes a mass supported on the primary spring alone. As the damper coefficient is increased the complex conjugate pair of roots move in the direction of the arrows and become under-damped. The damped natural frequency is given by the imaginary part of the roots. Further increases in damping coefficient results in a reduction in the real part of the roots and hence the damping in the system. In the limit as $\varsigma \to \infty$ the damper acts as a rigid link and the system collapses to a mass supported on the primary and secondary springs in parallel, i.e. an undamped system. The natural frequency is $\sqrt{N+1}$ times that of the original undamped system, when $\varsigma = 0$. When $\varsigma \ll 1$ the real root $\hat{s}_1$ is very large and negative, and as ς increases the real root moves towards the origin.

When $N>8$ there are two values of ς that satisfy Eq. (7). These solutions are distinct critical damping coefficients for the complex roots of the system, ς_{lower} and ς_{upper} say. When $N \gg 8$, then $\varsigma_{\text{lower}} \approx 1$, the system is critically damped for approximately the same value of damping coefficient as the corresponding Voigt model. The upper value $\varsigma_{\text{upper}} \approx \sqrt{N}/4$ corresponds to a larger value of damping coefficient that also yields critical damping. Taking $N = 15$ as an example, Fig. 2(b) illustrates the root locus when $N>8$. Again, the complex conjugate pair of roots is purely imaginary when $\varsigma = 0$, and initially become increasingly damped as ς

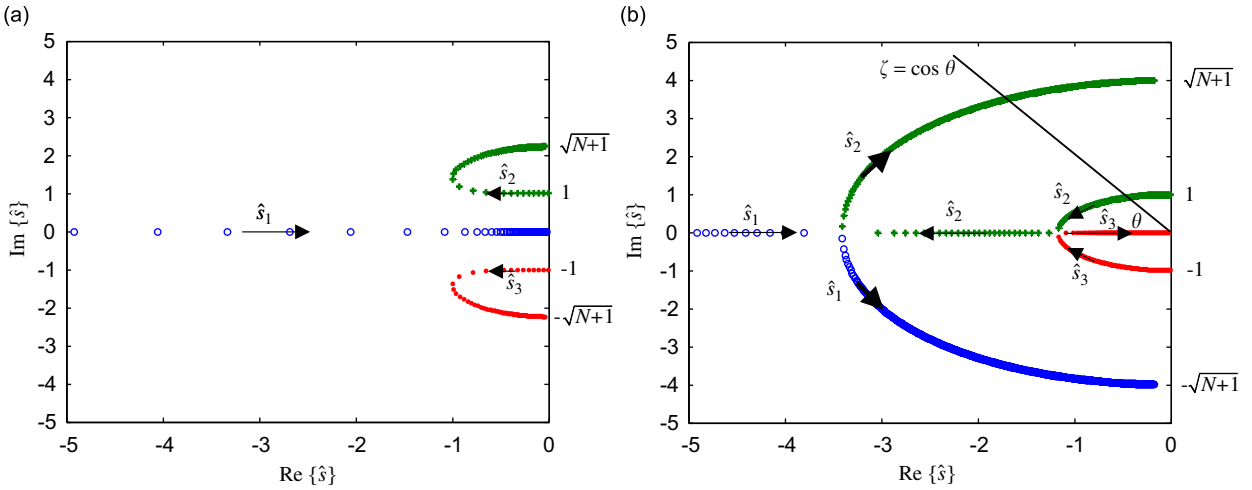

Fig. 2. Examples of the solutions to the characteristic equation of the Zener model as ς is increased from 0.001 to 20 in increments of 0.005: (a) root loci for $N=4$. (b) Root loci for $N=15$.

increases. When $\varsigma=\varsigma_{\text{lower}}$ the root pair become real, one becoming increasingly negative and one moving towards the origin. The root that is real when $\varsigma\ll 1$, ($\hat{s}_1$), is initially large and negative, and moves towards the origin as ς increases. When $\varsigma=\varsigma_{\text{upper}}$ this root and the root moving towards the left on the real axis, ($\hat{s}_2$), become complex; they become less damped as ς increases further until there is effectively zero damping in the system as in the previous case.

In a sdof system, where the mass is supported on a parallel combination of a spring and damper (Voigt model), the governing equation of motion has two roots. These roots are complex when the damping ratio is less than one and are real when the damping ratio is greater than one. The damping ratio of the system is defined by $-\text{Re}\{\hat{s}_{1,2}\}/|\hat{s}_{1,2}|$ [7]. In a system where the dashpot is elastically supported, the damping of the system cannot be uniquely defined because when $\varsigma<\varsigma_{\text{lower}}$ and $\varsigma_{\text{upper}}<\varsigma$ there are always two complex roots and one real root. However, the damping ratios corresponding to the complex roots can be defined in a similar way to the Voigt model [8]. For each value of ς, the damping ratio for these roots is given by

$$\zeta=\cos\theta=\frac{-\text{Re}\{\hat{s}_{1,2}\}}{|\hat{s}_{1,2}|}. \tag{8}$$

This is illustrated in Fig. 2(b). It can be seen that there are two roots that have the same angle θ. Thus, the same damping ratio ζ is obtained for two different values of ς, and for each N there are two values of damping ratio for each oscillatory root. This is shown in the contour plot of Fig. 3(a) for $0\leqslant N\leqslant 30$ and $0\leqslant\varsigma\leqslant 3$. Also plotted in Fig. 3(a) are the lines given by Eq. (7a,b). The region enclosed by the two curves represents combined values of N and ς that result in over-damped motion.

The damped natural frequency normalised by ω_0 is plotted in Fig. 3(b). When $N<8$, the damped natural frequency either increases or decreases first then increases as ς increases. However, when $N\geqslant 8$, the damped natural frequency first decreases as ς increases, and then it increases again. This can also be seen in Fig. 3(b).

Of practical interest is the maximum damping that can be achieved for a given N when $N\leqslant 8$. The form of Eq. (6) is the same as that in Ref. [9], which describes integrated force feedback control of a truss structure. In Ref. [9], an expression is given for the maximum possible damping ratio of the system. This can be adapted to the Zener model, which results in a maximum possible damping coefficient for $N\leqslant 8$, of

$$\zeta_{\max}=\frac{\sqrt{N+1}-1}{2}. \tag{9}$$

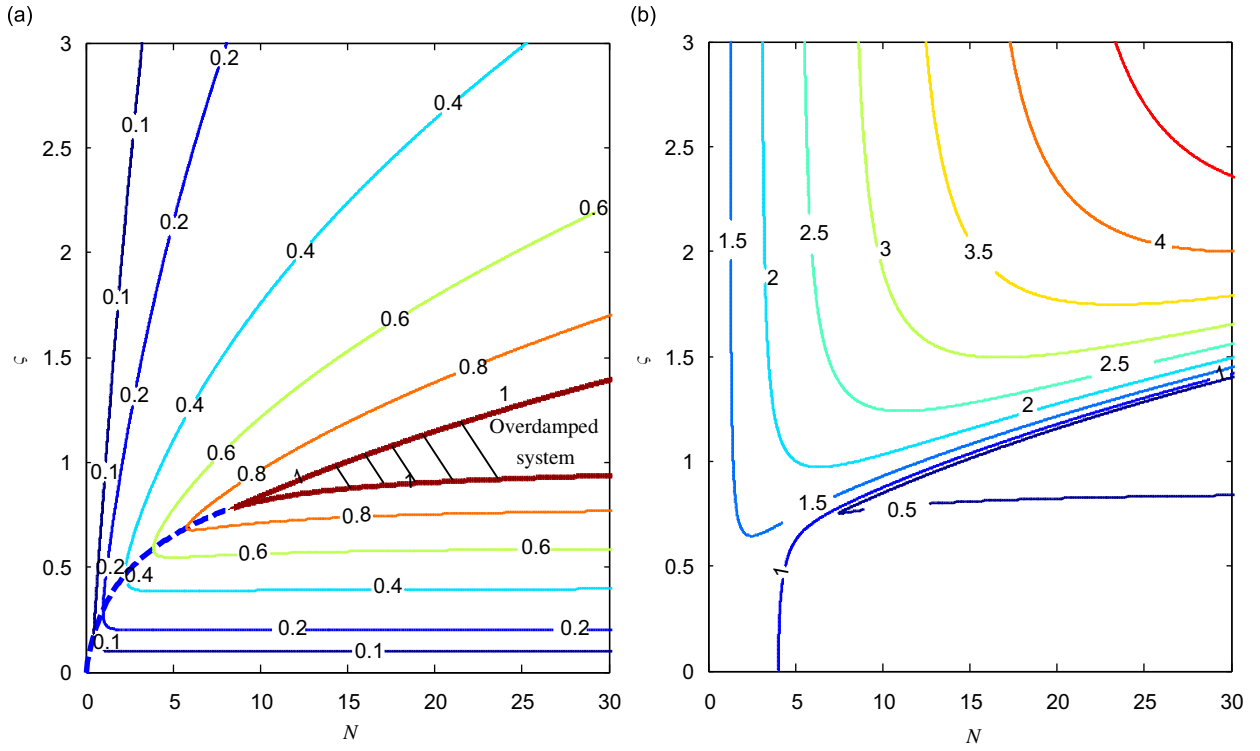

Fig. 3. Dynamic characteristics of free vibration of the Zener model: (a) Contour plot showing the damping ratio of roots $\hat{s}_{1,2}$. The dashed line shows the maximum damping ratio for $N<8$. (b) Contour plot showing the damped natural frequency normalised by ω_0.

The corresponding value of ς is determined by setting

$$\frac{\mathrm{Re}\{\hat{s}_{1,2}\}}{|\hat{s}_{1,2}|} = \frac{\sqrt{N+1}-1}{2} \tag{10}$$

and solving for ς, which results in

$$\varsigma = \frac{N}{2(N+1)^{3/4}}, \quad N \leqslant 8. \tag{11}$$

This is also plotted in Fig. 3(a) as a dashed line. The minimum real part of the underdamped root for the case when $N \leqslant 8$ is given by

$$\mathrm{Re}(\hat{s})\big|_{\min} = \frac{N}{4} \tag{12}$$

and this occurs when

$$\varsigma = \frac{N}{N+2}. \tag{13}$$

In Fig. 4, part of the root locus of $\hat{s}_2$ when $N = 4$ is plotted. Also plotted is the root locus of a second order system with an undamped natural frequency normalised by ω_0 of $(1+\sqrt{N+1})/2$. The tangent to the root locus of $\hat{s}_2$ drawn from the origin intersects *with* the root locus of the second-order system *and* the line $N/4$. Thus, the maximum damping ratio can be interpreted as the damping ratio for an equivalent second order system, which has an undamped natural frequency of $\omega_n/\omega_0 = (1+\sqrt{N+1})/2$ and a root to its normalised characteristic equation that has a real part equal to $-N/4$.

To illustrate the effect of the purely real root on the free vibration of the Zener model, two simulations are presented in Figs. 5(a) and (b). The first is the normalised impulse response of the system, $x(t)/(\hat{f}/m\omega_d)$, where

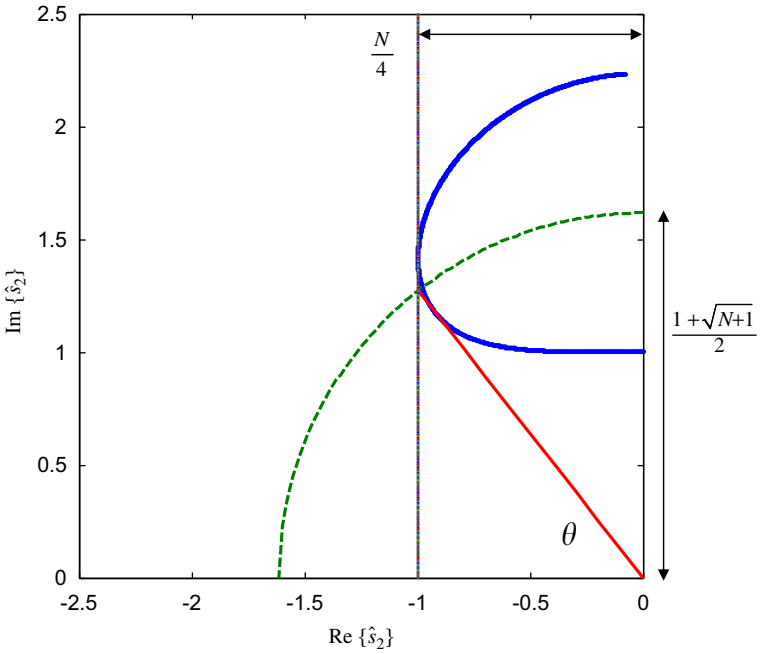

Fig. 4. Graph showing part the root locus of $\hat{s}_2$ when $N = 4$. The solid line is the root locus and the dashed line is the root locus of a second order system with an undamped natural frequency normalised by ω_0 of $(1 + \sqrt{N+1})/2$.

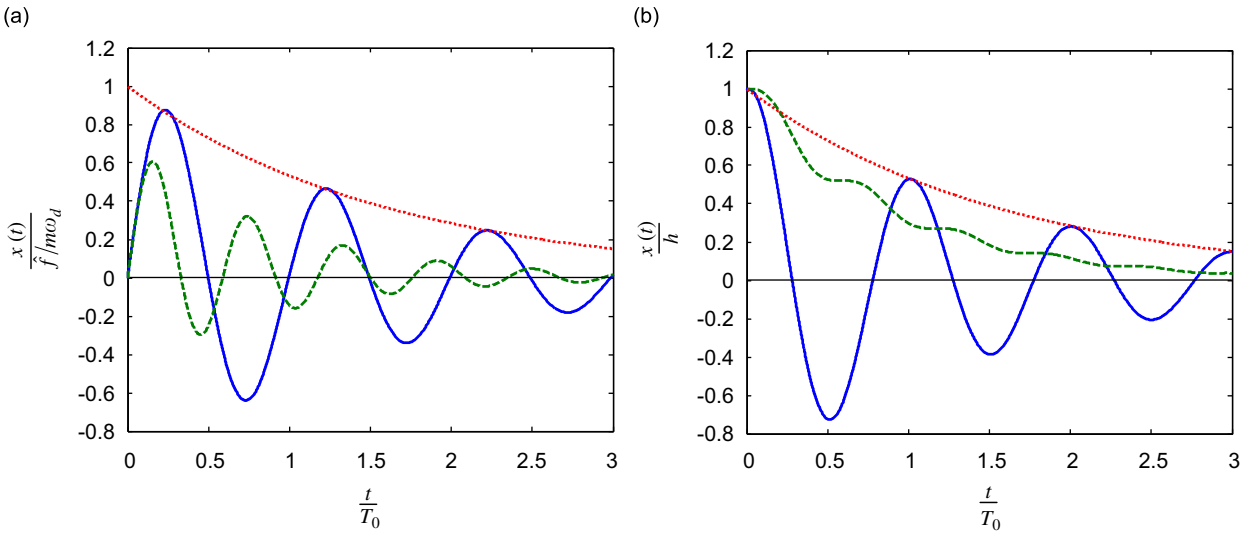

Fig. 5. Free vibration of the Zener model for two different initial conditions. $N = 2$ and $\varsigma = 0.1$: (a) Impulse response of the Zener system. Solid line, $\varsigma = 0.1$; dashed line, $\varsigma = 1.92$; dotted line, $\exp(-\zeta\omega_0 t)$. (b) Response of the Zener model to an initial displacement h. Solid line, $\varsigma = 0.1$; dashed line, $\varsigma = 1.92$; dotted line, $\exp(-\zeta\omega_0 t)$.

$\hat{f}$ is a unit impulse and ω_d is the damped natural frequency, and the second is the normalised response to a displacement input $x(t)/h$, where h is the initial displacement. Both responses are plotted as a function of non-dimensional time t/T_0 where $T_0 = 2\pi/\omega_0$ is the undamped natural period of the system when $N = 0$. To determine the constants in Eq. (5), the following equations have to be solved for the impulse response and the

displacement input response, respectively:

$$\begin{bmatrix} A \\ B \\ C \end{bmatrix} = \begin{bmatrix} 1 & 1 & 1 \\ \hat{s}_1 & \hat{s}_2 & \hat{s}_3 \\ \hat{s}_1^2 & \hat{s}_2^2 & \hat{s}_3^2 \end{bmatrix}^{-1} \begin{bmatrix} 0 \\ 1 \\ 0 \end{bmatrix} \quad \text{and} \quad \begin{bmatrix} A \\ B \\ C \end{bmatrix} = \begin{bmatrix} 1 & 1 & 1 \\ \hat{s}_1 & \hat{s}_2 & \hat{s}_3 \\ \hat{s}_1^2 & \hat{s}_2^2 & \hat{s}_3^2 \end{bmatrix}^{-1} \begin{bmatrix} 1 \\ 0 \\ 0 \end{bmatrix}. \tag{14a,b}$$

The values of $\hat{s}_i$ are determined numerically by solving Eq. (6) for $N = 2$ and $\varsigma = 0.1$ and 1.92 (which correspond to a value of $\zeta = 0.1$).

The main difference between the Zener and the Voigt models is the additional purely real root. This root is large and negative (−9.8) when $\varsigma = 0.1$ and small and negative (−0.18) when $\varsigma = 1.92$. The effects of this root on the free response can be observed in Figs. 5(a) and (b). It can be seen that the real root has a negligible effect when $\varsigma = 0.1$ as both the impulse response and the displacement input response are similar to that of the Voigt model and are thus dominated by the complex roots. However, when $\varsigma = 1.92$ the effect of the purely real root on the response is very much dependent on the initial conditions. For the impulse response, the complex roots dominate the response, but for the displacement input it is clear that the purely real root dominates the response.

As noted by Muller [5], because there is always one purely real root, the characteristic Eq. (6) can be written as

$$(\hat{s} + s_0)(\hat{s}^2 + a\hat{s} + b) = 0, \tag{15}$$

where s_0, a and b can be determined by comparing Eqs. (6) and (15). In general, Eq. (15) has a complicated form from which little new knowledge can be gained. However, there are two situations when the characteristic equation can be factorised easily, which is when

$\varsigma \ll N$. In which case Eq. (6) becomes

$$(\hat{s} + \varsigma + j)(\hat{s} + \varsigma - j)\left(\hat{s} + \frac{N}{2\varsigma}\right) = 0. \tag{16a}$$

$\varsigma \gg N$. In which case Eq. (6) becomes

$$\left(\hat{s} + \frac{N^2}{4(1+N)\varsigma} + j\sqrt{N+1}\right)\left(\hat{s} + \frac{N^2}{4(1+N)\varsigma} - j\sqrt{N+1}\right)\left(\hat{s} + \frac{N}{2(1+N)\varsigma}\right) = 0. \tag{16b}$$

The magnitudes of the real parts of the roots of the characteristic equation, which govern the decay of free vibration, are calculated numerically for $N = 4$ and plotted in Fig. 6 (all are negative) as a function of ς.

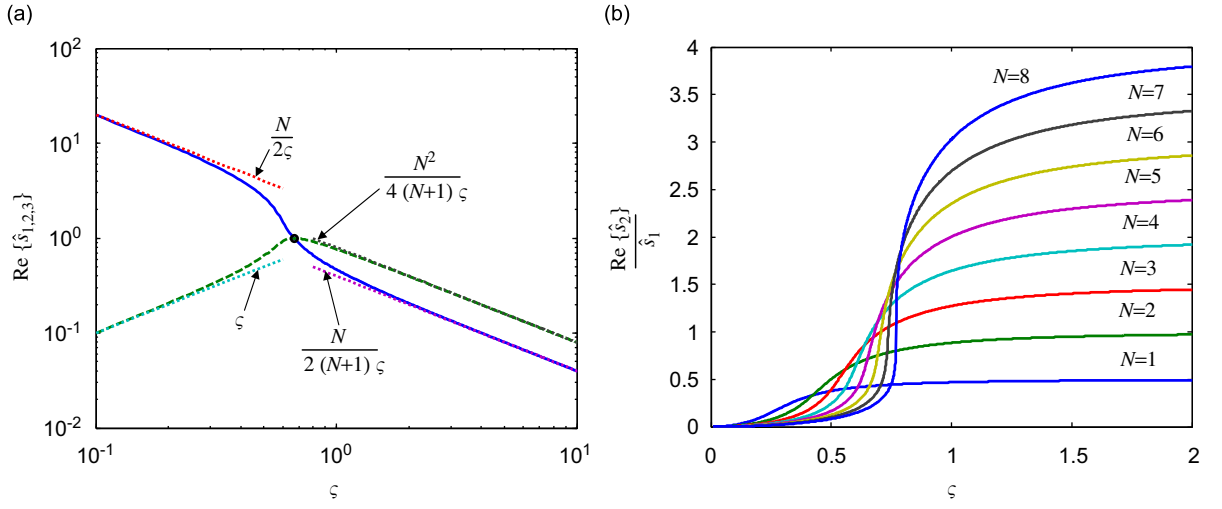

Fig. 6. Graphs to show the behaviour of the real parts of the roots for the Zener model as ς increases: (a) Magnitudes of the real part of the roots when $N = 4$ as ς increases (they are all negative). The dotted lines show the asymptotic behaviour. The roots are equal (°) when $\varsigma = N/(6\sqrt{N/2-1})$. (b) The ratio of $\mathrm{Re}\{\hat{s}_2\}/\hat{s}_1$ plotted as a function of ς for different values of N. $\mathrm{Re}\{\hat{s}_2\}/\hat{s}_1 \approx N/2$ when $\varsigma \gg 1$.

The real parts of the roots of Eq. (16a) and (16b) are also plotted. It can be seen that they are the asymptotes for the real parts of the roots when $\varsigma \ll 1$ and $\varsigma \gg N$. It can also be seen that the purely real root is much larger than the real part of the complex roots when $\varsigma \ll 1$, but when $\varsigma \gg 1$ the real part of the complex roots is greater than the purely real root. When the real part of the complex roots is equal to the purely real root, then

$$\varsigma = \frac{N}{6\sqrt{N/2-1}}. \tag{17}$$

The ratio of the real parts of the roots is plotted as a function of ς in Fig. 6(b) for different values of N. It can be seen in Figs. 6(a) and (b) that when $\varsigma \gg 1$ then $\mathrm{Re}\{\hat{s}_2\}/\hat{s}_1 \approx N/2$. Note that this is only a function of N.

Generally, the root with the smallest real part dominates the decay of free vibration, thus Eqs. (16a) and (16b) can be used to obtain analytical expressions for the free response of the Zener model in certain situations.

3. Forced vibration

This section is concerned with the forced response of the Zener model. Two situations are considered; the first is harmonic excitation and is described in Section 3.1, and the second is for white noise excitation and is discussed in Section 3.2.

3.1. Harmonic excitation

The dynamic response of the Zener model to forced *harmonic* excitation has been reported comprehensively in the literature, for example [1,2]. Therefore, only the key results are presented here, but in a way that is consistent with the results for free vibration discussed in Section 2. Two responses are considered; the non-dimensional displacement response of the system or the *dynamic magnification factor* given by $D(j\Omega) = X/(F_e/k)$, where $\Omega = \omega/\omega_0$, and the ratio of the transmitted force F_t to the excitation force F_e, or the *transmissibility* given by $T(j\Omega) = F_t/F_e$. These can be derived from Eq. (2) in a straightforward manner by assuming a harmonic excitation force $F_e e^{j\omega t}$. The dynamic magnification factor is given by

$$D(j\Omega) = \frac{1 + j(2/N)\varsigma\Omega}{1 - \Omega^2 + j(2/N)\varsigma\Omega(N + 1 - \Omega^2)}. \tag{18}$$

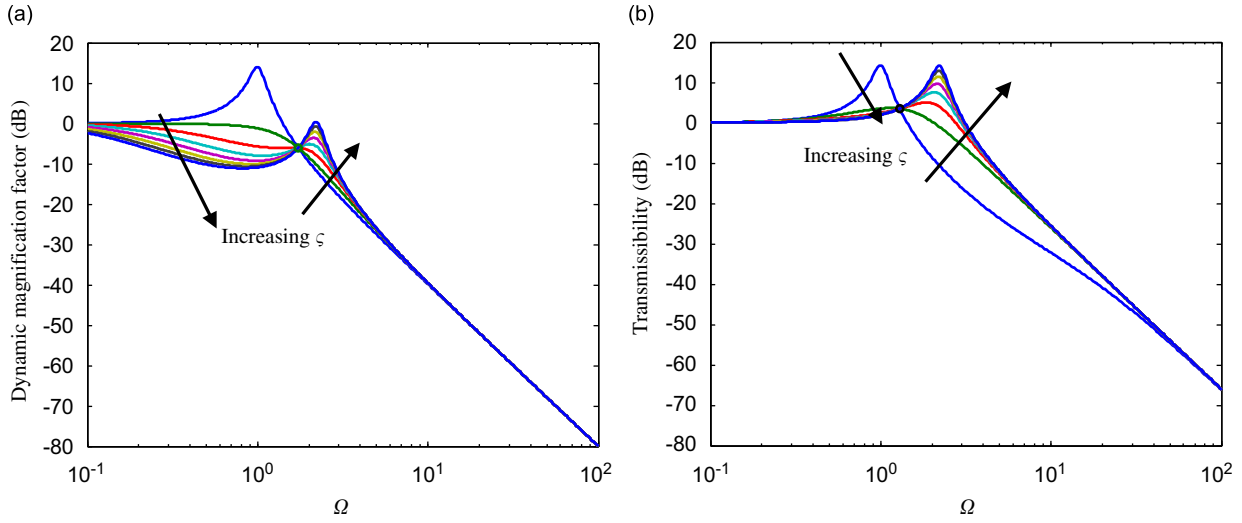

Fig. 7. Forced harmonic vibration response of the Zener model (dynamic magnification factor and transmissibility) for $N = 4$ as ς varies from 0.1 to 4 in steps of 0.5: (a) Magnitude of the dynamic magnification factor for the Zener model. (b) Magnitude of the transmissibility for the Zener model.

The modulus is plotted in Fig. 7(a) for values of ς from 0.1 to 4 in steps of 0.5. It can be seen that the resonance peak reduces initially as ς increases, and then it increases again, but with the peak occurring at a higher frequency. In the limit when $\varsigma \to 0$, $\Omega \to 1$, and when $\varsigma \to \infty$, $\Omega \to \sqrt{N+1}$. The modulus passes through the point $|X/(F_e/k)| = 2/N$ [1], for *all* values of ς, which is marked by $^\circ$ in Fig. 7(a). This occurs when the non-dimensional frequency $\Omega = \sqrt{(N+2)/2}$. The peak in the dynamic magnification factor is a minimum at this frequency, when the non-dimensional damping coefficient is [1]

$$\varsigma = \frac{N}{\sqrt{2(N+2)}}. \tag{19}$$

The damping value given by Eq. (19) is referred to as *optimum damping* in the literature as it yields the smallest displacement response at resonance. From the above discussion, it can be seen that the magnitude of the peak in the dynamic magnification factor is a function of N and ς. To compare the forced response of the Zener model with the free vibration characteristics depicted in Fig. 3, the *reciprocal* of the peak value is plotted as a contour graph as a function of N and ς in Fig. 8(a); Eq. (19) is also plotted for comparison. The peak in the dynamic magnification factor can only be less than unity when $N > 2$. It can be seen that for $N > 2$ and for ς less than about 0.3, the reciprocal of the peak value $\approx 2\varsigma$. Thus, the relationship between the damping of the complex roots and the non-dimensional damping coefficient is $\zeta \approx \varsigma$.

Inspection of Fig. 8(a) also shows that there is a wide range of values of ς for a given N greater than about 2 that results in the system having a maximum dynamic magnification factor of one. This does not occur at a resonance frequency, however, but at zero frequency as can be seen in Fig. 7(a). This can also be seen in Fig. 8(b), which shows the contour plot of the normalised frequency at which the *maximum* value of the dynamic magnification factor. When $N \gg 1$ the frequency at which the peak occurs decreases as ς increases (as it would in the Voigt model), until $\varsigma = 1/\sqrt{2}$ when $\Omega = 0$. For low values of N the situation is quite different. For ς greater than about $1/\sqrt{2}$, as N increases the frequency at which the peak occurs also increases. The peak value, however, decreases as can be seen in Fig. 8(a), and when it decreases below unity, the maximum value occurs when $\Omega = 0$. The line marked "all contours" gives the values of N and ς when the peak value just dips below unity.

Further insight can be gained by examining the *transfer* function of the system rather than the frequency response function. This is given by

$$D(\hat{s}) = \frac{\hat{s} + (N/2\varsigma)}{\hat{s}^3 + (N/2\varsigma)\hat{s}^2 + (N+1)\hat{s} + (N/2\varsigma)}. \tag{20}$$

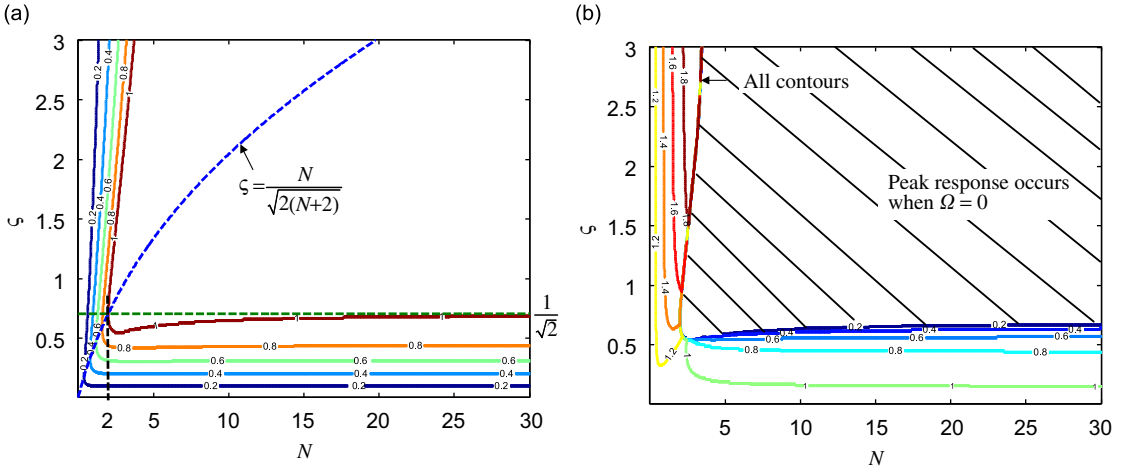

Fig. 8. Forced harmonic vibration response of the Zener model (dynamic magnification factor): (a) Contour plot showing the *reciprocal* of the maximum value of the dynamic magnification factor. The dashed line $\varsigma = N/\sqrt{2(N+2)}$ results in a minimum peak. (b) Contour plot showing the frequency normalised by ω_0 at which the maximum of the dynamic magnification factor.

When $\varsigma \ll N$, the denominator factorises as in Eq. (16a), and Eq. (18) reduces to

$$D(\hat{s}) \approx \frac{1}{(\hat{s}+\varsigma+j)(\hat{s}+\varsigma-j)}, \tag{21}$$

which means that for the frequency response function, the effect of the real root is effectively cancelled by the zero, which is given by $-N/(2\varsigma)$ (found be setting the numerator to zero and solving for $\hat{s}$). Thus, the oscillatory roots dominate the response for all frequencies.

If $\varsigma \gg N$, Eq. (20) can be written as

$$D(\hat{s}) \approx \frac{\hat{s}+(N/2\varsigma)}{\left(\hat{s}+\dfrac{N^2}{4(N+1)\varsigma}+j\sqrt{N+1}\right)\left(\hat{s}+\dfrac{N^2}{4(N+1)\varsigma}-j\sqrt{N+1}\right)\left(\hat{s}+\dfrac{N}{2(N+1)\varsigma}\right)}. \tag{22}$$

It can be seen that in this case the numerator does not cancel with the purely real root as it does when $\varsigma \ll N$ as discussed above. Thus, if the damping is high the purely real root cannot be neglected as it plays a role in the frequency response of the system. However, at high frequencies $|D(j\Omega)| \approx 1/\Omega^2$ as can be seen by inspecting Eq. (22) and Fig. 7(a).

Examination of Fig. 8(a) shows that there seems to be a marginal advantage in using an elastically supported damper because for small values of N the normalised peak response can be limited to unity for a smaller damping coefficient compared to the Voigt model.

A parameter that characterises the performance of an isolator is its Transmissibility, which, for an isolator described by the Zener model, is given by

$$T(j\Omega) = \frac{F_t}{F_e} = \frac{1+j(2/N)(N+1)\varsigma\Omega}{1-\Omega^2+j(2/N)\varsigma\Omega(N+1-\Omega^2)}. \tag{23}$$

It can be seen that Eq. (23) is identical to Eq. (18) except for the additional term $(N+1)$ in the numerator. The modulus of the Transmissibility is plotted in Fig. 7(b) for values of ς from 0.1 to 4 in steps of 0.5. As with the dynamic magnification factor, the resonant peak reduces initially as ς increases, and then it increases again but with the peak occurring at a higher frequency. It has the same frequency limits as $\varsigma \to 0$ and $\varsigma \to \infty$ as with the dynamic magnification factor. The modulus passes through the point $|T(j\Omega)| = (N+2)/N$ [1], for *all* values of ς, which is marked by $^\circ$ in Fig. 7(b). This occurs when the non-dimensional frequency $\Omega = \sqrt{2(N+1)/(N+2)}$. The peak in the transmissibility is a minimum at this frequency, when the

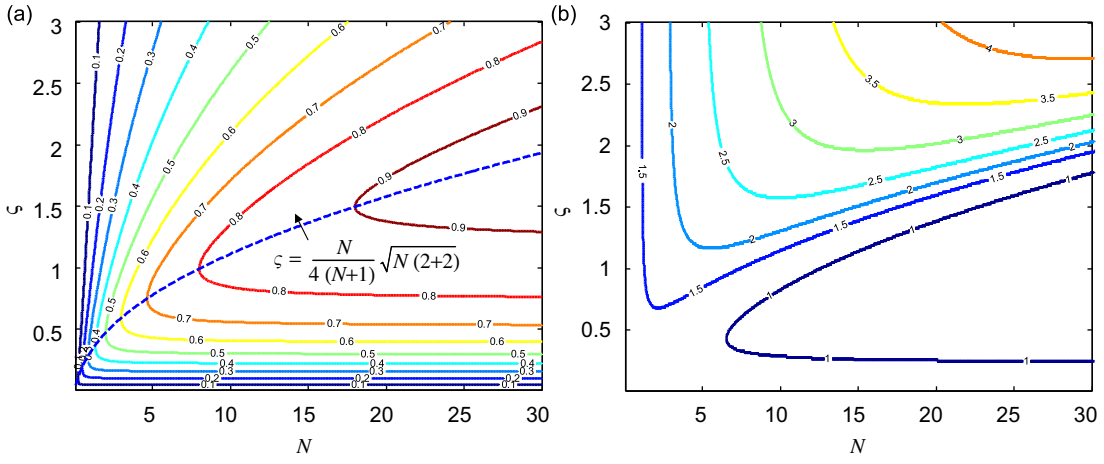

Fig. 9. Forced harmonic vibration of the Zener model (transmissibility): (a) Contour plot showing the *reciprocal* of the maximum value of the transmissibility. The dashed line shows the value of ς those results in a minimum peak. (b) Contour plot showing the frequency normalised by ω_0 at which the peak response of the transmissibility occurs.

non-dimensional damping coefficient is [1]

$$\varsigma = \frac{N}{4(N+1)}\sqrt{2(N+2)}. \tag{24}$$

The damping value given by Eq. (24) is referred to as *optimum damping* in the literature as it yields the lowest transmissibility at resonance.

The contour plots for the *reciprocal* of the maximum value of the transmissibility and the non-dimensional frequency at which this occurs are plotted in Figs. 9(a) and (b), respectively. Eq. (23) is also plotted for comparison in Fig. 9(a). These figures can be compared with the corresponding contour plots for the dynamic magnification factor in Fig. 7. It can be seen that there are significant differences. For a wide range of system parameters, the peak in the dynamic magnification factor was unity when the frequency was zero. This is not so with the Transmissibility; only if $N \gg 1$ and $\varsigma \gg 1$ does the maximum occur at zero frequency. One notable feature in Fig. 9, is that the natural frequency changes rapidly with ς in the region where the damping has been optimised according to Eq. (24).

The *transfer* function of the transmissibility is given by

$$T(\hat{s}) = \frac{(N+1)\left(\hat{s} + \left(\dfrac{N}{2\varsigma(N+1)}\right)\right)}{\hat{s}^3 + \left(\dfrac{N}{2\varsigma}\right)\hat{s}^2 + (N+1)\hat{s} + \left(\dfrac{N}{2\varsigma}\right)}. \tag{25}$$

When $\varsigma \ll N$, the denominator factorises as in Eq. (16a), and Eq. (25) reduces to

$$T(\hat{s}) \approx \frac{(N+1)\left(\hat{s} + \left(\dfrac{N}{2\varsigma(N+1)}\right)\right)}{(\hat{s}+\varsigma+j)(\hat{s}+\varsigma-j)\left(\hat{s} + \dfrac{N}{2\varsigma}\right)}. \tag{26}$$

It can be seen that unless $N \ll 1$ the purely real root in the denominator does not cancel with the zero, and so all three roots of the characteristic equation influence the frequency response function. This is different to dynamic magnification factor discussed above. At high frequencies, the transmissibility is given by $|T(j\Omega)| \approx (N+1)/\Omega^2$, i.e., independent of ς, and rolls off at 40 dB/decade. Conversely, for a system with a rigidly connected damper the high frequency transmissibility is $|T(j\Omega)| \approx \varsigma/\Omega$ and presents a decay slope of 20 dB/decade. It can be concluded that the Zener model out-performs the conventional system at high frequencies, i.e. when $\Omega > 1/\varsigma(N+1)$.

3.2. White noise excitation

Many systems are excited by random rather than harmonic vibration. To make the analysis tractable, white-noise excitation is considered. As with harmonic excitation, both the dynamic magnification factor and transmissibility are considered for the Zener model.

The mean square displacement response is given by [10]

$$\bar{x}^2 = S_0 \int_0^\infty |D(j\Omega)|^2 \, \mathrm{d}\Omega, \tag{27}$$

where S_0 is the amplitude of the excitation spectral density. Substituting for $D(j\Omega)$ from Eq. (18) into Eq. (27) and evaluating the integral gives, in non-dimensional form

$$\frac{\bar{x}^2}{S_0\omega_0\pi/4} = \frac{1}{\varsigma} + \frac{4\varsigma}{N^2}. \tag{28}$$

When $\varsigma \ll N$

$$\frac{\bar{x}^2}{S_0\omega_0\pi/4} \approx \frac{1}{\varsigma}. \tag{29a}$$

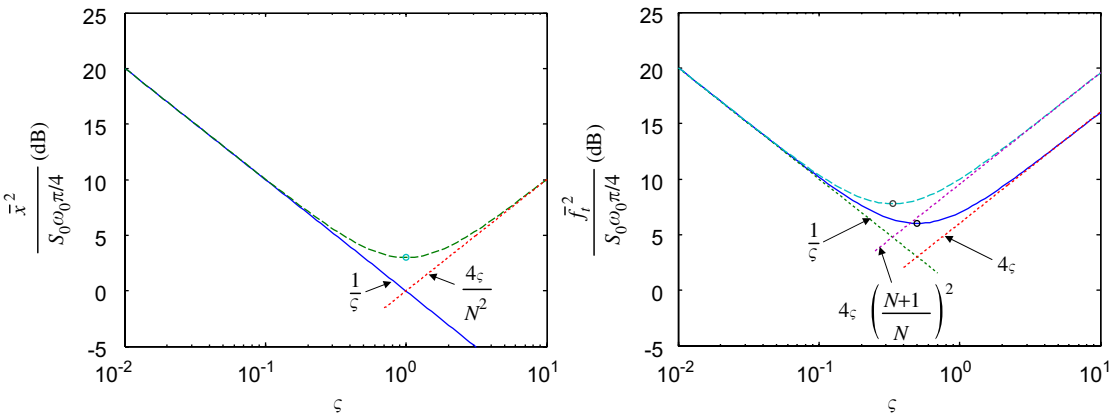

Fig. 10. Normalised mean square responses of the Zener model for white noise excitation: (a) Normalised mean square displacement response of the mass. Solid line, the displacement response when $N\to\infty$, dashed line for $N=2$. (b) Transmitted force. Solid line, the transmitted force when $N\to\infty$, dashed line for $N=2$.

When $\varsigma \gg N$

$$\frac{\bar{x}^2}{S_0\omega_0\pi/4} \approx \frac{4\varsigma}{N^2}. \tag{29b}$$

Eq. (29a) is also the normalised displacement response for a sdof system with a rigidly connected damper ($N\to\infty$). Eqs. (28) and (29) are plotted in Fig. 10(a) for $N=2$. It can be seen that the mean square response initially decreases as ς increases, but then increases again. The minimum in the response can be determined by setting the two asymptotes given in Eqs. (29a) and (29b) to be equal. The result is an optimum value of $\varsigma = N/2$ and a minimum normalised mean square response of

$$\left.\frac{\bar{x}^2}{S_0\omega_0\pi/4}\right|_{\min} = \frac{4}{N}. \tag{30}$$

This point is marked as $^\circ$ in Fig. 10(a).

The mean square force transmitted to the base is given by

$$\bar{f}_t^2 = S_0 \int_0^\infty |T(j\Omega)|^2 \, \mathrm{d}\Omega. \tag{31}$$

Substituting for $T(j\Omega)$ from Eq. (23) into Eq. (31) and evaluating the integral gives, in non-dimensional form

$$\frac{\bar{f}_t^2}{(\pi/4)S_0\omega} = \frac{1}{\varsigma} + 4\varsigma\left(\frac{N+1}{N}\right)^2. \tag{32}$$

When $\varsigma \ll N$

$$\frac{\bar{f}_t^2}{S_0\omega_0\pi/4} \approx \frac{1}{\varsigma}. \tag{33a}$$

When $\varsigma \gg N$

$$\frac{\bar{f}_t^2}{S_0\omega_0\pi/4} \approx 4\varsigma\left(\frac{N+1}{N}\right)^2. \tag{33b}$$

If $N\to\infty$ then Eq. (32) reduces to

$$\frac{\bar{f}_t^2}{S_0\omega_0\pi/4} = \frac{1}{\varsigma} + 4\varsigma, \tag{34}$$

which is the normalised mean square force for the system with a rigidly connected damper. Eq. (34) has asymptotes for $\varsigma \ll 1$ of $1/\varsigma$ and for $\varsigma \gg 1$ of ς. Eqs. (32) and (34) are plotted in Fig. 10(b) together with the corresponding asymptotes. It can be seen that, as with the displacement response, the mean square force initially decreases as ς increases, but then increases again. The minimum in the response can be determined by setting the two asymptotes given in Eqs. (33a) and (33b) to be equal. The result is an optimum value of $\varsigma = N/(2(N+1))$ and a minimum normalised mean square response of

$$\left.\frac{\bar{f}_t^2}{S_0\omega\pi/4}\right|_{\min} = \frac{4(N+1)}{N}. \tag{35}$$

If $N \to \infty$, the minimum normalised mean square response is 4 which occurs when $\varsigma = 1/2$. The minima are shown as ϱ in Fig. 10(b). It can be seen that the minimum mean square force for a rigidly connected damper is smaller than that for an elastically connected damper.

4. Discussion

Table 1 summarises the optimum values of the non-dimensional damping coefficient ς_{opt} for free and forced vibrations of the Zener model derived in Sections 2 and 3. These are also plotted in Fig. 11 for comparison. It can be seen that there is not a single optimum value; it depends upon the type of excitation and the response variable of interest. For free vibration, two optima are given, one for $N<8$ and one for $N \geqslant 8$. It has been shown that the complex roots can only be critically damped when $N \geqslant 8$ and this can be achieved with two values of ς. When $N<8$ two of the roots of the characteristic equation are always complex, but there is a value of ς that can achieve maximum damping for these roots. In general, there does not appear to be any advantage in using an elastically connected damper for free or transient vibration, unless there is a particular response that cannot be achieved using a parallel combination of a spring and a damper.

There are two optimum damping values for harmonic excitation, one for the displacement response of the system and one for the force transmitted to the rigid base. Both damping values ensure the response at the resonance frequency is minimised, and have been reported previously in the literature. There seems to be a marginal advantage in using an elastically connected damper if the displacement response is of interest, in that it is possible to achieve critical damping for the system with a smaller damper than in the Voigt model provided that N is chosen carefully. The main advantage is when the transmitted force is of interest. It is possible to have a high-frequency response that decreases with the square of frequency, but with some damping being added to the system to reduce the response at resonance. This is not possible with a rigidly connected damper. However, there is a trade-off between reducing the amplitude of the high-frequency response and reducing the amplitude of the resonance peak. The additional spring in series with the damper gives more flexibility in tuning the system for a particular requirement. It should be noted, however, that the frequency at which the peak occurs is particularly sensitive to the damping coefficient for N greater than about 10.

Table 1
Summary of the optimum non-dimensional damping coefficients ς_{opt} for free and forced vibration of the Zener model

Free vibration		Forced vibration			
$N<8$	$N \geqslant 8$	Harmonic excitation		White noise excitation	
		Dynamic magnification factor	Transmissibility	Mean square displacement response	Mean square transmitted force
$\dfrac{N}{2(N+1)^{3/4}}$	$N\dfrac{\sqrt{2}}{8}\sqrt{\dfrac{N^2+20N-8}{(N+1)^3} \pm \dfrac{\sqrt{N(N-8)^3}}{(N+1)^3}}$	$\dfrac{N}{\sqrt{2(N+2)}}$	$\dfrac{N}{4(N+1)}\sqrt{2(N+2)}$	$\dfrac{N}{2}$	$\dfrac{N}{2(N+1)}$

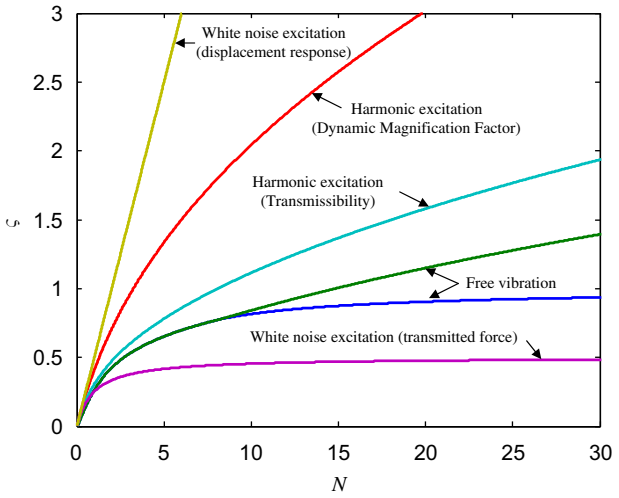

Fig. 11. Optimum values of ς for the Zener model for different excitation conditions.

Examination of Figs. 10(a) and (b) and Table 1 shows that there is no advantage in using an elastically connected damper if the excitation is white noise and the mean square displacement or transmitted force response is of interest. In fact it is detrimental in both cases. If the system is excited by both harmonic and random vibration, then it is possible that an elastically supported damper may offer advantages, but this would have to be considered on a case-by-case basis.

5. Conclusions

This paper has described the free and forced dynamic behaviour of a sdof system in the case where the damper is elastically supported (Zener model). There are three roots to the characteristic equation for this system; two of these are complex conjugates and the third root is purely real. It has been shown that it is not possible to achieve critical damping of the complex roots unless the secondary stiffness is at least eight times that of the primary stiffness. Expressions have been derived for the minimum damping required to critically damp the complex roots when this is possible. Expressions have also been derived for the maximum damping of the complex roots when critical damping is not possible. For comparison and completeness, the behaviour of the system when excited by harmonic vibration has also been presented. It has been shown that there could be some advantages in using a spring in series with a damper when the transmitted force to the base is of interest, but when the displacement response of the system is of interest then the benefits of such a system are marginal. Finally, the response of the Zener model excited by a force that is spectrally white has been considered. Optimum values of the damping have been determined for the cases when the mean square displacement response of the mass, and the mean square force transmitted to the rigid base are of interest. It is shown that the spring in series with the damper affords no advantages, the best situation being when the damper is rigidly connected.

Acknowledgements

The first author would like to acknowledge the support of the Leverhulme Trust for a Study Abroad Fellowship, and also to FAPESP, Brazil.

Appendix A. Solution of the characteristic equation for the Zener model

The closed-form solution of a third-order polynomial equation, which is the form of the characteristic equation for the Zener model given in Eq. (6), was determined in 1545 by Girolamo Cardano [11]. However, in this paper the symbolic algebra software package, Maple [12], was used to determine the roots of Eq. (6),

which is repeated here for convenience:

$$\hat{s}^3 + \left(\frac{N}{2\varsigma}\right)\hat{s}^2 + (N+1)\hat{s} + \left(\frac{N}{2\varsigma}\right) = 0. \tag{A.1}$$

The roots are given by

$$\hat{s}_1 = R_1, \tag{A.2a}$$

$$\hat{s}_{2,3} = R_2 \pm j\frac{\sqrt{3}}{2}Q, \tag{A.2b}$$

where

$$R_1 = \frac{(18\varsigma^2N^2 - 36\varsigma^2N - N^3 + 6\varsigma\sqrt{(3-3\varsigma^2)N^4 + (48\varsigma^4 - 60\varsigma^2)N^3 + (24\varsigma^2 + 144\varsigma^4)N^2 + 144\varsigma^2N + 48\varsigma^4})^{1/3}}{6\varsigma}$$
$$+ \cdots + \frac{N^2 - 12\varsigma^2(N^2+1)}{6\varsigma(18\varsigma^2N^2 - 36\varsigma^2N - N^3 + 6\varsigma\sqrt{(3-3\varsigma^2)N^4 + (48\varsigma^4 - 60\zeta^2)N^3 + (24\varsigma^2 + 144\varsigma^4)N^2 + 144\varsigma^2N + 48\varsigma^4})^{1/3}}$$
$$- \frac{N}{6\varsigma}$$

$$R_2 = -\frac{N^2 - 12\varsigma^2(N^2+1)}{12\varsigma(18\varsigma^2N^2 - 36\varsigma^2N - N^3 + 6\varsigma\sqrt{(3-3\varsigma^2)N^4 + (48\varsigma^4 - 60\varsigma^2)N^3 + (24\varsigma^2 + 144\varsigma^4)N^2 + 144\varsigma^2N + 48\varsigma^4})^{1/3}}$$
$$- \cdots - \frac{N}{6\varsigma},$$

$$Q = \frac{(18\varsigma^2N^2 - 36\varsigma^2N - N^3 + 6\varsigma\sqrt{(3-3\varsigma^2)N^4 + (48\varsigma^4 - 60\varsigma^2)N^3 + (24\varsigma^2 + 144\varsigma^4)N^2 + 144\varsigma^2N + 48\varsigma^4})^{1/3}}{6\zeta}$$
$$- \cdots - \frac{N^2 - 12\zeta^2(N^2+1)}{6\varsigma(18\varsigma^2N^2 - 36\varsigma^2N - N^3 + 6\varsigma\sqrt{(3-3\varsigma^2)N^4 + (48\varsigma^4 - 60\varsigma^2)N^3 + (24\varsigma^2 + 144\varsigma^4)N^2 + 144\varsigma^2N + 48\varsigma^4})^{1/3}}.$$

When there is critical damping the imaginary part of the roots given by Eq. (A.2b) is zero. Thus, by setting $Q = 0$ and rearranging the resulting equation the two positive solutions for ς in terms of N can be determined and are given by

$$\varsigma = N\frac{\sqrt{2}}{8}\sqrt{\frac{N^2 + 20N - 8}{(N+1)^3} \pm \frac{\sqrt{N(N-8)^3}}{(N+1)^3}}. \tag{A.3}$$

References

[1] J.E. Ruzicka, T.E. Derby, *Influence of Damping in Vibration Isolation*, T.S.a.V.I. Centre, US Department of Defense, 1972.

[2] T.F. Derby, P.C. Calcaterra, Response and optimization of an isolator with relaxation type damping, *Shock and Vibration Bulletin* 40 (5) (1970) 203–216.

[3] A.D. Nashif, D.I.G. Jones, J.P. Henderson, *Vibration Damping*, Wiley, New York, 1985.

[4] I. Yamakawa, On the free vibration and the transient state of one-degree-of-freedom system with elastically supported damper, *Bulletin of JSME* 4 (16) (1961) 641–644.

[5] P. Muller, Are the eigensolutions of a 1-d.o.f. system with viscoelastic damping oscillatory or not?, *Journal of Sound and Vibration* 285 (2005) 501–509.

[6] A. Muravyov, S.G. Hutton, Free vibration response characteristic of a simple elasto-hereditary system, *Journal of Vibration and Acoustics—Transactions of the ASME* 120 (1998) 628–632.

[7] B.C. Kuo, *Automatic Control System*, fifth ed., Prentice-Hall International, Englewood Cliffs, NJ, 1987.

[8] S.S. Rao, *Mechanical Vibrations*, second ed., Addison-Wesley, Reading, MA, 1990.

[9] A. Preumont, *Vibration Control of Active Structures*, second ed., Kluwer Academic Publishers, Dordrecht, 2002.

[10] D.E. Newland, *An Introduction to Random Vibrations and Spectral Analysis*, Longman, London, 1975.

[11] G. Cardano, *Ars Magna: The Great Art, or the Rules of Algebra* (translated by R.B. McClenon, in: D.E. Smith (Ed.), *A Source Book in Mathematics*, Dover, New York, 1959, pp. 203–206).

[12] Maplesoft, 615, Kumpf Drive, Waterloo, Ontario, Canada N2V 1KB.

Available online at www.sciencedirect.com
ScienceDirect
Journal of Sound and Vibration 301 (2007) 678–689
JOURNAL OF SOUND AND VIBRATION
www.elsevier.com/locate/jsvi

Static analysis of a passive vibration isolator with quasi-zero-stiffness characteristic

A. Carrella, M.J. Brennan, T.P. Waters*

Institute of Sound and Vibration Research, University of Southampton, Southampton, Hampshire SO17 1BJ, UK

Received 7 April 2006; received in revised form 17 October 2006; accepted 18 October 2006
Available online 8 December 2006

Abstract

The frequency range over which a linear passive vibration isolator is effective, is often limited by the mount stiffness required to support a static load. This can be improved upon by employing nonlinear mounts incorporating negative stiffness elements configured in such a way that the dynamic stiffness is much less than the static stiffness. Such nonlinear mounts are used widely in practice, but rigorous analysis, and hence a clear understanding of their behaviour is not readily available in the literature. In this paper, a simple system comprising a vertical spring acting in parallel with two oblique springs is studied. It is shown that there is a unique relationship between the geometry and the stiffness of the springs that yields a system with zero dynamic stiffness at the static equilibrium position. The dynamic stiffness increases monotonically with displacement either side of the equilibrium position, and this is least severe when the oblique springs are inclined at an angle between approximately 48° and 57°. Finally, it is shown that the force–displacement characteristic of the system can be approximated by a cubic equation.

1. Introduction

Isolation of undesirable vibrations is a problem that affects many engineering structures. In the ideal case of a mass m supported by a linear stiffness k on a rigid foundation, isolation does not occur until a frequency of $\sqrt{2k/m}$. It is evident that a smaller stiffness results in a wider frequency range of isolation. However, a smaller stiffness results in a larger static displacement of the mass, and this trade-off between isolation and static displacement is well known [1,2]. To overcome this limitation nonlinear springs have been used to obtain a high static stiffness and hence a small static displacement, and a small dynamic stiffness, which results in a low natural frequency [3,4]. By careful choice of system parameters it is possible to achieve an isolator with zero dynamic stiffness, a so-called *quasi-zero-stiffness* (QZS) mechanism [5,6]. Applications of QZS mechanisms range from space research (e.g. to simulate zero gravity, [7]) to isolation of high-precision machinery [8]. Systems with quasi-zero-stiffness characteristic are of interest also in other fields, for example in geodynamics [9–11]. The precision of instruments such as *seismographs* or *gravimeters* requires very long periods of oscillation.

*Corresponding author.
E-mail address: tpw@isvr.soton.ac.uk (T.P. Waters).

0022-460X/$ - see front matter © 2006 Elsevier Ltd. All rights reserved.
doi:10.1016/j.jsv.2006.10.011

QZS mechanisms are generally achieved by combining a negative stiffness element with a positive stiffness element. A number of configurations have been proposed, many of which use nonlinearities such as spring orientation or buckling to create the negative stiffness effect [3,4]. Perhaps the simplest of these is shown in its unloaded condition in Fig. 1. When it is loaded with a suitably sized mass, the springs compress such that the oblique springs, k_o are in the horizontal position and the static load is taken by the vertical spring, k_v. This is the static equilibrium position, and it is the motion about this position that is of primary interest. When the system of springs is used in this way, the oblique springs act as a negative stiffness in the vertical direction counteracting the positive stiffness of the vertical spring. A typical force–deflection curve for the system in Fig. 1 is shown in Fig. 2, where the changing stiffness as a function of displacement can be seen. For the particular case shown in Fig. 2 the geometry and stiffness are chosen such that at the static equilibrium position, x_e, the dynamic stiffness is zero. The penalty for this, however, is that the system becomes stiffer than the vertical spring alone for large excursions from this position.

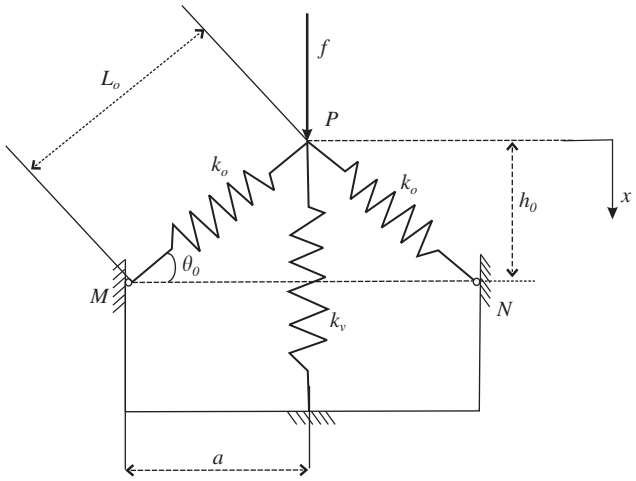

Fig. 1. Schematic representation of the simplest system which can exhibit quasi-zero stiffness.

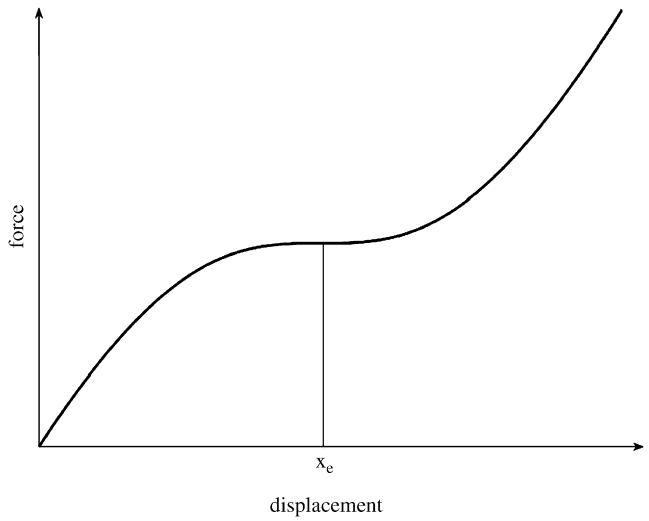

Fig. 2. Typical force–displacement characteristic of the isolator shown in Fig. 1.

In this paper, this trade-off between achieving a low dynamic stiffness for small excursions and acceptable stiffness for large excursions is investigated. An optimum relationship between the ratio of the oblique spring stiffness and the vertical spring stiffness is sought, as is an optimum angle for the oblique springs.

2. Force–displacement characteristic of a system with two oblique springs

It is instructive to examine first the behaviour of the oblique springs alone. Consider the system in Fig. 1, but with the vertical spring k_v removed. The two linear springs each of stiffness k_o hinged at points M and N, respectively, have initial length L_0. A force f is applied at point P which is a horizontal distance a from points M and N and initially at height h_0 above these points. The springs are initially at an angle θ_0 from the horizontal. The vertical component of the applied force is related to the spring stiffness k_o by

$$f = 2k_o(L_0 - L)\sin\theta, \tag{1}$$

where L is the length of the compressed spring, and $\sin\theta = (h_0 - x)/L$. Noting that $L_0 = \sqrt{h_0^2 + a^2}$ and $L = \sqrt{(h_0 - x)^2 + a^2}$, Eq. (1) can be written as

$$f = 2k_o(h_0 - x)\left(\frac{\sqrt{h_0^2 + a^2}}{\sqrt{(h_0 - x)^2 + a^2}} - 1\right), \tag{2}$$

which can be written in non-dimensional form as

$$\frac{f}{k_o L_0} = 2(\sqrt{1 - \gamma^2} - \hat{x})\left\{\left[\hat{x}^2 - 2\sqrt{1 - \gamma^2}\hat{x} + 1\right]^{-1/2} - 1\right\}, \tag{3}$$

where $\hat{x} = x/L_0$ and

$$\gamma = \frac{a}{L_0} = \cos\theta_0 \tag{4}$$

is a *geometrical parameter*. When $\gamma = 0$ the springs are initially vertical and when $\gamma = 1$ the springs, initially, lie horizontally. Fig. 3 shows the non-dimensional force plotted against the non-dimensional displacement for different values of γ.

It can be seen that the system has a highly nonlinear characteristic. The turning points of the curves represent zero stiffness but are unstable and the mechanism will "snap through" to a stable position if forced

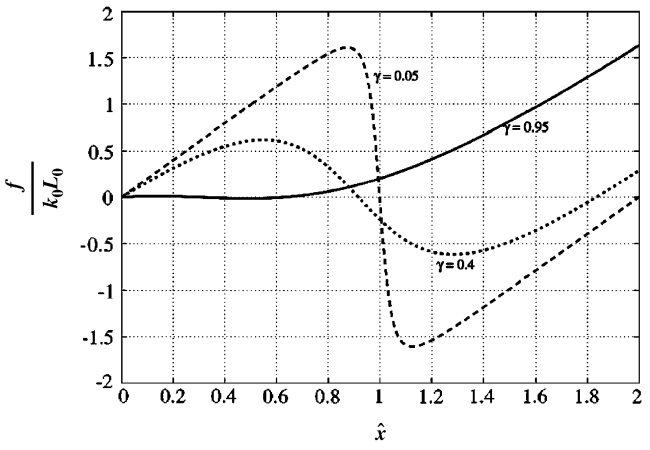

Fig. 3. Force–deflection characteristic of the system in Fig. 1. When $\gamma = 0$ the springs are vertical and when $\gamma = 1$ they are horizontal. The stiffness is negative between the maxima and the minima.

into this region. The maximum non-dimensional force that the system can accept before it snaps through is given by

$$\frac{f_{\max}}{k_o L_0} = 2\left[1 - \left(1 - \sqrt{1-\gamma^2}\right)^{1/3}\right]^{3/2}, \tag{5}$$

which occurs at

$$\hat{x}_{\max} = \sqrt{1-\gamma^2} - \gamma\sqrt{\gamma^{-2/3} - 1}. \tag{6}$$

The non-dimensional stiffness, K/k_o, of this system can be calculated by differentiating the force with respect to the displacement to give

$$\frac{K}{k_o} = 2\left[1 - \frac{\gamma^2}{\left(\hat{x}^2 - 2\sqrt{1-\gamma^2}\hat{x} + 1\right)^{3/2}}\right]. \tag{7}$$

The stiffness is a minimum at the equilibrium position, $\hat{x}_e = \sqrt{1-\gamma^2}$, and is given by

$$\frac{K}{k_o} = 2\left(1 - \frac{1}{\gamma}\right), \tag{8}$$

which becomes increasingly negative as the angle of inclination of the springs is increased.

The system can be modified to exhibit QZS at a point of stability by adding a vertical spring of equal and opposite (positive) stiffness, and such a system is the focus of the following section.

3. A QZS mechanism

For the system in Fig. 1, the vertical spring k_v is in parallel with the vertical components of the oblique springs. Choosing now to non-dimensionalise force f by $k_v L_0$, the resulting non-dimensional spring force $\hat{f}$ is given by

$$\hat{f} = \hat{x} + 2\alpha(\sqrt{1-\gamma^2} - \hat{x})\left\{\left[\hat{x}^2 - 2\sqrt{1-\gamma^2}\hat{x} + 1\right]^{-1/2} - 1\right\}, \tag{9}$$

where $\alpha = k_o/k_v$ is the ratio of the spring stiffnesses. For large α Eq. (9) tends to Eq. (3).

The non-dimensional stiffness of the system can be found by differentiating Eq. (9) with respect to the displacement to give

$$\hat{K} = 1 + 2\alpha\left[1 - \frac{\gamma^2}{\left(\hat{x}^2 - 2\sqrt{1-\gamma^2}\hat{x} + 1\right)^{3/2}}\right]. \tag{10}$$

The non-dimensional force as a function of the non-dimensional displacement is plotted in Fig. 4 for several values of γ and when $\alpha = 1$. For large initial angles (such as $\gamma = 0.05$ and 0.4 in Fig. 4) the inclined springs dominate the behaviour resulting in a region of negative stiffness. For small initial angles of inclination, such as $\gamma = 0.95$, the vertical spring dominates such that the combined stiffness of the mechanism is always positive and only weakly nonlinear. At a unique intermediate angle of inclination, represented by γ_{QZS}, there is a stationary point of inflexion, which corresponds to a stable equilibrium position with zero stiffness. This occurs at the equilibrium position $\hat{x}_e = \sqrt{1-\gamma^2}$ at which the (maximum) negative stiffness from the inclined springs is exactly balanced by the positive stiffness of the vertical spring. This is seen more clearly in Fig. 5 in which the non-dimensional stiffness is plotted as a function of the non-dimensional displacement for the same set of parameter values.

There is a unique relationship between the geometrical parameter $\gamma = a/L_0$ and the spring coefficient ratio $\alpha = k_o/k_v$ that yields the desired stable QZS characteristic. If Eq. (10) is evaluated at the static equilibrium

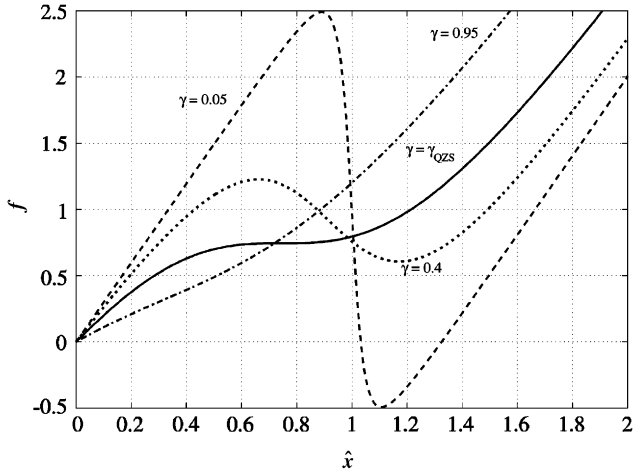

Fig. 4. Force–displacement characteristic of the three spring system when $\alpha = 1$: the solid line is the QZS system.

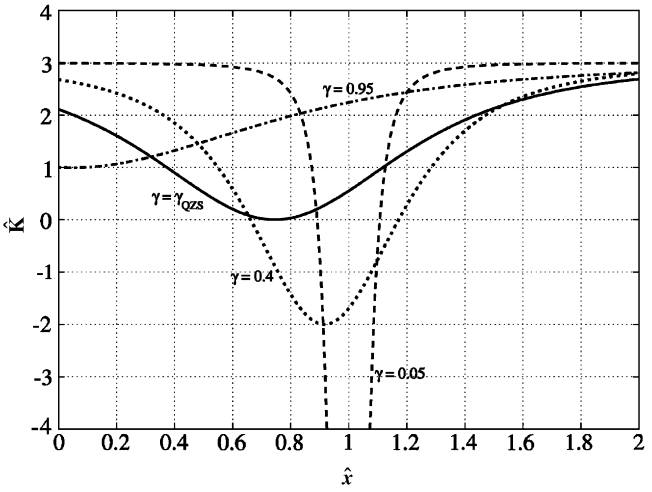

Fig. 5. Non-dimensional stiffness of a QZS mechanism when $\alpha = 1$: the solid line is representative of a stable system (always positive stiffness) with zero stiffness at the static equilibrium position. The stiffness is very small (quasi-zero) for a small deviation from this position.

position $\hat{x}_e = \sqrt{1-\gamma^2}$ and set to zero, then the value γ_{QZS} that gives quasi-zero-stiffness is

$$\gamma_{\mathrm{QZS}} = \frac{2\alpha}{2\alpha + 1} \tag{11a}$$

for a given value of α. Equivalently, the value of α that ensures QZS behaviour for a given γ is

$$\alpha_{\mathrm{QZS}} = \frac{\gamma}{2(1-\gamma)}. \tag{11b}$$

Hereafter, the subscript QZS on either α or γ is used to denote that the other parameter is not independent, but has been chosen in accordance with Eq. (11) so as to achieve stable QZS.

The combinations of stiffness ratio α and geometrical parameter γ that give rise to stable QZS are shown in graphical form in Fig. 6. For small initial angles ($\gamma \approx 1$) the inclined springs need to be orders of magnitude larger than the vertical spring. When the initial angle of inclination is a moderate 37°–66°, say, ($0.4 < \gamma < 0.8$)

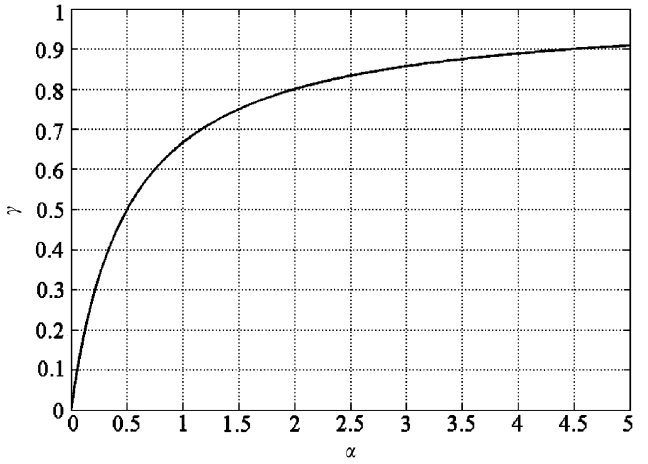

Fig. 6. Combinations of geometrical parameter γ and stiffness ratio α that yield QZS.

then vertical and inclined springs of similar stiffnesses can be employed, although this will result in larger static deformations of the springs.

4. Optimisation of the QZS mechanism

Although Eqs. (11a), (11b) relate the geometrical and stiffness parameters to give a QZS system, there is an infinite number of possible combinations of these parameters. However, the range of displacements over which the stiffness is smaller than the vertical spring alone, for example, is very much dependent upon the geometrical parameter. This relationship is explored further in this section.

By enforcing the QZS condition on α and γ in Eq. (11), the non-dimensional stiffness given by Eq. (10) can be written as a function of just the geometrical parameter as

$$\hat{K}_{\mathrm{QZS}} = 1 + \frac{\gamma_{\mathrm{QZS}}}{(1-\gamma_{\mathrm{QZS}})}\left[1 - \frac{\gamma_{\mathrm{QZS}}^2}{\left(\hat{x}^2 - 2\sqrt{1-\gamma_{\mathrm{QZS}}^2}\hat{x} + 1\right)^{3/2}}\right]. \tag{12}$$

This is plotted in Fig. 7 for several values of γ_{QZS}. It can be seen from the figure that the stiffness is zero at the static equilibrium position, $\hat{x}_e = \sqrt{1-\gamma_{\mathrm{QZS}}^2}$, and the displacement range over which there is a small stiffness depends on γ_{QZS}.

Of interest is the range of displacements about the equilibrium position for which the stiffness is less than a prescribed stiffness $\hat{K}_o$, say. (Note that a value of $\hat{K}_o = 1$ means that the stiffness of the system is equal to that of the vertical spring.) The displacement at which the stiffness is equal to the threshold value is found by setting $\hat{K}_{\mathrm{QZS}} = \hat{K}_o$ in Eq. (12) and solving for $\hat{x}$, which yields

$$\hat{x}|_{\hat{K}=\hat{K}_o} = \hat{x}_e \pm \hat{d}, \tag{13}$$

where $\hat{x}_e$ is the static equilibrium position and $\hat{d}$ is the excursion, normalised by L_0, from this position when $\hat{K} = \hat{K}_o$, and is given by

$$\hat{d} = \gamma_{\mathrm{QZS}}\sqrt{\left[\frac{1}{1-\hat{K}_o(1-\gamma_{\mathrm{QZS}})}\right]^{2/3} - 1}. \tag{14}$$

This is plotted in Fig. 8 as a function of γ_{QZS} for various values of $\hat{K}_o$. It can be seen that the value of γ_{QZS} for which $\hat{d}$ is a maximum, changes depending on the value of $\hat{K}_o$. It is not possible to determine a closed-form

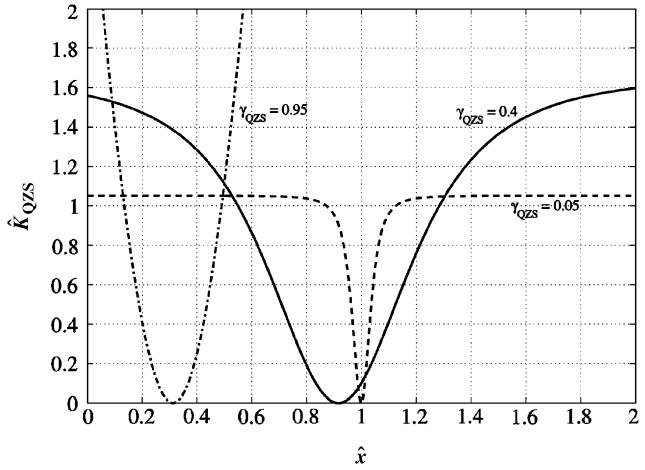

Fig. 7. Non-dimensional stiffness for different combinations of geometrical and stiffness parameters that yield QZS.

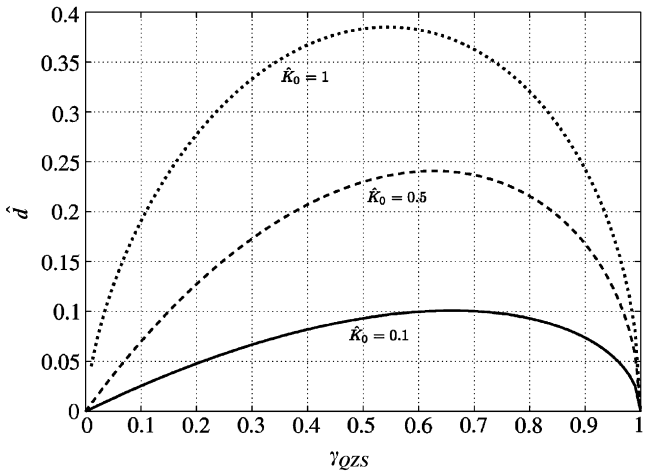

Fig. 8. Non-dimensional displacement from the static equilibrium position as a function of γ_{QZS}.

solution for this from Eq. (14), but it can be evaluated when $\hat{K}_o \ll 1$ and when $\hat{K}_o = 1$. For the case when $\hat{K}_o \ll 1$ Eq. (14) can be approximated by

$$\hat{d} \approx \gamma_{QZS}\sqrt{\frac{2}{3}\hat{K}_o(1-\gamma_{QZS})}, \tag{15}$$

which when differentiated with respect to γ_{QZS}, and set to zero gives the optimal geometrical parameter

$$\gamma_{opt} = \frac{2}{3}, \quad \hat{K}_o \ll 1. \tag{16}$$

If this is substituted into Eq. (11b) the optimum value of the stiffness ratio is $\alpha_{opt} = 1$, which means that all the springs have the same stiffness. If $\hat{K}_o$ is set to unity in Eq. (14) and the same procedure followed, the optimum geometrical parameter is found to be

$$\gamma_{opt} = \left(\frac{2}{3}\right)^{3/2}, \quad \hat{K}_o = 1. \tag{17}$$

An approximate general expression that relates γ and $\hat{K}_o$ for values of $0 \leqslant \hat{K}_o \leqslant 1$ can be determined by assuming a relationship of the form

$$\gamma_{\text{opt}} \approx \left(\frac{2}{3}\right)^{c_1\hat{K}_o + c_2}. \tag{18}$$

The constants c_1 and c_2 can be found by using Eqs. (16) and (17) for $\hat{K}_o = 0$ and 1, respectively, to give

$$\gamma_{\text{opt}} \approx \left(\frac{2}{3}\right)^{(\hat{K}_o/2)+1}. \tag{19}$$

This shows that there is only a weak relationship between the optimum geometry and the prescribed maximum stiffness of the system in which the angle for the oblique springs ranges from about 48° to 57°. The corresponding optimum stiffness ratio α_{opt} ranges from 1 to 0.6.

By substituting Eq. (19) into Eq. (14) an expression can be found that gives the maximum excursion from the static equilibrium position as a function of the maximum stiffness of the system during this excursion. It is given by

$$\hat{d} = \left(\frac{2}{3}\right)^{(\hat{K}_o/2)+1} \sqrt{\frac{1}{\left\{1 - \hat{K}_o\left[1 - \left(\frac{2}{3}\right)^{(\hat{K}_o/2)+1}\right]\right\}^{2/3}} - 1}. \tag{20}$$

Fig. 9 shows the largest excursion from the static equilibrium position that can be achieved without the system having stiffness larger than $\hat{K}_o$. The solid line is the solution calculated using Eq. (14), where the optimum value of γ_{QZS} for a given $\hat{K}_o$ is determined numerically. The dotted line is calculated using Eq. (20). Note that there is very little difference between the two solutions.

If the allowable increase in stiffness due to excursions about the equilibrium position is small, i.e. $\hat{K}_o \ll 1$, then Eq. (20) can be expanded to give the approximate relationship

$$\hat{d} \approx \frac{2}{9}\sqrt{2\hat{K}_o}, \quad \hat{K}_o \ll 1. \tag{21}$$

The analysis presented so far is based on the assumption that γ_{QZS} and α_{QZS} are related by Eq. (11). However, it is possible that, due to manufacturing tolerances Eq. (11) may not hold exactly. The question is whether the behaviour of the system is very sensitive to a change in the stiffness ratio. To investigate

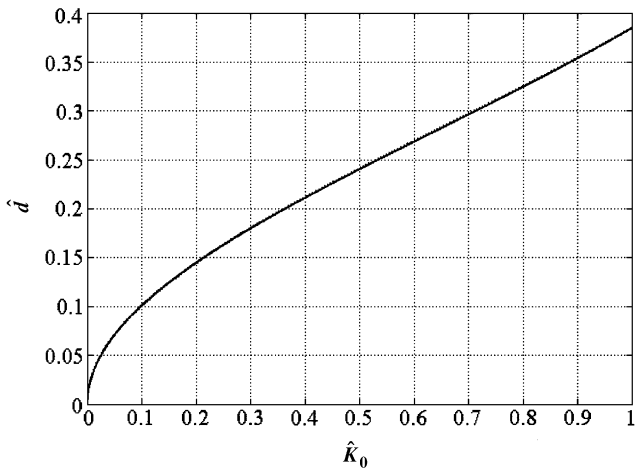

Fig. 9. Numerical and analytical representation of the maximum excursion from the static equilibrium position, $\hat{d}$, over which the system has a stiffness smaller than $\hat{K}_0$. (— numerical; -- equation (20)).

this let there be a fractional deviation ε from α_{QZS} such that $\alpha = \alpha_{QZS}(1 \pm \varepsilon)$. Substituting this into Eq. (10) gives

$$\hat{K} = \hat{K}_{QZS} \pm 2\varepsilon\alpha_{QZS}\left[1 - \frac{\gamma_{QZS}^2}{\left(\hat{x}^2 - 2\sqrt{1-\gamma_{QZS}^2}\hat{x} + 1\right)^{3/2}}\right], \tag{22}$$

where $\hat{K}_{QZS}$ is the stiffness when $\alpha = \alpha_{QZS}$ and $\gamma = \gamma_{QZS}$. Since excursions about the static equilibrium position are of interest the stiffness is evaluated at this position, where $\hat{K}_{QZS} = 0$. Substituting $\hat{x} = \hat{x}_e = \sqrt{1-\gamma^2}$ into Eq. (22) results in

$$\hat{K}\big|_{\hat{x}=\hat{x}_e} = -(\pm\varepsilon). \tag{23}$$

This means that the non-dimensional stiffness of the system at the static equilibrium position is of equal magnitude but opposite sign to the fractional change in the stiffness ratio at the static equilibrium position. Thus, for example, if the spring ratio is 1% smaller than α_{QZS} then the dimensional stiffness of the system at the static equilibrium position, which should be zero in optimal conditions, will be $0.01k_v$.

Although there are benefits to incorporating springs configured to act as a negative stiffness, there are also some disadvantages. As shown in Fig. 3, the oblique springs only act as a negative stiffness over a certain displacement range. Outside this range they act as a positive stiffness, adding to the stiffness of the vertical spring. This can be seen in Fig. 5. The peak positive stiffness can be obtained by setting $x \gg h_0$ such that $\hat{x} \gg 1$ and Eq. (12) becomes

$$\hat{K}\big|_{x \gg h_0} = \frac{1}{1-\gamma_{QZS}}. \tag{24}$$

The optimal value for γ_{QZS} lies between 2/3 and $(2/3)^{3/2}$ depending on the stringency with which low stiffness is required. Thus, the cost of having a QZS mechanism is that for large excursions from the static equilibrium position the stiffness can increase to between about two and three times that of the vertical spring.

5. Approximation to the stiffness of the QZS isolator

The relationship between force and displacement given in Eq. (9) and shown graphically in Fig. 2 is similar to that of a cubic function. It would considerably simplify subsequent dynamic analysis of the QZS system if its stiffness could be described by a polynomial. A simplified cubic expression of the force is therefore sought and the error in the approximation quantified.

Using a Taylor series expansion, the force can be expressed as a power series of order N [12]

$$f(y) = f(y_0) + \sum_{n=1}^{N} \frac{f^n(y_0)}{n!}(y - y_0)^n, \tag{25}$$

where y_0 is the point at which the function is expanded and f^n denotes the nth derivative of f. Since the displacement of the system about the static equilibrium position is of interest, the power series for the force is expanded about this point. By expanding Eq. (9) using Eq. (25) and substituting for $\hat{y} = \hat{x} - \sqrt{1-\gamma^2}$ an approximate expression for the force is found to be

$$\hat{f}(\hat{y}) \approx \frac{\alpha}{\gamma^3}\hat{y}^3 + \left[1 - 2\alpha\frac{(1-\gamma)}{\gamma}\right]\hat{y} + \sqrt{1-\gamma^2}, \tag{26}$$

which consists of a cubic term, a linear term and a constant term. An approximate expression for the stiffness can be obtained by differentiating Eq. (26) to give

$$\hat{K} \approx 3\frac{\alpha}{\gamma^3}\hat{y}^2 + \left[1 - 2\alpha\frac{(1-\gamma)}{\gamma}\right]. \tag{27}$$

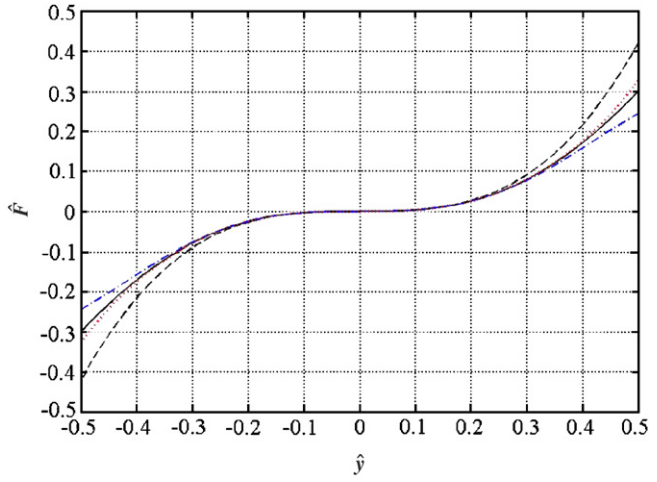

Fig. 10. Force–displacement characteristic of the QZS mechanism when $\gamma = 2/3$ and $\alpha = 1$. (— exact expression; - - - third-order expansion; - · - fifth-order expansion; .... seventh-order expansion).

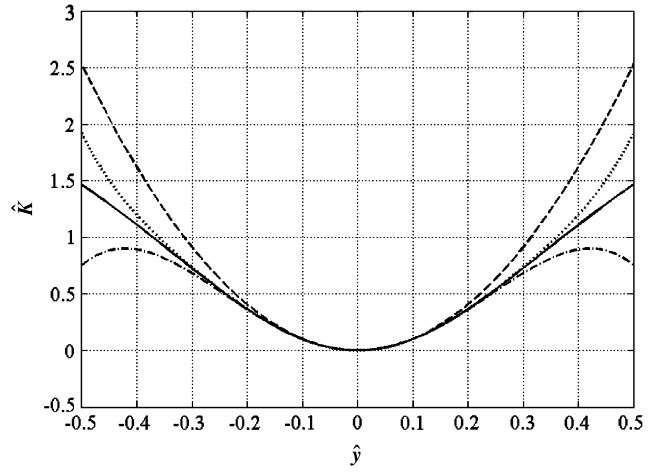

Fig. 11. Stiffness of the QZS mechanism as a function of deflection when $\gamma = 2/3$ and $\alpha = 1$. (— exact expression; - - - third-order expansion; - · - fifth-order expansion; .... seventh-order expansion).

If γ and α are chosen according to Eq. (11), the linear term in Eq. (26) disappears. Moreover, if the force is transformed by $\hat{F} = \hat{f} - \sqrt{1-\gamma_{\mathrm{QZS}}^2}$ to remove the constant term, then Eq. (26) can be written as

$$\hat{F}(\hat{y}) = \frac{1}{2\gamma_{\mathrm{QZS}}^2(1-\gamma_{\mathrm{QZS}})}\,\hat{y}^3, \tag{28}$$

which is plotted in Fig. 10. Also shown in the same figure are the curves corresponding to the approximation to the force if the fifth- and seventh-order terms in the series are included. Differentiating Eq. (28) gives the approximate stiffness of the QZS system to be

$$\hat{K}_{\mathrm{QZS}} \approx \frac{3}{2}\frac{1}{\gamma_{\mathrm{QZS}}^2(1-\gamma_{\mathrm{QZS}})}\,\hat{y}^2, \tag{29}$$

which is shown in Fig. 11, again compared with higher-order expansions.

The error between the approximate stiffness and the actual stiffness increases as the displacement from the static equilibrium position increases. This can be quantified at the maximum excursion when the stiffness

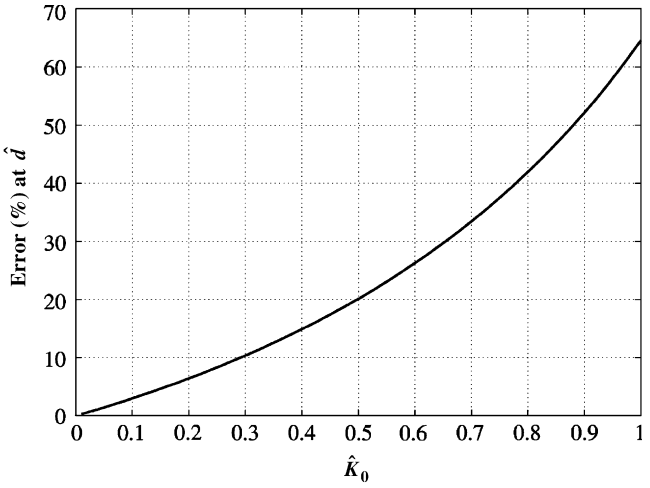

Fig. 12. Error in the approximation for the stiffness evaluated at the maximum excursion from the static equilibrium position such that the stiffness is smaller than $\hat{K}_0$.

equals $\hat{K}_o$ by the following:

$$\text{error}(\%) = \left| 1 - \frac{\hat{K}_{\text{approximate}}}{\hat{K}_{\text{actual}}} \right| \times 100, \tag{30}$$

where $\hat{K}_{\text{approximate}}$ is given by Eq. (29) and $\hat{K}_{\text{exact}}$ is given by Eq. (12), both evaluated at the maximum excursion for the corresponding $\hat{K}_o$. The percentage error is plotted in Fig. 12. It can be seen that the error is relatively small if the threshold stiffness $\hat{K}_o$ and hence the excursion from the static equilibrium position are small, but is significant as the threshold stiffness becomes comparable to that of the vertical spring ($\hat{K}_o \sim 1$).

6. Conclusions

The static characteristics of a quasi-zero stiffness mechanism have been investigated. The main feature of such a mechanism is the use of a negative stiffness element to achieve a low stiffness without having a large static deflection. A simple system consisting of three springs has been studied, and the optimum relationship between the geometry and the relative stiffnesses of the springs has been investigated. It has been found that to achieve a large excursion from the static equilibrium position such that the stiffness of the system does not exceed a prescribed value, there is an optimum geometry and a corresponding optimum relationship between the stiffnesses. It has also been found that for the spring configuration studied the oblique springs have to be inclined at an angle between approximately 48° and 57°. An approximate polynomial expression for the stiffness of the system has also been determined and the errors in this expression compared to the exact expression have been quantified.

References

[1] J.P. Den Hartog, *Mechanical Vibrations*, McGraw-Hill, New York, 1956.
[2] C.M. Harris, A.G. Piersol, *Shock and Vibration Handbook*, fifth ed., McGraw-Hill, New York, 2002.
[3] E.I. Rivin, *Passive Vibration Isolation*, ASME Press, New York, 2001.
[4] P. Alabuzhev, A. Gritchin, L. Kim, G. Migirenko, V. Chon, P. Stepanov, *Vibration Protecting and Measuring Systems with Quasi-Zero Stiffness*, Hemisphere Publishing, New York, 1989.
[5] D.L. Platus, Negative-stiffness-mechanism vibration isolation systems, *SPIE—Vibration Control in Microelectronics, Optics and Metrology* 1619 (1991) 44–54.
[6] J. Zhang, D. Li, S. Dong, An ultra-low frequency parallel connection nonlinear isolator for precision instruments, *Key Engineering Materials* 257–258 (2004) 231–236.

[7] K. Denoyer, C. Johnson, Recent achievements in vibration isolation systems for space launch and on-orbit applications, *52nd International Astronautical Congress*, Toulouse, France, 2001.
[8] J. Dankowski, State of the art vibration isolation of large coordinate measuring machine with an adverse environment, *Second Euspen International Conference*, Turin, Italy, 2001.
[9] P. Lorrain, Low natural frequency vibration isolator or seismograph, *Review of Scientific Instruments* 45 (1974) 198–202.
[10] L. Lacoste, Lacoste and Romberg straight-line gravity meter, *Geophysics* 48 (1983) 606–610.
[11] J. Winterflood, High Performance Vibration Isolation for Gravitational Wave Detection, PhD Thesis, University of Western Australia—Department of Physics, 2001.
[12] E.T. Whittaker, G.N. Watson, *A Course of Modern Analysis*, fourth ed., Cambridge Mathematical Library, 1990.

Appendix C

Lab demonstrator of the HSLDS characteristic

This appendix describes the design and construction of a test rig whose purpose was to give a visual demonstration of the effect of the combination of elements with positive and negative stiffness [74].
The scale of the apparatus is such that it is ideal to show the drastic reduction of natural frequency that can be achieved with an HSLDS mechanism without needing any instruments or data processing, but only the naked eye.

In order to provide a simple theoretical background to this otherwise purely demonstrative exercise, a linearised analysis of the system is presented. The device has a single rotational degree of freedom. It has two set of springs acting in parallel. One set is permanent and has positive stiffness. The other is negative and can be removed or adjusted. When acting simultaneously the dynamic stiffness is reduced and this results in an appreciable increase in the period of oscillations.

C.1 Linear mathematical model

A schematic representation of the mechanism is shown Fig.C.1. It consists of a horizontal beam suspended on a *support* spring of stiffness k_s attached at a distance d from the centre of rotation of the beam. An additional *correction* spring of coefficient k_c, can be attached to the beam through the rigid link OQ. This system is illustrated in [24] where its nonlinear behaviour is also studied.

Consider first the case when the corrective spring is detached. The system is reduced to a horizontal beam simply supported at one end. When displaced from its initial horizontal equilibrium position by an angle θ_0, and assuming small angles of oscillations[a], the conservative equation of motion of the simply supported beam is

$$I\ddot{\theta} + \kappa\,\theta = 0 \tag{C.1}$$

where I is the second moment of inertia of the beam about the vertical axis passing through the hinge, $\ddot{\theta}$ is the angular acceleration and $\kappa = k_s d^2$ is the angular stiffness. It follows that the restoring moment of the *supportive* springs is $M_s = k_s d^2\,\theta$. The frequency of oscillation for the simple pendulum is therefore given by

$$f_n = \frac{1}{2\pi}\sqrt{\frac{\kappa}{I}} \tag{C.2}$$

Consider now the case when the correction spring is connected. In Fig.C.1 this is attached between a fixed point P, at a vertical distance h from the centre of rotation O, and a point Q of the beam at a distance a from O. When displaced by an angle θ, as in Fig.C.1, the correction spring is stretched and its force generates a moment which does not oppose the rotation but favours it. This is the very concept of the negative stiffness.

The moment due to the correction spring, M_c, is

$$M_c = F_c\,r \tag{C.3}$$

where $F_c = k_c(L - L_0)$ is the constant spring force which arises by stretching the spring from its initial length L_0 to $L = a + h$[b] and r is the moment arm given by

$$r = \frac{a\,h}{L}\,\theta \tag{C.4}$$

Thus the corrective moment can be written as

$$M_c = k_c\left(1 - \frac{L_0}{L}\right)\,a\,h\,\theta \tag{C.5}$$

When both supportive and corrective springs are attached the total moment

[a] For small angles $\sin\theta \approx \theta$,$\cos\theta \approx 1$

[b] This is true because of the assumption of small angles

acting on the HSLDS mechanism is given by,[24]

$$M_{tot} = M_s - M_c = \left[k_s d^2 - k_c \left(1 - \frac{L_0}{a+h}\right) a\, h\right] \theta \tag{C.6}$$

from which is follows that the natural frequency of vibration of the HSLDS system is

$$(f_n)_{HSLDS} = \frac{1}{2\pi}\sqrt{\frac{\kappa_{tot}}{I}} = \frac{1}{2\pi}\sqrt{\frac{k_s d^2 - k_c \left(1 - \frac{L_0}{a+h}\right) a\, h}{I}} \tag{C.7}$$

By inspection of Eqn.(C.7) it can be seen that by adjusting the system parameters the frequency can be made as small as desired. Setting the connection of the support spring to be fixed (i.e. d), the most suitable parameter to be made adjustable is a. In particular, by increasing a the natural frequency can be drastically reduced, and even made zero if

$$a = a_{max} = \frac{d^2 k_s + k_c\, h\, (L_0 - h) + \sqrt{4d^2 h^2 k_c k_s + \left[d^2 k_s + h k_c (L_0 - h)\right]^2}}{2 h k_c} \tag{C.8}$$

Note that if $a > a_{max}$ the angular stiffness becomes negative and the system is unstable.

C.2 Experimental rig and results

The experimental rig in its HSLDS configuration is shown in Fig.C.2. The support and corrective springs are indicated. The adjustment parameter a is also shown.

The two supportive springs have a nominal stiffness $k_s = 254$ N/m, whilst that of the corrective springs, which have an initial length $L_0 = 24$ cm, is $k_c = 368$ N/m. The horizontal distance between the support springs and the centre of rotation is $d = 12$ cm and the fixed point (as P in Fig.C.1) is at a distance $h = 19$ cm from O. The maximum value a can attain, from Eqn.(C.8) is $a_{max} = 16.5$ cm. The adjustment parameter a is thus changed to three different lengths in the experiment in order to achieve different natural frequencies. Namely $a = 13$, 14.5 and 15.5 cm.

The measured transient response is due to an initial vertical displacement of

the free-end of the beam of 7 mm which is equivalent to the initial conditions

$$\theta(0) = \theta_0 \approx 1^\circ \qquad \dot{\theta}(0) = 0 \tag{C.9}$$

and acquired with a low-frequency accelerometer placed at the tip of the beam. This complies with the assumption of small angles and therefore the linearised theory applies.

Fig.C.3 a,b,c shows the comparison between the measured acceleration (in Volts) for the case when only the supporting springs were attached and that of the HSLDS systems with the three different values of a. It can be seen that the period of oscillation of the simply supported beam is more than 4 times smaller than the HSLDS with the lowest frequency ($a = 15.5$ cm). In order to show clearly the difference in frequency of oscillation the Discrete Fourier Transform (DFT) of the measured signals was computed and its magnitude plotted. This is shown in Fig. C.4. The DFT has been computed by simply using the Matlab® 'fft' function over the whole length of the acquired data.

C.3 Conclusions

In this appendix a device capable of achieving a very low frequency of oscillation has been designed, built and tested.

The demonstrator is a horizontal beam hinged at one end and suspended on two springs. Assuming small rotations, the mathematical model of the pendulum has been described with a linear model. A set of correction springs provide the necessary negative rotational stiffness which can be adjusted by suitably changing their initial length. As a result the frequency of oscillation has been reduced by more than four times.

As in most experimental work, the qualification and quantification of the damping is a rather difficult task. Because the main purpose of this experiment was to engineer a device with high-static-low-dynamic-stiffness no further investigations have been conducted on damping identification. An issue to be addressed in future work is the design of a rig that has one main mechanism of energy dissipation. A survey of the literature has disclosed a number of methods

to identify and quantify nonlinear behaviour from experimental measurements of transient response. Amongst these one of the most interesting allows to compute the instantaneous natural frequency and damping ratio rather easily. It is called 'FREEVIB' and is based on the analysis of the Hilbert Transform of the signal [73].

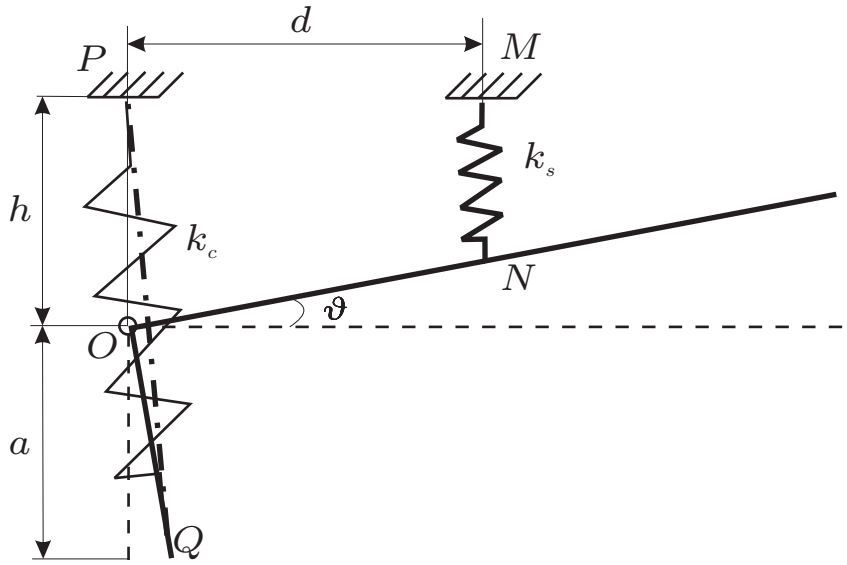

Figure C.1: Schematic representation of the HSLDS demonstrator

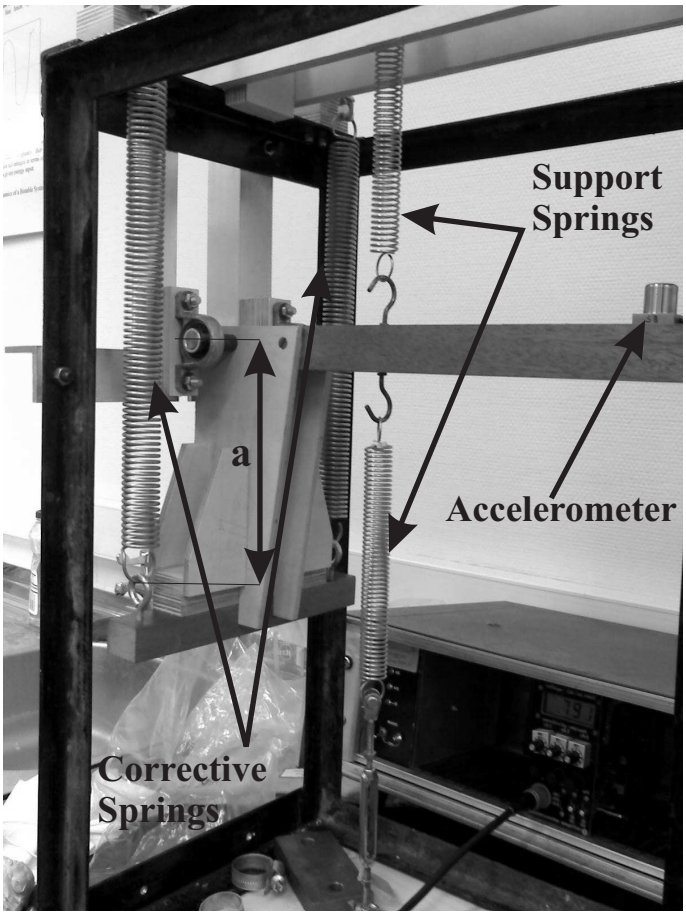

Figure C.2: *Experimental Rig*

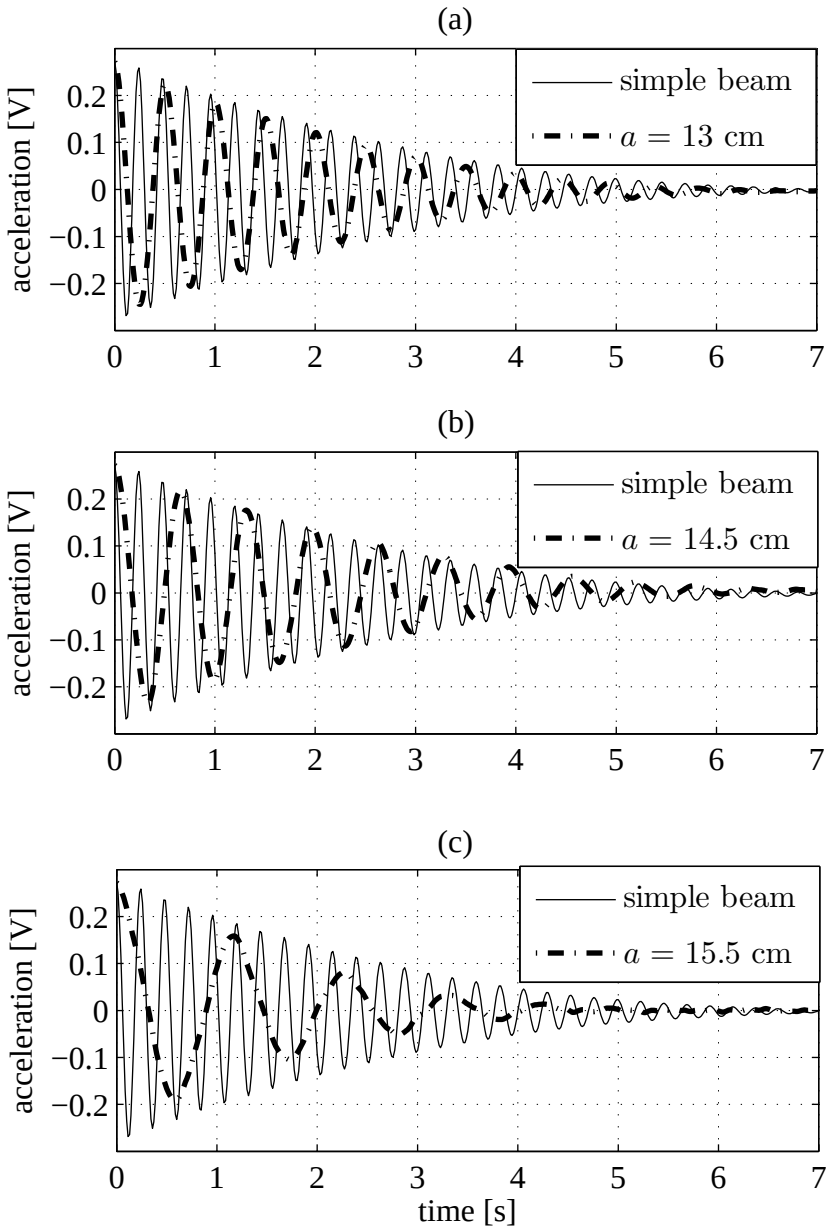

Figure C.3: Transient response of the system for different values of a: the period of the simple pendulum is more than 4 times shorter than the period of the HSLDS mechanism when $a = 15.5$cm (c)

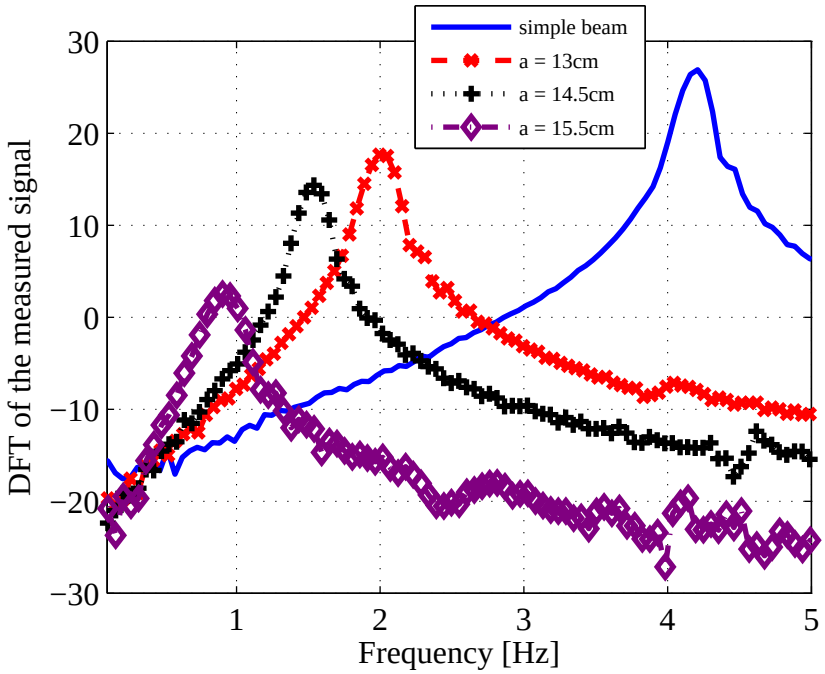

Figure C.4: DFT magnitude of the measured acceleration. The analysis of the frequency content clearly shows the reduction in natural frequency achieved with the insertion of the corrective springs